Volcanology of the basaltic lava succession within the Auckland pit of the Bombay Quarry, Bombay Volcanic Complex, South Auckland Volcanic Field

A thesis submitted in fulfilment
of the requirements for the degree
of
Masters of Science (Research)
in Earth Sciences
at
The University of Waikato
by

Aliasgar Kapasi

The University of Waikato
2016

THE UNIVERSITY OF
WAIKATO
Te Whare Wānanga o Waikato

Abstract

The South Auckland Volcanic Field (SAVF), which was active 1.59 – 0.51 million years ago and comprises around 82 volcanic centres, represents a complete history of a monogenetic field preserved in the geological record. The Auckland pit in the Bombay Quarry was recently exposed, revealing an infilled palaeovalley of volcanic and sedimentary deposits possibly associated with the nearby Bombay Volcanic Complex. A set of vertical drill cores from across the quarry were available for this study.

The stratigraphy of the volcanic and sedimentary deposits and the facies architecture were examined and described from the drill cores available, and a set of stratigraphic logs were produced. Volcanic and sedimentary units identified were: basement Waitemata and Tauranga group sediments, three individual ponded basalt lavas with intercalated scoria and Quaternary alluvium and/or Kauroa ash deposits. Facies identified include: moderately vesicular basalt (A.1), vesicular basalt with vesicle trails (A.2), non-vesicular basalt (A.3), poorly vesicular basalt (A.4), scoria deposit (B), scoriaceous basalt (C) and intercalated silt/clay (D).

Petrographic characteristics were analysed by optical microscopy, which show that all three basalt lavas have minerals comprising: olivine and clinopyroxene phenocrysts, and a groundmass of plagioclase, opaques and mafic minerals, however, the proportions of each mineral vary between samples. Olivine, clinopyroxene and plagioclase elemental compositions for each of the three basalt units were determined by electron microprobe analysis and revealed that the middle basalt had relatively lower proportion of Mg- and Ca-rich minerals compared to the upper and lower basalts. Furthermore, mineral compositions were consistent with the broad group B rock type of the SAVF lavas.

Bulk-rock geochemical characteristics were analysed by X-ray fluorescence spectrometry where the basalt samples were classified as basanites and ne-hawaiites. The lower and upper basalts have a relatively wide range of

major and trace element compositions; whereas, the middle basalt has less variation.

The three basalt lava flows represent pahoehoe and/or transitional lava flows, which occurred during magmatic eruptions separated by periods of volcanic quiescence represented by Quaternary alluvium and/or Kauroa ash deposits. The magma source beneath the Bombay area reveals that it consists of dominantly a garnet-bearing peridotite source where only group B type lavas were erupted over time. This process indicates a polygenetic-like eruption history within a monogenetic field, which may be an ideal analogue for understanding the future of shield volcanism in the South Auckland and Auckland Volcanic Field.

Acknowledgements

This project would not have been possible without the encouragement, assistance and support I received. I am grateful to have the opportunity to acknowledge and thank them.

My primary thanks goes to Dr. Adrian Pittari for his constant patience, support, guidance and knowledge, which has made this study possible. Thank you to Professor David Lowe for his help in the initial stages for this study.

Thank you to Holcim New Zealand and, in particular Keith Miller, for access to the Holcim Quarry at Bombay and for allowing me access to the Auckland pit, drill cores and internal company data and photographs for this study.

This research would not have been possible without the knowledge and guidance from the Earth Sciences staff; Renat Radosinksy, Kirsty Vincent, Annette Rodgers and Shaun Barker; as well as the help from Ian Schipper (Victoria the University of Wellington) on the electron microprobe.

I am very grateful of funding received from the internal University of Waikato research funds, including a scholarship stipend, and the Broad Memorial Fund.

To my family and friends, thank you for always believing in me, giving me the confidence and being supportive of my endeavours.

Table of Contents

List of Figures

Chapter Two: Geological Setting

Chapter Three: Stratigraphy and Facies

Chapter Five: Whole rock basalt geochemistry

Chapter Six: Discussion

List of Tables

Chapter Four: Petrography and Mineralogy

Chapter Five: Whole rock geochemistry

Chapter One

Introduction

1.1 Introduction

The South Auckland Volcanic Field (SAVF) is an example of one of many monogenetic volcanic fields throughout New Zealand, and it represents a complete history of basaltic monogenetic volcanism still preserved in the geological record. The field was active 1.59 – 0.51 million years ago (Briggs *et al.,* 1994) and many of the presently known 82 volcanic centres are exposed and easily accessible. The study of individual volcanic centres within the SAVF can help improve our understanding of the eruption history, dynamics and controls on monogenetic fields, as well as volcanic processes occurring at tuff rings, maars, scoria cones and effusive centres in both the SAVF and other fields around the world. The Bombay Quarry is located on the western side of the SAVF and a previous study on the Waikato pit was completed by Gibson (2011). However, since the study of Gibson (2011) the more recent Auckland pit was opened, and drill cores which were not previously available became accessible. This exposed section provides an insight into the volcanic history of the Bombay Quarry and also an understanding of the nature of volcanic and sedimentary units deposited within the Auckland pit.

1.2 Aims and Objectives

Previous research and studies into the volcanism of the South Auckland Volcanic Field have improved our understanding of the history of a monogenetic volcanic field. The Bombay Volcanic Complex is essentially a lava shield with multiple vent complexes and at the Bombay Quarry it's on the southwestern flanks, where there are multiple lava flows, various vent structures (e.g. scoria cones, spatter cones, tuff rings) and intercalated tephra and sediments.

The main aim of this thesis is to reconstruct the volcanic history associated with an exposed section on the southwestern flank of the Bombay Volcanic Complex, within the Auckland pit, Bombay Quarry. From a wider perspective, the findings from this study could assist in assessing the importance of polygenetic volcanoes within monogenetic fields and also if the Bombay Volcanic Complex would be an ideal analogue for understanding the future of shield volcanism in the Auckland Volcanic Field (i.e. Rangitoto Island).

The objectives for this study therefore, are;

1. To document the stratigraphic relationship and facies architecture of the volcanic and sedimentary deposits.
2. To describe the petrographic textures of the basalts and determined their mineral compositions.
3. To identify the bulk-rock geochemical composition of the basalts to better understand the magmatic processes.

1.3 Location of Study Area

The South Auckland Volcanic Field covers the Pukekohe, Bombay, Tuakau, Pukekawa and Onewhero regions (Briggs *et al.*, 1994) over an area of approximately 300 km^2 (Rafferty & Heming, 1979). The field hosts 82 volcanic centres and a wide range of volcanic activity.

The study area chosen was the Auckland pit, Bombay Quarry (lat. 37º12’46.67″ S long. 174º59’22.40″ E). The Bombay Volcanic Complex is situated on the eastern side of the SAVF, 3.5 km southwest of Bombay which is part of the Bombay Hills; to the south is the Waikato region and the Auckland region to the north. The complex consists of at least one tuff ring, a tuff cone, numerous scoria and spatter cones and at least three large deposits of ponded basalt lava.

1.4 Methods

To achieve the above objectives, the methodology involved field work, including stratigraphic logging of drill core and facies descriptions, and laboratory work: optical microscopic petrography from thin sections, including point counting, mineral geochemistry (electron microprobe analysis) and bulk-rock geochemical (X-ray fluorescence spectroscopy) analysis. Detailed descriptions of each method are outlined in Chapters 3, 4 and 5.

1.5 Chapter Outlines

Chapter 2 reviews monogenetic volcanic fields, the tectonic and volcanic setting of New Zealand and volcanism of the South Auckland Volcanic Field. Previous studies on the South Auckland Volcanic Field and especially on the Bombay Quarry are discussed.

Chapter 3 overviews of the geological features of the quarry, presents the results of field work on the stratigraphy and facies variations from drill core observations, and summaries the facies architecture throughout the stratigraphic succession that has been identified.

Chapter 4 focuses on the petrographic analysis of basalt lavas within the Auckland pit. Microscopic petrography of the basalt lavas and scoria samples are described and quantitative results of point counting are presented. Mineralogy of the basalt lavas is analysed, described and quantitative results from electron microprobe analysis are presented.

Chapter 5 focuses on the bulk-rock geochemical analysis of the basalt lavas; the major and trace elements are described and compared to other previous literature to describe any correlations that occur within the SAVF.

Chapter 6 interprets the data and observations presented in the preceding chapters, and discusses and summarises the eruption history of the Auckland pit in relation to the region of the Bombay Volcanic Complex.

Chapter Two

Geological Setting

2.1 Monogenetic Volcanoes

Monogenetic volcanic fields consist of small co-genetic/individual, commonly mafic volcanoes, built in a single relatively short-lived eruption cycle that never erupt again. Such volcanism is commonly associated with eruptions of basaltic to basaltic-andesite magmas and is common worldwide (White, 1991). The variety of volcanic landforms produced in such fields is dependent on whether or not water is present at or near the surface at the time of eruption. Eruptions involving groundwater result in hydrovolcanic eruptions which produce tuff cones, tuff rings and maar volcanoes (White, 1991; Nemeth & Kereszturi, 2015). Areas lacking groundwater or surface water produce eruptions that consist of lava flows and scoria cones (White, 1991; Nemeth & Kereszturi, 2015). A typical monogenetic volcanic field includes all of these landforms, and the relative proportion of each are primarily controlled by a combination of magma flux rates, physicochemical properties of magma, the bulk ratio of magma to external water/water-bearing sediments and the environment into which the volcanoes erupt (Nemeth & Kereszturi, 2015). Recent research has found that these monogenetic volcanoes can show systematic geochemical variations, reflecting the processes of melt extraction and deep fractionation (Nemeth & Kereszturi, 2015).

Basaltic magmas are known for producing quiet eruptions dominated by lava flows. Scoria cones are volumetrically minor associates of many such eruptions, generally formed during early stages of eruption when excess gas escapes the erupting magma (White, 1991). For basaltic eruptions, the relative proportion of scoria versus fluid lava is determined by the magma gas content and the rate of eruption (White, 1991). Within monogenetic volcanic fields scoria cones and lava flows are formed from magmatic eruptions. However, erupting

magma that encounters water will produce violent phreatomagmatic eruptions which build tuff cones, tuff rings and maars within the lowlands of the monogenetic volcanic field.

Volcanoes in the South Auckland Volcanic Field take the form of scoria cones, tuff rings, maars and tuff cones (Németh *et al.,* 2012). Scoria cones are the most common landform and show a great diversity in size, morphology and eruptive products. The four volcanic fields in the Auckland Volcanic Province of Okete, Ngatutura, South Auckland and Auckland are spaced at 30 km intervals and progressively young to the north (Németh *et al.,* 2012). The Indo-Australian Plate motion is to the north, which is inconsistent with the age trend of volcanism from south to north, if it was to be considered moving over a stationary mantle plume source. Instead, the age trend implies a northward movement of the mantle source. The volcanic fields in the Northland Volcanic Province show no younging trends and hence must have discrete sources from those of Auckland (Németh *et al.,* 2012). The subsurface geology of the SAVF is considered to play an important role in the nature and style of magmatic versus phreatomagmatic volcanism, related to the availability of local surface or groundwater, and a pronounced structural control by upper crustal faults which provided pathways for dike intrusion (Németh *et al.,* 2012).

2.2 New Zealand's Tectonic Setting

New Zealand lies along the plate boundaries between the Pacific and Indo-Australian plates, where both subduction and strike-slip movement occurs. The North Island of New Zealand is located towards the eastern margin of the Indo-Australian plate, bounded by the convergence and associated subduction of the Pacific Plate at the Hikurangi Trench. The plate boundary then moves onto land at Kaikoura and down the west side of the South Island where a strike-slip tectonic setting has, and still is actively producing the Southern Alps of the present day. To the south of the Southern Alps, the Indo-Australian plate is subducted underneath the Pacific plate at the Puysegur Trench, forming New Zealand's tectonic setting (Fig. 2.1). This boundary development has had a large influence on the volcanism of the North Island through the Neogene and Quaternary (Taylor, 2012).

The New Zealand landmass was located on the eastern side of Gondwana during the Mesozoic Era and consisted of several basement terranes (King, 2000). These terranes were uplifted, faulted and folded due to the convergence and subduction deformation regime New Zealand was experiencing, prior to the development of the plate boundary structure before 25 Ma (Furlong & Kamp, 2009). The movement of the Pacific Plate southward set the precursors for the subduction to begin at the Hikurangi and Puysegur Trenches. This began the movement of the New Zealand tectonic system away from an extension regime and towards one of a strike-slip deformation regime (Furlong & Kamp, 2009) (Fig. 2.1).

Post 25 Ma, the New Zealand landmass deformed under transpression, as the initial stages of subduction had started and the slab had begun to migrate south (Furlong & Kamp, 2009). The basement terrane, forming the main South Island body, moved south off the East Coast of the North Island to the middle of what is now the current South Island (Furlong & Kamp, 2009). The plate boundary began propagating through the New Zealand landmass, producing the onset of arc volcanism in Northland and the Coromandel in the Late Miocene (Cole, 1986). The propagation of the plate boundary through New Zealand produced both uplift, and basin subsidence along the reactivation of faults trending northward in the Auckland region (Edbrooke, 2001).

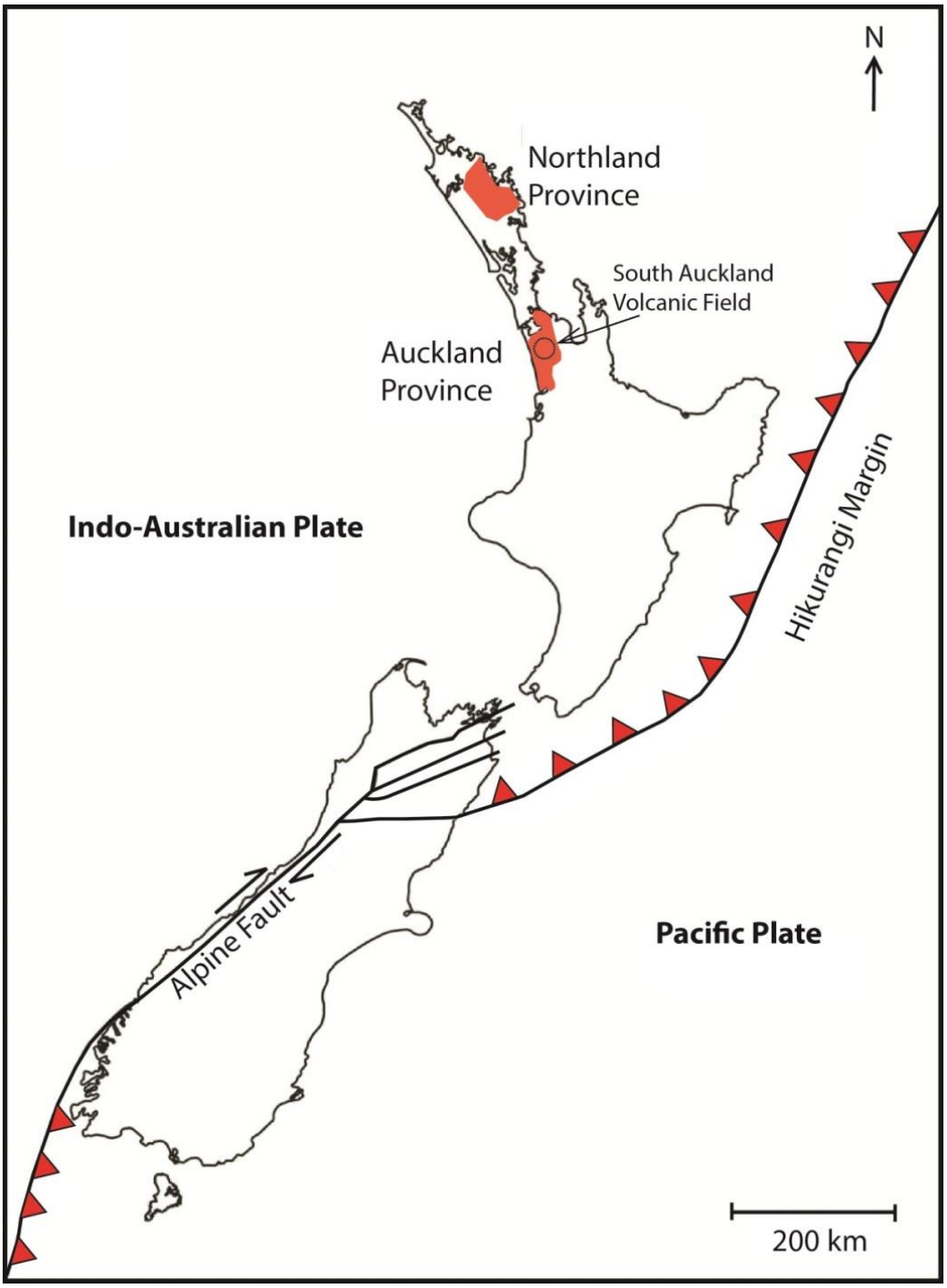

Figure 2.1: Active plate boundary in New Zealand showing the Hikurangi Margin where subduction takes place and strike-slip boundary in the South Island along the Alpine Fault (modified from Gibson, 2011).

During the early Miocene, the development of the Indo-Australian-Pacific plate boundary initiated subduction-related volcanism in the Northland Peninsula, followed later on the Coromandel Peninsula and finally the Taupo Volcanic Zone (TVZ) which produced large volumes of magma, varying in composition from basalt through andesite to rhyolite (Cook *et al.*, 2005). The geological record also implies that volumetrically minor amounts of basaltic magma were erupted in a number of distinct intraplate volcanic fields in northern North Island of New Zealand; these fields are the Northland Volcanic Province (Kaikohe–Bay of Islands and Whangarei volcanic fields) and Auckland Volcanic Province (Okete, Ngatutura, South Auckland, and Auckland volcanic fields). Each volcanic field contains numerous, relatively small-volume, predominantly monogenetic volcanoes that produce volcanic products of mainly basaltic composition and include maars, scoria cones and lava flows - all with small volumes. The North Island intraplate volcanic activity has occurred from the Miocene to recent times (Cook *et al.*, 2005) and the Auckland province shows an age trend of progressive younging (Briggs *et al.*, 1994) northwards.

Cook *et al.*, (2005) noted that the subducting Pacific Plate beneath the North Island can only be tracked to 250 km deep. This cannot be tracked underneath the South Auckland Volcanic Field and that the volcanism is caused by decompressional melting in the extensional environment of western and northern North Island. The intraplate volcanoes in New Zealand are generally separate from the active plate boundary zone and have no apparent tectonic relationship with the active margin (Briggs *et al.*, 1994).

2.3 South Auckland Volcanic Field

The South Auckland Volcanic Field covers the Pukekohe, Bombay, Tuakau, Pukekawa and Onewhero regions (Briggs *et al.*, 1994) over an area of approximately 300 km^2 (Rafferty & Heming, 1979) (Fig. 2.2). It is situated in an extensional tectonic environment around 160 km behind the active volcanic front of the TVZ, and is considered to represent an intraplate association developed on the Australian plate (Briggs *et al.*, 1994).

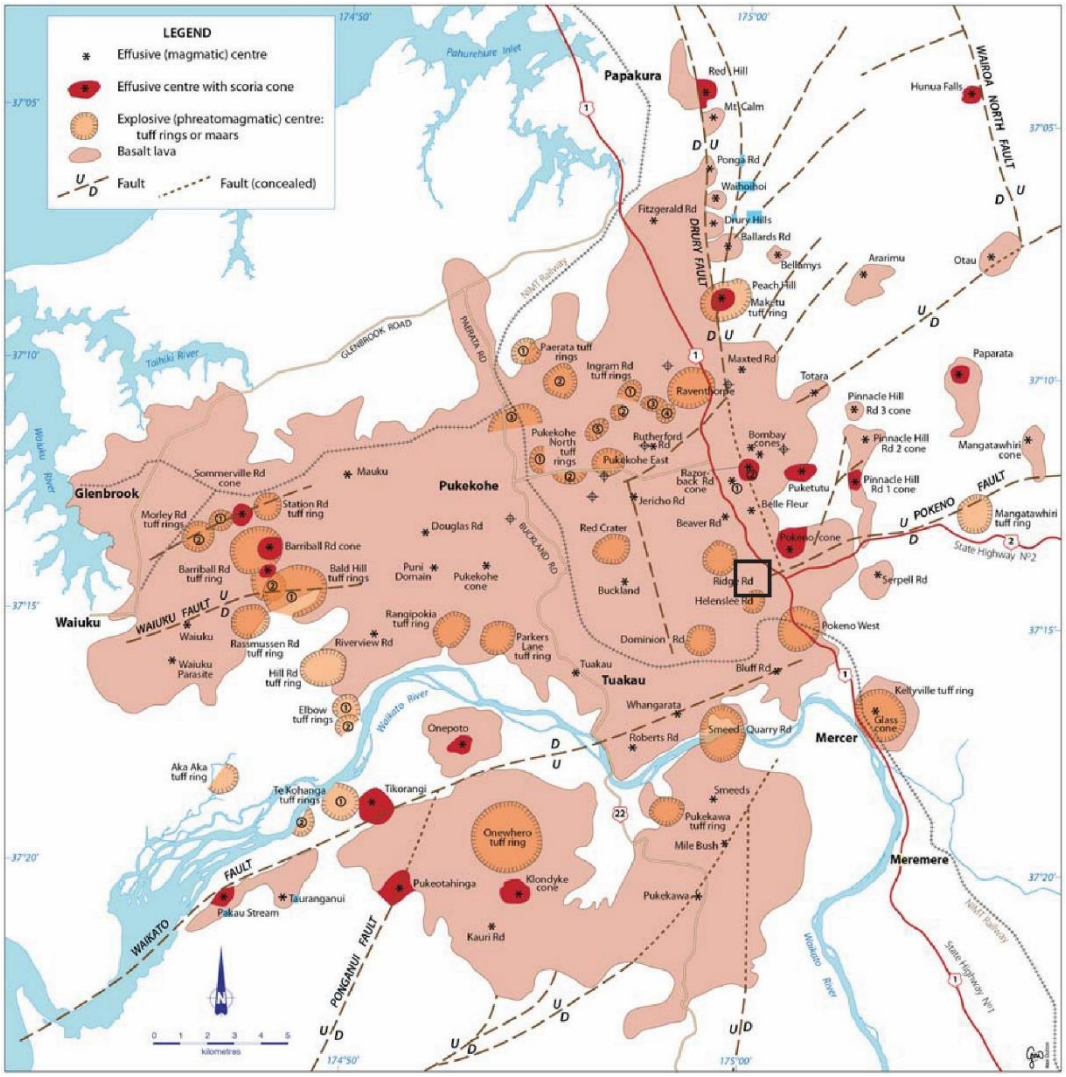

Figure 2.2: Distribution of volcanic centres and underlying geology of the SAVF. The study area is shown as box (adapted from Németh *et al.*, 2012).

The number of volcanic centres recorded for the South Auckland Volcanic Field has changed over time: using a combination of mapped locations and use of volcanic ages from previous literature, the number of tuff rings, scoria cones and effusive deposits has been recounted and in present day the accepted number of volcanic centres is ~ 82. Briggs *et al.*, (1994) outlined that where volcanoes in the SAVF were either overlapping one another or had small distances between them they would be classified as one centre. The SAVF was active between the ages of 1.59 and 0.51 Ma (Briggs *et al.*, 1994) and it is located 30 km south of the

younger Auckland Volcanic Field, active since 250 ka (Cook *et al.,* 2005). Two eruption styles of volcanism occurred: magmatic, producing scoria cones and lava flows, and phreatomagmatic, producing tuff rings and maar craters (Briggs *et al.*, 1994; Taylor, 2012).

Because the SAVF is much older, the volcanoes are not as well preserved as those of the younger Auckland field (Hayward, 2015). Unlike the Auckland volcanoes, the South Auckland Volcanic Field has been covered by the Hamilton Ash Formation, comprising a sequence of multiple rhyolitic tephra beds and associated paleosols, up to c. 6 m thick (Tonkin, 1970; Kamp & Lowe, 1981; Selby & Lowe, 1992; Lowe & Percival, 1993; Lowe *et al.,* 2001). The Hamilton Ash beds were deposited by airfall, from eruptions that occurred between c. 350,000 and c. 100,000 years ago from the Taupo Volcanic Zone (Lowe *et al.*, 2001). Much of the ash has been eroded on the higher parts of the volcanic fields, like the tuff rings and Hunua Ranges (Hayward, 2015). However, many of the gently sloping lava flow fields of the shield volcanoes are still deeply buried by the ash cover.

Many of the volcanic centres in the South Auckland Field are located either along or adjacent to faults, or inferred extensions of faults (Cook *et al.*, 2005).They are situated in a down-faulted area bound in the south by the Waikato fault and east by the Drury fault of Mesozoic greywacke, sandstone and argillite that form the basement rocks (Rafferty, 1977). The volcanoes south of the Waikato fault and east of the Drury fault lie on the uplifted basement rocks.

Overlying the Mesozoic basement, with a pronounced angular unconformity, is the Te Kuiti Group of Eocene – Oligocene age that predominantly consists of a transgressive sequence of coal measures overlain by marginal marine to outer shelf calcareous mudstone, sandstone and limestone (Edbrooke, 2001; Tripathi *et al.,* 2008) . The Waitemata Group of Miocene age unconformably overlies the Te Kuiti Group which comprises a basal, transgressive sequence of coarse, lithic, shallow marine sediments that pass rapidly up into bathyal, turbidite sandstone and pelagic mudstone sequences (Edbrooke, 2001). The Kaawa Formation of Pliocene age, unconformably overlies the Waitemata and/or Te Kuiti Groups, comprising fine-to medium-grained,

pumiceuos sandstone (Edbrooke, 2001). The Tauranga Group of Pliocene – Pleistocene, comprises mainly of pumiceous, terrestrial and minor estuarine sediments that are present and mostly exposed in extensive lowland areas west and south of Auckland, as the Puketoka Formation and Taupo Pumice alluvium. Silicic volcanic materials that dominate the sediments were derived initially from eruptions in the Coromandel Volcanic Zone (CVZ) and later from the Taupo Volcanic Zone (TVZ) (Rafferty & Heming, 1979; Edbrooke, 2001).

Tuff rings in the South Auckland Volcanic Field occur commonly in clusters or nested, and range from 0.5 to 2.5 km in diameter (Rafferty & Heming, 1979). Several tuff rings have formed nested scoria cones where strombolian activity occurred after phreatomagmatic eruptions (Rafferty & Heming, 1979). Rafferty (1977) suggested that the processes that formed the South Auckland volcanism were also the cause of the Pleistoscene displacement of the major faults in the area, including the Drury, Pokeno, Wairoa and Waikato faults and approximately half of the volcanic centres are either directly on, or very close to, faults in the volcanic field. This indicates that the volcanism is largely fault-controlled (Briggs *et al.*, 1994). Faults pre-dating the volcanism are present but covered in the extensive lavas that largely cover the field (Briggs *et al.*, 1994).

Cook *et al.*, (2005) shared the view that it is unlikely that the South Auckland volcanism occurred from magma chambers, but is characterised by short-lived eruptions derived from small batches of magma sourced directly from the mantle. This is typical of monogenetic basaltic fields elsewhere in the world (Connor & Conway, 2000).

Initial study on the "Franklin County" was undertaken by Schofield (1958), who studied basalts in South Auckland and suggested that they were between early - mid Pleistocene in age. Schofield (1958) reported the Franklin basalts to consist of basalt flows and basaltic tuffs commonly containing Waitemata Group lithics. The lavas are all basaltic and all contain olivine, augite, plagioclase and opaques (Rafferty, 1977). Schofield (1958) originally divided the South Auckland basalts into two groups: Franklin basalts and Bombay basalts, based on cone morphology and degree of weathering. However, Briggs *et al.*, (1994), Cook (2002) and Cook *et al.*, (2005) established that there was no basis

for this subdivision. Rafferty (1977) and Rafferty and Heming (1979) decided that this would limit further classification using geochemical characteristics and, therefore, divided the basaltic products of the SAVF into two different groups: a hypersthene-rich subalkaline group and a nepheline-rich alkaline group. Cook (2002) studied the geochemistry of a characteristic group of volcanic samples from the SAVF, and Cook et *al.*, (2005) further analysed the differences between these two distinct groups of basalt, calling them Group A and Group B (respectively), using a greater range of samples taken by Cook (2002).

Previous volcanic studies in the SAVF have been completed by: Rosenberg (1991), mechanisms of phreatomagmatic volcanism; Cook (2002), petrogenesis and evolution of alkalic basaltic magmas; Ilanko (2010), Barriball Road tuff ring; Gibson (2011), tuff rings at Kellyville, Onewhero and Bombay; Taylor (2012), Raventhorpe and Pokeno west tuff rings; and Mullane (2015), geophysical study of Kellyville and Onewhero tuff rings.

2.4 Previous Work at Bombay Quarry

The volcanic complex at the Bombay Quarry is the product of many eruptions and consists of at least one tuff ring, a tuff cone, numerous scoria and spatter cones, plus at least two large deposits of ponded basalt lava. Alloway *et al.*, (2004) has provided an age date for a tephra layer at the base of one of the tuff rings present in the quarry. The tephra layer AT-71 was dated using isothermal plateau fission track dating (ITPFT) at 1 - 1.2 Ma. It is correlated with a post-Ongatiti tephra layer (AT-47) from Schnapper Rock at Beachlands from the Taupo Volcanic Zone (Gibson, 2011).

The Bombay Quarry is operated by Holcim Aggregates, who have commissioned geotechnical surveys and reports on the area, specifically relating to factors that can influence either the quality of the basalt or their safety to mine it. Ormiston Associates Ltd (1999) reported on the basalt resource at Bombay Quarry using drilling, geological studies and resource modelling. The geological model generally indicates that the basalt deposit comprises a high quality central core of basalt, surrounded by shells of successively decreasing rock quality. It is

further complicated by an explosion crater which has replaced part of the southern corner of the high quality basalt with low quality scoria and volcanic debris (Gibson, 2011).

Cook (2002) studied multiple volcanic centres in the South Auckland Volcanic Field that were geochemically analysed to determine the petrogenesis and evolution of alkali basaltic magmas within the SAVF. One of the centres included the Bombay Quarry where Cook analysed the ponded basalt lava (ne-hawaiites), scoria deposit (alkali ol-basalt) and tuff deposit (alkali ol-basalt – ne-hawaiites). Cook determined that the Bombay Quarry volcanic deposits consist of group B rock type that was derived from relatively small degrees of melting of a garnet peridotite source from the upper mantle region.

Gibson (2011) studied the tuff rings within the Waikato pit which is situated next to the currently exposed Auckland pit in the Bombay Quarry where tuff rings were analysed to determine their magmatic activity and illustrate the style of eruptions as well as their controlling factors. Gibson (2011) studied the upper tuff ring deposit on top of the Waikato pit where the tuff ring eruption was relatively constant and alternated between two sets of conditions: fallout dominated eruption pulses with some base surges that have high water content.

The Bombay Quarry tuff ring represents a relatively steady eruption with a general decrease in grainsize and a general decrease in water content, eruption energy and fragmentation. Fallout processes were dominant and fragmentation depth was generally intermediate. Juvenile material was dominant and lithic type was generally evenly distributed between Mercer Sandstone and Koheroa Siltstone. Gibson (2011) determined that the Mercer Sandstone is the most likely aquifer for the subsurface water source of the tuff ring eruption due to its high porosity and transmissivity. Gibson (2011) also studied a basalt sample from the Waikato pit and identified it as a ne-hawaiite considered group B rock type in the SAVF lavas.

Chapter Three

Stratigraphy and Facies

3.1 Introduction

The volcanic succession in the Auckland pit of the Bombay Quarry was formed about 1.0 – 1.2 million years ago (Alloway *et al.*, 2004), as dated from a tephra layer at the base of one of the tuff rings present in the quarry. The succession consists of a tuff ring, numerous scoria and spatter cones, at least three large deposits of ponded basalt lava as well as intercalated sediments. This chapter will cover the field and drill core examination methods, the main geological features of the Auckland pit and the lithologic facies and their stratigraphic variation identified within drill cores.

Access to the tuff ring and faces of the quarry was not permitted due to health and safety reasons therefore the focus of this chapter is on the volcanic succession intersected in drill core. Previous literature on the tuff ring within the quarry was presented in the MSc thesis of Gibson (2011), who focussed on the nearby Waikato pit.

3.2 Methods

Field work was undertaken at the Auckland pit and in the core storage facility at the Bombay Quarry, South Auckland to determine the stratigraphy and facies variation of the basalt lava flows and intercalated sediments that are preserved within the pit. Using the drill core provided by Holcim, detailed stratigraphic logs were constructed for each drill core over a period of four months. Twelve detailed stratigraphic logs were constructed and four to eight samples were collected from different depths in each drill core representing the different volcanic/sedimentary units present within the Auckland pit; a total of 84 samples were collected. In each drill core photographs of the volcanic and

sediment units were taken, before any samples were collected, to provide a visual aid later. The full list of samples is included in the sample catalogue presented in Appendix I and stratigraphic logs including both the graphic logs and written descriptions are presented in Appendix II.

Three cross section lines of correlated drill holes were produced to show the range and variation of volcanic/sedimentary units throughout the Auckland pit. Volcanic units that were logged in the drill cores were described, focussing on the phenocryst minerals and their sizes and estimated percentages, colour, vesicle sizes and shapes, and the degree of weathering that has occurred. Sedimentary units logged focussed on the colour and grain size variation of sediment. Vesicle percentages in this study are defined by: 0 %, non-vesicular; 0–10 %, very poorly vesicular; 10–35 %, poorly vesicular; 35–60 %, moderately vesicular; 60–80 %, very vesicular; and > 80 %, extremely vesicular, modified from Cas *et al.,* (2008).

As mentioned above, for health and safety reasons, access to the rock exposures within the quarry was not possible, therefore the main focus was on the drill core data available. However, representative photographs of different aspects of the quarry were taken from a safe distance.

Grain size analysis by dry sieving was undertaken on four samples of scoria deposits. Samples were sieved using an interval of 1 phi. A sieve stack was assembled from - 6 to - 1 phi where the dry scoria samples were put on the top of the sieve stack and placed on the agitator for several minutes to allow the scoria sample to sieve through the stack. Each interval of the sieve stack was carefully removed retaining the sieved sample and weighed. This process of repeated for the remaining scoria samples.

3.3 Historic and Geological Overview

The Bombay Quarry is located 3 km northeast of Pokeno township and access to the quarry is off State Highway 1, at the Nikau Road off-ramp and Ridge road (Fig. 3.1). Previous geological exploration comprised several stages of drilling programs that were conducted between early 1988 and mid 1989 supervised by Applied Geology Associates Ltd (Ormiston, 1999). The geological model based on initial drilling comprised a lensoidal body of relatively homogeneous basalt thinning and wedging out at the edges. The geological interpretation of the deposit, rock volume and quality was hindered by the number of widely spread drill holes giving the impression of a simple basalt body (Ormiston, 1999).

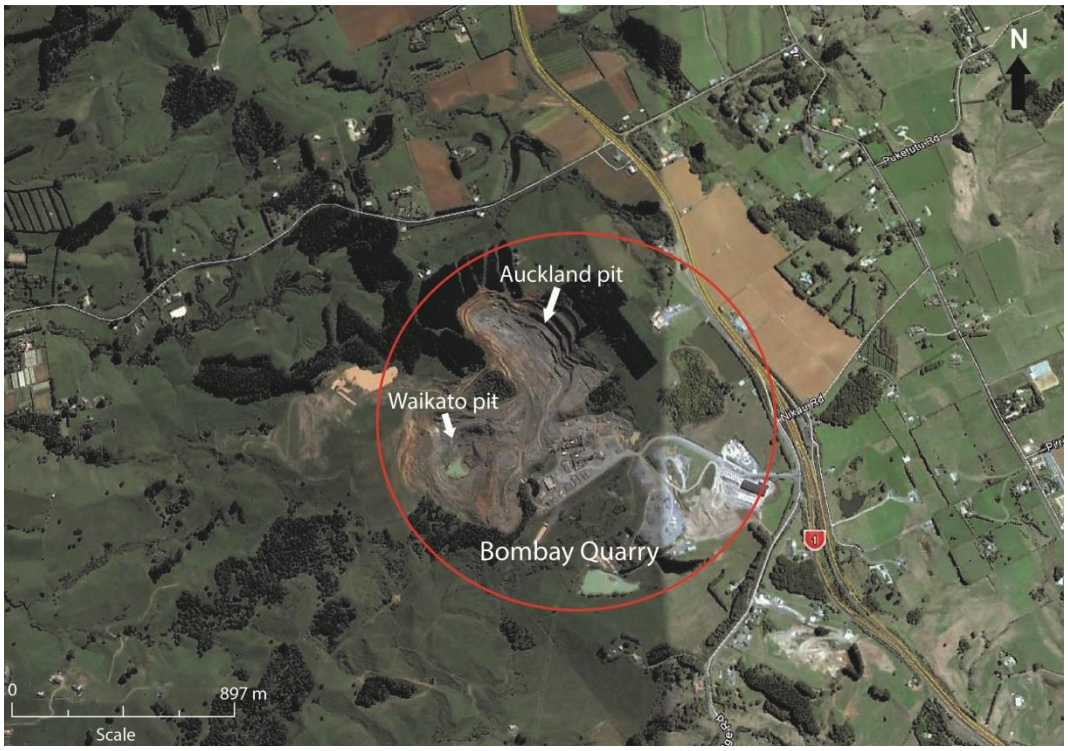

Figure 3.1: Location of Bombay Quarry, South Auckland off State Highway 1 (modified from Google Earth 2016).

The Bombay Quarry was opened in 1997 and, almost immediately, variations in the rock quality from the predicted relatively uniform high grade basalt resource model were encountered within the Waikato pit. Quarrying has indicated that the geological model from 1988 - 1989 was too simplistic and that, instead of there being a continuous body of homogeneous high strength basalt (Ormiston, 1999), the deposit comprises several volcanic bodies including scoria and spatter cones, tuff rings, basalt lava flows (Fig. 3.2) and a rhyolitic distal tephra layer at the base of the tuff ring (Fig. 3.3). Significant volumes of low strength, intercalated silts/clay within the area reduced the volume of high quality basalt. Additional drilling from early - mid 1999 was completed within the quarry to further refine the distribution and quality of the basalt flow (Ormiston, 1999). A new pit, the Auckland pit, was opened in 2011 approximately 400 m northeast of the Waikato pit, and quarrying in the Waikato pit finished in early 2012.

Figure 3.2: Photograph taken this study, looking towards north within the Auckland pit showing a succession of several volcanic deposits.

Figure 3.3: Photograph of the northwestern end of the Auckland pit taken this study showing the contact between the tuff ring deposit, silt sediment and the basalt lava flow. The distal rhyolitic tephra layer overlies the silt sediment at the northern point of the Auckland pit as shown.

The region of the Bombay Quarry, South Auckland comprises a variety of volcanic and sedimentary deposits including Waitemata and Tauranga group sediments; overlain by the Quaternary basaltic volcanic centres and associated lava flows then further overlain by tephra deposits (Ormiston, 1999).

The Miocene Waitemata Group in the area consists of weak interbedded turbidite sandstones and mudstones with calcareous units (Ormiston, 1999). Overlying the Waitemata group are the Tauranga Group sediments of Pliocene to Pleistocene age and comprise shallow water to weak terrestrial pumiceous sediments (Ormiston, 1999). In drill cores studied here the basement unit comprises red to brown fine-grained silt and light grey to dark grey mud which were later eroded into a palaeovalley beneath the Auckland pit.

Quaternary volcanic deposits in the area unconformably overlie the older Waitemata and Tauranga group sediments. The volcanic deposits comprise many small basaltic spatter cones, scoria cones and explosion craters (tuff rings). The spatter cones and scoria cones consist of flows interbedded with tuff (volcanic ash <2 mm), lapilli (scoria and basalt 2 mm – 64 mm) and a minor amount of ejected scoria. The explosion craters comprise fragmented country rock and basalt in a matrix of tuff and also some of these craters are infilled with basalt lava flows.

The Auckland pit has been excavated into several large ponded basalt lavas infilling a palaeovalley. The geological description below is based on field and photographic observations made in this study. The basalt lavas are columnar-jointed, platy-jointed and horizontal jointed. Several scoria and spatter cones occur above or are intercalated within the basalt succession. The basalt lavas display a pattern of concentric shells with high quality high strength basalt forming the core, and poor quality basalt towards the walls of the palaeovalley. The high strength basalt runs in a north-west and south-east direction. The majority of the material extends westwards under the overburden, which includes the tuff ring deposit and underlying sediments, forming the existing high wall. The overall dimension of the Auckland pit is 500 m long, 250 m wide and there is approximately 40 m thick of the basalt lavas within the palaeovalley.

Basalt jointing patterns vary within the Auckland pit. The observations are from remote view points and photographs, as access to the faces was not possible. Towards the northern most end of the pit jointing patterns vary from horizontal basalt joints near the base as well as dipping platy basalt in the lower to middle area followed by horizontal joints, and then columnar joints at the top of the basalt (Fig. 3.4). On the western and eastern sides jointing patterns also vary: the lower area consists of horizontal joints, the middle and upper areas of platy joints that are orientated to be dipping at a shallow angle towards the centre of the pit (Fig. 3.5). The upper point of the eastern side consists of columnar basalt joints (c. f. platy joints on the western side) (Fig. 3.6).

Figure 3.4: Photograph of the northern point of the Auckland pit taken this study showing the variation in jointing patterns of the basalt.

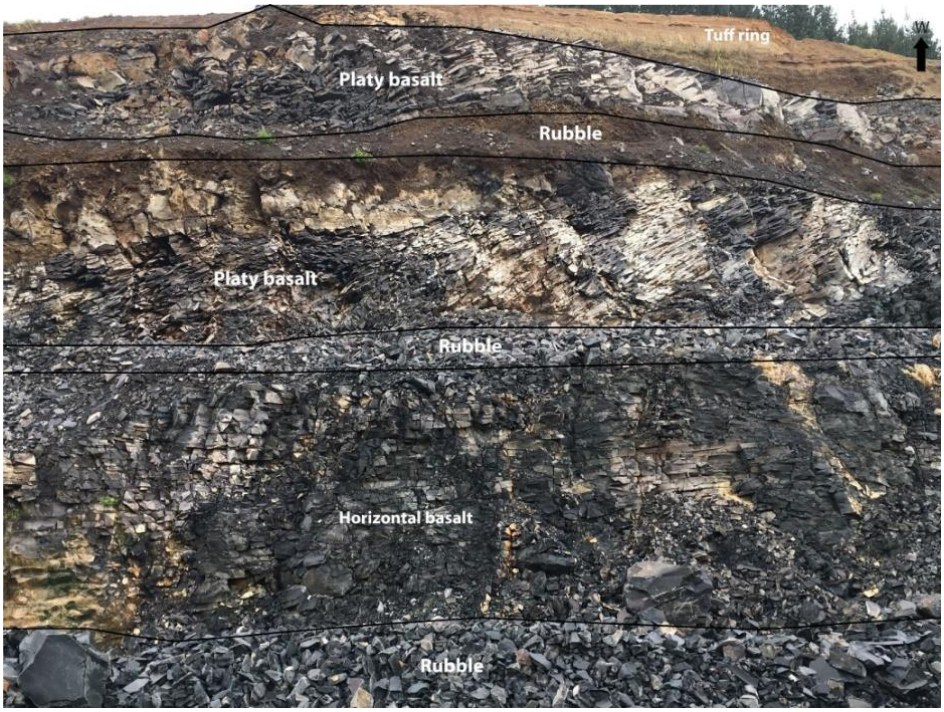

Figure 3.5: Photograph of the western side of the Auckland pit taken this study showing the variation in jointing patterns of the basalt.

Figure 3.6: Photograph of the eastern side of the Auckland pit taken this study showing the variation in jointing patterns of the basalt.

At the time of writing, Holcim recently exposed a sequence on the western side of the pit where they were removing overburden material. The exposed outcrop shows a dike intrusion that crosses through the middle of the pit and in this area it has reached the surface and released a small flow that has infilled a depression (Fig. 3.7).

Figure 3.7: Photograph of the western side of the Auckland pit revealing a dike intrusion that has reached the surface and released a small flow (courtesy of Keith Miller, Holcim, 2016).

3.4 Stratigraphy

A topographic map of the Auckland pit, showing the locations of drill cores logged in this study and cross-section lines is shown in figure 3.8. Multiple cross-section lines were created to cover enough stratigraphic logs (from drill cores) to show the different stratigraphic variation present within the pit. There are three basalt lava flows, scoria deposits, scoriaceous basalts and intercalated silt/clay sediments that have occurred throughout the Auckland pit. Stratigraphic logs have been grouped together on the cross-section line, to produce a visual representation and correlation of the geological units across the pit (Figs. 3.9, 3.10, 3.11). Drill core C321 was also logged (Fig. 3.8) however it does not occur on the cross-section line. Log C321 (Fig. 3.12) was included in this study because it clearly shows the three basalt lava flows and intercalated sediments on the southeast margin of the pit.

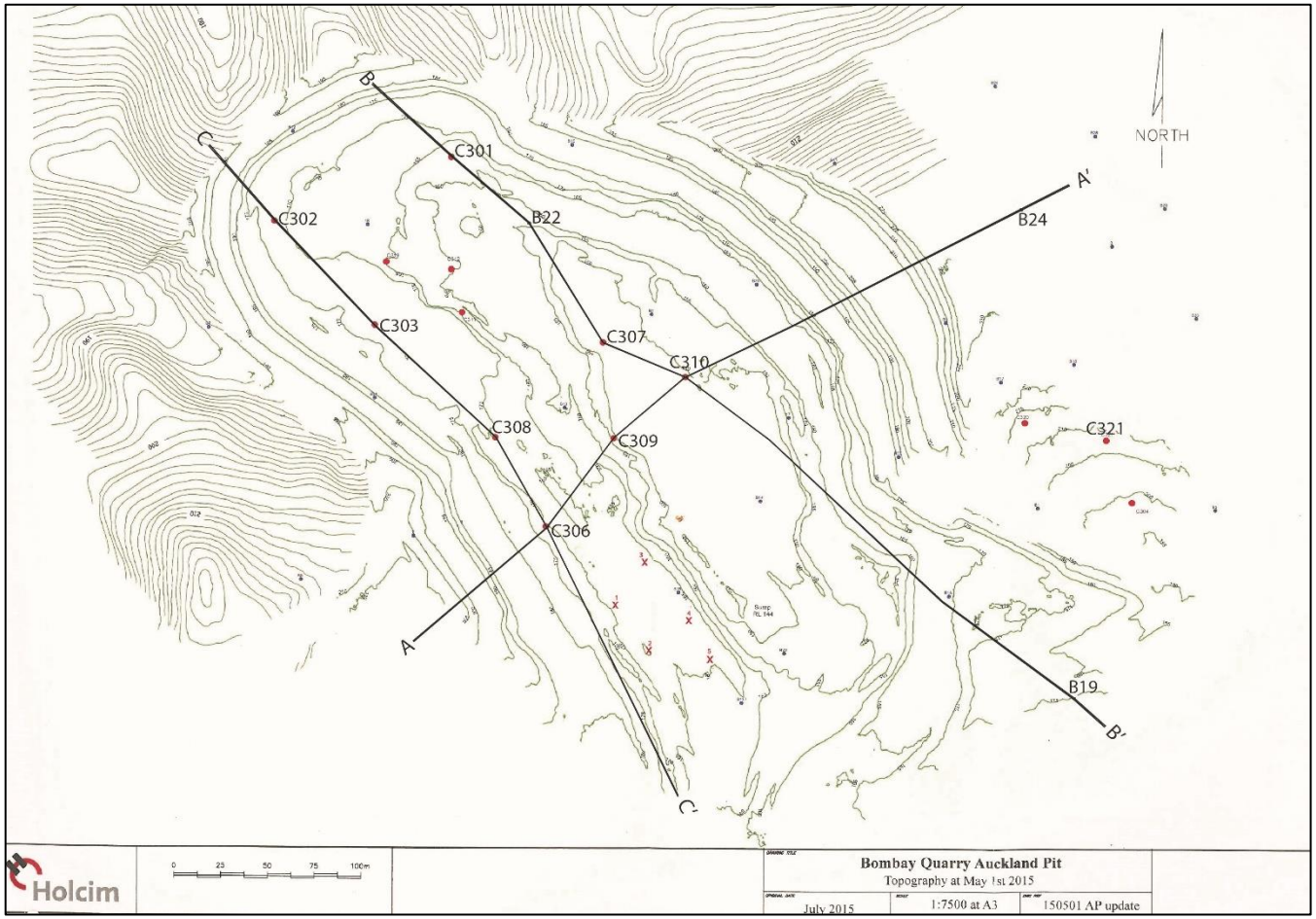

Figure 3.8: Map of the Auckland pit, Bombay Quarry, with drill core locations used in this study and cross-section lines (base map from Holcim unpublished data, 2015).

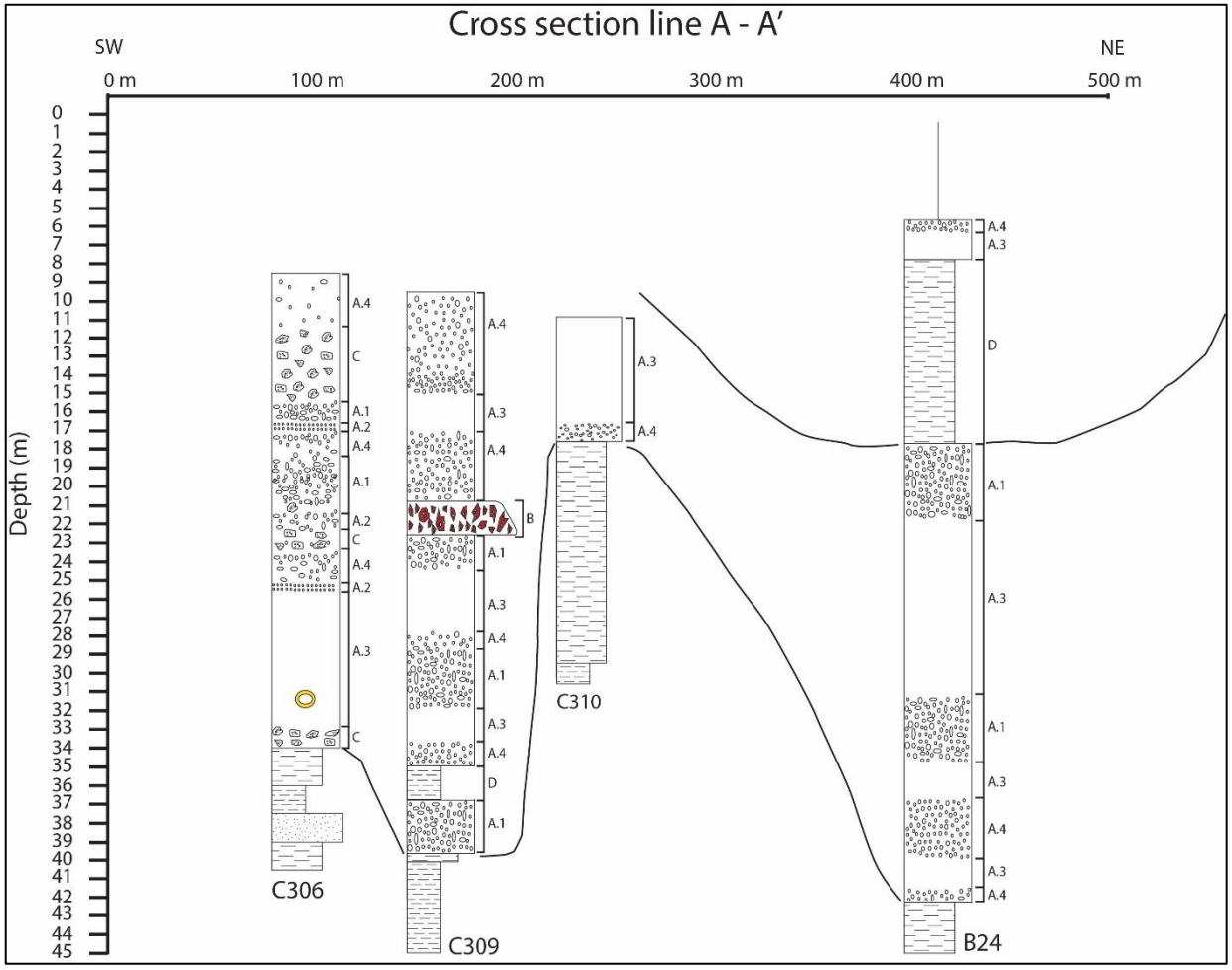

Figure 3.9: Cross-section line A - A' (see Fig. 3.8) with stratigraphic logs and facies A1-A4, B-D (see text for facies description).

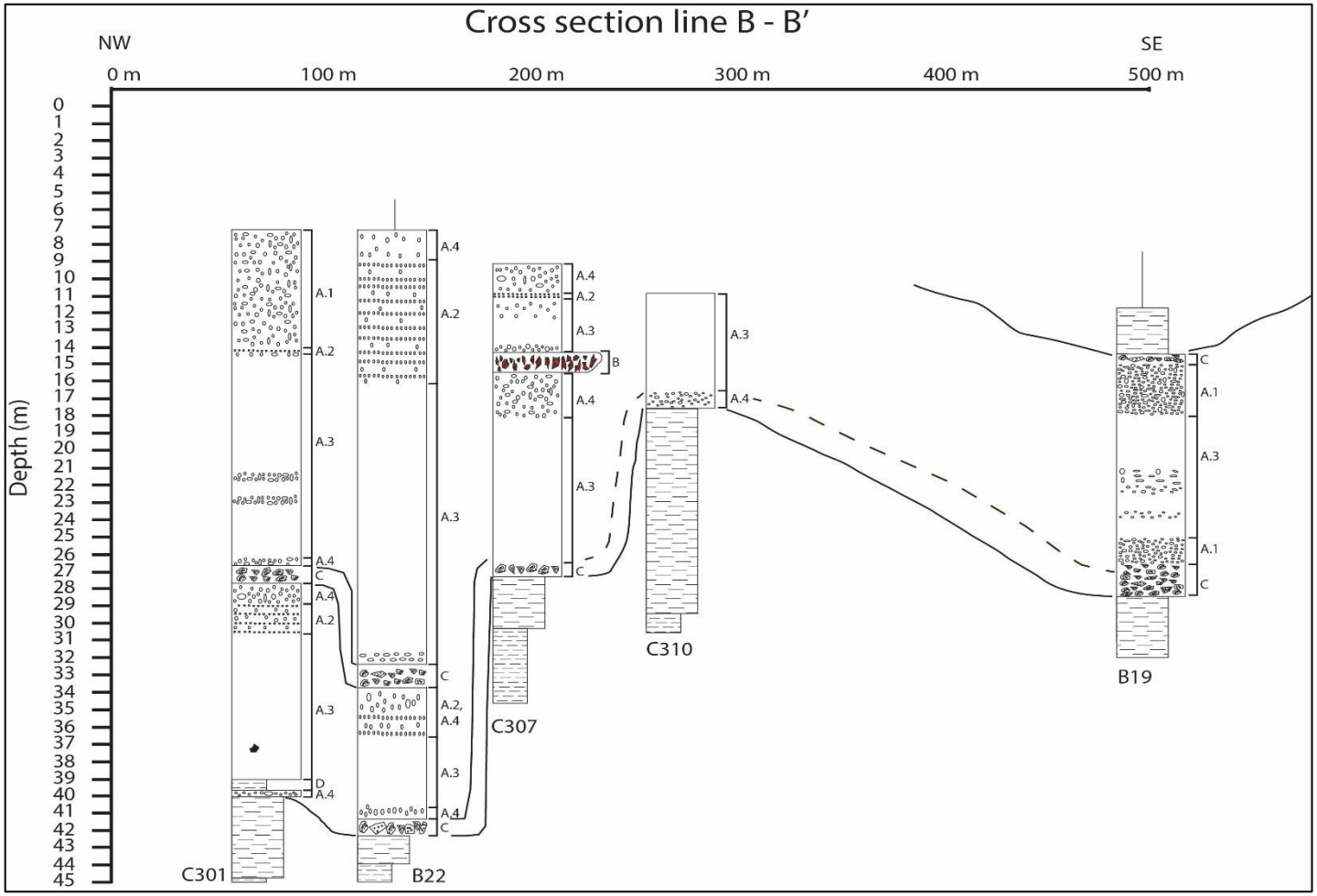

Figure 3.10: Cross-section line B- B' (see Fig. 3.8) with stratigraphic logs and facies A1-A4, B-D (see text for facies description).

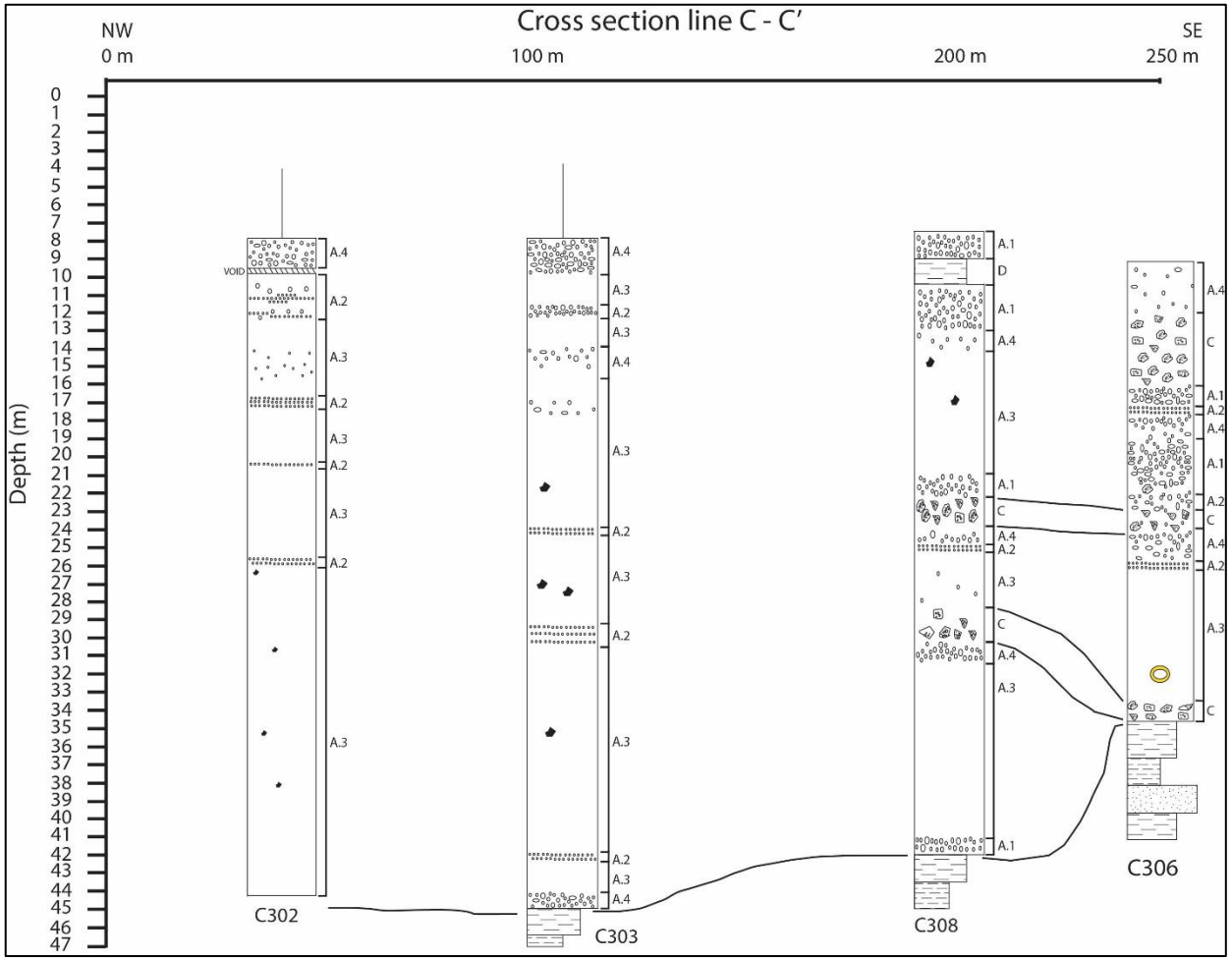

Figure 3.11: Cross-section line C - C' (see Fig. 3.8) with stratigraphic logs and facies A1-A4, B-D (see text for facies description).

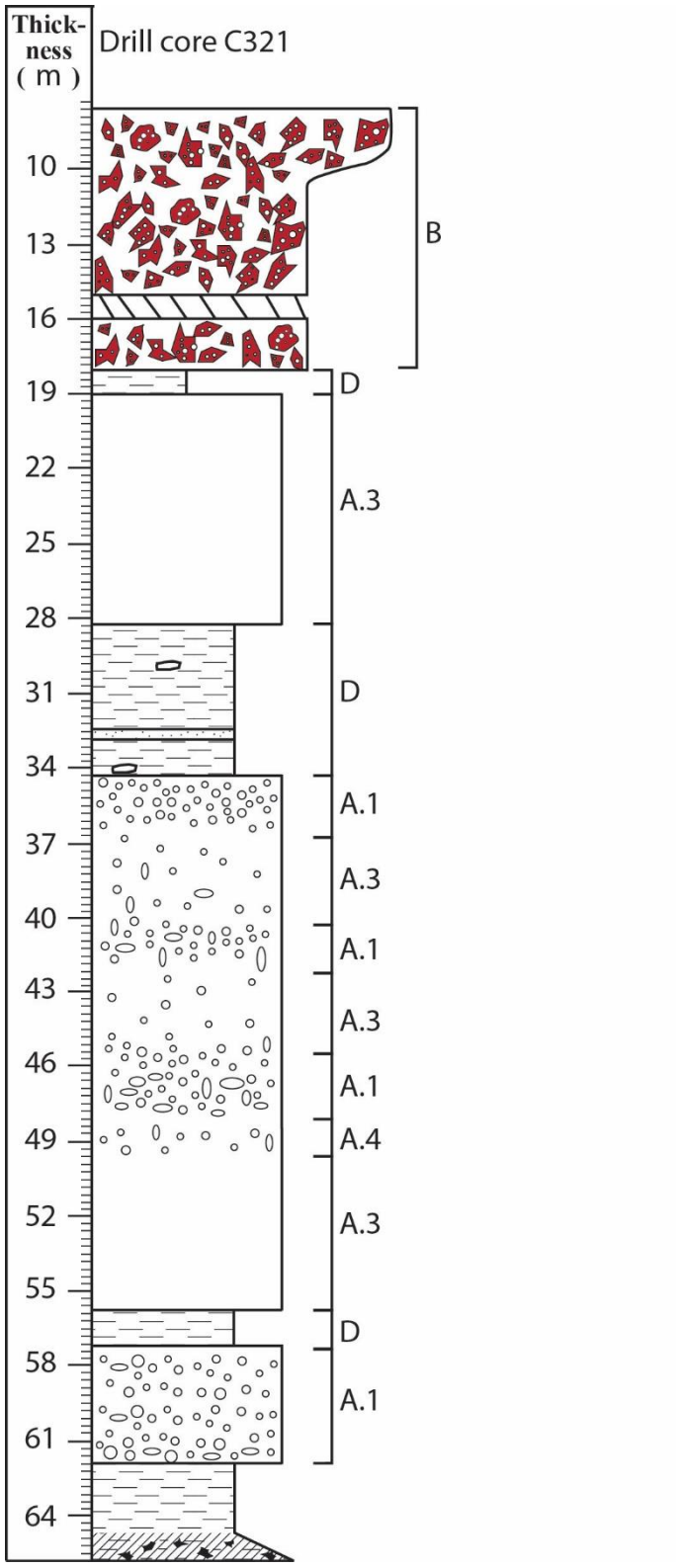

Figure 3.12: Drill core log C321 (see Fig. 3.8) showing the stratigraphy and facies A1-A4, B-D (see text for facies description).

Drill core data have identified the underlying contacts with the quarry basalt deposit to be Tauranga group in some places, and Waitemata Group in others (John O'Brien Associates et al., 1994). The Tauranga and Waitemata group deposits occur in all the drill core logs with varying minimum thicknesses from 2.2 m to 12.8 m (Figs. 3.9, 3.10, 3.11).

Overlying the country rock in logs C301, C309 and C321, there is a lower basalt lava flow that has a sharp lower contact and a thickness of 0.6 m to 4.4 m (Figs. 3.9, 3.10, 3.12). However the lower basalt lava flow does not occur anywhere else in the drill cores examined in this study.

In sharp contact with the lower basalt flow there is a overlying zone of intercalated silt and clay with thicknesses of 0.5 m to 1.7 m and only occurs in logs C301, C309 and C321 (Figs 3.9, 3.10, 3.12). There is not any intercalated silt/clay within the other logs at this stratigraphic level.

Up the sequence, there is a middle basalt lava flow that sharply overlies the intercalated silt/clay with a thickness of 6.7 m to 24.5 m in logs C301, C309 and C321. However, in the other logs the middle basalt lava flow overlies the sharp contact with older Tauranga and Waitemata groups (Figs. 3.9, 3.10, 3.11).

A scoria deposit that overlies the sharp contact with the middle basalt lava flow, with thicknesses of 1.1 m to 1.7 m, occurs in logs C307 and C309 (Figs. 3.9 and 3.10). In the other logs, however, there is a scoriaceous basalt that overlies the middle basalt lava flow (instead of a scoria deposit) with thicknesses of 1.3 m to 2 m (Fig. 3.10). In drill core C321, intercalated silt/clay overlies the sharp contact with the middle basalt lava flow with a thickness of 1 m (Fig 3.12).

At the top of the sequence in logs C307 and C309, the upper basalt lava flow overlies in sharp contact with the scoria deposit (or scoriaceous basalt in the other logs), with thicknesses of 2.10 m to 28.2 m. However, in logs B24 and C321, the upper basalt lava flow sharply overlies the intercalated silt/clay with a thickness of 6.2 m to 10.10 m (Figs. 3.9, 3.12).

In drill core log C321, which lies on the higher eastern side of the Auckland pit (Fig. 3.8), the upper basalt lava flow occurs at the top of the

sequence in all the drill core logs (Figs. 3.9, 3.10, 3.11). Overlying the upper basalt flow is the intercalated silt/clay, which has a thickness of 1 m. Overlying the silt/clay is a large scoria deposit of thickness 10.9 m (Fig. 3.12).

Due to the nature of the topography of the palaeovalley underlying the Auckland pit, there are stratigraphic volcanic variations throughout some of the logs. Cross-section line C - C' (Figs. 3.8, 3.11) which runs in a northwest to southeast direction along the pit, shows that there is a massive thick unit of the middle basalt lava flow with thicknesses of 25.50 m to 37.5 m, compared to the other drill core logs that show the different thickness variation of volcanic units (e.g. Intercalated sediments and scoria, scoriaceous deposits; Figs. 3.9, 3.10). Drill core log B19 and B24 also has a massive thick unit of the middle basalt flow with thicknesses of 14 m and 24.5 m, respectively (Figs. 3.9, 3.10).

Using observations from the stratigraphic logs, a geological map of the Auckland pit is shown in Fig. 3.13 with tuff ring and sedimentary deposit stripped off. Using the top stratigraphic unit of each of the drill cores, a visual representation of the underlying geology can be seen at the Auckland pit (Fig. 3.13). Within the Auckland pit the youngest basalt lava flow occurs near the top, whereas surrounding the valley on the higher ridges there is a tuff/ash layer deposit. Also to the north-east, there is a single scoria deposit further away from the tuff/ash layer. Within the younger basalt lava flow, there is a small scoriaceous basalt layer to the west of the pit. Tuff ring boundaries are visualised by photos surrounding the pit.

Southwest of the Auckland pit is the Waikato pit which is confined to a different palaeovalley to the Auckland pit. This has a similar stratigraphic sequence of the top layer (Fig. 3.13), showing the youngest basalt lava flow within the valley and a tuff/ash layer surrounding the basalt lava flow at higher elevation. The Waikato pit representation of the geology was created from unpublished drill core data provided by Holcim.

Figure 3.13: Map of the Auckland and Waikato pit showing the underlying geology after the removal of tuff rings and sediments. The Auckland pit is based on stratigraphic logs from this study, while the Waikato pit is based on the stratigraphic logs provided by Holcim (Image from Google Earth 2016).

3.5 Basalt Facies

The basalt lava flows are weathered at their bases and tops in some places. They are also broken in some places at the base, middle and top of each lava flow in many cases probably due to the drilling rig intercepting the jointing pattern of the basalt and causing it to break naturally. Furthermore, while retrieving the core the machine could have fragmented the basalt as it was removed for analysis. Otherwise, the basalt lava flows are fairly coherent; coherent basalt lava is represented by facies A. Pyroclastic and brecciated facies are represented by facies B and C, respectively.

Facies A

Facies A is a bluish-grey, finely porphyritic basalt with olivine and augite phenocrysts < 2 mm. Sub-facies are distinguished by the vesicularity, and by vesicle texture and arrangement.

A.1 is moderately vesicular (40 – 60 %) basalt containing both small vesicles up to 1 – 10 mm in diameter and large vesicles, up to 10 – 20 mm in diameter. Vesicles range from spherical to elongate in morphology (Fig. 3.14).

Figure 3.14: Moderately vesicular basalt in drill core.

A.2 is vesicular basalt in which vesicles are elongated and aligned along vesicle trails. Vesicle trails are 10 – 40 mm apart and have an overall thickness range of 0.1 – 9.5 m (Fig. 3.15).

Figure 3.15: Vesicular basalt with vesicle trails in drill core.

A.3 is non-vesicular basalt that has a high strength and is dense with few very small vesicles < 2 mm (Fig. 3.16). In some drill core logs, local vesicularity may vary up to 5 – 10 %, approaching A.4 facies.

Figure 3.16: Non-vesicular basalt in drill core.

A.4 is poorly vesicular (10 – 30 %) basalt containing both small vesicles up to 1 – 5 mm in diameter and large vesicles up to 10 – 20 mm in diameter. Vesicles range from spherical to elongate in morphology (Fig. 3.17). Within some drill core logs the local vesicularity varies up to 60 %, approaching A.1 facies.

Figure 3.17: Poorly vesicular basalt in drill core.

Facies B

Facies B is a reddish brown, very vesicular (60 – 80 %) lapilli to bomb/block scoria deposit. Lapilli and bomb/block sizes range from 5 – 120 mm (Fig. 3.18). Grain size analysis shows that in drill core C307 and C309, it is dominantly a very coarse to coarse lapilli deposit, while in C321 it is dominantly a block/bomb deposit with some coarse to medium lapilli as well (Fig. 3.19).

Figure 3.18: Scoria deposit in drill core showing different scoria clasts.

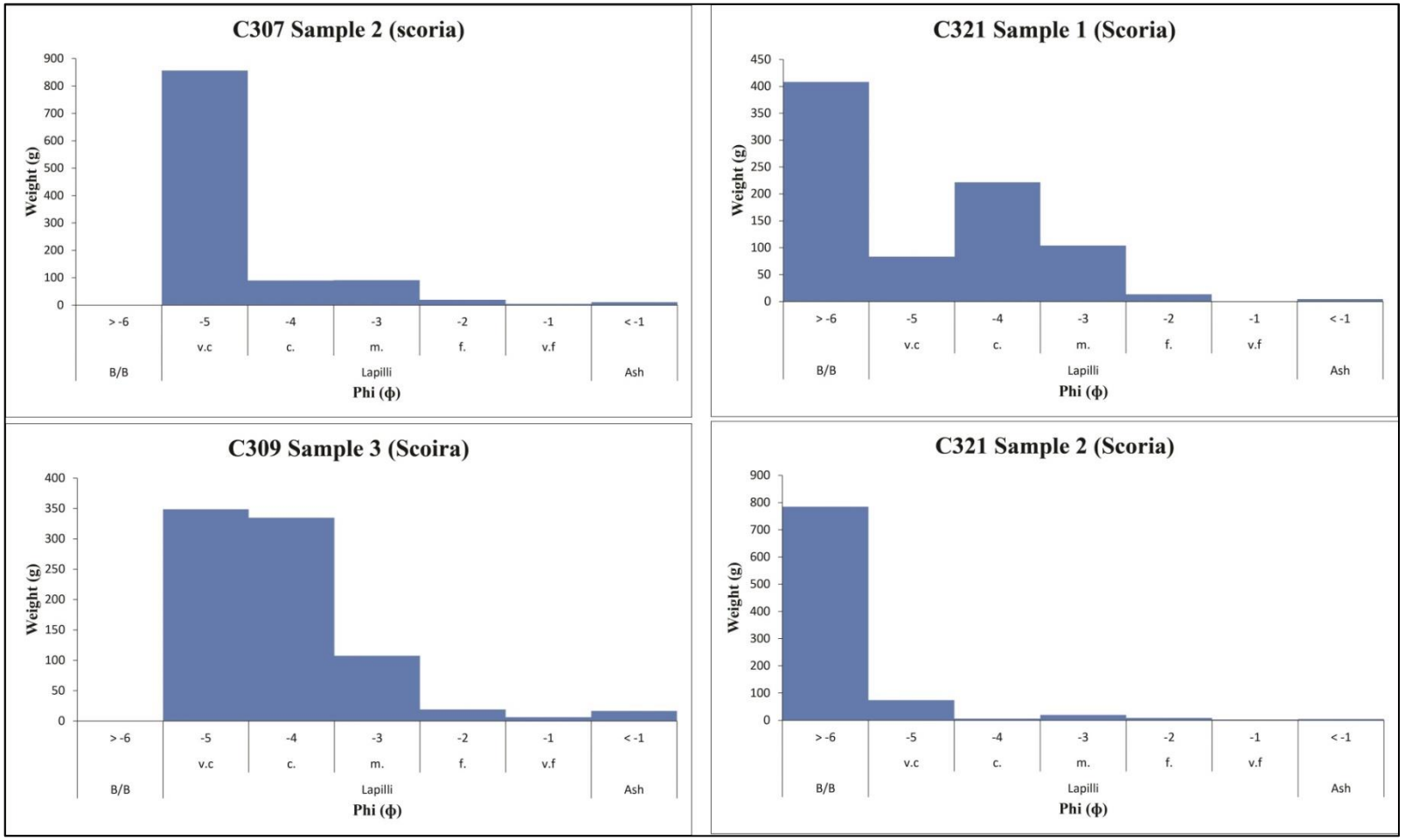

Figure 3.19: Grain size analysis for facies B in drill core logs C307, C309 and C321 (B/B is blocks/bombs).

Facies C

Facies C is a highly weathered, broken and moderately vesicular (40 – 60 %) scoriaceous basalt, with small spherical vesicles, 1 – 3 mm in diameter, and large vesicles, 10 – 20 mm in diameter (Fig. 3.20).

Figure 3.20: Scoriaceous basalt in drill core.

3.6 Intercalated Silts/Clay Sediments

In the Auckland pit there are intercalated sediments present between both the lower and middle, and middle and upper basalt lava flows, representing periods of time when there were no local basalt eruptions. Drill core logs C301, C309, C308 and B24 (Figs. 3.9 to 3.11) have one interval of deposited sediment material that occurred between basalt eruptions, whereas log C321 has two to three intervals of sediment deposition (Fig. 3.12).

Facies D

The entire succession of the intercalated sediments is classified as facies D.

Brown to dark brown fine-grained mud occurs lower in the stratigraphic sequence between the lower and middle basalt lava flow sequence in logs C301 and C309 with thicknesses of 0.5 m and 1.7 m (Figs. 3.9, 3.10, 3.21, 3.22).

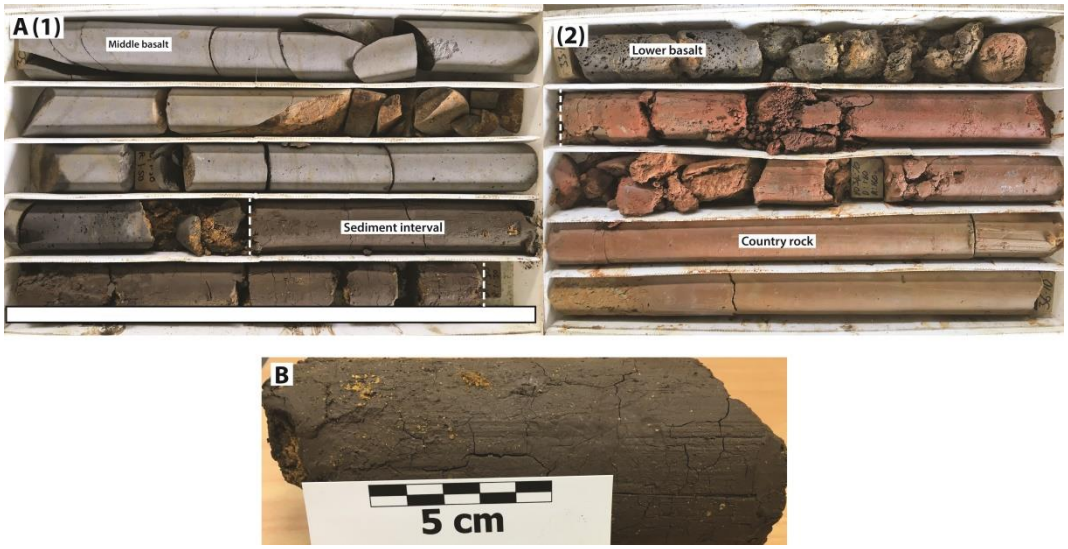

Figure 3.21: (A) Interval of drill core C301 (30.20 m top left of box 1 to 36.10 m bottom right of box 2) showing the sediment interval between sharp contacts of the lower and middle basalt flow. Scale bar is 0.64 m. (B) Close-up of the mud in log C301. (Dotted line represents contact zone).

Figure 3.22: (A) Interval of drill core C309 (24.80 m top left to 28.0 m bottom right) showing the sediment interval between sharp contacts of the lower and middle basalt flow. Scale bar is 0.64 m. (B) Close-up of the mud in log C309. (Dotted line represents contact zone).

There is also a light yellow-brown fine-grained silt that occurs between the middle and upper basalt lava flows in log B24 and C308 with thicknesses of 9.9 m and 1.5 m (Figs. 3.9, 3.11, 3.23, 3.24), respectively.

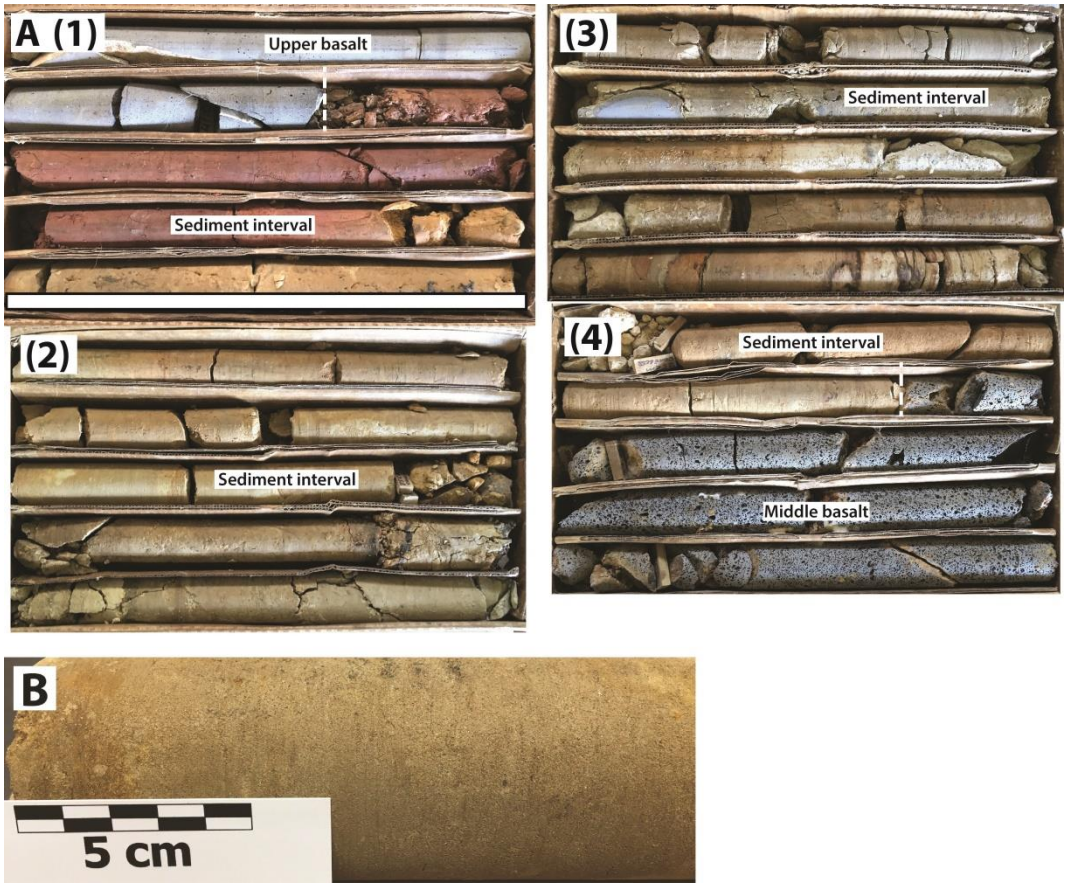

Figure 3.23: (A) Interval of drill core B24 (40.20 m top left of box 1 to 53.60 m bottom right of box 4) showing the sediment interval between the sharp contacts of the middle and upper basalt flow. Scale bar is 0.64 m. (B) Close-up of the fine-grained silt within the sediment interval of log B24. (Dotted line represents contact zone).

Figure 3.24: (A) Interval of drill core C308 (0 m top left to 4.40 m bottom right) showing the sediment interval between the sharp contacts of the middle and upper basalt flow. Scale bar 0.64 m. (B) Close-up of the fine-grained silt with mud texture in log C308. (Dotted line represents contact zone).

In drill core C321, however, there is a sequence of intercalated reddish-brown to pale yellow silt/clay with thickness of 6.2 m between the contacts of the middle and upper basalt flow, with an intercalated layer of fine grained yellowish rhyolitic distal tephra of thickness 0.2 m (Figs. 3.12, 3.25).

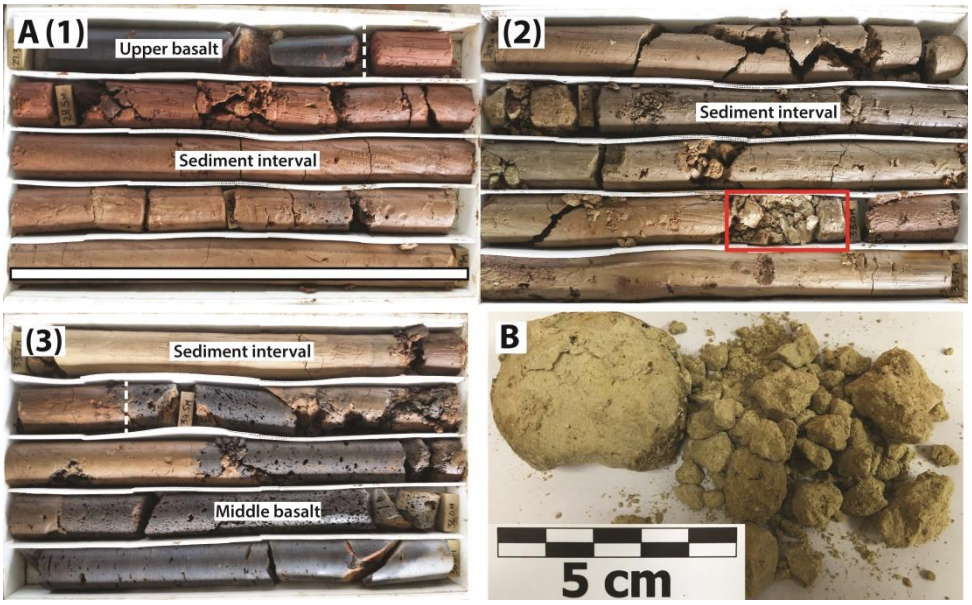

Figure 3.25: (A) Interval of drill core C321 (27.30 m top left of box 1 to 36.60 m bottom right of box 3) intercalated silts/clay deposited between the sharp contacts of the middle and upper basalt flow. Scale bar 0.65 m. Red box indicating the tephra layer. (B) Close-up of the tephra in log C321. (Dotted line represents contact zone).

3.7 Facies Architecture

The Auckland pit has a complex stratigraphic variation due to the different volcanic phases that have occurred over time. The basalt lava flows within the Auckland pit have characteristics of moderately vesicular (A.1), vesicle trail-rich (A.2), non-vesicular (A.3) and poorly vesicular (A.4) facies. It also has scoria (B) and scoriaceous basalt (C) facies present between the basalt lava flows. Generally the top and bottom of each basalt flow is vesicular (A.1 and A.4), while the centre is non-vesicular (A.3) with zones of vesicle trails (A.2) and gradational variations in vesicularity (A.1, A.4).

The lower basalt lava flow consists of facies A.1 and A.4 with a thickness of 0.6 m to 4.4 m. It only occurs in logs C301, C309 and C321 (Figs. 3.9, 3.10, 3.12).

The middle basalt lava flow comprises facies A.1 and A.4 at the top and bottom with thicknesses ranging from 0.7 m to 5.3 m. The centre comprises facies A.3 with thicknesses of 1.6 m to 17.8 m and there are also intercalated zones of facies A.2 with thicknesses of 0.10 m to 2.8 m. Gradational variations between facies A.1 and A.4 sometimes alternate with facies A.3 and range in thicknesses from 0.2 m to 3.6 m (Fig. 3.9, 3.10, 3.11). In some logs (C306, C307, B19 and C308) there is scoriaceous basalt (facies C) intercalated with facies A.3, with thicknesses of 0.5 m to 3.8 m (Fig. 3.9, 3.10, 3.11).

Cross-section line C – C’ has a massive thick unit of the middle basalt flow with zones of facies A.2, and gradational variations between facies A.1 and A.4. Along the cross-section line C - C’ from the north-west to south-east (see Fig. 3.8) the middle basalt lava flow increases in vesicularity and the concentration of facies A.3 increases with intercalated facies A.1, A.2, A.4 and facies C also occurring (Fig. 3.11).

The upper basalt lava flow comprises facies A.1 and A.4 at the top and bottom with thicknesses of 0.2 m to 6.8 m. The centre comprises facies A.3 with thicknesses of 1.5 m to 18 m and intercalated zones of facies A.2 with thicknesses

of 1 m to 7 m. There are gradational variations of facies A.1 and A.4 within the facies A.3, with thicknesses of 0.3 m to 1 m (Figs. 3.9, 3.10, 3.11).

The scoria deposit, which comprises entirely facies B, occurs between the middle and upper basalt lava flow with a thicknesses of 1.1 m and 1.7 m in logs C307 and C309 (Figs. 3.9, 3.10). However in log C321, facies B occurs above facies D with a thickness of 10.9 m (Fig. 3.12).

The scoriaceous basalt, which comprises entirely facies C, occurs between the middle and upper basalt lava flow with a thickness of 1.3 m and 2 m in logs C301 and B22 (Fig. 3.10), respectively. It also occurs at the bottom of the middle basalt lava flow with a thickness of 0.65 m to 2 m in logs B19, B22, C306 and C307 (Figs. 3.9, 3.10, 3.11).

Facies D, which entirely comprises silt/clay sediment, occurs between the lower and middle basalt lava flow with a thickness of 0.5 m to 1.7 m in logs C301, C309 and C321 (Figs. 3.9, 3.10, 3.12). Facies D also occurs between the middle and upper basalt lava flow with a thickness of 1.5 m to 9.9 m in logs B24, C308 and C321 (Figs. 3.9, 3.11, 3.12). In log C321 facies D overlies the upper basalt lava flow with a thickness of 1 m (Fig. 3.12).

The stratigraphic succession of the volcanic and intercalated sediments within the Auckland pit varies in unit thickness and facies architecture. The succession shows that deposition of sediment (volcanic quiescence) has occurred between intervals of the basalt lava flow emplacement, as well as small deposits of scoria and scoriaceous basalt.

Chapter Four

Petrography and Mineralogy

4.1 Introduction

This chapter describes the petrographic characteristics of the basalt lava flows and scoria deposit within the Auckland pit, identifying minerals and their compositions, component proportions, and textures. The results obtained will aid in identifying the differences and similarities between the lower, middle and upper basalt lava flows, which will then help understand the eruption and emplacement processes of each unit.

4.2 Methods

4.2.1 Thin Section Preparation

49 thin sections were made from core samples that were representative of the different stratigraphic units and facies identified in Chapter 3; 44 of basalt lava flows and 5 of scoria. The core samples were cut using a diamond saw to produce a block which would cover a glass slide, leaving margins of 1 - 2 mm. The side to be mounted to the glass was ground, using a diamond grinder, to ensure a flat surface. Once dry the rock surface was impregnated with Nuplex K36 two-part resin with a predetermined ratio of 2 g resin to 1 g of hardener. The sample was left to absorb this mixture and when absorption was complete the excess of this mixture was removed by scraping the surface with a wooden tongue depressor to avoid contamination with the exposed surface of the rock. These samples were then left to set overnight. The impregnated surface was then ground using a #600 polish powder on a frosted glass plate until the excess of the mixture was removed and the initial rock surface was again exposed, leaving only depressions infilled. Glass sides were frosted on one side using a diamond discoplan to ensure a flat

surface. The dried polished samples were mounted onto the frosted side of the glass slide with Hillquist thin section resin using a ratio of 2.3 g resin to 1 g hardener. Bubbles were removed by circulating the frosted slide along the surface. The samples were left to dry overnight. The mounted blocks were then cut to ~1 mm thickness using the Struers Discoplan-TS. The samples were then trimmed to ~30 μm thick through the same method. Cover slips were applied to seal the sample using a petropoxy 145 at a ratio of 5 ml resin to 0.5 ml hardener. The samples were then left to dry overnight.

4.2.2 Optical Microscopy

All thin sections were examined under the microscope. Thin sections were observed under a transmitted light petrographic microscope in both plane and cross polarised light to identify and describe the different mineral components and textures for basalt lavas and scoria.

Quantitative data on mineral and groundmass abundances were obtained by point counting on 24 thin sections that were selected based on their stratigraphic variations and overall representation of the Auckland pit. For each sample, the stage interval was set at 0.4 mm and 300 counts per slide were recorded to ensure a fair representation of the sample. All 24 thin sections of the basalt lava included counts of: phenocrysts (olivine, clinopyroxene), groundmass components, xenoliths and vesicles. Where there was uncertainty on the identity of a mineral within the groundmass, it was recorded as a ‘mafic mineral’. Raw point count data is included in Appendix III.

4.2.3 Polished Thin Section Preparation

Three polished thin sections were prepared for electron microprobe analysis. These thin sections followed the same initial steps as the samples with cover slips with cutting, grinding, impregnation, mounting to glass and the initial cut to remove the block from the glass. These samples were then ground back on the discoplan until the majority of plagioclase crystals were at a dark yellow – white interference colour under crossed polarised light. #500 grit paper was used

to grind the sample back further until the majority of crystals were at the right colouration. The thin section was then polished until there was a flat, reflective surface.

4.2.4 Electron Microprobe Analysis

Electron microprobe analysis (EMPA) was used to gain geochemical data on olivine, clinopyroxene and plagioclase within three polished thin sections one each of the lower, middle and upper basalt lava flows that were identified within the drill cores.

The JEOL-8230 Superprobe electron microprobe analyser at Victoria University of Wellington was used, with the assistance of Ian Schipper. The elemental composition of individual minerals was investigated in all samples. Each polished thin section was carbon-coated to ensure conductivity. Crystals were analysed with an electron gun accelerating voltage of 15 kV, current of 12 nA and a focus beam of diameter 1 µm. Standardisation used a set of previously analysed crystals. Raw data from the electron microprobe analysis is presented in Appendix IV.

4.3 Phenocrysts

The lower, middle and upper basalt lava flows within the Auckland pit, are all dense, hypocrystalline, fine-grained, porphyritic basalt comprised of olivine and clinopyroxene phenocrysts, plagioclase, opaque Fe-Ti oxides and mafic groundmass minerals, xenoliths and vesicles. The olivine and clinopyroxene phenocrysts are set in a heterogeneous, plagioclase lath-dominant, intergranular fine-grained, groundmass. There are also subtle heterogeneous variations of the phenocrysts and groundmass minerals across the lower, middle and upper basalt lava flow, which will be covered in this chapter. The basalt overall, is non-to very poorly vesicular; however, vesicle distribution is also heterogeneous throughout the basalt flow. This section, and the following sections 4.4 - 4.6 describe the petrographic characteristics of the basalt lavas. The scoria will be described independently in section 4.7.

4.3.1 Olivine

Olivine occurs as a predominant phenocryst typically euhedral to subhedral ranging from 0.5 mm to 3.5 mm long; there are also some phenocrysts that rarely range from 3.5 mm to 7.5 mm long. Some olivine phenocrysts are partially resorbed with embayments. Most olivine phenocrysts have thin brown-orange iddingsite margins; although some have unaltered rims (Fig. 4.1). Point count data reveal the range in the proportion of olivine phenocrysts within all three basalt lava flows to be 1.20 - 13.33 % of the bulk rock (Table 4.1).

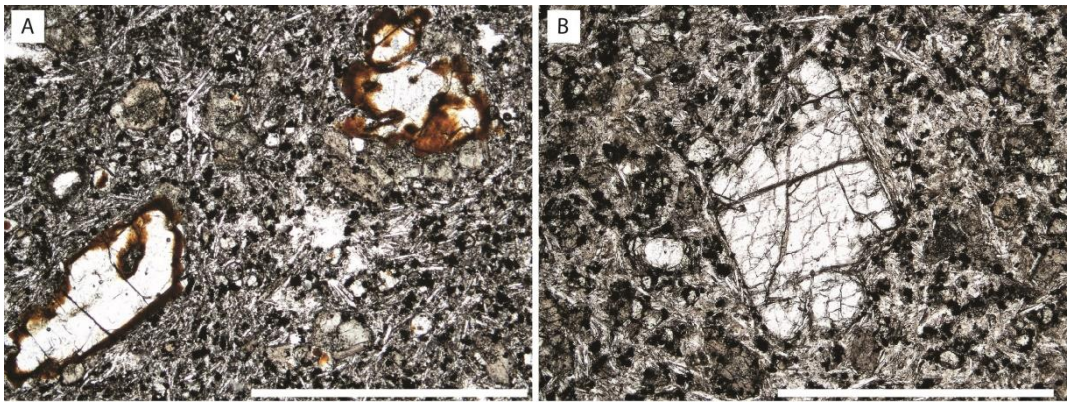

Figure 4.1: (A) Olivine phenocryst under plane polarised light (PPL) with altered iddingsite rims. Scale bar 2 mm. (B) Unaltered olivine phenocryst (PPL). Scale bar is 2 mm.

4.3.2 Clinopyroxene

Clinopyroxene which is characterised by a distinctive brownish – green colour, occurs as subhedral to anhedral phenocrysts typically 0.5 mm to 2.5 mm long. Microphenocrysts of clinopyroxene also occur and are anhedral and typically 0.1 mm to 0.5 mm long (Fig. 4.2). Point count data reveal that the range in the proportion of clinopyroxene phenocrysts and microphenocrysts within all three basalt lava flows to be 2.67 - 15.67 % of the bulk rock (Table 4.1).

Table 4.1: Component percentages from point count data (lighter blue = upper basalt; medium blue = middle basalt; dark blue = lower basalt).

	Log C301				Log C309			Log C306			Log B24	
Thin Section No.	**44**	**45**	**46**	**47**	**11**	**12**	**13**	**22**	**23**	**27**	**28**	**30**
Olivine (Phenocrysts) **%**	**3.33**	**3.00**	**5.00**	**5.00**	**13.00**	**5.33**	**13.33**	**2.67**	**3.67**	**1.20**	**10.67**	**5.00**
Clinopyroxene (Phenocrysts & Microphenocrysyts) **%**	**8.33**	**5.00**	**4.33**	**3.00**	**3.33**	**5.67**	**2.67**	**6.33**	**6.00**	**7.20**	**3.67**	**10.00**
Plagioclase (Groundmass) **%**	**16.67**	**39.00**	**60.33**	**10.00**	**5.33**	**46.33**	**7.00**	**21.33**	**10.67**	**40.80**	**14.67**	**32.33**
Opaques (Groundmass) **%**	**14.00**	**15.00**	**11.67**	**0.00**[1]	**19.67**	**15.00**	**19.67**	**21.67**	**16.00**	**19.20**	**16.33**	**15.34**
Mafic Minerals (Groundmass) **%**	**37.67**	**35.67**	**17.33**	**46.67**	**50.67**	**27.67**	**55.33**	**47.67**	**56.00**	**30.80**	**38.00**	**37.33**
Vesicles **%**	**20.00**	**2.33**	**1.34**	**35.33**	**8.00**	**0.00**	**2.00**	**0.33**	**7.66**	**0.00**	**12.66**	**0.00**
Lithic **%**	**0.00**	**0.00**	**0.00**	**0.00**	**0.00**	**0.00**	**0.00**	**0.00**	**0.00**	**0.80**	**4.00**	**0.00**
Total %	**100.00**	**100.00**	**100.00**	**100.00**	**100.00**	**100.00**	**100.00**	**100.00**	**100.00**	**100.00**	**100.00**	**100.00**

[1] Dark groundmass, opaques not distinguishable

Table 4.1: (continued).

	Log B22		Log C303	Log C307		Log C302			Log C308		Log C310	Log B19
Thin Section No.	**33**	**35**	**1**	**41**	**42**	**3**	**5**	**6**	**7**	**25**	**20**	**37**
Olivine (Phenocrysts) **%**	**2.67**	**3.67**	**3.67**	**4.33**	**2.34**	**4.33**	**2.67**	**2.33**	**4.67**	**6.33**	**5.00**	**3.33**
Clinopyroxene (Phenocrysts & Microphenocrysyts) **%**	**15.67**	**6.67**	**10.33**	**5.00**	**3.33**	**2.67**	**8.67**	**5.33**	**4.00**	**7.67**	**5.67**	**11.67**
Plagioclase (Groundmass) **%**	**47.00**	**39.67**	**44.67**	**22.67**	**33.00**	**12.00**	**36.00**	**54.67**	**8.00**	**9.67**	**21.00**	**33.33**
Opaques (Groundmass) **%**	**13.66**	**17.33**	**16.67**	**22.00**	**18.33**	**15.00**	**18.67**	**17.67**	**14.33**	**18.67**	**26.33**	**19.00**
Mafic Minerals (Groundmass) **%**	**21.00**	**32.66**	**23.66**	**33.67**	**43.00**	**45.00**	**16.33**	**18.33**	**48.67**	**47.66**	**42.00**	**27.00**
Vesicles **%**	**0.00**	**0.00**	**1.00**	**12.33**	**0.00**	**21.00**	**17.66**	**1.00**	**20.33**	**10.00**	**0.00**	**5.67**
Lithic **%**	**0.00**	**0.00**	**0.00**	**0.00**	**0.00**	**0.00**	**0.00**	**0.67**	**0.00**	**0.00**	**0.00**	**0.00**
Total %	**100.00**	**100.00**	**100.00**	**100.00**	**100.00**	**100.00**	**100.00**	**100.00**	**100.00**	**100.00**	**100.00**	**100.00**

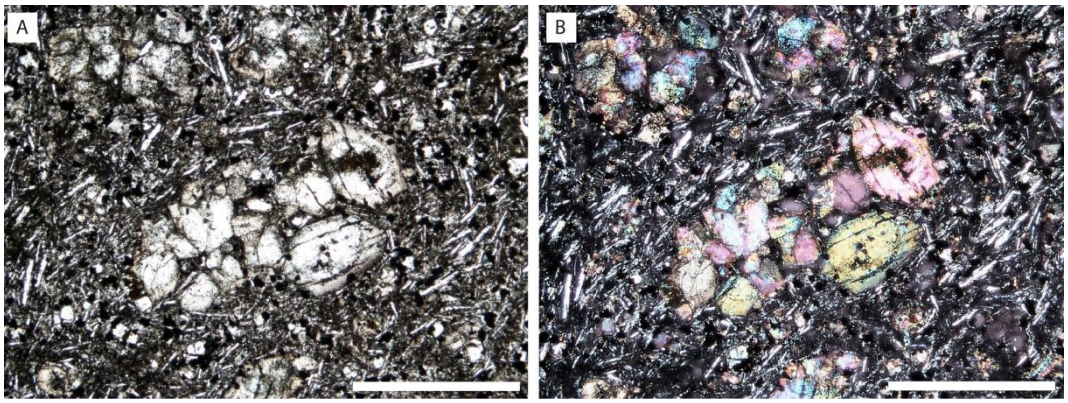

Figure 4.2: (A) PPL, and (B) XPL pair of photomicrographs showing a clinopyroxene phenocryst in the centre, and microphenocrysts in the top left. Scale bar 2 mm. Birefringence colours in photograph vary from actual birefringence colours observed.

4.4 Groundmass

Crystalline groundmass within the lower, middle and upper basalt lava flow is heterogeneous, fine grained and intergranular, comprised of thin plagioclase laths, mafic minerals (Mg-Fe silicates) and granular opaques. Plagioclase is the dominant mineral that occurs within the groundmass in all three basalt lavas, with variations in abundance and size. There are also subtle heterogeneous variations of the groundmass throughout the lower, middle and upper basalt lava flows.

4.4.1 Plagioclase

Plagioclase is characterised by white-yellowish laths, typically 0.05 mm to 0.5 mm long, however, some plagioclase laths can be up to 0.6 to 1.25 mm long (Fig. 4.3). Within thin sections where plagioclase crystals are large enough, polysynthetic crystal twinning can be observed, occurring in all three basalt lava flows. Point count data reveal that the range of plagioclase proportions across the three basalt lava flows is 7.00 - 60.33 % of the bulk rock (Table 4.1).

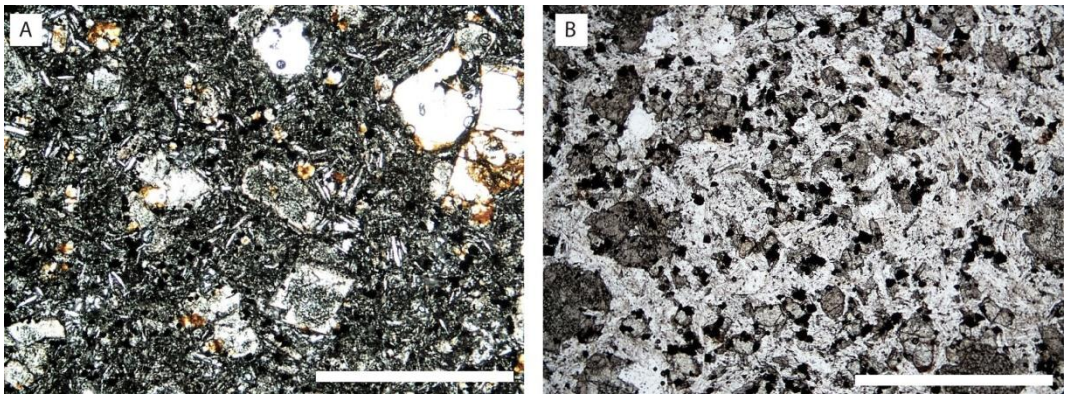

Figure 4.3: (A) Plagioclase laths, opaques and mafic minerals within the fine grained groundmass (PPL). Scale bar 2 mm. (B) Plagioclase-dominant groundmass with opaques and mafic minerals (PPL). Scale bar 2 mm.

4.4.2 Opaques

Opaques (presumed to be titanomagnetite) are characterised by black cubic-shaped grains sometimes irregular, and typically with an average size of 0.01 mm; distinctive coarser-grained titanomagnetite (0.05 mm - 0.1 mm) also occurs (Fig. 4.3). Point count data reveal that the range in the proportion of opaques within the three basalt lava flows is from 13.66 - 26.33 % of the bulk rock (Table 4.1).

4.4.3 Mafic Minerals

Mafic minerals, which are small olivine and clinopyroxene minerals, occur within the groundmass and are difficult to distinguish due to their small grain size. However mafic minerals within the basalt lava flows are generally anhedral and typically 0.02 mm to 0.1 mm in size (Fig. 4.3). Point count data reveal that the range in the proportion of mafic minerals within the three basalt lava flows is from 16.33 - 56.00 % of the bulk rock (Table 4.1).

4.5 Vesicles

Basalt lava flows are generally vesicular, and can vary in vesicularity throughout the stratigraphic succession. In thin section, the vesicles tend to range in shape from round to elongate to irregular; and typically in size from 0.05 to 7.5 mm. Some thin sections show a bimodal vesicle size; large, irregular vesicles formed by vesicle coalescene, and also smaller round vesicles (Fig. 4.4). Point count data reveal that the range in the proportion of vesicles within the three basalt lava flows is 0.00 - 35.33 % of the bulk rock (Table 4.1), although these percentages should be treated as semi-quantitative because of the statistical error associated with counting large objects (i.e. vesicles) over a small area (i.e. thin section area).

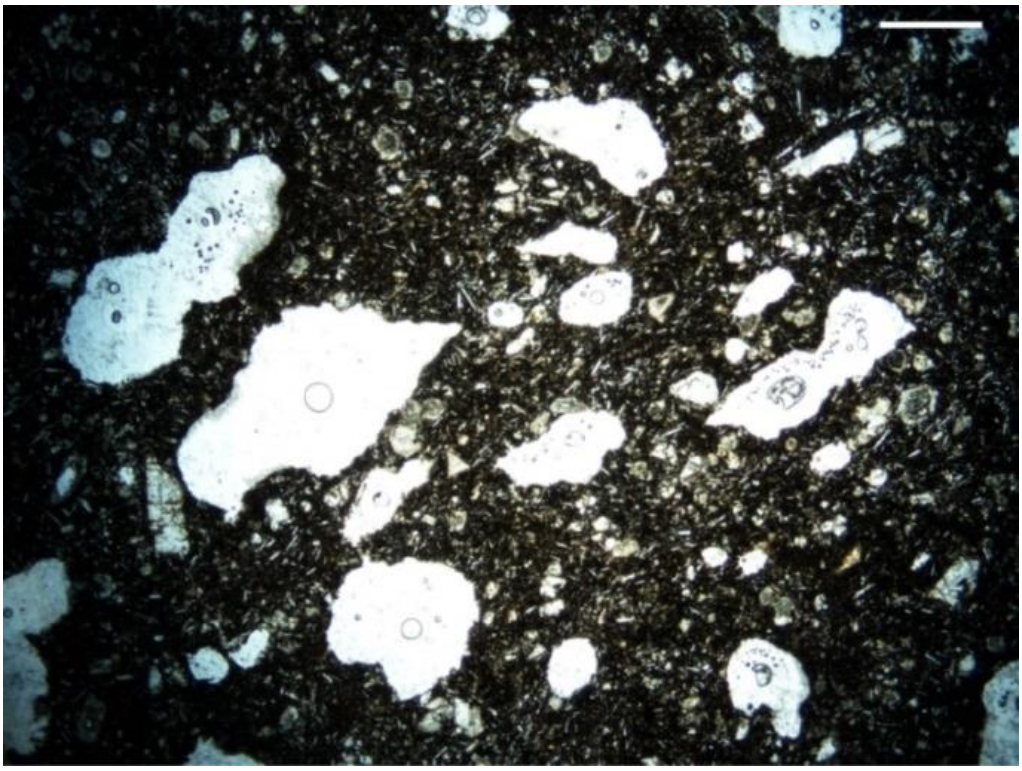

Figure 4.4: Representative vesicle texture of the basalt lava flows, showing the difference in shape and sizes of the vesicles. Scale bar 1 mm.

4.6 Xenoliths

The SAVF lavas often contain xenoliths that may be completely exotic material (country rock ripped off conduit walls) or restite material from mantle source region (Cook, 2002). Xenoliths observed within thin sections in this study are quartzose xenoliths, which are equigranular and have an internal grain size typically of 0.1 mm to 0.2 mm (Fig. 4.5). Some xenoliths exhibit a fine grained radial crystal growth around their rims (Fig. 4.5). Point count data reveal that the range in the proportion of xenoliths within the three basalt lava flows are 0.00 % - 4.00 % of the bulk rock, although the higher end of this range may have an inherent statistical error associated with counting large objects (i.e. xenoliths) over a small area (i.e. thin section area) (Table 4.1).

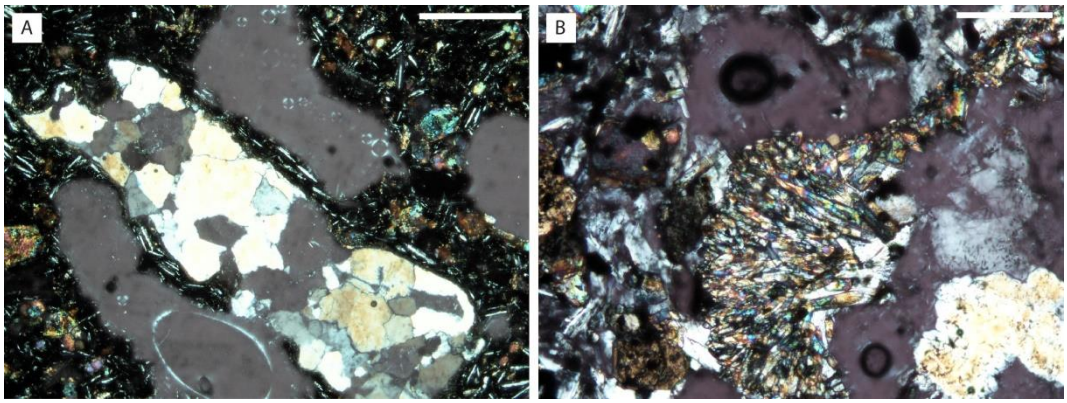

Figure 4.5: (A) Equigranular quartzose lithic present within basalt (XPL). Scale bar 2 mm. (B) Growth of small needle-like crystals around the rim of the lithic (XPL). Scale bar 1 mm. Grey patches are the glue residue from the cover slips. Birefringence colours in photograph vary from actual birefringence colours observed.

4.7 Scoria Petrography

Olivine phenocrysts in the scoria deposit have relatively thicker iddingsite alteration rims and are subhedral, typically 0.25 to 2.5 mm in size. Clinopyroxene microphenocrysts, which are subhedral, are typically 0.1 to 0.2 mm in size. The groundmass in the scoria deposit, ranges from predominantly crystalline (Fig. 4.6A) to opaque and glassy (Fig. 4.6B). Small plagioclase laths were observed typically 0.05 to 0.2 mm long. Some opaques were distinguishable within the

groundmass, typically cubic and an average size of 0.01 mm. Vesicles are round to elongate to irregular in shape and many are also interconnected; their size ranges from 0.25 to 0.5 mm (Fig. 4.6C). A xenolith was also present with an equigranular crystalline texture with an internal grain size typically 0.25 to 0.5 mm.

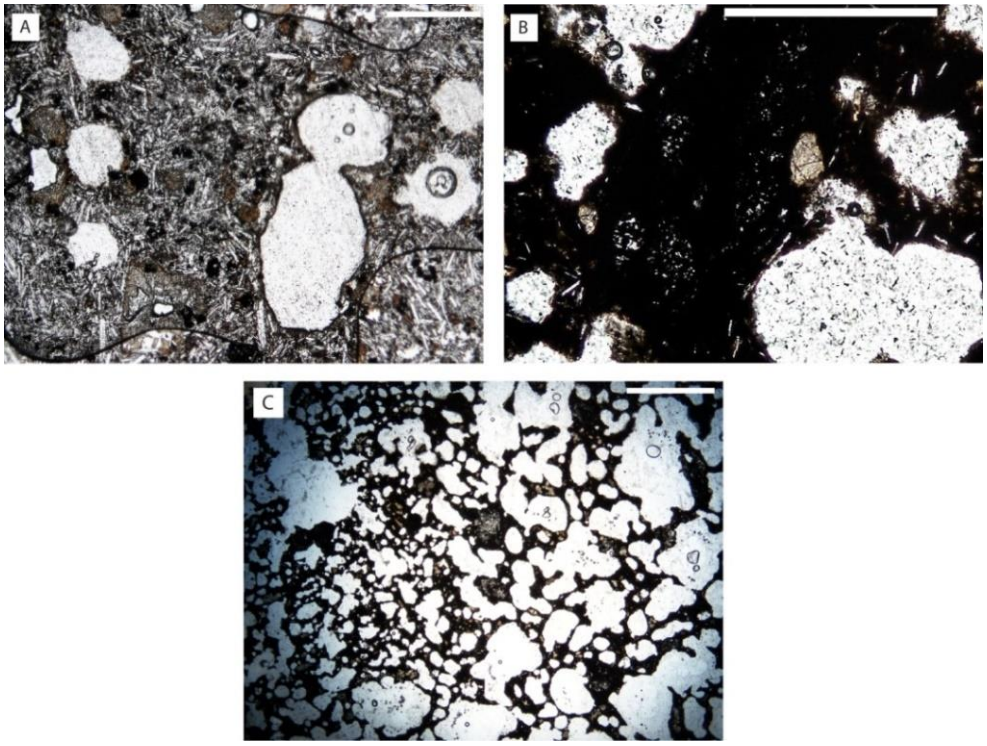

Figure 4.6: (A) Scoria groundmass containing plagioclase laths, opaques, mafic minerals and vesicles (PPL). Scale bar 2 mm. (B) Dark glassy groundmass (XPL) with small plagioclase laths and vesicles. Scale bar 2 mm. (C) Vesicular scoria (XPL). Scale bar 1 mm. Birefringence colours in photograph vary from actual birefringence colours observed.

4.8 Mineral Composition

The main crystals occurring within the basalt lava flows at the Auckland pit are olivine and clinopyroxene as phenocrysts and plagioclase in groundmass. Microprobe analysis of these minerals from the three basalt lava flows, show their variations in elemental composition. The complete dataset of microprobe analyses for olivine, clinopyroxene and plagioclase is presented in appendix IV. Representative analyses for the minerals in the lower, middle and upper basalt lavas are presented here.

4.8.1 Olivine

Representative microprobe analyses of olivine from the three basalt lava flows are shown in Table 4.2.

Table 4.2: Representative element compositions (wt. %) of olivine phenocrysts by EMPA.

Sample:	11 (upper basalt)		12 (middle basalt)		13 (lower basalt)	
No.	**6**	**38**	**44**	**70**	**95**	**105**
SiO_2	39.034	39.835	37.004	37.56	39.478	39.127
TiO_2	0.022	-	0.013	0.008	0.021	0.025
Al_2O_3	0.059	0.124	0.023	0.041	0.082	0.058
Cr_2O_3	0.036	0.045	-	-	0.015	0.026
NiO	0.17	0.209	0.106	-	0.129	0.165
FeO	18.239	14.037	29.386	25.846	14.575	17.092
MnO	0.287	0.172	0.479	0.34	0.16	0.189
MgO	42.973	46.949	33.524	36.855	45.815	44.274
CaO	0.22	0.159	0.246	0.163	0.153	0.151
Na_2O	0.004	0.018	0.031	-	0.012	0.008
Total	**101.044**	**101.548**	**100.812**	**100.813**	**100.44**	**101.115**
Fa %	19.24	14.37	32.97	28.24	15.15	17.81
Fo %	80.76	85.63	67.03	71.76	84.85	82.19

Overall compositions of olivine ranged from Fo_{85} to Fo_{63} (Fig. 4.7). Olivine phenocryst compositions are in agreement with those determined by Cook (2002) and Cook *et al.*, (2005) who plotted olivine compositions with Fo values ranging from 91.8 – 59.6.

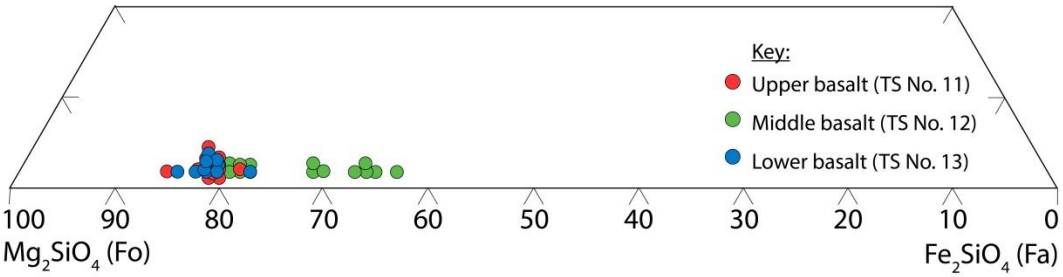

Figure 4.7: Olivine compositions between magnesium-rich (Mg) forsterite and iron-rich (Fe) fayalite. Compositions are in mol. %. (TS = thin section). Data points are spread vertically for ease of visualisation only.

4.8.2 Clinopyroxene

Representative microprobe analyses of clinopyroxene from the three basalt lava flows are shown in Table 4.3.

Table 4.3: Representative element compositions (wt. %) of clinopyroxene phenocrysts by EMPA.

Sample:	11 (upper basalt)		12 (middle basalt)		13 (lower basalt)	
No.	**5**	**37**	**45**	**69**	**79**	**102**
SiO_2	41.381	45.218	50.177	49.851	41.477	42.39
TiO_2	5.159	3.297	1.246	0.913	5.422	4.649
Al_2O_3	10.846	7.77	3.897	6.056	11.156	9.933
Cr_2O_3	0.018	0.084	0.308	0.978	0.008	0.004
NiO	0.012	-	0.022	0.001	-	-
FeO	8.914	7.824	8.401	7.032	9.339	9.285
MnO	0.103	0.085	0.156	0.157	0.122	0.112
MgO	10.535	12.245	14.608	15.616	10.056	10.546
CaO	22.815	23.146	21.207	18.924	22.824	22.806
Na_2O	0.46	0.427	0.496	0.763	0.53	0.439
Total	**100.243**	**100.096**	**100.518**	**100.291**	**100.934**	**100.164**
Wo %	51.36	50.01	44.11	41.02	51.76	51.00
Fs %	15.66	13.19	13.64	11.90	16.53	16.21
En %	32.98	36.80	42.26	47.08	31.72	32.80

Overall compositions ranged from $Wo_{51.76\text{-}41.02}$ $En_{47.08\text{-}31.72}$ $Fs_{17.10\text{-}11.69}$ respectively (Fig. 4.8) which plot predominantly in the diopside field of the Wo-En-Fs ternary diagram. However, some compositions exceed the diopside field with higher Wo content, and some others occur within the augite field. Clinopyroxene phenocryst compositions are in agreement with those determined by Cook (2002) and Cook *et al.,* (2005) who plotted clinopyroxene compositions with $Wo_{53.0\text{-}44.8}$ - $En_{45.9\text{-}25.7}$ - $Fs_{29.5\text{-}9.9}$ that also occur within the diopside field.

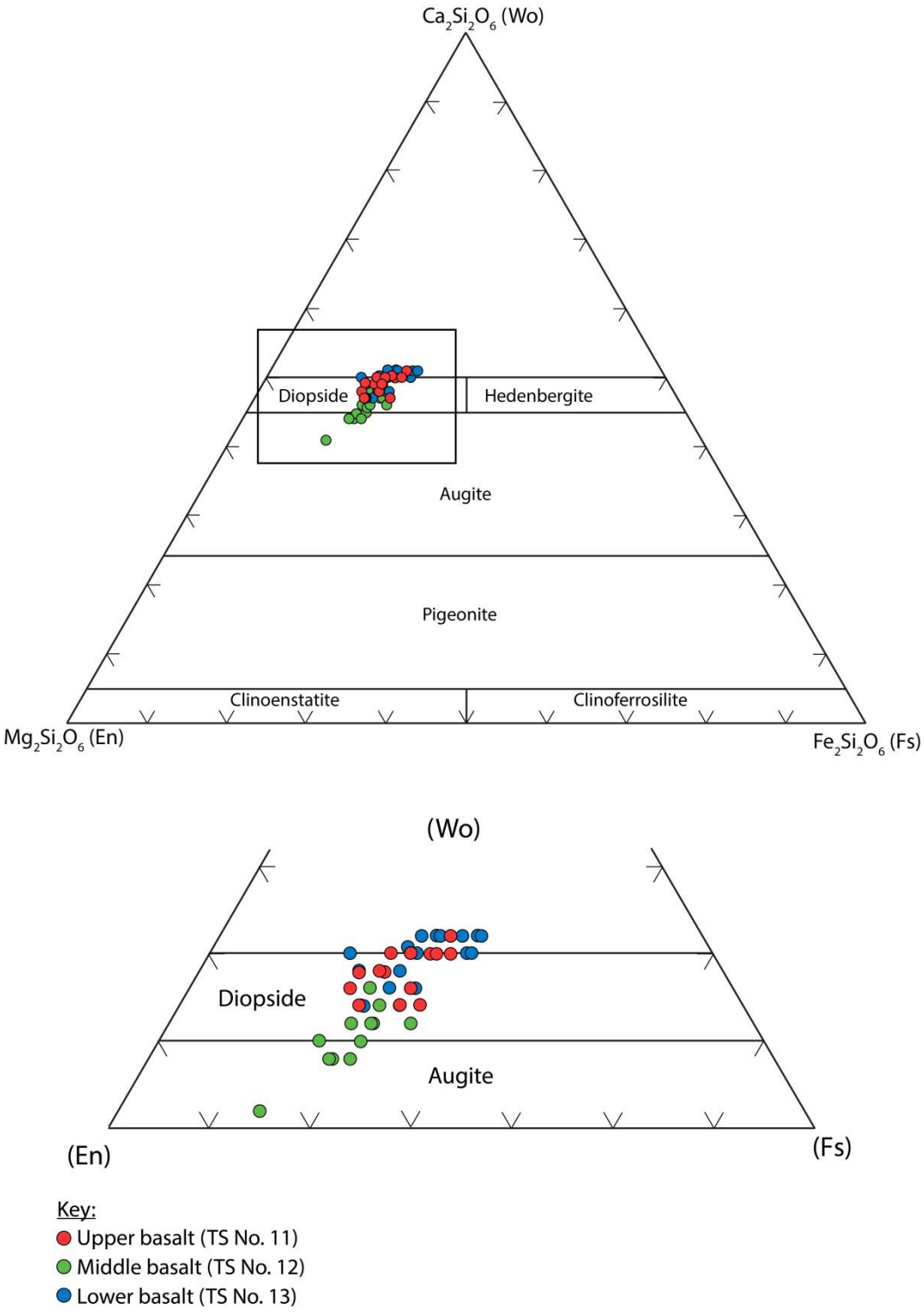

Figure 4.8: Wollastonite - enstatite - ferrosilite ternary diagram for pyroxene crystals found in basalt lava flows. Compositions are in mol. %. Box shape shows enlarged composition field. (TS = thin section).

4.8.3 Plagioclase

Plagioclase is an abundant groundmass phase. Representative microprobe analyses of plagioclase from the three basalt lava flows are shown in Table 4.4.

Table 4.4: Representative element compositions (wt. %) of plagioclase crystals by EMPA.

Sample:	11 (upper basalt)		12 (middle basalt)		13 (lower basalt)	
No.	**4**	**21**	**36**	**42**	**58**	**65**
SiO_2	53.758	51.789	55.265	54.680	51.868	52.605
TiO_2	0.095	0.110	0.083	0.081	0.097	0.083
Al_2O_3	29.538	30.963	27.982	28.931	30.540	30.166
FeO	0.565	0.717	0.557	0.549	1.052	0.802
MnO	-	-	0.009	0.005	-	0.015
MgO	0.051	0.093	0.013	0.034	0.053	0.061
CaO	11.430	13.021	9.755	10.663	12.801	12.020
Na_2O	4.445	3.476	5.459	4.845	4.000	4.360
K_2O	0.479	0.295	0.342	0.339	0.254	0.334
Total	**100.361**	**100.464**	**99.465**	**100.127**	**100.665**	**100.446**
An %	57.02	66.22	48.68	53.76	62.93	59.19
Ab %	40.13	31.99	49.29	44.21	35.59	38.85
Or %	2.85	1.79	2.03	2.03	1.49	1.96

Overall compositions ranged from $Ab_{51.14\text{-}31.99}$ $An_{66.22\text{-}46.83}$ $Or_{4.04\text{-}1.41}$ respectively (Fig. 4.9) which plot predominantly in the range from labradorite to low-Na andesine on the Ab-An-Or ternary diagram. Plagioclase crystal compositions are in agreement with those determined by Cook (2002) and Cook *et al.*, (2005) who plotted plagioclase compositions of $An_{69.6\text{-}40.6}$ in group A basalts and $An_{69.6\text{-}37.8}$ in group B basalts. Group A basalts have plagioclase phenocrysts, while group B basalts do not have plagioclase phenocrysts, but have a dominant plagioclase groundmass. From this study, plagioclase only occurs in the groundmass which is consistent with these basalts being of group B type.

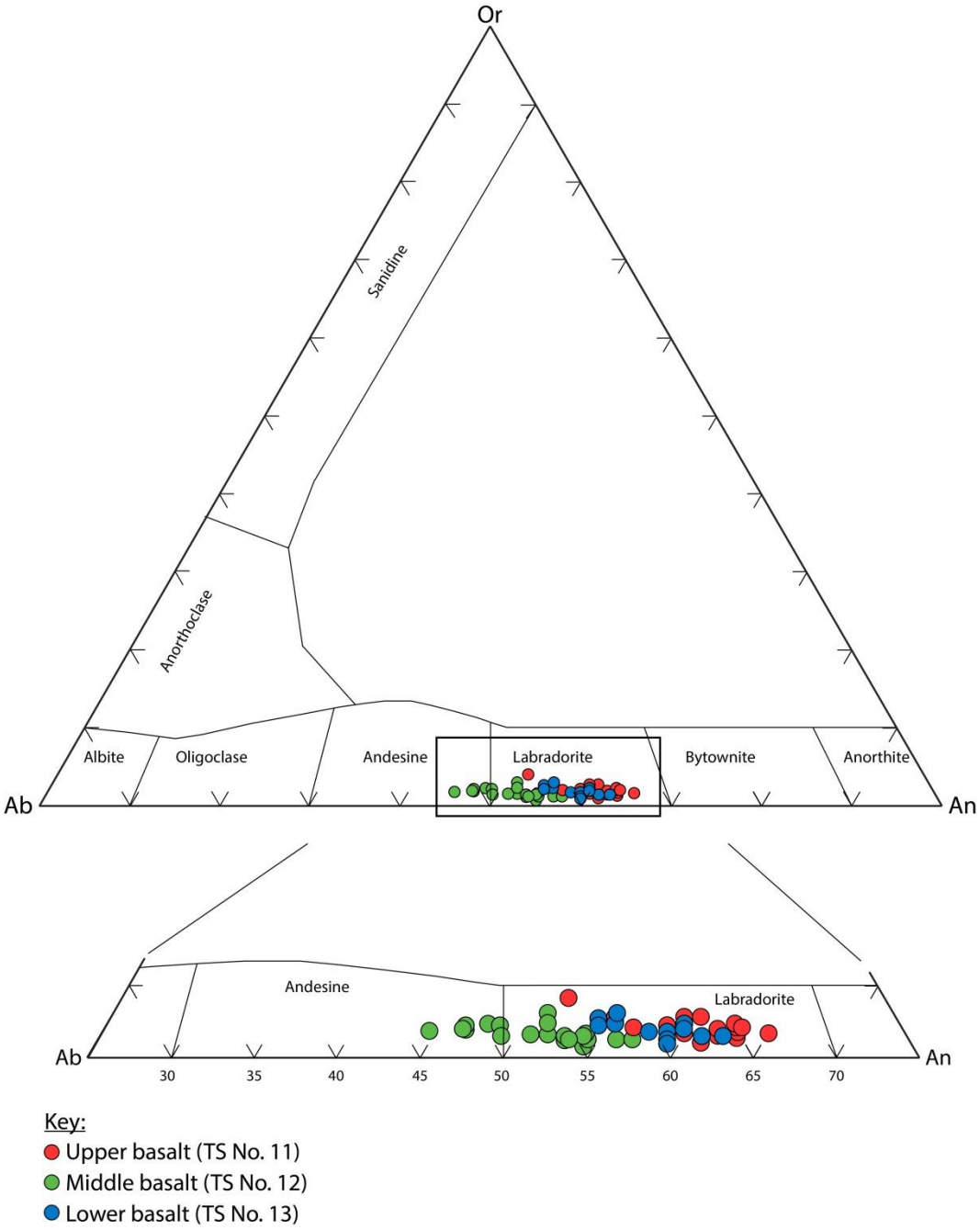

Figure 4.9: Albite - anorthite - orthoclase ternary diagram for plagioclase crystals found in basalt lava flows. Compositions are in mol. %. Box shape shows enlarged composition field. (TS = thin section).

4.9 Comparison between the mineral geochemistry of the three basalt lava flows

This chapter documents the diverse mineral compositions of the phenocrysts and groundmass within the three basalt lava flows in the Auckland pit. From the electron microprobe analysis, the olivine and clinopyroxene phenocrysts compositions and plagioclase groundmass compositions are in agreement with those determined by Cook (2002) and Cook *et al.,* (2005) in that they all occur within the group B rock classification of the SAVF lavas.

The upper and lower basalt flows have similar compositions of olivine, clinopyroxene and plagioclase, while the middle basalt has relatively more Fe-enriched olivine, and lower Ca content in clinopyoxene and plagioclase compositions, which is different and unique to the upper and lower basalt flows (Figs. 4.7, 4.8, 4.9).

4.9.1 Lower basalt

Compositions of olivine in the lower basalt are very Mg-rich, ranging from $Fo_{84.85\text{-}77.96}$ and the abundance of olivine phenocrysts varies from 5.00 - 13.33 % (Fig. 4.7, Table 4.1). The clinopyroxene compositions are very calcic ranging from $Wo_{51.76\text{-}47.78}$ $En_{39.85\text{-}31.72}$ $Fs_{17.10\text{-}11.69}$ which are predominantly within the diopside field and slightly above, and have phenocryst abundances of 2.67 – 3.00 % (Fig. 4.8, Table 4.1). Groundmass plagioclase compositions are Ca-rich, ranging from $Ab_{41.49\text{-}35.20}$ $An_{63.12\text{-}56.12}$ $Or_{3.51\text{-}1.49}$ which are dominantly labradorite, and have an abundance of 7.00 - 10.00 % groundmass (Fig. 4.9, Table 4.1). From point count data, the lower basalt is olivine dominant, however, only two samples were examined.

4.9.2 Middle basalt

The middle basalt is a unique basalt lava flow that has a different mineral composition range from the upper and lower basalt flows. The olivine

compositions are lower in Mg then the lower basalt, but still relatively high in the range of $Fo_{81.43-63.59}$ and have phenocryst abundance of 1.20 - 6.33 % (Fig. 4.7, Table 4.1). The clinopyroxene compositions are less calcic than the lower basalt, ranging from $Wo_{48.24-41.02}$ $En_{47.08-37.79}$ $Fs_{15.38-11.90}$ which are predominantly within the augite and diopside field and have phenocryst abundance of 2.67 - 11.67 % (Fig. 4.8, Table 4.1). Plagioclase compositions are also less calcic then the lower basalt, ranging from $Ab_{58.89-46.83}$ $An_{51.44-39.67}$ $Or_{3.34-1.41}$, predominantly in the andesine to labradorite field, and has a groundmass abundance of 9.67 - 60.33 % (Fig. 4.9, Table 4.1). From point count data, the middle basalt is predominantly clinopyroxene dominant, however, in some logs olivine and clinopyroxene have a similar range of abundances.

4.9.3 Upper basalt

The upper basalt is very similar to the lower basalt with subtle variations in composition. Compositions of olivine are more Mg-rich then the middle basalt but also similar to the lower basalt, ranging from $Fo_{85.63-78.29}$ and the abundance of phenocrysts are 2.67 - 13.00 % (Fig. 4.7, Table 4.1A). The clinopyroxene compositions are calcic, similar to the lower basalt but different to the middle basalt, ranging from $Wo_{51.36-47.79}$ $En_{39.72-32.98}$ $Fs_{15.66-12.10}$ which are predominantly within the diopside field and above, and have phenocryst abundances of 3.33 - 15.67 % (Fig. 4.8, Table 4.1). Plagioclase compositions are more calcic then the middle basalt and similar to the lower basalt, ranging from $Ab_{48.69-31.99}$ $An_{66.22-54.27}$ $Or_{4.04-1.78}$, predominantly in the labradorite field, and has a groundmass abundance of 5.00 - 47.00 % (Fig. 4.9, Table 4.1).

4.10 Summary

Cook (2002) and Cook *et al.,* (2005) determined that the SAVF lavas are classified into two distinctive groups; either group A or group B rocks. Group A and B have dominant olivine phenocrysts, although their abundance varies between samples from the same rock type. In terms of their Fo-content, the olivine in each group exhibits a distinctive range of compositions with the most Fo-rich crystals occurring in group B (Cook, 2002). Clinopyroxene in group A

and B rocks are characterised by their contrasting compositions. Phenocrysts of clinopyroxene in group A are typically calcic augite compositions, whereas those from group B are predominantly diopside (Cook, 2002). Plagioclase is the dominant groundmass phase in both group A and B rocks; however, plagioclase is present as a phenocryst within group A rocks. Compositions are predominately labradorite and range to andesine (Cook, 2002). Nepheline is restricted to the group B rocks, occurring as groundmass only.

The overall mineral composition of olivine and clinopyroxene across the three basalt lavas studied here are relatively similar in compositions, however, in the middle basalt, the lower Mg-rich compositions are more distinguishable. Plagioclase, which occurs in the groundmass across the three basalt lavas have high calcium-rich compositions, however, the middle basalt has lower calcic compositions which is unique compared to the other basalts. Therefore analyses of the basalts samples within this study show that all the samples are classified within the group B rock type of the SAVF lavas determined by Cook (2002) and Cook *et al.,* (2015).

Chapter Five

Whole rock basalt geochemistry

5.1 Introduction

This chapter presents the whole rock major and trace element geochemical data that were obtained for this study. Two types of basalt lavas, based on geochemical differences occur in the SAVF (Rafferty & Heming, 1979; Cook, 2002). Rafferty and Heming (1979) divided the basaltic products into two different groups: a hypersthene-rich subalkaline group and a nepheline-rich alkaline group. Cook (2002) further analysed the differences between these two distinct groups of basalt, associating the basalts group A and B, respectively. Here, X-ray fluorescence spectrometry (XRF) has been used to identify the chemical composition of the three basalt lava flows within the Auckland pit and these are then compared to previous literature on the SAVF lavas. Detailed major and trace element data are included in Appendix V.

5.2 Method

X-ray fluorescence spectrometry (XRF) was used for whole rock major and trace element geochemical analysis, using the Bruker S8 Tiger XRF machine at the University of Waikato. 24 fresh basalt samples were analysed: 2 from the lower basalt, 15 from the middle basalt and 7 from the upper basalt.

Major element geochemistry was analysed using fusion glass disks. The rock samples were first heated in the oven overnight to remove any moisture. The samples were then crushed into a fine powder using a tungsten carbide mill in order to homogenise them. The parts of the mill used were carefully cleaned to ensure no contamination between samples. The powdered samples were then added to crucibles by adding 0.33 – 0.35 g of powdered sample with 2.50 – 2.55 g of 1.2:2.2 flux (35% Li-tetraborate, 65% Li-metaborate) with a pinch of

ammonium iodide to prevent the contents of the crucible from sticking. Crucibles were step-heated every 15 minutes in a Bradway Fusion Furnace at temperatures of 700°C, 800°C, and 1050°C, with the furnace shaker mixing the contents. The contents were then poured onto a graphite disk mould and cooled down within the furnace. Once the disk had cooled, the fused disks were then analysed with the XRF.

Trace elements compositions were analysed using pressed powder pellets. Pressed pellets were formed by adding approximately 8 - 9 g of powdered sample and 25 drops of PVA binder in a paper cup using a wooden spatula, to ensure no contamination, as the XRF does not detect carbon. Once well-mixed the sample was put into an aluminium cup to be compressed with a hydraulic press loaded to 200 bars. The pressed pellets were then heated for approximately 2 hours to evaporate off the binder. These were then analysed by XRF.

Loss on ignition (LOI) was determined by measuring 2 g of powdered sample into a crucible and heated up to 1100°C in a Bradway Fusion Furnace for about an hour, then measuring the weight difference. The raw results from the XRF analysis are in Appendix V.

CIPW norm calculations were used to classify igneous rocks by the normative mineralogy of the rock based on the chemical data. Using the XRF data, the major elements (wt. %) were normalised to 100 % volatile free. Then using the online Excel sheet written by Kurt Hollocher the normalised data were entered into the program and the normalization factor of Fe^{3+}/ (total iron) = 0.10 was set as recommended by the software for basalts. The program produced a wt. % of normative minerals that should theoretically occur within that rock sample. The CIPW normative mineral compositions (wt. %) were plotted on a nepheline (Ne)-diopside (Di)-olivine (Ol)-hypersthene (Hy)-quartz (Q) diagram (Thompson, 1984; Rollinson, 1993) to identify basalt classifications.

A total alkali versus silica diagram (TAS) is one of the most useful classification schemes for volcanic rocks. XRF data for major elements (wt. %) were first normalised to 100 % volatile free, then the sum of the Na2O + K2O content and the SiO2 content were plotted onto the TAS diagram. Using the

plotted data on the TAS diagram and the Ne–Di–Ol–Hy–Q diagram, basalt rocks were classified based on their fit, relative to the two diagrams. CIPW norm calculations for 24 basalt samples are presented in Appendix V.

5.3 Rock Classification

Geochemical data of bulk-rock XRF analyses are presented in Table 5.1.

Table 5.1: Bulk-rock XRF analyses of the upper, middle and lower basalts in the Auckland pit. (Major elements normalized to 100 % volatile free).

	Upper Basalt						
	ne-hawaiite	basanite	basanite	basanite	basanite	ne-hawaiite	basanite
Equivalent thin section no.[1]	**7**	**11**	**28**	**33**	**41**	**44**	**45**
Major elements (wt. %)							
SiO_2	47.711	42.571	43.635	47.279	47.518	48.025	48.000
Al_2O_3	15.545	12.680	12.844	14.978	14.938	15.397	15.598
TiO_2	2.263	3.139	2.958	2.234	2.222	2.417	2.251
MnO	0.186	0.177	0.188	0.178	0.192	0.190	0.179
Fe_2O_3	13.536	14.176	14.645	13.202	13.413	13.384	12.808
Na_2O	3.962	3.678	3.310	4.902	4.878	3.893	5.430
MgO	6.295	11.024	10.412	6.590	6.412	6.090	5.832
K_2O	1.864	1.432	1.076	1.874	1.935	1.847	1.997
CaO	7.866	10.324	10.299	8.012	7.714	8.003	7.063
P_2O_5	0.771	0.799	0.634	0.751	0.779	0.754	0.841
Total[2]	**100.24**	**101.07**	**100.11**	**100.43**	**100.23**	**100.13**	**102.35**
LOI[2]	1.32	0.25	0.05	0.3	0.75	1.66	16.55
Trace elements (ppm)							
F	364	782	455	403	516	472	364
S	0	578	162	5	38	0	0
Cl	158	135	89	258	296	180	258
Sc	11	11	15	13	10	11	6
V	167	263	306	170	161	170	129
Cr	184	285	330	215	205	205	113
Co	55	93	78	57	57	62	45
Ni	100	254	264	103	128	103	71
Cu	53	69	45	55	49	52	40
Zn	119	124	108	111	122	122	103
Ga	28	23	24	27	26	27	22
As	6	6	6	6	7	6	6
Rb	29	23	19	30	31	33	28
Sr	839	720	622	785	791	890	684
Y	23	23	22	23	24	23	18
Zr	370	271	223	351	363	371	338
Nb	59	52	42	54	58	59	46
Mo	6	7	5	6	6	6	5
Sn	3	0	2	3	3	4	0
Sb	0	0	0	0	0	0	0
Cs	13	19	18	13	12	13	10
Ba	291	258	199	275	293	300	265
La	62	48	41	56	52	61	50
Ce	101	99	78	102	112	107	98
Nd	39	40	31	41	41	37	37
Tl	0	0	0	0	0	0	0
Pb	3	3	3	3	3	3	3
Th	8	7	7	8	8	8	7
U	3	3	3	3	3	3	3

[1] Samples analysed correspond to thin sections described in Chapter 4.
[2] LOI and total are original figures.
LOI = Loss on ignition; Total Fe expressed as Fe_2O_3.

Table 5.1: Continued.

	Middle Basalt					
	ne-hawaiite	ne-hawaiite	ne-hawaiite	basanite	ne-hawaiite	ne-hawaiite
Equivalent thin section no.[1]	**1**	**3**	**5**	**6**	**12**	**20**
Major elements (wt. %)						
SiO_2	47.687	47.428	47.493	47.815	47.280	47.213
Al_2O_3	15.146	15.027	15.132	15.438	14.684	14.596
TiO_2	2.201	2.437	2.249	2.130	2.249	2.403
MnO	0.179	0.193	0.190	0.179	0.179	0.191
Fe_2O_3	13.229	13.748	13.219	12.936	13.351	13.453
Na_2O	4.516	3.781	4.908	5.468	4.245	4.013
MgO	6.496	6.900	6.307	5.855	7.542	7.630
K_2O	1.864	1.795	1.916	2.067	1.795	1.742
CaO	7.906	7.931	7.816	7.282	7.927	8.010
P_2O_5	0.776	0.759	0.769	0.830	0.747	0.749
Total[2]	**98.95**	**100.44**	**99.96**	**100.45**	**99.89**	**98.17**
LOI[2]	0.4	1.66	0.38	0.31	1.09	1.78
Trace elements (ppm)						
F	245	493	517	289	503	475
S	0	100	0	0	30	58
Cl	221	163	254	389	220	140
Sc	10	11	10	9	10	11
V	166	178	162	148	164	170
Cr	189	225	197	143	216	224
Co	50	66	60	54	52	53
Ni	101	149	105	85	130	142
Cu	49	56	49	51	55	44
Zn	113	126	121	113	112	116
Ga	27	25	26	26	25	25
As	7	8	9	8	6	8
Rb	31	28	29	33	28	29
Sr	868	798	794	825	800	826
Y	25	29	23	23	24	25
Zr	364	350	360	386	347	338
Nb	61	57	58	59	55	59
Mo	6	6	6	6	6	6
Sn	3	1	2	2	3	5
Sb	0	0	0	0	1	1
Cs	12	13	12	12	13	13
Ba	308	501	280	305	292	288
La	58	59	53	51	56	55
Ce	103	105	110	114	99	97
Nd	45	42	38	35	37	41
Tl	0	0	0	0	0	0
Pb	3	3	3	3	3	3
Th	8	8	8	8	8	8
U	3	3	3	3	3	3

[1] Samples analysed correspond to thin sections described in Chapter 4.

[2] LOI and total are original figures.

LOI = Loss on ignition; Total Fe expressed as Fe_2O_3.

Table 5.1: Continued.

	Middle Basalt					
	ne-hawaiite	ne-hawaiite	ne-hawaiite	ne-hawaiite	ne-hawaiite	ne-hawaiite
Equivalent thin section no.[1]	**22**	**23**	**25**	**27**	**30**	**35**
Major elements (wt. %)						
SiO_2	48.042	47.493	47.430	47.096	47.604	47.121
Al_2O_3	15.445	14.646	14.916	14.318	15.244	14.469
TiO_2	2.178	2.363	2.321	2.302	2.254	2.307
MnO	0.176	0.187	0.193	0.192	0.177	0.178
Fe_2O_3	12.979	13.258	13.384	13.631	13.098	13.310
Na_2O	5.065	4.728	4.875	4.231	4.959	4.736
MgO	5.941	6.868	6.254	7.468	6.246	7.296
K_2O	2.006	1.888	1.939	1.864	1.925	1.840
CaO	7.329	7.821	7.915	8.141	7.703	8.003
P_2O_5	0.837	0.748	0.774	0.756	0.791	0.738
Total[2]	**100.18**	**99.77**	**99.65**	**98.45**	**100.25**	**100.35**
LOI[2]	0.22	0.08	0.15	0.05	0.1	0.64
Trace elements (ppm)						
F	321	361	443	444	287	398
S	0	0	93	0	0	98
Cl	304	503	353	194	293	276
Sc	11	9	10	11	10	11
V	147	168	165	172	157	167
Cr	148	209	217	213	168	208
Co	49	57	62	57	50	58
Ni	86	132	117	139	93	134
Cu	49	53	58	53	50	57
Zn	118	120	121	115	117	114
Ga	26	27	26	27	27	25
As	6	8	7	7	7	6
Rb	32	30	31	37	31	29
Sr	860	815	822	866	817	776
Y	24	24	24	25	23	23
Zr	393	361	365	353	373	339
Nb	61	60	60	60	60	54
Mo	6	6	6	6	6	6
Sn	3	3	3	4	2	2
Sb	0	1	0	2	0	1
Cs	12	13	13	13	13	13
Ba	314	297	308	302	299	281
La	63	59	56	55	58	53
Ce	106	107	101	107	106	96
Nd	42	44	35	43	40	38
Tl	0	0	0	1	1	0
Pb	3	3	3	3	3	3
Th	8	8	8	8	8	8
U	3	3	3	3	3	3

[1] Samples analysed correspond to thin sections described in Chapter 4.

[2] LOI and total are original figures.

LOI = Loss on ignition; Total Fe expressed as Fe_2O_3.

Table 5.1: Continued.

	Middle Basalt			Lower Basalt	
	ne-hawaiite	ne-hawaiite	ne-hawaiite	basanite	ne-hawaiite
Equivalent thin section no.[1]	**37**	**42**	**46**	**13**	**47**
Major elements (wt. %)					
SiO_2	47.285	47.277	47.117	42.259	47.085
Al_2O_3	14.956	14.595	14.624	12.342	14.936
TiO_2	2.295	2.380	2.351	3.010	2.588
MnO	0.180	0.192	0.184	0.199	0.198
Fe_2O_3	13.129	13.335	13.370	15.082	13.860
Na_2O	4.970	4.158	4.685	3.944	3.672
MgO	6.580	7.568	7.253	10.909	7.088
K_2O	1.853	1.783	1.834	1.462	1.562
CaO	7.993	7.964	7.839	10.025	8.254
P_2O_5	0.758	0.746	0.741	0.769	0.755
Total[2]	**100.74**	**98.59**	**100.07**	**101.38**	**98.56**
LOI[2]	0.26	0.27	0.51	0.22	0.22
Trace elements (ppm)					
F	313	488	433	678	586
S	0	0	0	986	154
Cl	330	271	282	168	242
Sc	9	10	11	11	11
V	172	175	171	252	185
Cr	206	224	222	273	220
Co	59	53	136	72	62
Ni	105	138	146	241	160
Cu	52	53	60	69	57
Zn	114	118	117	114	130
Ga	26	26	25	22	27
As	8	7	8	7	8
Rb	29	30	30	23	25
Sr	786	827	786	673	848
Y	23	25	23	22	26
Zr	353	349	340	261	352
Nb	55	60	56	49	62
Mo	6	6	6	5	6
Sn	2	4	1	0	2
Sb	0	2	0	0	0
Cs	13	13	13	18	15
Ba	299	292	281	247	427
La	52	56	51	46	54
Ce	108	107	98	97	111
Nd	38	36	39	36	35
Tl	0	0	0	0	0
Pb	3	3	3	3	3
Th	8	8	8	7	8
U	3	3	3	3	3

[1] Samples analysed correspond to thin sections described in Chapter 4.

[2] LOI and total are original figures.

LOI = Loss on ignition; Total Fe expressed as Fe_2O_3.

The geochemistry of the lower, middle and upper basalts from the Auckland pit has been classified based on their total alkalis ($Na_2O + K_2O$) versus silica (SiO_2) (TAS) abundance (Fig. 5.1) (Rollinson, 1993). All samples are plotted within the basanite and trachybasalt regions: also plotted is the Gibson (2011) basalt sample from the Waikato pit, which plots as a trachybasalt.

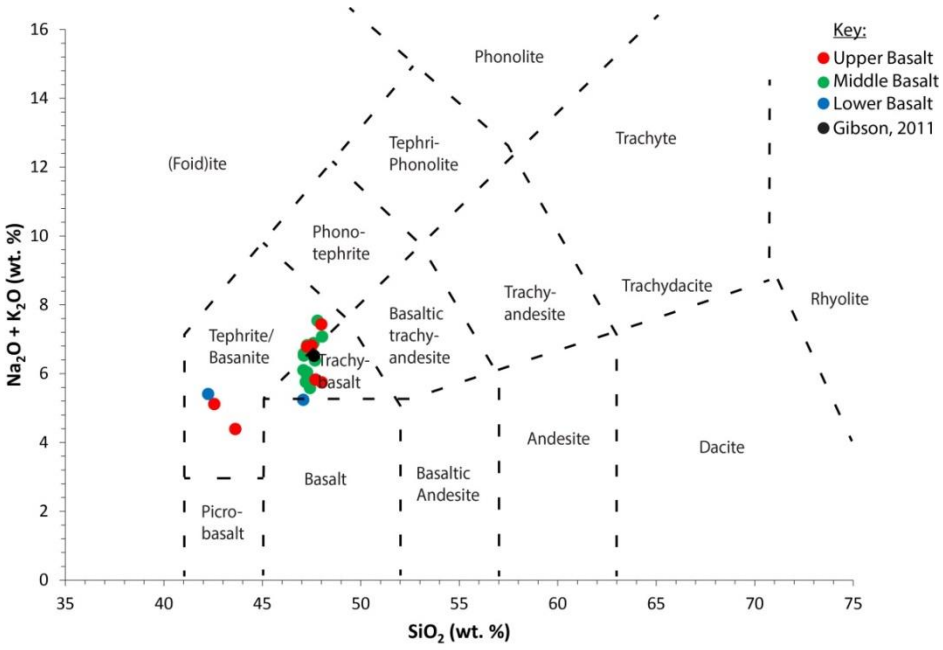

Figure 5.1: Chemical classification of volcanic rocks using the total alkalis versus silica (TAS) diagram. Plots of basalt samples throughout the Auckland pit. Gibson's (2011) basalt sample from the Waikato pit is also included for comparison.

Using a variant to the standard TAS diagram (Fig. 5.2), the basalts can be further classified into group A or group B SAVF lavas (Cook, 2002). Figure 5.2 determines that group A basalts dominantly plot in the subalkaline field with group B plotting in the alkaline field. Basalt samples in this study predominantly lie within the alkaline group B region. Gibson's (2011) basalt sample from the Waikato pit is also similar composition to Auckland pit basalt samples, which are all in group B of Cook (2002).

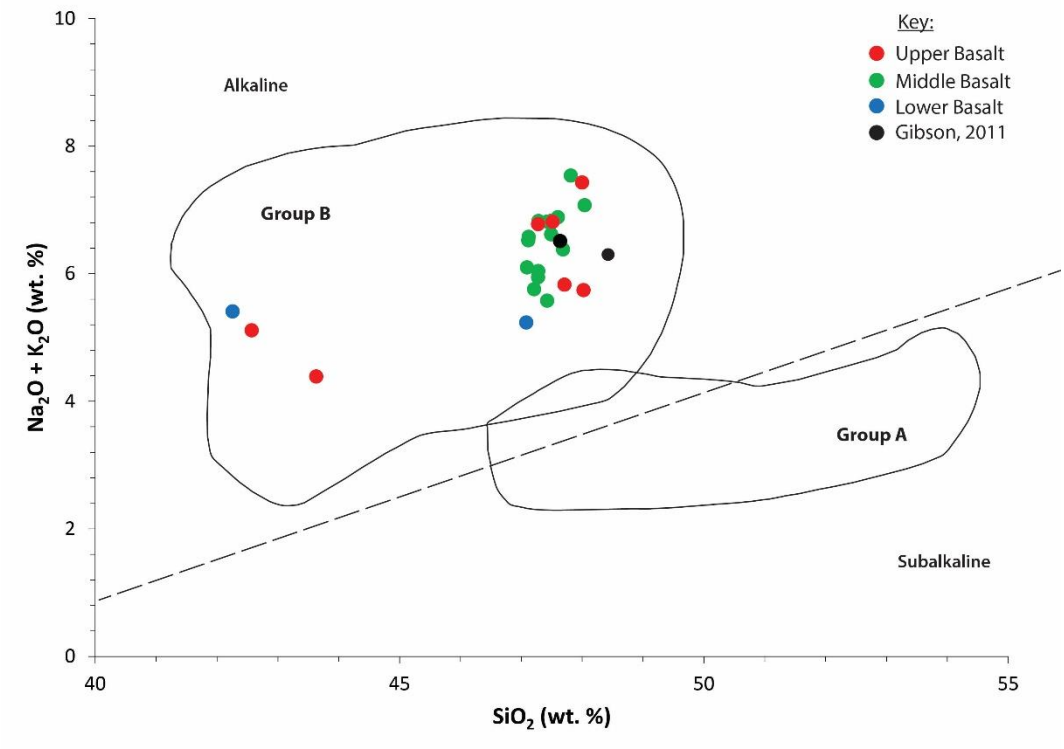

Figure 5.2: $Na_2O + K_2O$ (wt. %) against SiO_2 (wt. %), with typical boundaries of Group A and B basalt from the SAVF (Cook, 2002). Gibson's (2011) basalt sample from the Waikato pit is also included for comparison.

The CIPW normative classification scheme (Rollinson, 1993) is used to plot the basalts and related basic and ultrabasic magmatic rocks, according to their CIPW normative mineral composition expressed as Ne–Di–Ol–Hy–Q diagram (Fig. 5.3). All samples plot within the Ne–Di–Ol diagram and are within the group B region supported by Cook (2002). Using the TAS and Ne–Di–Ol diagrams, the CIPW classification scheme has identified two basalts in this study: basanites and ne-hawaiites (Table 5.1).

Group B represents a basanite to hawaiite group and is derived from the upper mantle (Cook, 2002). The data below suggests that magma sources from the Auckland pit were generated in the upper mantle.

Based on Cook (2002) and Cook *et al.*, (2005) discrimination of group A and B basalts is best determined from abundances of high field strength elements (HFSE), i.e. Nb and Zr. Subalkaline group A basalts have low HFSE abundances of Nb (9-29 ppm) and Zr (97-219 ppm), while group B basalts are comparatively

much higher (Nb, 35-102 ppm; Zr, 194-491 ppm) which are in agreement with the basalt samples in this study (Table 5.1).

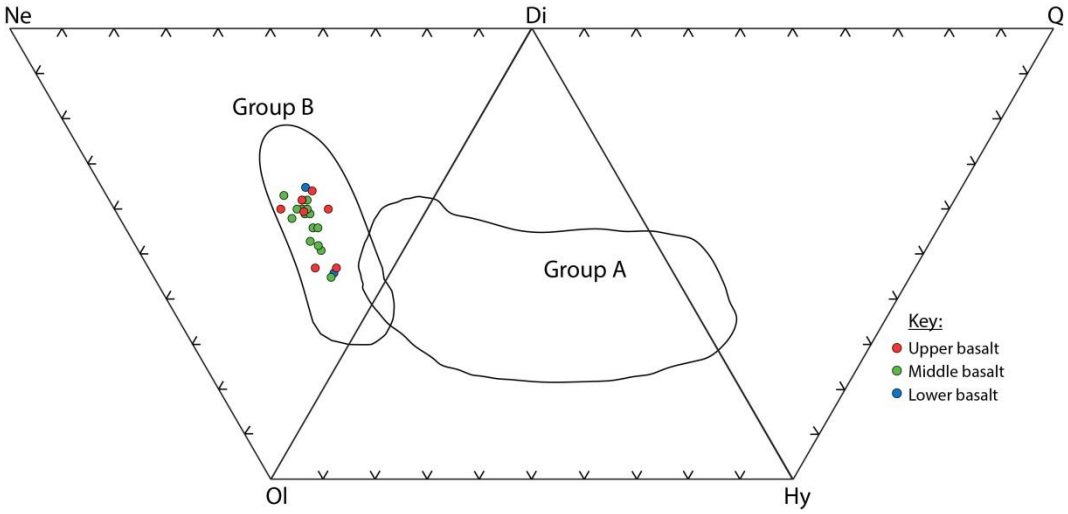

Figure 5.3: Classification of basalts according to their CIPW normative mineral compositions. Group A and B regions obtained from Cook (2002).

5.4 Major Elements Geochemistry

The geochemical data from the XRF (Table 5.1) are in agreement with the range of expected results for the SAVF lavas as obtained by Cook (2002). SiO_2 values have a broad range from 42 – 48 wt. % as basanite to trachybasalt. The geochemical data indicate several trends across the major elements (SiO_2, Al_2O_3, TiO_2, Fe_2O_3, Na_2O, K_2O and CaO) plotted against MgO wt. % (Fig. 5.4).

Basalt lava flows from the Auckland pit range in MgO content from 5.8 – 11.2 wt. %. There is a strong trend of SiO_2 increasing with a decrease in MgO content. There is also a strong trend of increasing Al_2O_3 and K_2O with decreasing MgO wt. %. A weak trend is also present of Na_2O increasing as MgO (wt. %) content decreases. In contrast, however, there is a weak trend of decreasing TiO_2, Fe_2O_3 and CaO with decreasing MgO (wt. %) content (Fig. 5.4).

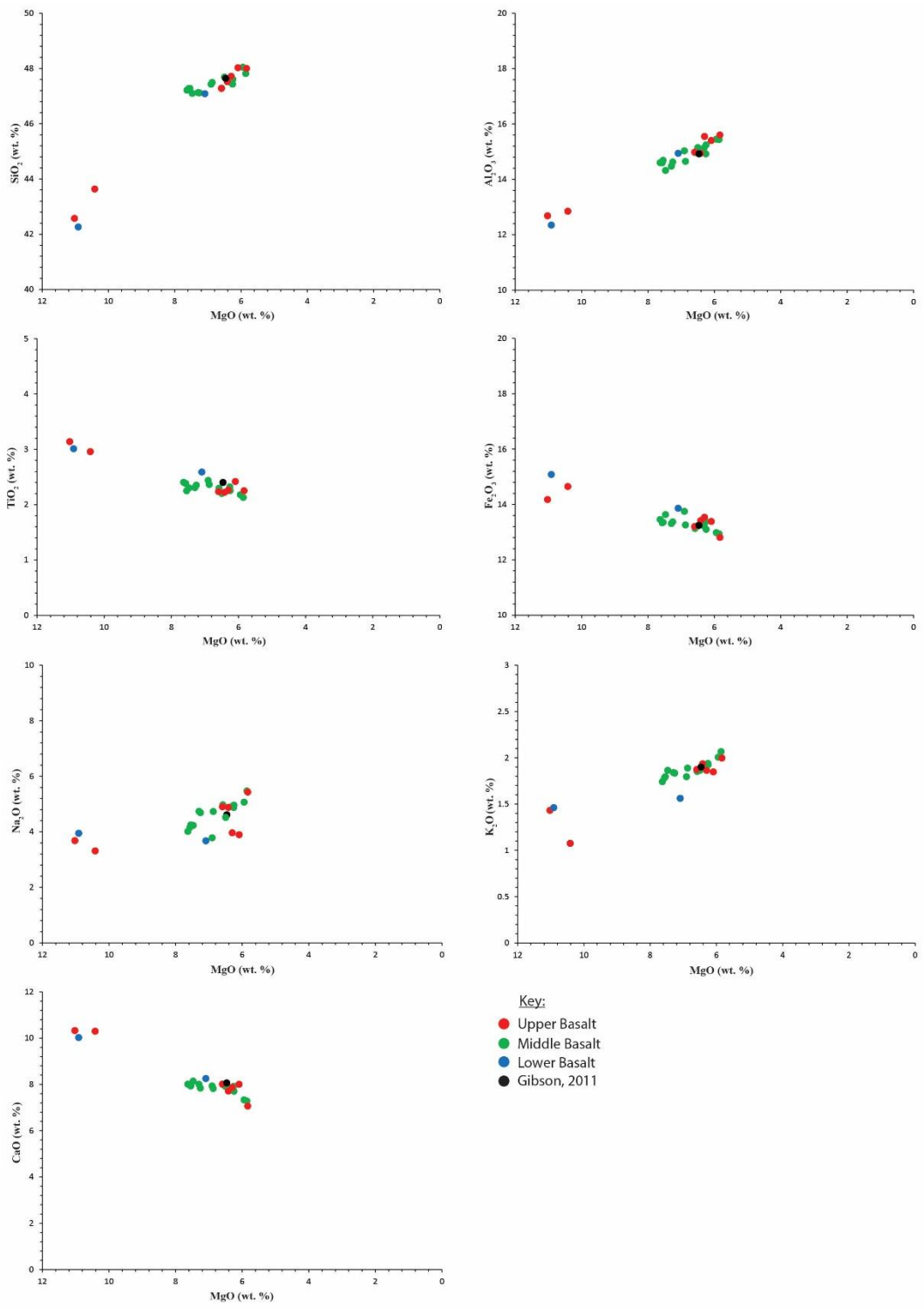

Figure 5.4: Plots of major element abundances versus MgO (wt. %) of the lower, middle and upper basalts from the Auckland pit. Gibson's (2011) basalt sample from the Waikato pit is also included for comparison.

The major element geochemical plots reveal similar trends for SiO_2, Al_2O_3, with precipitation of Na_2O and K_2O which is consistent. As MgO decreases (more felsic) CaO also decreases as the plagioclase mineral is removing it from the melt, therefore K_2O + Na_2O increases in proportion as nothing is removing it. Overall, the trends show typical fractional crystallisation. However, with the increase in silica, it is expected that MgO, Fe_2O_3, TiO_2 and CaO decrease, as the main mafic minerals of olivine and clinopyroxene are precipitated.

The lower, middle and upper basalts in the Auckland pit are displaying the same trends as expected. However, there are small variations of wt. % of the major elements that are plotted against MgO wt. %. This does not change the overall geochemistry and, therefore, they all lie within the group B region defined by Cook (2002).

Three outliers (no. 11, 28 and 13; Table 5.1) of high MgO values occur due to the very high percentage of olivine phenocrysts present within these samples (see Table 4.1 in chapter 4), which correspond to dilution (low values) of SiO_2, Al_2O_3, K_2O, Na_2O, and enrichment in Fe_2O_3 and TiO_2; also higher CaO, although this cannot be explained by olivine phenocryst proportions.

5.5 Trace Elements Geochemistry

From the geochemical data, only eight selected trace elements (V, Cr, Ni, Rb, Sr, Zr, Nb and Ba) were plotted against MgO wt. % (Fig 5.5). The samples classified as basanites and ne-hawaiites generally plot in accordance with the findings of Cook (2002). All trace elements show some comparable trends to the major elements.

There is a strong trend of decreasing V, Cr and Ni, with decreasing MgO wt. %. There is a strong trend of increasing Rb, Sr and Zr, with decreasing MgO wt. %. Nb and Ba show flat trends with decreasing MgO wt. %.

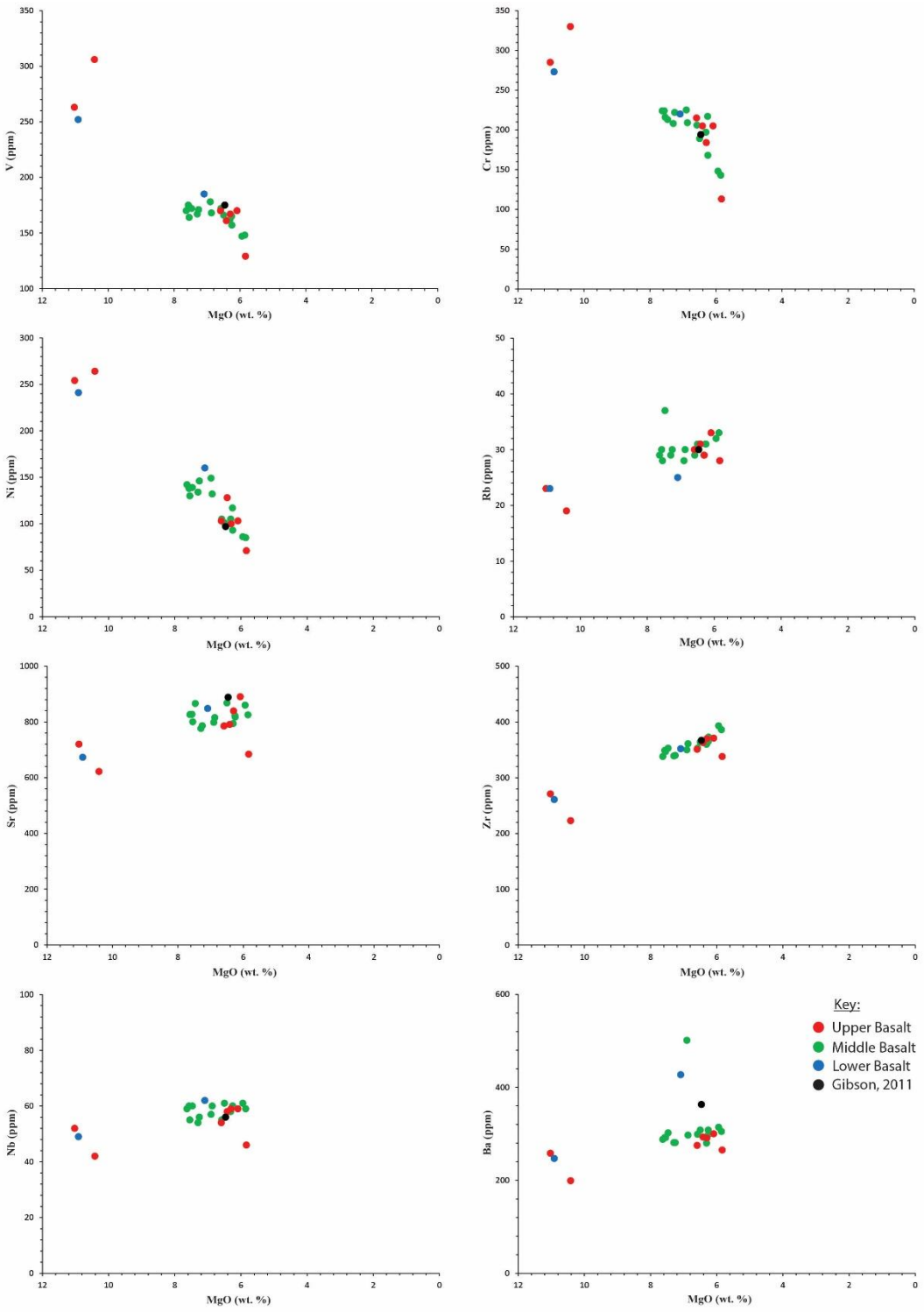

Figure 5.5: Selected trace element abundances versus MgO (wt. %) of the lower, middle and upper basalts from the Auckland pit. Gibson's (2011) basalt sample from the Waikato pit is also included for comparison. Elements Ni, Cr and V are compatible while Rb, Sr, Zr, Nb and Ba are incompatible.

5.6 Comparison of Basalts with other Literature

Cook (2002) studied the SAVF lavas and determined that there are two types of basalt lavas based on differences in geochemical composition. Basalts were identified with subalkalic and alkalic compositions, associating the basalts group A and B respectively.

This study revealed the Auckland pit basalts to be classified into group B and have MgO in the range of 5.8 – 11.1 wt. %. Cook (2002) classified the basalts in group B further to illustrate that the majority of basanites have MgO greater than 10 wt. % and ne-hawaiites with values of 5.3 – 7.5 wt. %. This range of MgO content is strongly in agreement with this study of basalts from the Auckland pit (Fig. 5.4).

Cook (2002) also determined that SAVF lavas in group B tend to span a distinct range of SiO_2 content between nephelinites (40 – 42.8 wt. %), basanites (41.6 – 45.2 wt. %), ne-hawaiites (43 – 47.9 wt. %) and alkali ol-basalts (42.9 – 47.4 wt. %). Basalts from the Auckland pit are in agreement with Cook (2002) which lie within the basanites and ne-hawaiites classification of basalts where SiO_2 ranges from 42 – 48 wt. %.

Major element compositions of the basalt flows within the Auckland pit lie within the group B region of Cook (2002) where there is a strong trend of increasing SiO_2, Al_2O_3, Na_2O and K_2O with decreasing MgO (wt. %), and also a strong trend of decreasing TiO_2, Fe_2O_3 and CaO with decreasing MgO (wt. %), (Fig. 5.4).

Trace elements compositions determined by Cook (2002) reveal that compatible trace elements of Ni and Cr in group B span similar abundances, ranging from 59 – 337 ppm and 61 – 404 ppm respectively, although the majority of the basanites have among the largest Ni and Cr abundances and most ne-hawaiites the smallest. Furthermore, group B has V abundances that range from 147 – 310 ppm with basanites containing the largest and ne-hawaiites the smallest. Basalts from the Auckland pit show the same abundances and trends as

Cook (2002) where basanites contain the largest abundances and ne-hawaiites the smallest (Fig. 5.5).

Incompatible trace elements determined by Cook (2002) include large ion lithophile elements (LILE) e.g. Ba, Rb and Sr, high field strength elements (HFSE) e.g. Zr and Nb, and light rare earth elements (LREE) e.g. La and Ce and Y. Cook (2002) determined that group B rocks exhibit a relatively large range of incompatible trace element concentrations that exhibit increasing trends with decreasing MgO (wt. %), ranging from silica-undersaturated basanites to less undersaturated ne-hawaiites and alkali ol-basalts. Basalts from the Auckland pit are in agreement with Cook's (2002) findings that show there is a moderate trend of increasing incompatible elements with decreasing MgO wt. % (Fig. 5.5).

Taylor (2012) studied the basalts from the Raventhorpe volcanic complex, and the Pokeno West volcanic complex, determining the basalts to be of group A and B and classified the basalts as; transitional basalts, olivine-tholeiitic basalts, basanites and alkali olivine-basalts. From major element compositions, Taylor (2012) identified a weak trend of decreasing TiO_2 with decreasing MgO wt. %, with Al_2O_3 and Fe_2O_3 showing flat trends for group A and B regarding major element composition. No relationship between SiO_2 and MgO wt. % exists within either group, however, they generally plot with the range of expected results for the SAVF. Taylor (2012) found that the trace elements generally plot in accordance with the findings of Cook (2002), however, the trace elements show no clear trends and are clustered. Basalts from this study show that all the basalts from the Auckland pit lie within group B, and are similar to the group B basalts of Taylor (2012). However, this study shows there is a strong trend of increasing SiO_2, Al_2O_3, Na_2O and K_2O with decreasing MgO (wt. %) and also a strong trend of decreasing TiO_2, Fe_2O_3 and CaO with decreasing MgO (wt. %) (Fig. 5.4) compared to Taylor's (2012) major elements data. Also trace elements show strong trends of decreasing compatible elements with decreasing MgO (wt. %), whereas incompatible elements show a moderate trend of increasing while MgO wt. % decreases (Fig. 5.5) compared to Taylor (2012) where all trace elements are clustered and show no trend.

Gibson (2011) studied the tuff ring from the Waikato pit, Bombay Quarry and determined that the basalt sample obtained from the pit was group B and classified the basalt as ne-hawaiite. Figure 5.4 and 5.5 show the basalt plotted from the Waikato pit with the Auckland pit basalts, which reveal the basalt from the Waikato and Auckland pit following the same trends for the major and trace elements within the group B SAVF lavas.

5.7 Summary

The three basalt lava flows within the Auckland pit have been analysed by its geochemical compositions and it has revealed that all the basalt flows lie within the expected group B region. The geochemical data also provide an insight into the three individual lavas. The lower and upper basalt flows are classified as basanites and ne-hawaiites, and have much variation in their major and trace element compositions. Therefore, when plotted, they span a relatively wide range of composition. However, the middle basalt, classified as ne-hawaiite, has less variation of major and trace elements compositions. Even though the basalts have different variations of elemental compositions, the overall geochemical analysis shows that the basalts within the Auckland pit are in agreement with the group B rock types in the SAVF.

Chapter Six

Discussion

6.1 Introduction

This chapter interprets the observations and data presented in the preceding chapters, in terms of the process origins of the volcanic and sedimentary units and the eruption history of the Auckland pit in relevance to the SAVF.

6.2 Origin of the palaeotopography

The volcanic succession within the Auckland pit lies within a palaeotopographic low, here interpreted to be a palaeovalley which is separate to the palaeotopographic low associated with the adjacent Waikato pit (c.f. Gibson, 2011). The valley has formed within the pre-existing Waitemata and Tauranga groups which are comprised of pumiceous, terrestrial and minor estuarine sediments (Kear & Schofield, 1978; Isaac *et al.*, 1994). The variation in the topography of the valley within the Auckland pit suggests that the basalt lavas have infilled the palaeovalley depression from a nearby volcanic eruption. Alternatively, the Auckland pit could represent an original vent topography, which the volcanic eruptions occurred from within the Auckland pit. Therefore the lava could have just ponded within such a crater, but this is unlikely, due to their being sedimentary intervals between the basalt lavas. The most likely scenario for the topographic variation is due to the eroded material being removed, to accommodate the basalt from a nearby vent to erupt and flow into the palaeovalley.

6.3 Basalt Lava Flow Processes

Basalt flows identified within the drill cores in the Auckland pit reveal that there are three individual lavas flows that may be either pahoehoe, aa, and/or transitional lava flows.

Pahoehoe lavas, are produced by inflation of the lava flow beneath a chilled surface crust (Hon *et al.,* 1994), and are the most abundant lava type in the Auckland pit logged in drill core. All pahoehoe flow units observed contain planar upper and lower contacts with very small spherical vesicles preserved just within these margins. The vesicles increase in size from the margins towards the centre of the lava flow. The paheohoe lavas identified in this study, show an increase in the vesicle size from both the upper and lower zones towards the centre, however, the concentration of vesicles decrease towards the centre; the central part of each flow is mainly dense, lacking vesicles (Figs. 3.9 to 3.11).

Pahoehoe lavas propagate by building out from small toes at the flow front beneath chilled, smooth, low-relief surface crusts (Hare & Cas, 2005). Pahoehoe sheet flows are produced by the radial spreading of pahoehoe toes on shallow slopes and coalescence of the surface crusts of adjacent toes, forming a continuous sheet under which molten lava is fed (Hon *et al.,* 1994). Steady inward thickening of the upper and lower crusts occurs around a constant fluid layer of freshly supplied lava (Hare & Cas, 2005). Some gas bubbles in the molten interior lava are trapped in the chilled flow base forming the lower vesicular zone, but most rise buoyantly to the top of the lava, where they are initially trapped beneath, and with further cooling, are incorporated within the upper crust, forming the upper vesicular zone; a dense core represents the non-vesicular zone.

The gas bubbles in lavas are not generally subject to shear stresses, hence vesicles are usually discrete and spherical, and locally the distribution is homogeneous (Aubele *et al.,* 1988; Wilmoth & Walker, 1993; Self *et al.,* 1996). Horizontal vesicle sequences (e.g. vesicle trails) are an exception, as these are interpreted to represent the final stages of lava movement in pahoehoe flows (Hare & Cas, 2005). Segregation veins form because incompatible volatiles are concentrated in the residual melt during crystallisation of the non-vesicular zone.

These periodically rise and spread out at the lower parts of the upper vesicular zone.

The Auckland pit lavas are dominated by pahoehoe lava flows, however, the vesicular distribution within some basalt intervals in drill core make it difficult to identify them as a pahoehoe lava flow (C306, C308; Fig. 3.11). Pahoehoe lavas characteristically form only on gentle slopes of less than 2^{o} (Hon *et al.*, 1994; Cashman & Kauahikaua, 1997). Although the topography prior to volcanism was more irregular and possibly slightly steeper, it must have been relatively flat to allow inflation of the pahoehoe flows to occur (Hare & Cas, 2005).

Aa lavas are generally emplaced at higher viscosities than pahoehoe lavas, and autobrecciation occurs during emplacement (Macdonald, 1953; Lipman & Banks, 1987). Talus from cooled, broken surface crust is dumped over the flow front and the side margins, and falls to the ground surface, or is incorporated into the fluid flow (Crisp & Baloga, 1994). The talus is overridden by lava upwelling from the fluid inner core, therefore producing a fragmented basal layer overlain by a coherent lava flow. The lava undergoes autobrecciation because the viscosity or yield strength of the lava beneath the crust is too high for it to flow within and heal torn-apart portions (Rowland & Walker, 1990). The exteriors of the autobrecciated clasts are characteristically rough as the ripped viscous lava retains an irregular shape.

Gas bubbles do not migrate significantly during emplacement due to the high viscosity of the lava. Vesicles in aa lava flows are generally irregular shapes, interconnected to a high degree and their distribution is heterogeneous (Polacci & Papale, 1997; Cashman *et al.*, 1999; Polacci *et al.*, 1999; Hare & Cas, 2005), because the lava is more viscous and less able to homogenise. The lack of segregation veins in aa flows is probably because the lavas are to viscous for residual melt to migrate through the surrounding crystal mush, as it does in pahoehoe flows.

Broken core represented by facies C observed within the basalt flows of the Auckland pit, was probably generated on steeper terrain within the Auckland

pit area, where the talus from the broken surface crust was thrown over the flow front and then incorporated into the interior of the lava flow.

Transitional lavas contain features which are common to both pahoehoe and aa lava flows (Hare & Cas, 2005). The flows observed in drill core commonly contain rubbly material at the top and base surrounding a coherent interior that can be subdivided into a upper vesicular zone, non-vesicular zone and lower vesicular zone (e.g. Log B19, top, 24.5 – 25 m, and base, 36.5 – 38.5 m; Fig. 3.10). The weathered vesicular clasts of scoriaceous basalt have been entrained into the interior of the flows during emplacement (e.g. Log C306, 3.2 – 7 m; Fig 3.9). Transitional lavas are generally considered to be either aa lava flows or pahoehoe flows, autobrecciated behind the flow-front (Keszthelyi, 2002). Possibly the magma was significantly undercooled prior to eruption, as evidenced by higher crystallinity and/or the eruption rate was initially higher than the other lava types. It is not clear which (if either) mechanism developed the transitional lava type in this study.

Facies A.1 is moderately vesicular basalt that occurs at the top and base of lava flow intervals. Facies A.1 is likely to be part of a pahoehoe lava flow which usually has an upper vesicular and lower vesicular zone; furthermore, the vesicle size tends to increase towards the centre of the basalt flow within this facies.

Facies A.2 is basalt lava with horizontal vesicle trails up to 10 – 40 mm apart. This facies represents the final stages of lava movement in a pahoehoe lava flow, as volatiles are concentrated in the residual melt during crystallisation and periodically rise and spread out at the lower parts of the upper vesicular zone.

Facies A.3 is high strength, dense, coherent, non-vesicular basalt produced predominantly within a pahoehoe flow. Vesicles which migrate and are trapped within the lower and upper vesicular zones leaving a dense coherent centre; this vertical facies arrangement is commonly associated with pahoehoe lava flows.

Facies A.4 is a poorly vesicular basalt that occurs in-between the non-vesicular and upper and lower vesicular zones. However, in this study facies A.4 occurs throughout the lava flows at different variations and depth. Facies A.4 most likely represents part of a pahoehoe lava flow, where the vesicularity might

represent fluctuations between the dense non-vesicular zone and vesicular zones on the outer parts within the lava flow.

Facies C is highly weathered, broken and moderately vesicular scoriaceous basalt that is likely to be the product of aa and/or transitional lava flow. Facies C is the autobrecciated part of aa/transitional lava flow. In some drill cores (e.g. Log C308, 16.5 – 18.30 m; Fig. 3.11) the autobreccia clasts are within a coherent pahoehoe basalt lava flow, indicating that the broken surface crust from the talus was thrown over the flow front moving lava. The broken surface crust was then incorporated into the centre of the lava flow which has then been preserved within the pahoehoe flow as it was deposited and cooled, suggesting a transitional lava flow deposition. In other drill cores (e.g. Log C301, 19.5 – 20.80 m; Fig. 3.10), the breccia is visible at the base of the lava flow indicating, that the breccia has broken apart and was dumped over the flow front, then was overridden by lava from the inner core, therefore producing a fragmented basal layer overlain by a coherent lava flow, typical of an aa lava flow.

6.4 Basalt Jointing Patterns

Within this study jointing patterns of the basalt lavas were only observed from remote viewing points and photographs from within the Auckland pit, as jointing patterns could not be assessed from drill core logs. Basalt joints identified within the Auckland pit are columnar, horizontal ‘sheeted’ and entablature ‘platy - prismatic’ joints.

Columnar joints form as a result of ordered contraction cracks propagating into cooling lava flows (Mallet, 1875). As the lava cools and solidifies, the fracture tips follow the solidification front, leaving behind a record of the ordering process in the form of roughly hexagonal columns (Goehring & Morris, 2008). As the cracks advance in the lava, they do so intermittently, leaving striations on the sides of columns (Ryan & Sammis, 1978) and tend to occur at the upper parts of the lava flow.

Horizontal sheets are a set of parallel, generally closely-spaced joints which divide the rock into layers, which are developed in essential conformity

with the topography and where the ground surface is flat. Sheeting joints generally form as a result of physical weathering which removes the superimposed load from the rock it exposes (Faust, 1978). This removal of overburden permits the rock to dissipate its stored strain energy, primarily in the formation of cracks oriented parallel to the ground surface (Faust, 1978).

Platy - prismatic joints are considered to be entablature joints where they occur with colonnade joints, which Budkewitsch & Robin, (1994) and Faust (1978) considered to be processes of convective heat transfer. Platy - prismatic joints are fracture cleavage which is superimposed onto pre-existing cooling joints of the curvilinear type (Bennecke, 1996). A colonnade is a single tier of columnar jointed rock where individual columns can be traced from the upper to the lower bounding surface and those surfaces are roughly perpendicular to the boundaries (Budkewitsch & Robin, 1994). Such columns do not separate against other joints in the tier and remain broadly parallel to a common direction (Budkewitsch & Robin, 1994). Colonnade joints are referred to as widely-spaced (40 – 200 cm) and relatively planar tiers (DeGraff *et al.,* 1989). An entablature is a tier that exhibits closely-spaced (20 – 40 cm), planar to irregularly curved joints which bound columns that may form radial patterns or otherwise deviate from the vertical direction, typically separating the upper and lower colonnades (DeGraff *et al.,* 1989). These jointing patterns were exposed by quarrying in the Auckland pit which may also be the result of these platy - prismatic joints from colonnade joints.

Looking into the Auckland pit from a remote view point, it can be observed that the lower area is considerably horizontal-jointed, middle area is entablature-jointed indicating closely spaced, irregular curved joints that have deviated from the common direction of colonnade joints and the upper area which consists of columnar joints, indicating the slow cooling process of the upper zone of the basalt flow (Figs. 3.4, 3.5, 3.6).

6.5 Scoria Facies

Most of the scoria deposits occur within the exposed outcrop of the Auckland pit, due to quarrying. The sequence consists of weakly stratified, moderate to very vesicular, well-sorted scoria lapilli clasts, with larger blocks/bombs intermittently distributed throughout the exposure, observed from view points and photographs within the pit. In drill cores, three scoria deposits were identified as Facies B. In each drill core, the scoria overlies the lava flows and an intercalated sediment deposit. The scoria cone was probably built up relatively quickly through explosive strombolian activity (Blackburn *et al.*, 1976) without any noticeable change in eruption conditions, perhaps reflecting more rapid accumulation of hot clasts (Head & Wilson, 1989). The scoria appears to be primarily fallout material within drill core observations, due to the nearby eruption of the scoria cone within the Bombay Quarry. The scoria thickness within the drill cores suggests that they were drilled from the outer flanks of the scoria cone. Strombolian eruptions commonly eject pyroclastic material beyond the vicinity of the scoria cone (Wood, 1980) and the scoria may have been preserved due to relatively rapid burial by lava flows.

6.6 Vent Source

The South Auckland Volcanic Field consists of volcanic centres that are much older, more weathered and eroded than those of the younger Auckland field. Although there are clearly explosive eruption vents near the Auckland pit (e.g. tuff ring, scoria cone), there is no evidence that these erupted the lava flows observed here. The vent location of the basalt lavas within the Auckland pit is unknown. Most of the volume of the SAVF comprises lava flows of several prominent basalt shields (e.g., Pukekohe and Bombay Volcanic Complex complexes; Pittari *et al.*, 2012). In this study, it is assumed that the basalts found within the Auckland pit are associated with the nearby Bombay Volcanic Complex, which has a peak 3 km northeast of the Bombay Quarry. The size and geomorphology of the Bombay Volcanic Complex and the surrounding area has not been defined, therefore, the basalt from the Auckland pit could have

originated from the flanks of the Bombay Volcanic Complex and not from the peak. There are also multiple deposits of basalts surrounding the area with overlapping volcanic and sedimentary deposits, which further illustrates that the deposits may be from vents that could be from the flanks or the peak of the Bombay Volcanic Complex.

The basalt lavas in the Auckland pit are considered to be pahoehoe lava flows which erupted from vents on the Bombay Volcanic Complex (geographic location unknown). These lavas travelled down through the valley reaching the location of the Auckland pit where they infilled the pre-existing palaeovalley and either ponded there due to the slope becoming gentle or the lava had sufficiently cooled by the time it reached the valley; in both cases stopping the lava flow.

Another alternative scenario is that the basalt lava accumulated within a vent instead of a valley; however, this scenario is unlikely due to there being three basalt lava flows with intercalated scoria and sediments, instead of there being one massive deposit of basalt lava. The most likely scenario is the basalt originated from the Bombay Volcanic Complex, as evidence suggested in this study, shows that the basalt thickness decreases from the northwest to southeast, and possibly reflecting the flow direction by which the lava was emplaced.

6.7 Intercalated Sediments and Tephra Layer

Intercalated sediments present between the basalt lava flows within the Auckland pit, indicate a period of volcanic quiescence where sedimentary material was deposited. Sediments between the basalt lava flows are considered to be mid-Quaternary alluvium deposits of commonly pumiceous rich sand and silt/mud, loess and paleosols. Parts of these sedimentary intervals are also considered to correlate to the Kauroa ash formation which comprises a sequence of extremely weathered, clay-rich, rhyolitic tephra deposits recognised largely in the Waikato region (Ward, 1967; Pain, 1975; Salter, 1979; Kirkman, 1980a). The Kauroa ash has been dated at 2.3 – 0.95 Ma (Lowe & Percival, 1993) which is correlated with the SAVF being active during 1.59 to 0.51 Ma (Pittari *et al.*, 2012; Briggs, 2012).

A tephra layer was identified within the drill cores in the Auckland pit and was also visible in outcrop between sediment deposits. The rhyolitic tephra layer is a normally-graded fall unit and it is suggested here that it correlates to the tephra layer AT-71 which was derived from the Taupo Volcanic Zone (TVZ) between 1 and 1.2 million years ago (Alloway *et al.,* 2004), and has also been found in the nearby Waikato pit (Gibson, 2011). This tephra layer is correlated with the post-Ongatiti tephra layer at Schnapper Rock in Beachlands (Alloway *et al.,* 2004; Gibson, 2011) and is also linked to the Mangakino volcanic centre that was active from the commencement of rhyolitic volcanism in the TVZ during 1.6 Ma through to the last eruption that took place around 0.91 Ma (Wilson, 1986a; Briggs *et al.,* 1993; Wilson *et al.,* 1995; Brink, 2012).

6.8 Magma Source

Two groups of basalts are distinguished in the SAVF based on mineralogy and geochemical compositions, but no temporal or spatial patterns exist in the distribution of the various lava types of each group within the field: Group A basalts are silica-undersaturated, transitional to quartz-tholeiitic basalts with relatively low total alkalis (3.0 – 4.6 wt. %) and Nb (7 – 29 ppm); Group B basalts are strongly silica-undersaturated basanites to nepheline-hawaiites with high total alkalis (3.3 – 7.9 wt. %) and Nb (32 – 102 ppm) (Cook *et al.,* 2005).

In this study, the basalts within the Auckland pit are associated with group B lavas determined by Cook (2002). Studies of the continental intraplate volcanic fields elsewhere in the world demonstrate that they commonly consist of alkalic basalts characterized by strongly silica-undersaturated to less silica-undersaturated compositions (Huang *et al.,* 1997; Zhang *et al.,* 2001). Despite their wide range of geographic distribution, these basalts commonly share ocean island basalt (OIB)-like geochemical characteristics. The South Auckland basalts have geochemical compositions and OIB-like geochemical characteristics (Cook, 2002), which differ from groups of alkalic basalts elsewhere, because each group appears to have evolved as a set of distinct lineages. In addition, group A and B basalts exhibit subtle, but distinct variations in abundances of the large ion lithophile elements (LILE), high field strength elements (HFSE), rare earth elements (REE)

and isotopic compositions (Cook *et al.,* 2005). Such variations are commonly attributed to source heterogeneity, or variable degrees of partial melting, or both (Zou & Zindler, 1996).

Contrasting geochemical trends and incompatible element ratios (e.g. K/Nb, Zr/Nb and Ce/Pb) are consistent with separate evolution of groups A and B from dissimilar parental magmas derived from distinct sub-continental lithospheric mantle sources. Differentiation within each group was controlled by olivine and clinopyroxene fractionation, supported by a number of melting experiments, involving garnet and spinel peridotite compositions of Green (1973a) which demonstrate that the primary magmas from group B can be generated from a garnet-bearing peridotite source (60 % olivine, 18 % orthopyroxene, 14 % clinopyroxene and 8 % garnet), by degrees of partial melting that range from < 2 to 15 %. In comparison, group A magmas were derived from a spinel peridotite source (58 % olivine, 25 % orthopyroxene, 15 % clinopyroxene and 2 % spinel), by degrees of partial melting in the range 7 – 30 % (Cook, 2002).

Overall, group A and B basalts evolved as a set of distinct volcanic lineages that do not appear to be related by processes such as variable degrees of melting of a common mantle source or by fractional crystallization of a common parental magma. Furthermore, there is no apparent temporal or spatial pattern between or among the various lava types that make up each group. The distinct geochemical differences between group A and B basalts reflect differences in their respective mantle sources, which is supported by contrasting incompatible element ratios, such as K/Nb, Sr/Nb, and Zr/Nb (Cook, 2002; Cook *et al.*, 2005). This source type may have resulted from subduction-related metasomatism of the sub-continental lithosphere. These events were associated with Mesozoic or earlier subduction and plume-related magmatism, when New Zealand was at the eastern margin of the Gondwana supercontinent (Cook *et al.*, 2005).

The fact that all the Auckland pit basalts, and probably the basalts from the Waikato pit, are all group B lavas, implies that the volcanic eruptions at this location must have used the same source that generates a garnet-bearing peridotite magma over time, beneath the Bombay Volcanic Complex. The Drury fault, which strikes in a north to south direction near the Bombay quarry on the eastern

side, may have provided an easy pathway for the magma to reach the surface and produce a basaltic eruption of group B lavas.

6.9 Comparison to the Volcanic Succession in the Waikato Pit

The Waikato pit is situated adjacent to the Auckland pit and the volcanic and sedimentary deposits are similar. The Waikato pit consists of Waitemata and Tauranga group country rock that has eroded into a palaeovalley, separated by a ridge line next to the Auckland pit. This implies that there are two distinctive palaeovalleys that exist within the Bombay Quarry.

Gibson (2011) identified two large deposits of basalt lava, however, in this study, three basalt lavas were identified from drill cores. This suggests the third (lower) basalt was not identified from the Waikato pit. However, there is a possibility of lower basalt being there but just not accessible without drilling further down into the pit to reveal the basalt lava. Gibson (2011) described the basalts as a dense, hypocrystalline, fine grained, porphyritic basalt with olivine and pyroxene phenocrysts, within a plagioclase lath groundmass, which are similar with basalts from the Auckland pit.

Several scoria and spatter cones were described by Gibson (2011) as highly vesicular (49 – 65 %), which are similar to several scoria deposits in this study, however spatter cones were not observed in the Auckland pit. Between the basalt lavas, Quaternary alluvium and/or Kauroa ash sediments were identified in this study. However, Gibson (2011) did not identify these sedimentary beds between lavas in the Waikato pit. However, the distal tephra layer dated at 1 – 1.2 Ma (Alloway *et al.,* 2004) that Gibson (2011) identified in the Waikato Pit is correlated to a tephra layer on the eastern side of the Auckland pit.

Gibson (2011) focused on the tuff ring deposit on the upper area of the Waikato pit. Two facies were identified within the tuff ring succession: well sorted coarse ash to fine lapilli (A) and poorly sorted coarse lapilli (B) which alternate in the exposed section. Gibson (2011) determined that overall, the tuff ring generally becomes finer upward through the tuff succession. In this study, a tuff ring deposit is also observed at the upper area of the Auckland pit, which may

be an extension of the tuff ring observed above the Waikato pit, or a tuff ring from a different phreatomagmatic eruption.

Geochemical analysis of the basalts from the Waikato pit identified by Cook (2002) and Gibson (2011) reveal the basalt lavas are of group B which are generated from a garnet-bearing peridotite source which is consistent with the basalts in the Auckland pit. This suggests that the basalts from both the Auckland and Waikato pit are from the same magma source beneath the Bombay area that only seems to produce group B lavas over time.

Overall, the volcanic succession of the Waikato and the Auckland pit seem to reveal a similar volcanic history, where different volcanic and sedimentary units are deposited within the two distinctive palaeovalley.

6.10 Eruption History of the Succession in the Auckland Pit

Before any eruptions occurred, the area of the Bombay Quarry consisted of Waitemata and Tauranga group country rock that had been eroded into a hill-and-valley landscape (Fig. 6.1A).

Effusive volcanism first occurred with the emplacement of the older (lower basalt) lava flow into the palaeovalley where it ponded (Fig. 6.1A). The eruption must have had a stable outpouring of lava, fire fountaining, or a mixture of both to deposit a relative small, but thick deposit. Multiple layers of horizontal 'sheeted' joints were formed where the basalt had formed lava-tubes (Figs. 3.5, 3.6).

A period of volcanic quiescence occurred where Quaternary sediments of alluvial pumiceous sand, silt/mud and/or Kauroa ash formation were deposited above the lower basalt flow (Fig. 6.1B) likely to have been derived locally from floodplains and/or from distal volcanism from the TVZ. An effusive eruption occurred depositing the massive and thick middle basalt lava over the Quaternary and Kauroa ash sediments (Fig. 6.1C) and produced multiple horizontal-sheeted joints. Entablature irregular curved joints occurred where the columns deviate from the common vertical direction of the colonnade joints.

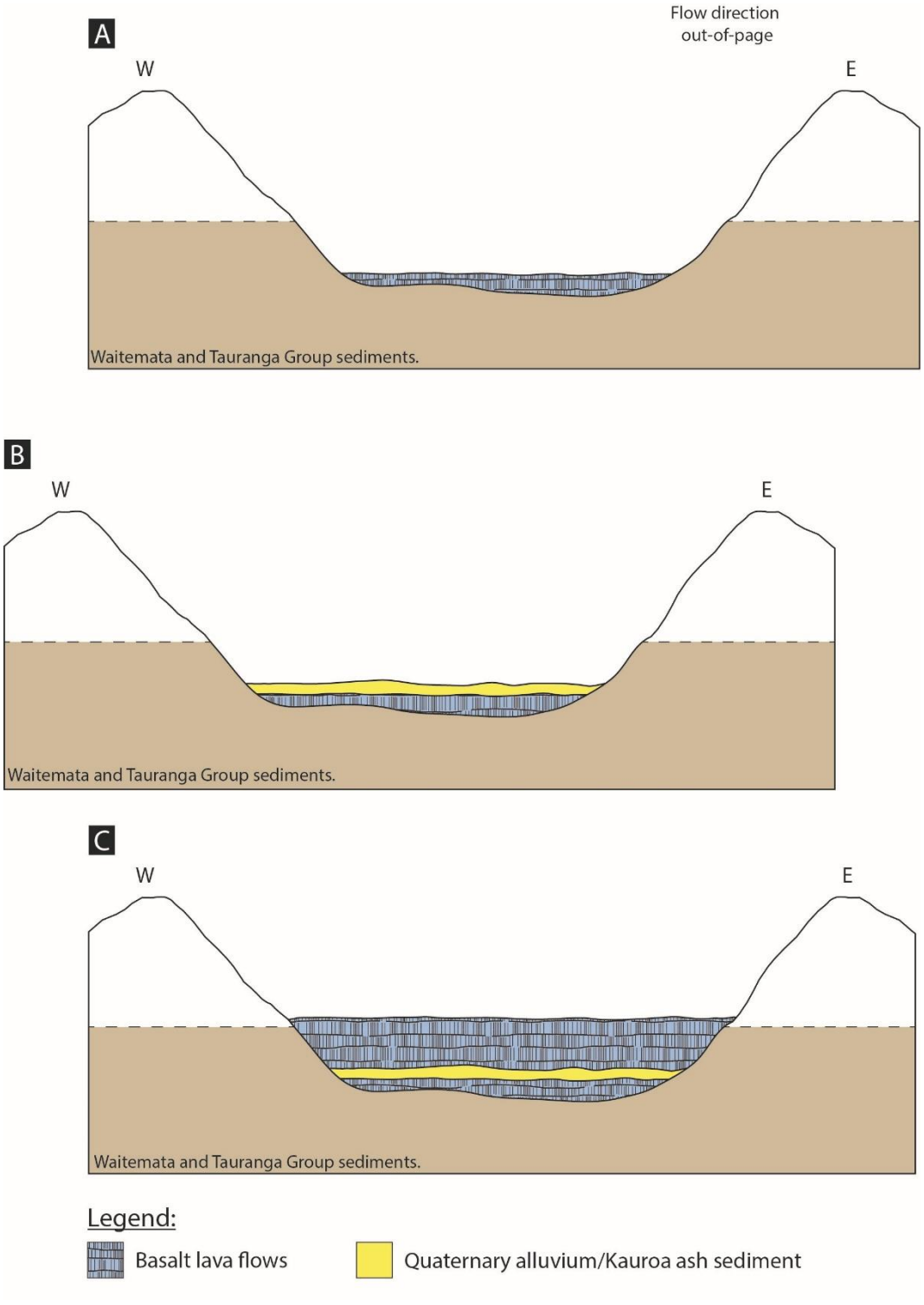

Figure 6.1: Illustration of the volcanic eruption of the Auckland pit. (A) Waitemata and Tauranga group exposed as basement rocks within the palaeovalley and deposition of the lower basalt. (B) Quaternary alluvium/Kauroa ash sediment deposition. (C) Deposition of middle basalt. (D) Deposition of intercalated scoria and tephra within the Quaternary

alluvium/Kauroa ash sediments. (E) Deposition on the upper basalt. (F) Deposition of Quaternary alluvium/Kauroa ash sediments and tuff ring.

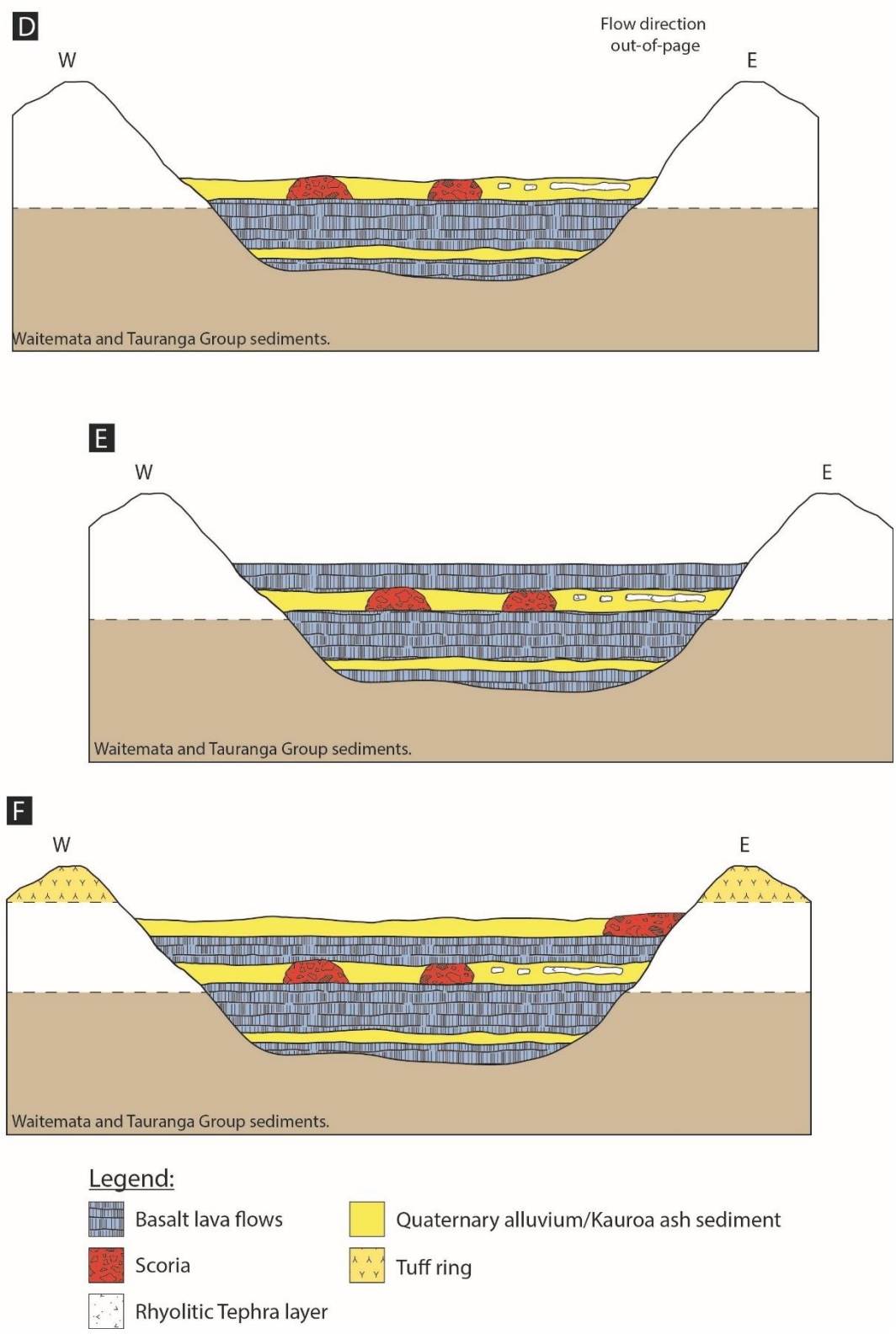

Figure 6.1: Continued.

Another period of volcanic quiescence followed the emplacement of the middle basalt, where further Quaternary sediments of alluvial pumiceous sand, silt/mud and/or Kauroa ash formation were deposited above the middle basalt flow (Fig. 6.1D). A tephra deposit is intercalated with the Kauroa ash formation where it is dated at 1 - 1.2 Ma (Alloway *et al.*, 2004) and is associated with the post-Ongatiti tephra layer.

During this time, explosive strombolian eruptions also occurred locally, within the area of the Auckland pit, producing at least two or more scoria cones (Fig. 6.1D; e.g., Cas, 1989). Strombolian eruptions are characteristic of basaltic volcanoes which consist of prolonged sequences of intermittent, short-lived explosions, usually lasting a few seconds to several minutes. Strombolian clasts of ejecting ash to bombs, typically reach heights of < 100 m above the vent and the plume generated by the explosion generally rise to < 200 m (Parfitt, 2004; Houghton & Gonnermann, 2008). Scoria cones would have been erupted at shorter trajectories and higher explosivity (Sumner *et al.*, 2005), forming massive deposits within the quarry walls.

Another effusive eruption occurred depositing a younger thick unit of lava (upper basalt), overlying the scoria and Quaternary alluvium and/or Kauroa ash sediments (Fig. 6.1E). The eruption must have had a steady supply of lava to produce columnar basalt that extended across the centre of the valley (Figs. 3.4, 3.6). Within the basalt, multiple layers of sheeted basalt are also present where the basalt had formed lava tubes, or where the basalt was overriding the base of the cooled lava surface.

Volcanic quiescence again allowed the deposition of further Quaternary alluvial sediments and/or Kauroa ash above the youngest basalt flow (Fig. 6.1F). A scoria cone erupted by a strombolian eruption from a nearby vent on the eastern side of the pit depositing basaltic lapilli and blocks/bombs above the uppermost Quaternary alluvium and/or Kauroa ash sediments (Fig. 6.1F).

The final stage of volcanism, which followed after another period of volcanic quiescence, involved a phreatomagmatic eruption that ensued as rising magma interacted with a water source and produced a tuff ring deposit above the

underlying volcanic succession (Fig. 6.1G). In the later stages, a dike intrusion occurred on the western side of the Auckland pit, intruding the Quaternary alluvium and/or Kauroa ash sediments which then reached the surface and released a small flow within a small depression.

In this study, the volcanic deposit of the tuff ring and the dike intrusion were not studied in the Auckland pit, and therefore the volcanic eruption history is from observations only.

Chapter Seven

Conclusions

This study focuses on the Auckland pit in the Bombay Quarry which lies on the western side of the South Auckland Volcanic Field that was active 1.59 – 0.51 Ma. The SAVF comprises at least 82 known volcanic centres that are exposed and easily accessible. The Bombay Volcanic Complex is a large basaltic volcano that comprises a succession of multiple volcanic and sedimentary deposits which are exposed within the Bombay Quarry and, in particular for this study, the recently opened Auckland pit.

Stratigraphic logs of drill core show that within the Auckland pit there are three individual basalt lava flows with intercalated scoria and sedimentary deposits that were emplaced within a palaeovalley.

Basalt facies show a range of vesicularities and textural characteristics which are generally arranged within each lava flow into an upper and lower vesicular zone and a dense coherent non-vesicular zone; this facies architecture is typical of pahoehoe to transitional lava flows. Intercalated sediment overlies each of the three basalt lava flows, representing periods of volcanic quiescence. Scoria deposits within the basalt indicate a change in magmatic eruption style to strombolian.

Petrography of the three basalts reveal that each lava flow has similar mineral characteristics of olivine, clinopyroxene, plagioclase, opaques, mafic minerals and vesicle texture, however, there are slight differences in their proportions for each lava flow.

From geochemical analysis, there is a slight difference in mineral compositions between the three lava flows. The upper and lower basalt flows have higher Mg-rich and calcic-rich compositions than the middle basalt with lower Mg-rich and calcic-rich mineral compositions. The three basalts, however, are all within the broad group B basalt type which is recognised with the SAVF lavas.

The Auckland pit has revealed that the succession of volcanic and sedimentary units, deposited within the palaeovalley is characteristic of a polygenetic eruption history. From this interpretation, the Waikato pit should also have a polygenetic eruption history, as it lies adjacent to the Auckland pit. Considering the Auckland pit lavas are related to the larger, broad Bombay Volcanic Complex nearby, it should be considered that the Bombay Volcanic Complex has multiple volcanic/sediment deposits and a polygenetic eruption history.

Future work on the Bombay Volcanic Complex could include a more detailed study of the palaeo-environment and origin of the sedimentary units to better focus on the history of the Bombay Volcanic Complex.

The evolution of the volcanic and sedimentary units in this thesis offers insight into the importance of polygenetic volcanoes within monogenetic fields and may be an ideal analogue for understanding the future of shield volcanism in both the South Auckland and Auckland Volcanic Fields (i.e. Rangitoto Island).

References

Alloway, B., Westgate, J., Pillans, B., Pearce, N., Newnham, R., Byrami, M. & Aarburg, S. (2004). Stratigraphy, age and correlation of middle Pleistocene silicic tephras in the Auckland region, New Zealand: a prolific distal record of Taupo Volcanic Zone volcanism. *New Zealand Journal of Geology and Geophysics*, vol. 47, pp. 447-479.

Aubele, J. C., Crumpler, L. S., & Elston, W. E. (1988). Vesicle zonation and vertical structure of basalt flows. *Journal of Volcanology and Geothermal Research*, *35*(4), 349-374.

Bennecke, W. M. (1996). Basalt Features Observed in Outcrops, Cores, Borehole Video Imagery and Geophysical Logs, and Basalt Hydrogeologic Study at the Idaho, *National Engineering Laboratory, Eastern Idaho.* MSc thesis, Boise State University, Boise, ID.

Blackburn, E. A., Wilson, L., & Sparks, R. J. (1976). Mechanisms and dynamics of strombolian activity. *Journal of the Geological Society*, *132*(4), 429-440.

Briggs, R.M., Gifford, M.G., Moyle, A.R., Taylor, S.R., Normaff, M.D., Houghton, B.F. & Wilson, C.J.N. (1993). Geochemical zoning and eruptive mixing in ignimbrites from Mangakino volcano, Taupo Volcanic Zone, New Zealand. *Journal of volcanology and Geothermal Research*, vol. 56, pp. 175-203.

Briggs, R. M., Okada., T., Itaya, T., Shibuya, H. & Smith, I. E. M. (1994). K-ar ages, paleomagnetism, and geochemistry of the South Auckland volcanic field, North Island, New Zealand. *New Zealand Journal of Geology and Geophysics*, vol. 37, pp. 143-153.

Briggs, R. (2012). The influence of subsurface hydrogeology on the nature and localisation of volcanism in the South Auckland Volcanic Field. *Geoscience Society of New Zealand Miscellaneous Publication 131A*, 17.

Brink, M. T. (2012). Emplacement processes of ignimbrites in the Ongatiti Valley, southeast Te Kuiti. MSc thesis, University of Waikato, Hamilton, New Zealand.

Budkewitsch, P., & Robin, P. Y. (1994). Modelling the evolution of columnar joints. *Journal of Volcanology and Geothermal Research*, *59*(3), 219-239.

Cas, R. A. F. (1989). 'Physical Volcanology', in R. W. Johnson (ed.). *Intraplate Volcanism*, Cambridge University Press, Cambridge, pp. 55-87.

Cas, R., Porritt, L., Pittari, A., & Hayman, P. (2008). A new approach to kimberlite facies terminology using a revised general approach to the nomenclature of all volcanic rocks and deposits: descriptive to genetic. *Journal of Volcanology and Geothermal Research*, *174*(1), 226-240.

Cashman, K. V., & Kauahikaua, J. P. (1997). Reevaluation of vesicle distributions in basaltic lava flows. *Geology*, *25*(5), 419-422.

Cashman, K. V., Thornber, C., & Kauahikaua, J. P. (1999). Cooling and crystallization of lava in open channels, and the transition of Pāhoehoe Lava to'A'ā. *Bulletin of Volcanology*, *61*(5), 306-323.

Cole, J. W., (1986). Distribution and tectonic setting of late Cenozoic volcanism in New Zealand. *In*: Smith, I.E.M. (*ed*.), Late Cenozoic volcanism in New Zealand. *Royal Society of New Zealand Bulletin*, *23*:7-20.

Connor, C. B. & Conway, F. M. (2000). Basaltic Volcanic Fields, in H. Sigurdsson (ed.). *Encyclopedia of Volcanoes*, Academic Press, California, pp. 331- 343.

Cook, C. (2002). Petrogenesis and evolution of alkalic basaltic magmas in a continental intraplate setting: the South Auckland Volcanic Field, New Zealand. Ph.D. thesis, University of Waikato, Hamilton, New Zealand.

Cook, C., Briggs, R. M., Smith, I. E., & Maas, R. (2005). Petrology and geochemistry of intraplate basalts in the South Auckland volcanic field, New Zealand: evidence for two coeval magma suites from distinct sources. *Journal of Petrology*, *46*(3), 473-503.

Crisp, J., & Baloga, S. (1994). Influence of crystallization and entrainment of cooler material on the emplacement of basaltic aa lava flows. *Journal of Geophysical Research: Solid Earth*, *99*(B6), 11819-11831.

DeGraff, J. M., Long, P. E., & Aydin, A. (1989). Use of joint-growth directions and rock textures to infer thermal regimes during solidification of basaltic lava flows. *Journal of Volcanology and Geothermal Research*, *38*(3), 309-324.

Edbrooke, S. W. (2001). *Geology of the Auckland Area*, Institute of Geological and Nuclear Sciences Limited, Lower Hutt, New Zealand.

Faust, G. T. (1978). *Joint systems in the Watchung basalt flows, New Jersey*. Professional Paper 864-B. United States Government Printing Office, Washington DC.

Furlong, K. P. & Kamp, P. J. J. (2009). The lithospheric geodynamics of plate boundary transpression in New Zealand: Initiating and emplacing subduction along the Hikurangi margin, and the tectonic evolution of the Alpine Fault system. *Tectonophysics*, 474 (1-4): 449-462.

Gibson, A. C. (2011). Volcanology of tuff rings at Kellyville, Onewhero and Bombay, South Auckland Volcanic Field. MSc thesis. University of Waikato, Hamilton, New Zealand.

Goehring, L., & Morris, S. W. (2008). Scaling of columnar joints in basalt. *Journal of geophysical research: Solid Earth*, *113*(B10).

Green, D. H. (1973a). Conditions of melting of basanite magma from garnet peridotite. *Earth and Planetary Science Letters* 17, 456–465.

Hare, A. G., & Cas, R. A. F. (2005). Volcanology and evolution of the Werribee Plains intraplate, basaltic lava flow-field, Newer Volcanics Province, southeast Australia. *Australian Journal of Earth Sciences*, *52*(1), 59-78.

Hayward, B. W. (2015). Helvetia Volcano–A Newly Recognised Tuff Ring and Maar In The South Auckland Volcanic Field. *Auckland GeoClub Magazine, No. 12.*

Head, J. W., & Wilson, L. (1989). Basaltic pyroclastic eruptions: influence of gas-release patterns and volume fluxes on fountain structure, and the formation of cinder cones, spatter cones, rootless flows, lava ponds and lava flows. *Journal of Volcanology and Geothermal Research*, *37*(3), 261-271.

Hon, K., Kauahikaua, J., Denlinger, R., & Mackay, K. (1994). Emplacement and inflation of pahoehoe sheet flows: Observations and measurements of active lava flows on Kilauea Volcano, Hawaii. *Geological Society of America Bulletin*, *106*(3), 351-370.

Houghton, B. F., & Gonnermann, H. M. (2008). Basaltic explosive volcanism: Constraints from deposits and models. *Chemie der Erde - Geochemistry*, *68*(2), 117-140.

Huang, Y., Hawkesworth, C., van Calsteren, P., Smith, I. E. M. & Black, P. (1997). Melting generation models for the Auckland volcanic field, New Zealand: constraints from U–Th isotopes. Earth and Planetary Science Letters 149, 477–489.

Ilanko, T. (2010). Eruption and emplacement processes of the Barriball Road tuff ring, South Auckland. MSc thesis, University of Waikato, Hamilton, New Zealand.

Isaac, M. J., Herzer, R. H., Brook, F. & Hayward, B. W. (1994). *Cretaceous and Cenozoic basins of Northland, New Zealand*. Institute of Geological and Nuclear Sciences Monograph no. 8, 203 pp.

John O'Brien Associates, Boffa Miskell Partners & John Thacker and Associates (1994), *Management Plan and Emergency Procedures Bombay Quarry*, Milburn New Zealand Ltd, Auckland.

Kamp, P. J., & Lowe, D. J. (1981). Quaternary stratigraphy, landscape, and soils of the Hamilton Basin. In *Geological Society of New Zealand Annual Conference* (pp. 14-28). University of Waikato, Hamilton, New Zealand.

Kear, D., Schofield, J. C., & Couper, R. A. (1978). *Geology of the Ngaruawahia subdivision* (No. 88). Dept. of Scientific and Industrial Research, New Zealand.

Keszthelyi, L., (2002). Classification of the mafic lava flows from ODP Leg 183. *In* Frey, F.A., Coffin, M.F., Wallace, P.J., and Quilty, P.G. (Eds.), *Proc. ODP, Sci. Results*, 183.

King, P. R. (2000). Tectonic reconstructions of New Zealand: 40 Ma to Present. *New Zealand Journal of Geology and Geophysics*, 43: 611-638.

Kirkman, J. H. (1980a). Mineralogy of the Kauroa Ash formation of south-west and west Waikato, North Island, New Zealand. *New Zealand Journal of Geology and Geophysics*, *23*(1), 113-120.

Lipman, P. W., & Banks, N. G. (1987). AA flow dynamics, Mauna Loa 1984.*US Geol Surv Prof Pap*, *1350*, 1527-1567.

Lowe, D. J., Percival, H. J. (1993). Clay mineralogy of tephras and associated paleosols and soils, and hydrothermal deposits, North Island. Guide Book for New Zealand PreConference Field Trip F.1, 10th International Clay Conference, Adelaide, Australia. 110 pp.

Lowe, D. J., Tippett, J. M., Kamp, P. J., Liddell, I. J., Briggs, R. M., & Horrocks, J. L. (2001). Ages on weathered Plio-Pleistocene tephra sequences, western North Island, New Zealand. *Les Dossiers de l'Archeo-Logis*, *1*, 45-60.

Macdonald, G. A. (1953). Pahoehoe, aa, and block lava. *American Journal of Science*, *251*(3), 169-191.

Mallet, R. (1875). On the origin and mechanism of production of the prismatic (or columnar) structure of basalt. *Philos. Mag.*, 50, 122–135, 201–226.

Mullane, K. J. C. (2015). Geophysical characterisation of the Onewhero and Kellyville volcanic complexes, South Auckland Volcanic Field. MSc thesis, University of Waikato, Hamilton, New Zealand.

Nemeth, K., Agustin-Flores, J., Briggs, R., Cronin, S. J., Kereszturi, G., Lindsay, J. M., Pittari, A. & Smith, I. E. M. (2012). Monogenetic volcanism of the South Auckland and Auckland Volcanic Fields. IAVCEI – IASIMC Conference, Auckland, New Zealand.

Nemeth, K., & Kereszturi, G. (2015). Monogenetic volcanism: Personal views and discussion, *International Journal of Earth Science*, vol. 104, pp. 2131-2146.

Ormiston Associates Ltd (1999). *Review of basalt resource at Bombay Quarry*, Auckland.

Pain, C. F. (1975). Some tephra deposits in the south-west Waikato area, North Island, New Zealand. *New Zealand journal of geology and geophysics*, *18* (4), 541-550.

Parfitt, E. A. (2004). A discussion of the mechanisms of explosive basaltic eruptions. *Journal of Volcanology and Geothermal Research,* vol. 134, pp. 77-107.

Pittari, A., Briggs, R., Ilanko, T., Gibson, A., Rosenberg, M., & Németh, K. (2012). Variation in deposit characteristics and eruption processes across the lifetime of a monogenetic field, the South Auckland volcanic field. *Geoscience Society of New Zealand Miscellaneous Publication 131A*, 70.

Polacci, M., & Papale, P. (1997). The evolution of lava flows from ephemeral vents at Mount Etna: insights from vesicle distribution and morphological studies. *Journal of Volcanology and Geothermal Research*, *76*(1), 1-17.

Polacci, M., Cashman, K. V., & Kauahikaua, J. P. (1999). Textural characterization of the pahoeho-a a transition in Hawaiian basalt. *Bulletin of Vocanology*, 60(8), 595-609.

Rafferty, W. J. (1977). The volcanic geology and petrology of South Auckland, MSc thesis, University of Auckland, Auckland, New Zealand.

Rafferty, W. J. & Heming, R. F. (1979). Quaternary alkalic and sub-alkalic volcanism in South Auckland, New Zealand. *Contributions to Mineralogy and Petrology*, *1*(2), 139-150.

Rollinson, H. (1993). Using geochemical data: Evaluation, Presentation, Interpretation. Longman Group Limited. Essex, England. 352 pp.

Rosenberg, M. D. (1991). The nature and mechanisms of phreatomagmatic volcanism in the South Auckland volcanic field. MSc thesis, University of Waikato, Hamilton, New Zealand

Rowland, S. K., & Walker, G. P. (1990). Pahoehoe and aa in Hawaii: volumetric flow rate controls the lava structure. *Bulletin of Volcanology*,*52*(8), 615-628.

Ryan, M. P., and C. G. Sammis (1978). Cyclic fracture mechanisms in cooling basalt. *Geol. Soc. Am. Bull.*, 89, 1295–1308.

Salter, R. T. (1979). A pedological study of the Kauroa Ash Formation at Woodstock. MSc thesis, University of Waikato, Hamilton, New Zealand.

Schofield, J. C. (1958). Notes on the volcanism and structure in Franklin County. *New Zealand Journal of Geology and Geophysics*, *1*, 541-559.

Selby, M. J., & Lowe, D. J. (1992). *The middle Waikato Basin and hills*. Auckland, New Zealand: Longman Paul.

Self, S., Thordarson, T., Keszthelyi, L., Walker, G. P. L., Hon, K., Murphy, M. T., & Finnemore, S. (1996). A new model for the emplacement of Columbia River basalts as large, inflated pahoehoe lava flow fields. *Geophysical Research Letters*, *23*(19), 2689-2692.

Sumner, J. M., Blake, S., Matela, R. J. & Wolff, J. A. (2005). 'Spatter'. *Journal of Volcanology and Geothermal Research, 142*, 49-65.

Taylor, S. N. (2012). Volcanology of the Raventhorpe and Pokeno West Volcanic Complexes, South Auckland Volcanic Field. MSc thesis, University of Waikato, Hamilton, New Zealand.

Thompson, R. N. (1984). Dispatches from the basalt front. I. Experiments. *Proceedings of the Geologists' Association*, *95*(3), 249-262.

Tonkin, P. J. (1970). Contorted stratification with clay lobes in volcanic ash beds, Raglan-Hamilton region, New Zealand.

Tripathi, A. R. P., Kamp, P. J., & Nelson, C. S. (2008). Te Kuiti Group (Late Eocene-Oligocene) lithostratigraphy east of Taranaki Basin in central-western North Island, New Zealand. Unpublished Petroleum Report PR3900. Ministry of Economic Development, New Zealand, 70 pp.

Ward, W. T. (1967). Volcanic ash beds of the lower Waikato Basin, North Island, New Zealand. *New Zealand Journal of Geology and Geophysics 10*: 1109-1135.

White, J. D. L. (1991). The *Depositional record of small, monogenetic volcanoes within terrestrial Basins*. SEPM Publication 45. Society for Sedimentary Geology.

Wilmoth, R. A., & Walker, G. P. (1993). P-type and S-type pahoehoe: a study of vesicle distribution patterns in Hawaiian lava flows. *Journal of Volcanology and Geothermal Research*, *55*(1), 129-142.

Wilson, C. J. N. (1986a). 'Reconnaissance Stratigraphy and Volcanology of Ignimbrites from Mangakino Volcano', in Smith, I.E.M. (ed). *Late Cenozoic Volcanism in New Zealand*. Royal Society of New Zealand Bulletin, vol.23, pp.179-193.

Wilson, C.J.N., Houghton, B.F., McWilliams, M.O., Lanphere, M.A., Weaver, S.D. & Briggs, R.M. (1995). 'Volcanic and Structural Evolution of Taupo Volcanic Zone, New Zealand: A Review'. *Journal of Volcanology and Geothermal Research, 68,* 1-28.

Wood, C. A. (1980). Morphometric evolution of cinder cones. *Journal of Volcanology and Geothermal Research*, *7*(3), 387-413.

Zhang, M., Stephenson, P. J., O'Reilly, S. Y., McCulloch, M. T. & Norman, M. (2001). Petrogenesis and geodynamic implications of late Cenozoic basalts in North Queensland, Australia: trace element and Sr–Nd–Pb isotope evidence. *Journal of Petrology 42*, 685–719.

Zou, H. & Zindler, A. (1996). Constraints on the degree of dynamic partial melting and source composition using concentration ratios in magmas. *Geochimica et Cosmochimica Acta 60*, 711–717.

Appendices

Appendix I

Sample Catalogue

University of Waikato No.	Sample No./ Thin section No.	Drill core	Drill core Sample No.	Rock/Sediment	Location	Thin Section	Point Counted	XRF	EPMA
W160301	1	C303	2	Basalt (Non-vesicular)	Auckland pit, Bombay Quarry	X	X	X	
W160302	2	C303	1	Basalt	Auckland pit, Bombay Quarry	X			
W160303	3	C302	1	Basalt	Auckland pit, Bombay Quarry	X	X	X	
W160304	4	C302	3	Basalt (Non-vesicular)	Auckland pit, Bombay Quarry	X			
W160305	5	C302	4	Basalt (Vesicle trails)	Auckland pit, Bombay Quarry	X	X	X	
W160306	6	C302	6	Basalt (Non-vesicular)	Auckland pit, Bombay Quarry	X	X	X	
W160307	7	C308	1	Basalt	Auckland pit, Bombay Quarry	X	X	X	
W160308	8	C308	3	Basalt	Auckland pit, Bombay Quarry	X			
W160309	25	C308	4	Basalt	Auckland pit, Bombay Quarry	X	X	X	
W160310	26	C308	6	Basalt	Auckland pit, Bombay Quarry	X			
W160311	10	C309	1	Basalt	Auckland pit, Bombay Quarry	X			
W160312	11	C309	2	Basalt	Auckland pit, Bombay Quarry	X	X	X	X
W160313	12	C309	4	Basalt (Non-vesicular)	Auckland pit, Bombay Quarry	X	X	X	X
W160314	13	C309	6	Basalt	Auckland pit, Bombay Quarry	X	X	X	X
W160315	16	C321	3	Basalt (Non-vesicular)	Auckland pit, Bombay Quarry	X			
W160316	17	C321	6	Basalt (Non-vesicular)	Auckland pit, Bombay Quarry	X			
W160317	18	C321	7	Basalt	Auckland pit, Bombay Quarry	X			
W160318	19	C321	9	Basalt (Weathered)	Auckland pit, Bombay Quarry	X			
W160319	20	C310	1	Basalt (Non-vesicular)	Auckland pit, Bombay Quarry	X	X	X	
W160320	21	C310	2	Basalt	Auckland pit, Bombay Quarry	X			
W160321	22	C306	1	Basalt	Auckland pit, Bombay Quarry	X	X	X	

University of Waikato No.	Sample No./ Thin section No.	Drill core	Drill core Sample No.	Rock/Sediment	Location	Thin Section	Point Counted	XRF	EPMA
W160322	23	C306	3	Basalt	Auckland pit, Bombay Quarry	X	X	X	
W160323	24	C306	2	Scoriaceous Basalt	Auckland pit, Bombay Quarry	X			
W160324	27	C306	4	Basalt (Non-vesicular)	Auckland pit, Bombay Quarry	X	X	X	
W160325	28	B24	1	Basalt	Auckland pit, Bombay Quarry	X	X	X	
W160326	29	B24	3	Basalt	Auckland pit, Bombay Quarry	X			
W160327	30	B24	4	Basalt (Non-vesicular)	Auckland pit, Bombay Quarry	X	X	X	
W160328	31	B24	5	Basalt	Auckland pit, Bombay Quarry	X			
W160329	32	B22	1	Basalt (Veins)	Auckland pit, Bombay Quarry	X			
W160330	33	B22	2	Basalt (Non-vesicular)	Auckland pit, Bombay Quarry	X	X	X	
W160331	34	B22	3	Scoriaceous Basalt	Auckland pit, Bombay Quarry	X			
W160332	35	B22	4	Basalt (Non-vesicular)	Auckland pit, Bombay Quarry	X	X	X	
W160333	36	B19	2	Basalt	Auckland pit, Bombay Quarry	X			
W160334	37	B19	3	Basalt	Auckland pit, Bombay Quarry	X	X	X	
W160335	38	B19	4	Basalt	Auckland pit, Bombay Quarry	X			
W160336	39	B19	5	Basalt	Auckland pit, Bombay Quarry	X			
W160337	40	B19	6	Scoriaceous Basalt	Auckland pit, Bombay Quarry	X			
W160338	41	C307	1	Basalt	Auckland pit, Bombay Quarry	X	X	X	
W160339	42	C307	3	Basalt (Non-vesicular)	Auckland pit, Bombay Quarry	X	X	X	
W160340	43	C307	4	Scoriaceous Basalt	Auckland pit, Bombay Quarry	X			
W160341	44	C301	1	Basalt	Auckland pit, Bombay Quarry	X	X	X	
W160342	45	C301	2	Basalt (Non-vesicular)	Auckland pit, Bombay Quarry	X	X	X	

University of Waikato No.	Sample No./ Thin section No.	Drill core	Drill core Sample No.	Rock/Sediment	Location	Thin Section	Point Counted	XRF	EPMA
W160343	46	C301	4	Basalt (Non-vesicular)	Auckland pit, Bombay Quarry	X	X	X	
W160344	47	C301	6	Basalt (Weathered)	Auckland pit, Bombay Quarry	X	X	X	
W160345	48	C309	3	Scoria (ϕ -5)	Auckland pit, Bombay Quarry	X			
W160346	49	C309	3	Scoria (ϕ -4)	Auckland pit, Bombay Quarry	X			
W160347	50	C321	1	Scoria (ϕ -6)	Auckland pit, Bombay Quarry	X			
W160348	51	C321	2	Scoria (ϕ -6)	Auckland pit, Bombay Quarry	X			
W160349	52	C307	2	Scoria (ϕ -5)	Auckland pit, Bombay Quarry	X			
W160350	53	C321	Box 6	Intercalated Sediments	Auckland pit, Bombay Quarry				
W160351	54	C321	Box 7	Intercalated Sediments	Auckland pit, Bombay Quarry				
W160352	55	C321	Box 8	Intercalated Sediments	Auckland pit, Bombay Quarry				
W160353	56	C306	6	Country Rock sediment	Auckland pit, Bombay Quarry				
W160354	57	C306	7	Country Rock sediment	Auckland pit, Bombay Quarry				
W160355	58	C306	8	Country Rock sediment	Auckland pit, Bombay Quarry				
W160356	59	C306	9	Country Rock sediment	Auckland pit, Bombay Quarry				

Appendix II

Stratigraphic Logs

Date: 11/11/15
Name: Drill core B19
Stratigraphic Column No.: 1 of 1
Region: South Auckland
Location: 'Auckland Pit' Bombay Quarry

Graphic Log Symbols

Small Vesicles
Large Vesicles
Scoriaceous Basalt
Siltstone
Basalt

Thickness (m)	Graphic Log	Photo No.	Sample No.	Lithological Notes
22	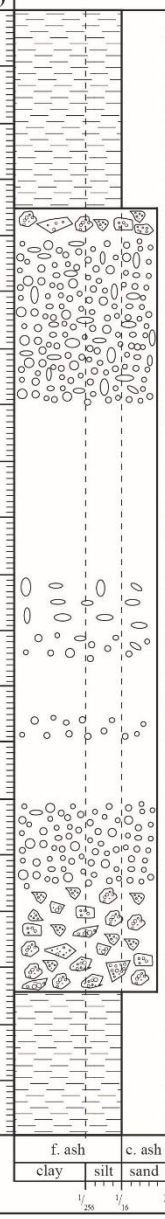		1.	21.90 - 24.50 m: Light yellow fine-grained silt/tuff
23				
24				Blue - grey finely porphyritic basalt (<1mm phenocrysts) Ol + Aug
25				24.50 - 25 m: Highly weathered reddish - blue scoriaceous basalt
26			2.	25 - 28 m: Moderately vesicular (40 - 60 %), vesicle size: small 1 - 5 mm spherical; large 10 - 20 mm elongated
27				
28				
29			3.	28 - 31 m: Non-vesicular
30				
31				31 - 32 m: Highly weathered, very poorly vesicular (0 - 10 %), small vesicle size: 3 mm elongated
32			4.	32 - 32.50 m: very poorly vesicular (0 - 10 %), vesicle size small: 1 - 3 mm spherical; large 10 - 20 mm spherical + elongated
33				32.50 - 33.50 m: Non-vesicular
34				33.50 - 34 m: Highly weathered, broken, very poorly vesicular (0 - 10 %), vesicle size 3 mm spherical
35				34 - 35 m: Non-vesicular
36			5.	35 - 36.50 m: Highly weathered, moderately vesicular (40 - 60 %), vesilce size 1 - 3 mm spherical
37			6.	36.50 - 38.50 m: Highly weathered, light reddish scoriaceous basalt
38				
39				
40			7.	38.50 - 41 m: Light yellow fine-grained siltstone
41				

f. ash | c. ash | lapilli | blocks/bombs
clay | silt | sand | gravel
1/256 | 1/16 | 2 | 64
Grainsize (mm)

Date: 11/11/15

Name: Drill core B22

Stratigraphic Column No.: 1 of 1

Region: South Auckland

Location: 'Auckland Pit' Bombay Quarry

Graphic Log Symbols

Small Vesicles
Large Vesicles
Vesicles trials
Scoriaceous Basalt
Mudstone
Siltstone
Basalt

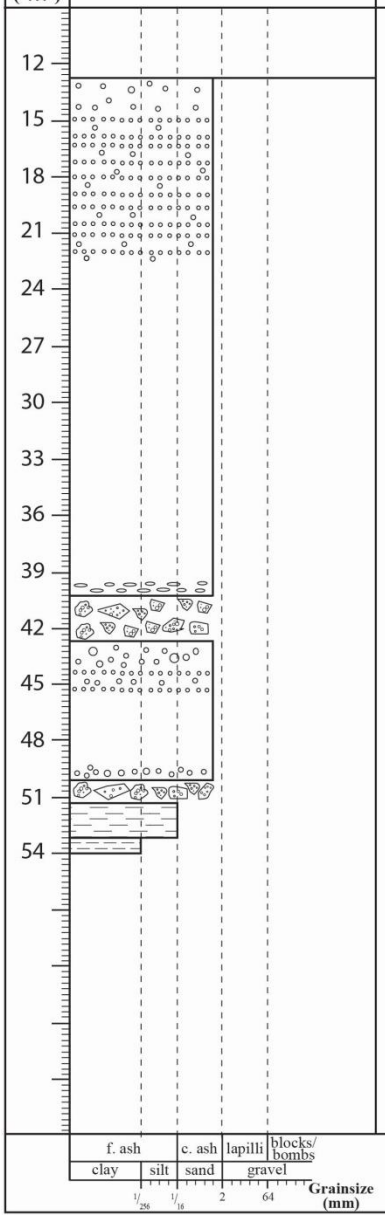

Thickness (m)	Photo No.	Sample No.	Lithological Notes
			0 - 12.50 m: No data
		1.	12.50 - 22 m: Very poorly vesicular (0 - 10 %), vesicle size: small 1 - 3 mm spherical; large 5 - 20 mm spherical + elongated, vesilce trails (10 - 30 mm apart)
		2.	22 - 40 m: Non-vesicular
		3.	40 - 40.7 m: Very poorly vesicular (0 - 10 %), small vesicles 1 - 2 mm spherical
			40.7 - 42.7 m: Highly weathered, brown scoriaceous basalt, moderately vesicular (40 - 60 %), vesicle size 1 - 3 mm
		4.	42.7 - 45.50 m: Poorly vesicular (15 - 30%), vesicle size: small 1 - 3 mm spherical; large 3 - 5 mm spherical, vesilce trails (10 mm apart)
		5.	45.50 - 49.50 m: Non-vesicular
		6.	49.50 - 50.50 m: Highly weathered, moderately vesicular (40 - 60 %), vesicle size: small 1 - 2 mm spherical; large 10 - 15 mm spherical + elongated
			50.50 - 51.15 m: Highly weathered, reddish scoriaceous basalt
			51.15 - 51.80 m: Dark reddish grading to light reddish fine-grained siltstone
			51.80 - 53 m: Light yellow siltstone
			53 - 54 m: Grey mudstone

Date: 26/01/16
Name: Drill core B24
Stratigraphic Column No.: 1 of 1
Region: South Auckland
Location: 'Auckland Pit' Bombay Quarry

Graphic Log Symbols

Small Vesicles
Large Vesicles
Silty-mud
Basalt

Thickness (m)	Graphic Log	Photo No.	Sample No.	Lithological Notes
38–40	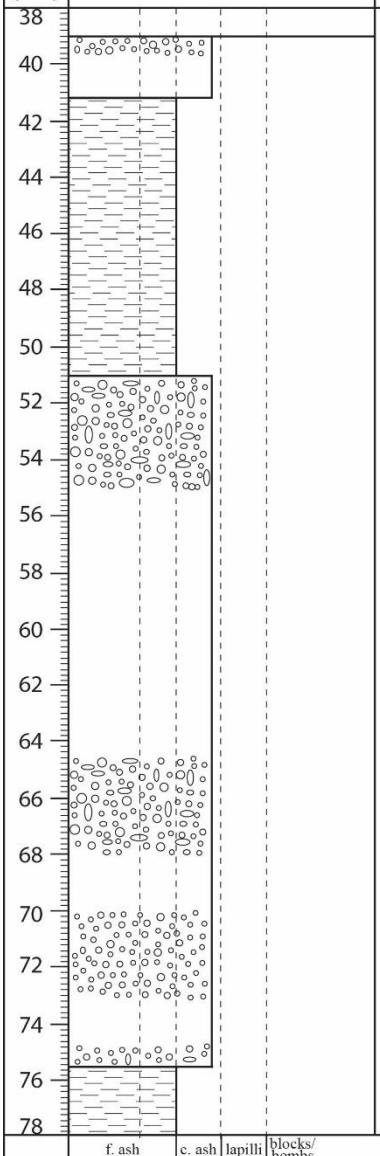		1.	Blue-grey finely porphyritic basalt (<1mm phenocrysts) Ol + Aug 39 - 39.5 m: Weathered moderately vesicular (40 - 60 %), small vesicles: 1 - 2 mm spherical
40–42				39.5 - 41.10 m: Non-vesicular
42–44			2.	
44–46				
46–48				41.10 - 51 m: Red to light brown Siltstone
48–50				
50–52			3.	
52–54				51 - 55 m: Moderately vesicular (40 - 60 %), vesicle size: small 1 - 4 mm spherical; large: 5 - 8 mm spherical + elongated
54–56				
56–58				
58–60			4.	55 - 64.50 m: Non-vesicular
60–62				
62–64				
64–66				64.50 - 68 m: Moderately vesicular (40 - 60 %), vesicle size: small 1 - 3 mm spherical; large 4 - 7 mm spherical + elongated
66–68				
68–70				68 - 70 m: Non-vesicular
70–72				70 - 73 m: Moderately vesicular (40 - 60 %), vesicle size: small 1 - 3 mm spherical; large 4 - 7 mm spherical + elongated
72–74				73 - 74.80 m: Non-vesicular
74–76			5.	74.80 - 75.50 m: Poorly vesicular (10 - 35 %), vesicle size: small 1 - 3 mm spherical; large 4 - 6 mm elongated
76–78				75.50 - 78 m: Weathered light red to light brown Siltstone

f. ash | c. ash | lapilli | blocks/bombs
clay | silt | sand | gravel
1/256 | 1/16 | 2 | 64
Grainsize (mm)

Date: 09/11/15
Name: Drill core C301
Stratigraphic Column No.: 1 of 1
Region: South Auckland
Location: 'Auckland Pit' Bombay Quarry

Graphic Log Symbols

Small Vesicles
Large Vesicles
Vesicles trials
Lithic cast
Scoriaceous Basalt
Mudstone
Siltstone
Basalt

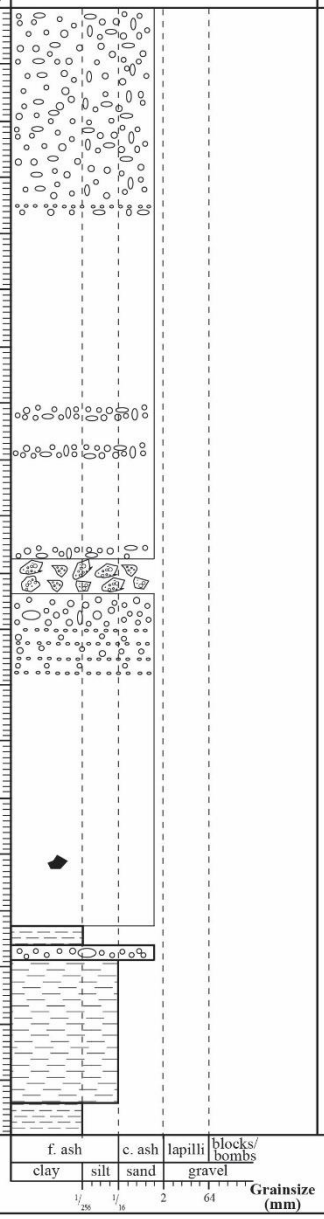

Thickness (m)	Photo No.	Sample No.	Lithological Notes
			Blue-Grey finely porphyritic basalt (<1mm phenocrysts) Ol +Aug
		1.	0 - 6.8 m: Moderately vesicular (40 - 60 %), vesicle size: small 1 - 5 mm spherical; large 5 - 10 mm spherical + elongated
			6.80 - 7.30 m: Very poorly vesicular (0-10 %), vesicle size small 1 - 3 mm spherical
			7 m: Vesicle trials (1 mm)
			7.30 - 19.10 m: Non-vesicular
		2.	14.40 m: Zone of vesicles
			15.80 m: Zone of vesilces
		3.	19.10 - 19.50 m: Poorly vesicular (10 - 30%), vesicle size: large 5 - 40 mm elongated
			19.50 - 20.80 m: Rubbly reddish brown scoriaceous basalt
			20.80 - 23.50 m: Very poorly vesicular (0 - 10 %), vesicle size 1 - 2 mm, vesicle trails (1 mm)
			23.50 - 32.60 m: Non-vesicular
		4.	30.30 m: Lithic 10 mm white crystalline
		5.	32.60 - 33.10 m: Brown mudstone
		6.	33.10 - 33.70 m: Highly weathered basalt. Poorly vesicular (10 - 30 %), vesicle size: 2 - 10 mm spherical + elongated
			33.70 - 34.70 m: Reddish fine-grained siltstone
		7.	34.70 - 37 m: Dull brown-reddish siltstone
			37 - 39.30 m: Light yellow siltstone
		8.	39.30 - 40 m: Dark grey mudstone

Date: 30/09/15
Name: Drill core C302
Stratigraphic Column No.: 1 of 1
Region: South Auckland
Location: 'Auckland Pit' Bombay Quarry

Graphic Log Symbols

Small Vesicles
Large Vesicles
Vesicles trials
Lithic cast
Basalt

Thickness (m)	Graphic Log	Photo No.	Sample No.	Lithological Notes
	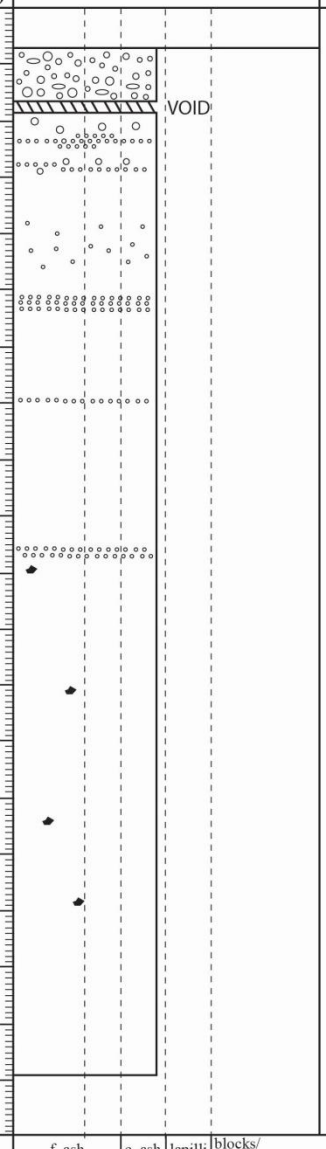			0 - 24.4 m: Overburden
			1.	Brownish-grey, crystal poor basalt; moderately vesicular (40 %). Bimodal, vesicular size: 1 - 4 mm + large 10 - 20 mm, small vesicles typically spherical; large vesicles typically spherical to elongated.
			2.	25.2 - 25.6 m: High % of large spherical vesicles
				25.6 - 27.7 m: Vesicles trails = 1 mm; also coalesced vesicle lines + large 5 - 10 mm spherical vesicles, poorly vesicular (10 %)
				28.5 - 28.9 m: Vesicle trails, isolated large irregular vesicles
			3.	Dark grey, finely porphyritic basalt (< 1 mm phenocrysts) Olivine + Augite
				28.9 - 30.6 m: Non-vesicular
				30.6 - 32.3 m: Vesicles vary 1 - 5 mm, poorly vesicular zone (5 - 10 %)
			4.	32.3 - 33.1 m: Non-vesicular
				33.1 - 34 m: Parallel vesicle trials 10 - 40 mm apart, sinlge line vesicles
				34 - 36.6 m: Non-vesicular
				36.6 - 37 m: Vesicular trails 10 - 40 mm apart
			5.	37 - 43 m: Non-vesicular, occasional vesicle trails
				42.9 m: 20 mm lithic cast, white crystalline with green band
				43 - 60.8 m: Non-vesicular
				47.2 m: 3 mm lithic cast, white crystalline with green band
				51.8 m: 20 mm lithic cast, white crystalline with green band
			6.	54.7 m: 10 mm lithic cast, white crystalline with green band

Date: 05/10/15

Name: Drill core C303

Stratigraphic Column No.: 1 of 1

Region: South Auckland

Location: 'Auckland Pit' Bombay Quarry

Graphic Log Symbols

Small Vesicles
Large Vesicles
Vesicles trials
Lithic cast
Silty-mud
Mudstone
Basalt

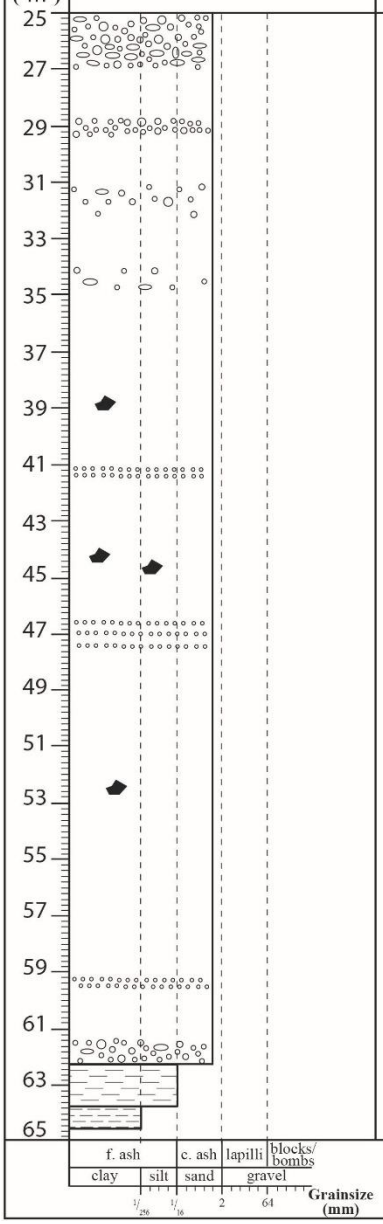

Thickness (m)	Photo No.	Sample No.	Lithological Notes
		1.	Brownish grey, slightly weathered, crystal poor basalt
			25 - 26.5 m: Poorly vesicular (30 %), vesicle size-small: 5 - 10 mm spherical; large 10 - 15 mm elongated
			26.5 - 27 m: High proportion of large vesicles
			28 - 31.50 m: Highly weathered yellowish brown basalt, Non-vesicular
			28.80 - 29.20 m: Moderately vesicular (40 %), vesicle size-small: 1 - 5 mm spherical; large 5 - 10 mm spherical; vesicle trails: 1 mm
			Dark-grey finely porphyritic basalt (<1mm phenocrysts) Olivine + Augite
			31.50 - 32.10 m: Slightly weathered, very poorly vesicular (10 %), small vesicles: 1 - 2 mm
			32.10 - 61.50 m: Non-vesicular
			34.5 - 34.8 m: Very poorly vesicular (5 %), vesicle size: 1 - 2 mm
			39.90 m: Lithic cast 5 mm white crystalline
			41 - 41.30 m: Single line vesicle trails: 4 - 10 mm; 15 - 30 mm apart
			44.30 m: Lithic cast 10 mm white crystalline
			44.6 m: Lithic cast 8 mm white crystalline
		2.	
			46.50 - 47.50 m: Single line vesicle trails: 1 mm
			52.60 m: Lithic cast 15 mm white crystalline
			59.30 - 59.40 m: Single line vesicle trails: 4 - 10 mm
			61.5 - 62.20 m: Moderately vesicular (40 %), vesicle size-small: 1 - 4 mm spherical; large 10 - 13 mm elonglated
			62.20 m: Sharp contact
			62.20 - 62.70 m: Brownish black, very finely grained silt/mud. Very thin bed
		3.	
		4.	62.70 - 63.70 m: Dark reddish brown very fine silt
			63.70 - 64.50 m: Light brown very fine mud?

Date: 28/10/15
Name: Drill core C306
Stratigraphic Column No.: 1 of 1
Region: South Auckland
Location: 'Auckland Pit' Bombay Quarry

Graphic Log Symbols

- Small Vesicles
- Large Vesicles
- Scoriaceous Basalt
- Vesicles trials
- Mudstone
- Silty/clay siltstone
- Course-sand
- Basalt

Thickness (m)	Graphic Log	Photo No.	Sample No.	Lithological Notes
2 4 6 8 10 12 14 16 18 20 22 24 26 28 30 32	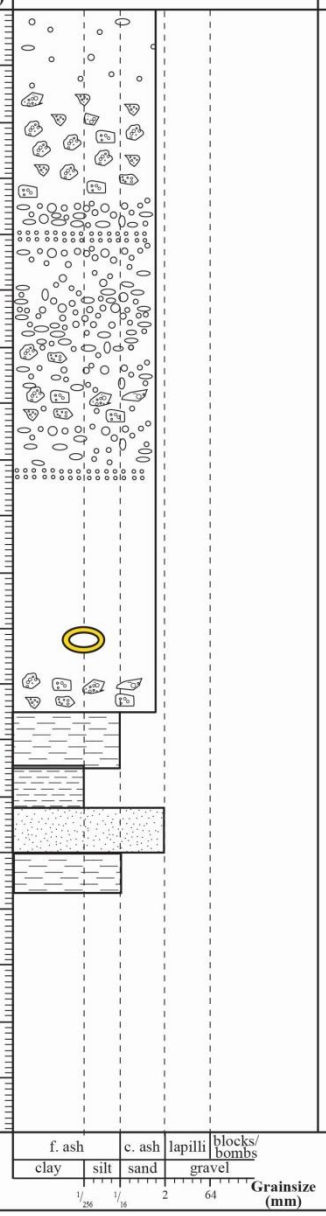		1.	Bluish-grey finely porphyritic basalt (<1mm phenocrysts) Ol +Aug
				0 - 3.2 m: Very poorly vesicular (0 - 10 %); small vesicles 1 - 5 mm spherical
			2.	3.2 - 7 m: Highly weathered Scoriaceous basalt; very broken pieces (10 - 50 mm), brownish to light brown
				7 - 7.70 m: moderately vesicular (40 - 60 %); vesicle size: small 1 - 5 mm spherical; large 5 - 15 mm spherical + elongated
			3.	7.70 - 8.10 m: Vesicle trails (1 mm)
				8.10 - 9.20 m: Very poorly vesicular (0 - 10 %); vesicle size 1 - 3 mm spherical
				9.20 - 12.20 m: Slighty weathered, moderately vesicular (40 - 60 %) broken pieces; vesicle size: small 1 - 2 mm spherical; large 15 - 20 mm spherical + elongated
				12.20 m: Vesicle trails (3 mm)
				12.20 - 15.50 m: Moderately weathered; Scoriaceous Basalt, poorly vesicular (20 - 30 %); small vesicle size: 1 - 4 mm spherical
				15.50 - 16.50 m: Poorly vesicular (20 - 30 %); vesilce size: 1 - 5 mm spherical; vesicle trails (1 mm)
				16.50 - 24.40 m: Non-vesicular
			4.	22.50 m: Yellowish circle within Basalt.
				24.40 - 25.50 m: Brownish to Reddish, silty, Scoriaceous Basalt
			5.	25 - 26.50 m: Dark purple-ish grey; silty clay
			6.	26.50 - 27 m: Reddish brown silty clay
			7.	27 - 28.50 m: Yellowish brown clay/mud
			8.	28.50 - 30 m: Pale-yellow to light grey course-sand
			9.	30 -31.50 m: Dull brown silty clay

Date: 09/11/15

Name: Drill core C307

Stratigraphic Column No.: 1 of 1

Region: South Auckland

Location: 'Auckland Pit' Bombay Quarry

Graphic Log Symbols

Small Vesicles
Large Vesicles
Vesicles trials
Scoria
Scoriaceous Basalt
Mudstone
Siltstone
Basalt

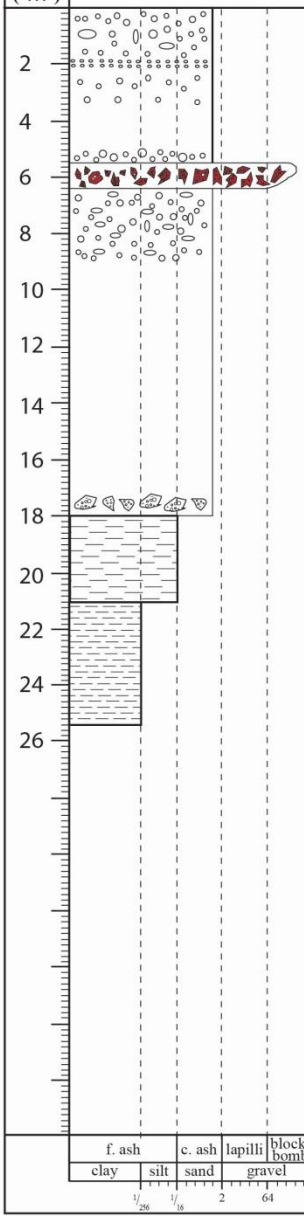

Thickness (m)	Photo No.	Sample No.	Lithological Notes
			Blue-Grey finely porphyritic basalt (<1mm phenocrysts) Ol + Aug
		1.	0 - 1 m: Poorly vesicular (10 - 30 %), broken, vesicle size: small 1 - 3 mm spherical; large 5 - 13 mm spherical + elongated
		2.	1 - 3.5 m: Very poorly vesicular (0 - 10 %), vesicle size 1 mm spherical
			2 m: Vesicle trails multiple (1 mm)
			3.5 - 5 m: Non-vesicular
			5 - 5.20 m: Very poorly vesicular (0 - 10 %), weathered at the bottom, vesicle size, small 1 - 3 mm spherical; large 10 - 20 mm elongated
			5.20 - 6.30 m: weathered brown-reddish scoria. Very vesicular (60 - 80 %), lapiili + blocks/bombs
			6.30 - 8.90 m: Moderately vesicular (40 - 60 %), vesicle size: small 1 - 3 mm spherical; large 5 - 8 mm elongated
		3.	8.90 - 17 m: Non-vesicular
		4.	17- 18 m: Highly weathered scoriaceous basalt. Reddish at base
		5.	18 - 19.50 m: Reddish brown fine-grained siltstone
		6.	19.50 - 21 m: Yellowish brown fine-grained Siltstone
			21 - 22.50 m: Light grey mudstone
			22.50 - 25 m: Dark greyish mudstone
		7.	25 - 25.50 m: Very light grey mudstone

Date: 03/11/15
Name: Drill core C308
Stratigraphic Column No.: 1 of 1
Region: South Auckland
Location: 'Auckland Pit' Bombay Quarry

Graphic Log Symbols

Small Vesicles
Large Vesicles
Vesicles trials
Lithic cast
Scoriaceous Basalt
Mudstone
Siltstone
Basalt

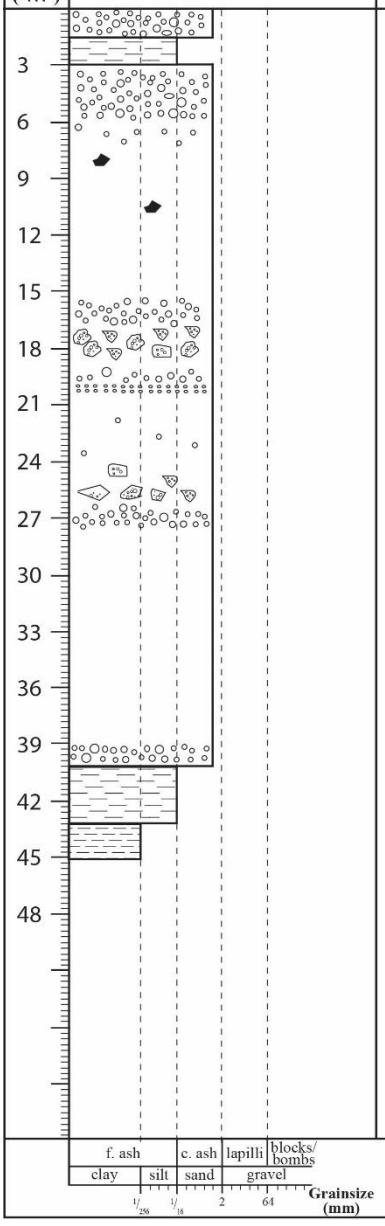

Thickness (m)	Photo No.	Sample No.	Lithological Notes
		1.	0 -1.50 m: Light grey, Moderately vesicular (40 - 60 %); vesicle size 1 - 3 mm spherical + elongated
		2.	
		3.	1.5 - 3 m: Yellowish-brown fine-grained silt
			3 - 6 m: Moderately weathered, broken pieces; moderately vesicular (40 - 60 %); vesicle size 1 - 3 mm
			6 - 7 m: Poorly vesicular (10 - 30 %); vesilce size: small 1 - 3 mm spherical, large: 5 - 10 mm spherical
			7 - 15.40 m: Non- vesicular
			8.10 m: Lithic 30 mm white crystalline with green band
			10.50 m: Lithic 10 mm white crystalline with green band
			15.40 - 15.80 m: Moderately vesicular (40 - 60 %); vesilce size: small 1 - 5 mm spherical, large 10 - 40 mm elongated
		4.	15.80 - 16.50 m: Dark brown, highly weathered Scoriaceous Basalt. Very broken
			16.50 - 18.30 m: Blue-ish grey broken Scoriaceous Basalt
			18.30 - 19.5 m: Poorly vesicular (10 - 30 %); vesilce size: small 1 - 3 mm spherical, large 5 - 10 mm elongated
			19.5 - 20.5 m: Moderaterly vesicular (40 - 60 %); vesicle size 5 - 10 mm spherical; multiple vesicle trails (1 mm)
			20.5 - 24 m: Non-vesicular; ocassional vesicle, size 3 mm
			24 - 25.6 m: Very broken brownish Scoriaceous Basalt
		5.	25.6 - 27.3 m: Moderately vesicular (40 - 60 %), vesicle size 1 - 3 mm spherical. Vesicle trail 1 mm at 26.60 - 27.3 m
			26.5 - 26.6 m: Zone of very vesicular (60 - 80 %), vesilce size 1 mm
		6.	
		7.	27.3 - 39.5 m: Non-vesicular
		8.	39.5 - 40.5 m: Moderately weathered; moderately vesicular (40 - 60 %), vesicle size: 1 - 4 mm spherical
			40.5 - 41.90 m: Dull reddish grey, fine grained siltstone
			41.90 - 43.5 m: Light grey siltstone
			43.5 - 44.30 m: Dark reddish brown, very fine grained mudstone
			44.30 - 45 m: Brownish black mudstone

Date: 26/01/16
Name: Drill core C309
Stratigraphic Column No.: 1 of 1
Region: South Auckland
Location: 'Auckland Pit' Bombay Quarry

Graphic Log Symbols

Small Vesicles
Large Vesicles
Vesicles trials
Scoria
Mudstone
Siltstone
Basalt

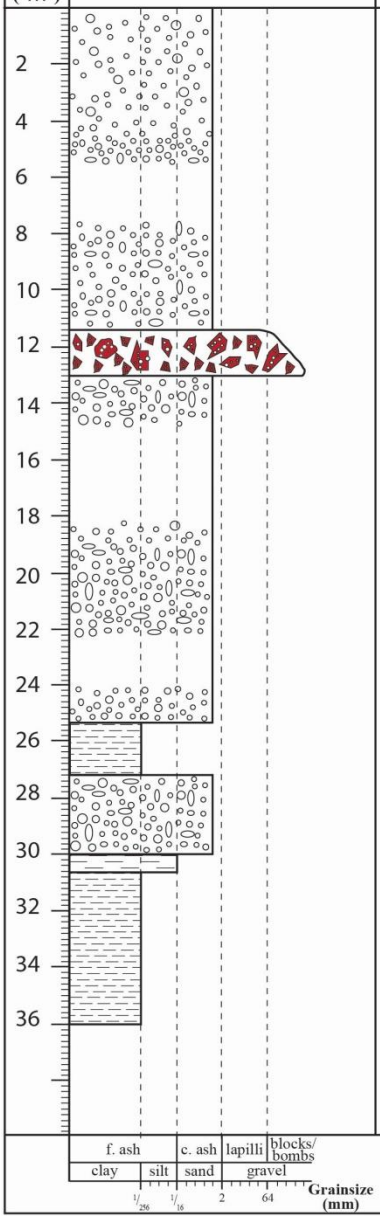

Thickness (m)	Photo No.	Sample No.	Lithological Notes
			Blue-grey finely porphyritic Basalt (<1mm phenocryts) Ol + Aug
		1.	0 - 4.5 m: Poorly vesicular (10 - 30 %), vesicle size: small 1 - 3 mm spherical; large 5 - 6 mm elongated
			4.5 - 5.5 m: Broken, moderately vesicular (40 - 60 %), small vesicles: 1 - 2 mm spherical + elongated
			5.5 - 7.5 m: Non -vesicular
		2.	7.5 - 11.30 m: Moderately vesicular (40 - 60 %), small vesicles: 1 - 2 mm spherical + elongated
		3.	11.30 - 13 m: Dark reddish scoria, Lapilli: 10 - 30 mm; Blocks/Bombs: 70 - 80 mm
			13 - 14.80 m: Slightly weathered, moderately vesicular (40 - 60 %), small vesicles: 1 - 2 mm spherical + elongated
		4.	14.80 - 18.20 m: Non-vesicular
			18.20 - 18.80 m: Poorly vesicular (10 - 30 %), vesicle size: small 1 - 3 mm spherical; large 5 - 7 mm spherical + elongated
			18.80 - 22.40 m: Very broken, weathered, moderately vesicular (40 - 60 %) small vesicles: 1 - 2 mm spherical + elongated
			22.40 - 24 m: Non-vesicular
		5.	24 - 25.50 m: Moderately vesicular (40 - 60 %), small vesicles: 1 - 2 mm spherical
			25.20 m: Vesicle trails (1 mm apart)
			25.50 - 27.20 m: Brown to dark brown mudstone
		6.	27.20 - 30 m: Moderately vesicular (40 - 60 %), small vesicles: 1 - 2 mm spherical + elongated
			30 - 30.60 m: Reddish silt/mud
		7.	30.60 - 33.20 m: Light brown mudstone
			33.20 - 36 m: Brown mudstone

Date: 03/11/15
Name: Drill core C310
Stratigraphic Column No.: 1 of 1
Region: South Auckland
Location: 'Auckland Pit' Bombay Quarry

Graphic Log Symbols

Small Vesicles
Large Vesicles
Mudstone
Siltstone
Basalt

Thickness (m)	Graphic Log	Photo No.	Sample No.	Lithological Notes
				Blue-Grey finely porphyritic basalt (< 1mm phenocrysts) Ol + Aug
				0 - 2.40 m: Very broken basalt
				0 - 5.80 m: Non-vesicular
			1.	
			2.	5.80 - 6.70 m: Poorly vesicular (10 - 30 %); vesilce size: 1 - 10 mm spherical
				6.70 - 7.50 m: Reddish brown fine-grained Siltstone
			3.	7.50 - 7.80 m: Dark purple-ish Siltstone
			4.	7.80 - 9.40 m: Light reddish Siltstone
				9.40 - 18.70 m: Light yellowish-grey Siltstone
			5.	
				12.70 - 13.50 m: Weathered Siltstone
			6.	16.50 - 18.70 m: Clayey Siltstone
			7.	18.70 - 19.50 m: Light blue-ish grey Mudstone

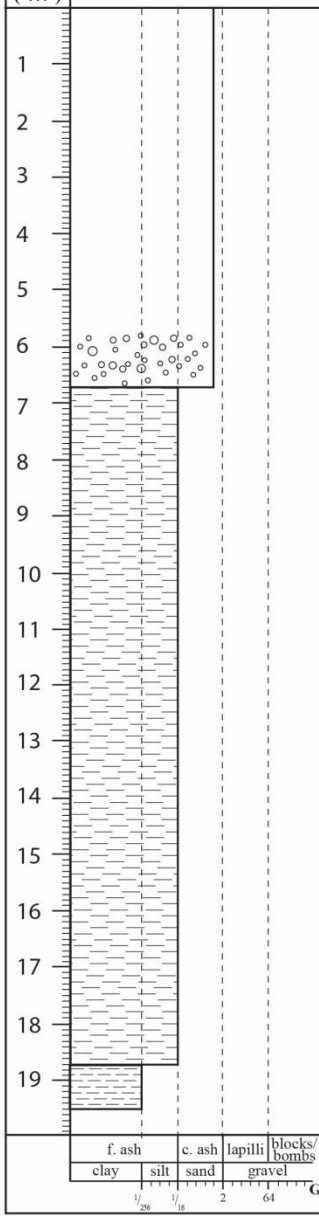

Date: 07/10/15

Name: Drill core C321

Stratigraphic Column No.: 1 of 1

Region: South Auckland

Location: 'Auckland Pit' Bombay Quarry

Graphic Log Symbols

Small Vesicles
Large Vesicles
Basalt block
Scoria
Peat
Fine-ash
Silty-mud
Basalt

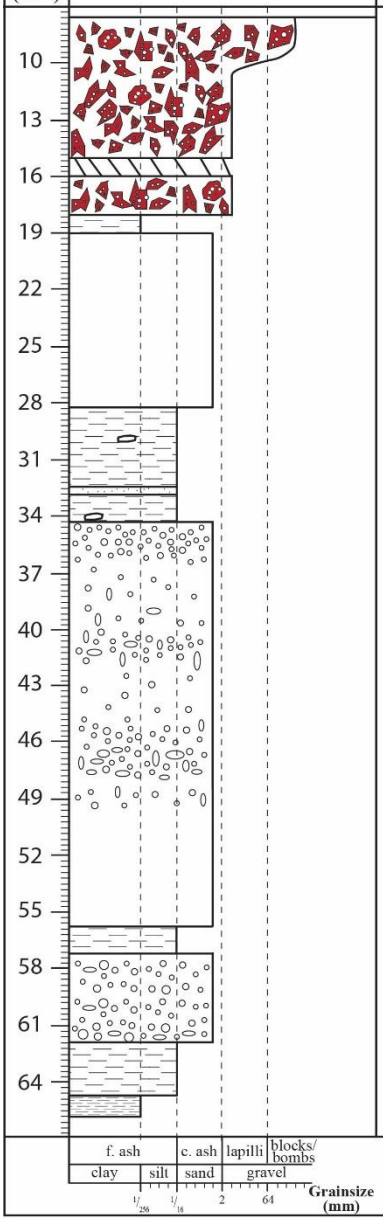

Thickness (m)	Photo No.	Sample No.	Lithological Notes
			0 - 7.1 m: No data
		1.	7.1- 10.5 m: Reddish brown, very vesicular (60 - 80 %), broken scoria. Lapilli: 5 - 60 mm sub-angular;
		2.	Blocks/Bombs: 60 - 120 mm angular. Vesicles size: 1 - 10 mm spherical
			10.5 - 15 m: Browish black, very vesicular (60 - 80 %), broken scoriaceous basalt. Vesicle size: 1 - 10 mm spherical to elongated.
			15 - 16.5 m: Zero recovery
			16.5 - 18 m: Reddish brown, very vesicular (60 - 80 %), broken scoria. Lapilli: 5 - 60 mm sub-angular; Blocks/Bombs: 60 - 120 mm angular.
		3.	Vesicles size: 1 - 10 mm spherical
			18 m: Sharp contact
			18 -19 m: Dark brown, finely grained clayey-silt
			Blue grey, finely porphyritic basalt (<1mm phenocrysts). Olivine + Augite
		4.	19 - 28.3 m: Non-vesicular
			19 - 20 m: Slightly weathered basalt
		5.	28.3 m: Planar contact
			28.3 - 34.5 m: Reddish brown to pale yellow clayey mud/silt
			30 m: Basalt block
			32.8 - 33 m: Very fine grained white ash layer
		6.	34.5 m: Basalt block
			Blue grey, finely porphyritic basalt (<1mm phenocrysts). Olivine + Augite
			34.5 - 36.6 m: Slightly weathered, clayey moderately vesicular (40 - 60 %), Vesicle size: 1 - 10 mm spherical
			36.6 - 40.5 m: Very poor vesicular zone (0 - 10 %). Vesicle size-small: 1 - 5 mm spherical; large: 10 - 15 mm elongated
		7.	40.5 - 42 m: Very broken basalt
			42 - 42.6 m: Moderately vesicular (40 - 60 %). Vesicle size-small: 2 - 10 mm spherical; large: 15 - 20 mm spherical-elongated
			42.6 - 45 m: Very poorly vesicular (0 - 10 %). Vesicle size: 5 - 10 mm
			45 - 48 m: Moderately vesicular (40 - 60 %). Vesicle size: 1 - 10 mm spherical to elongated
			48 - 49.5 m: Poorly vesicular (10 - 30 %), vesicle size-small: 1 - 5 mm
		8.	spherical; large: 10 - 15 mm spherical-elongated
			49.5 - 56.5 m: Non-vesicular
			56.5 - 57.6 m: Brown, fine grained clayey-silt
		9.	57.6 - 62 m: Slightly weathered, moderately vesicular (40 - 60 %), broken blue grey basalt. Vesicle size-small: 1 - 5 mm spherical; large: 10 - 15 mm spherical + elongated
		10.	62 - 65 m: Reddish to light brown fine-ash silt
			65 - 66 m: Black, course-grained mud

Appendix III

Point Counting Results

	Log C301				Log C309			Log C306			Log B24	
Thin Section No.	**44**	**45**	**46**	**47**	**11**	**12**	**13**	**22**	**23**	**27**	**28**	**30**
Olivine	10	9	15	15	39	16	40	8	11	3	32	15
(Phenocrysts) **%**	**3.33**	**3.00**	**5.00**	**5.00**	**13.00**	**5.33**	**13.33**	**2.67**	**3.67**	**1.20**	**10.67**	**5.00**
Clinopyroxene	25	15	13	9	10	17	8	19	18	18	11	30
(Phenocrysts) **%**	**8.33**	**5.00**	**4.33**	**3.00**	**3.33**	**5.67**	**2.67**	**6.33**	**6.00**	**7.20**	**3.67**	**10.00**
Plagioclase	50	117	181	30	16	139	21	64	32	102	44	97
(Groundmass) **%**	**16.67**	**39.00**	**60.33**	**10.00**	**5.33**	**46.33**	**7.00**	**21.33**	**10.67**	**40.80**	**14.67**	**32.33**
Opaques	42	45	35	0[1]	59	45	59	65	48	48	49	46
(Groundmass) **%**	**14.00**	**15.00**	**11.67**	**0.00**[1]	**19.67**	**15.00**	**19.67**	**21.67**	**16.00**	**19.20**	**16.33**	**15.34**
Mafic Minerals	113	107	52	140	152	83	166	143	168	77	114	112
(Groundmass) **%**	**37.67**	**35.67**	**17.33**	**46.67**	**50.67**	**27.67**	**55.33**	**47.67**	**56.00**	**30.80**	**38.00**	**37.33**
Vesicles	60	7	4	106	24	0	6	1	23	0	38	0
%	**20.00**	**2.33**	**1.34**	**35.33**	**8.00**	**0.00**	**2.00**	**0.33**	**7.66**	**0.00**	**12.66**	**0.00**
Lithics	0	0	0	0	0	0	0	0	0	2	12	0
%	**0.00**	**0.00**	**0.00**	**0.00**	**0.00**	**0.00**	**0.00**	**0.00**	**0.00**	**0.80**	**4.00**	**0.00**
Point Counted	300	300	300	300	300	300	300	300	300	250	300	300
Total %	**100.00**	**100.00**	**100.00**	**100.00**	**100.00**	**100.00**	**100.00**	**100.00**	**100.00**	**100.00**	**100.00**	**100.00**

[1] Dark groundmass, opaques not distinguishable.

	Log B22		Log C303	Log C307		Log C302			Log C308		Log C310	Log B19
Thin Section No.	**33**	**35**	**1**	**41**	**42**	**3**	**5**	**6**	**7**	**25**	**20**	**37**
Olivine	8	11	11	13	7	13	8	7	14	19	15	10
(Phenocrysts) **%**	**2.67**	**3.67**	**3.67**	**4.33**	**2.34**	**4.33**	**2.67**	**2.33**	**4.67**	**6.33**	**5.00**	**3.33**
Clinopyroxene	47	20	31	15	10	8	26	16	12	23	17	35
(Phenocrysts) **%**	**15.67**	**6.67**	**10.33**	**5.00**	**3.33**	**2.67**	**8.67**	**5.33**	**4.00**	**7.67**	**5.67**	**11.67**
Plagioclase	141	119	134	68	99	36	108	164	24	29	63	100
(Groundmass) **%**	**47.00**	**39.67**	**44.67**	**22.67**	**33.00**	**12.00**	**36.00**	**54.67**	**8.00**	**9.67**	**21.00**	**33.33**
Opaques	41	52	50	66	55	45	56	53	43	56	79	57
(Groundmass) **%**	**13.66**	**17.33**	**16.67**	**22.00**	**18.33**	**15.00**	**18.67**	**17.67**	**14.33**	**18.67**	**26.33**	**19.00**
Mafic Minerals	63	98	71	101	129	135	49	55	146	143	126	81
(Groundmass) **%**	**21.00**	**32.66**	**23.66**	**33.67**	**43.00**	**45.00**	**16.33**	**18.33**	**48.67**	**47.66**	**42.00**	**27.00**
Vesicles	0	0	3	37	0	63	53	3	61	30	0	17
%	**0.00**	**0.00**	**1.00**	**12.33**	**0.00**	**21.00**	**17.66**	**1.00**	**20.33**	**10.00**	**0.00**	**5.67**
Lithics	0	0	0	0	0	0	0	2	0	0	0	0
%	**0.00**	**0.00**	**0.00**	**0.00**	**0.00**	**0.00**	**0.00**	**0.67**	**0.00**	**0.00**	**0.00**	**0.00**
Point Counted	300	300	300	300	300	300	300	300	300	300	300	300
Total %	**100.00**	**100.00**	**100.00**	**100.00**	**100.00**	**100.00**	**100.00**	**100.00**	**100.00**	**100.00**	**100.00**	**100.00**

Appendix IV

Electron Microprobe Analysis

Sample:	11 (upper basalt)							
Phenocryst:	Olivine							
No.	**6**	**9**	**10**	**12**	**14**	**15**	**16**	**18**
(wt. %)								
SiO_2	39.034	39.286	39.095	38.435	39.476	39.282	39.289	39.026
TiO_2	0.022	0.021	0.004	0.038	0.017	0.017	0.019	0.009
Al_2O_3	0.059	0.054	0.069	0.021	0.066	0.054	0.057	0.072
Cr_2O_3	0.036	0.013	0.018	0.022	-	0.033	0.032	0.009
NiO	0.17	0.121	0.14	0.076	0.125	0.146	0.129	0.1
FeO	18.239	18.504	17.326	20.184	18.183	18.095	18.276	19.102
MnO	0.287	0.247	0.206	0.319	0.234	0.233	0.241	0.201
MgO	42.973	43.716	44.3	40.851	43.757	43.724	43.582	43.248
CaO	0.22	0.316	0.157	0.295	0.205	0.199	0.256	0.278
Na_2O	0.004	0.006	0.006	-	0.031	-	0.023	0.014
Total	**101.044**	**102.284**	**101.321**	**100.241**	**102.094**	**101.783**	**101.904**	**102.059**
Fa %	19.24	19.19	18.00	21.71	18.91	18.85	19.05	19.86
Fo %	80.76	80.81	82.00	78.29	81.09	81.15	80.95	80.14

Sample:	11 (upper basalt)							
Phenocryst:	Olivine							
No.	**19**	**20**	**21**	**22**	**24**	**29**	**33**	**38**
(wt. %)								
SiO_2	39.124	38.755	39.088	39.014	39.1	39.102	39.038	39.835
TiO_2	0.025	0.021	0.001	-	0.032	-	0.013	-
Al_2O_3	0.024	0.064	0.087	0.05	0.055	0.062	0.04	0.124
Cr_2O_3	0.018	0.043	0.031	0.06	0.044	0.004	0.031	0.045
NiO	0.168	0.124	0.146	0.099	0.046	0.126	0.119	0.209
FeO	17.856	18.039	17.481	17.863	18.456	17.793	18.137	14.037
MnO	0.23	0.229	0.238	0.239	0.228	0.166	0.267	0.172
MgO	43.965	43.594	43.788	43.734	43.446	43.797	43.474	46.949
CaO	0.21	0.298	0.192	0.284	0.223	0.199	0.311	0.159
Na_2O	-	0.011	0.003	-	0.019	0.024	0.023	0.018
Total	**101.62**	**101.178**	**101.055**	**101.343**	**101.649**	**101.273**	**101.453**	**101.548**
Fa %	18.56	18.84	18.30	18.65	19.25	18.57	18.97	14.37
Fo %	81.44	81.16	81.70	81.35	80.75	81.43	81.03	85.63

Sample:	12 (middle basalt)							
Phenocryst:	Olivine							
No.	**39**	**40**	**43**	**44**	**47**	**48**	**58**	**60**
(wt. %)								
SiO_2	38.583	38.739	38.405	37.004	37.001	36.424	38.791	38.446
TiO_2	0.024	0.011	0.033	0.013	0.012	0.002	0.003	0.011
Al_2O_3	0.035	0.048	0.044	0.023	0.031	0.04	0.045	0.022
Cr_2O_3	-	0.036	0.035	-	0.025	0.014	0.012	0.038
NiO	0.181	0.131	0.12	0.106	0.077	0.064	0.152	0.111
FeO	20.271	19.919	21.144	29.386	30.131	32.473	19.891	21.4
MnO	0.243	0.272	0.263	0.479	0.483	0.595	0.252	0.275
MgO	41.585	42.341	40.671	33.524	33.472	31.826	41.826	40.558
CaO	0.187	0.196	0.189	0.246	0.216	0.296	0.184	0.174
Na_2O	-	0.01	-	0.031	-	0.009	0.017	0.023
Total	**101.109**	**101.703**	**100.904**	**100.812**	**101.448**	**101.743**	**101.173**	**101.058**
Fa %	21.48	20.89	22.59	32.97	33.56	36.41	21.07	22.85
Fo %	78.52	79.11	77.41	67.03	66.44	63.59	78.93	77.15

Sample:	12 (middle basalt)							
Phenocryst:	Olivine							
No.	**61**	**62**	**63**	**66**	**67**	**68**	**70**	**71**
(wt. %)								
SiO_2	37.246	38.702	38.743	37.367	36.694	39.256	37.56	36.734
TiO_2	0.026	0.024	0.011	0.011	0.022	0.01	0.008	0.025
Al_2O_3	0.053	0.057	0.031	0.028	0.026	0.044	0.041	0.035
Cr_2O_3	-	-	0.002	0.027	0.007	0.036	-	0.018
NiO	0.109	0.145	0.133	0.122	0.056	0.001	-	0.006
FeO	25.925	19.336	18.89	27.097	30.817	17.809	25.846	30.057
MnO	0.383	0.25	0.213	0.389	0.533	0.145	0.34	0.481
MgO	37.14	42.104	42.653	36.129	33.045	43.829	36.855	33.903
CaO	0.184	0.211	0.225	0.202	0.214	0.198	0.163	0.173
Na_2O	-	0.01	0.026	0.031	0.029	0.011	-	-
Total	**101.066**	**100.839**	**100.927**	**101.403**	**101.443**	**101.339**	**100.813**	**101.432**
Fa %	28.15	20.49	19.91	29.62	34.35	18.57	28.24	33.22
Fo %	71.85	79.51	80.09	70.38	65.65	81.43	71.76	66.78

Sample:	13 (lower basalt)										
Phenocryst:	Olivine										
No.	**82**	**83**	**84**	**85**	**86**	**88**	**89**	**90**	**95**	**105**	**108**
(wt. %)											
SiO_2	39.023	39.019	39.116	39.24	39.101	39.033	38.895	39.479	39.478	39.127	38.45
TiO_2	0.025	0.04	0.013	0.017	0.004	0.029	0.026	0.007	0.021	0.025	0.022
Al_2O_3	0.224	0.058	0.054	0.075	0.069	0.05	0.082	0.072	0.082	0.058	0.022
Cr_2O_3	0.032	0.046	0.014	0.001	0.008	0.058	0.022	0.038	0.015	0.026	0.037
NiO	0.112	0.104	0.132	0.138	0.101	0.107	0.081	0.179	0.129	0.165	0.049
FeO	17.519	18.72	17.889	18.041	19.243	18.496	18.248	17.751	14.575	17.092	20.75
MnO	0.268	0.265	0.244	0.209	0.161	0.224	0.234	0.182	0.16	0.189	0.248
MgO	43.02	43.173	43.549	43.721	43.312	42.963	43.432	44.356	45.815	44.274	41.188
CaO	0.285	0.302	0.158	0.167	0.144	0.248	0.252	0.188	0.153	0.151	0.38
Na_2O	0.006	0.01	0.013	0.021	0.023	0.022	0.012	0.027	0.012	0.008	0.03
Total	**100.514**	**101.737**	**101.182**	**101.63**	**102.166**	**101.23**	**101.284**	**102.279**	**100.44**	**101.115**	**101.176**
Fa %	18.60	19.57	18.73	18.80	19.96	19.46	19.08	18.34	15.15	17.81	22.04
Fo %	81.40	80.43	81.27	81.20	80.04	80.54	80.92	81.66	84.85	82.19	77.96

Sample:	11 (upper basalt)						
Phenocryst:	Clinopyroxene						
No.	**5**	**7**	**8**	**11**	**13**	**17**	**23**
(wt. %)							
SiO_2	41.381	43.807	48.693	45.985	42.451	48.791	48.3
TiO_2	5.159	4.163	2.132	2.814	4.6	2.169	2.287
Al_2O_3	10.846	8.927	4.843	7.525	10.247	4.816	5.059
Cr_2O_3	0.018	-	0.018	0.145	0.024	0.016	0.006
NiO	0.012	0.021	-	-	0.039	0.001	-
FeO	8.914	8.583	7.735	7.759	8.88	7.476	7.829
MnO	0.103	0.129	0.134	0.1	0.129	0.116	0.131
MgO	10.535	11.444	13.865	12.541	10.809	13.735	13.435
CaO	22.815	23.034	23.227	23.133	22.845	23.286	22.776
Na_2O	0.46	0.464	0.368	0.436	0.464	0.384	0.365
Total	**100.243**	**100.572**	**101.015**	**100.438**	**100.488**	**100.79**	**100.188**
Wo %	51.36	50.46	47.84	49.61	50.98	48.29	47.88
Fs %	15.66	14.67	12.44	12.99	15.47	12.10	12.84
En %	32.98	34.87	39.72	37.41	33.55	39.61	39.28

Sample:	11 (upper basalt)						
Phenocryst:	Clinopyroxene						
No.	**30**	**31**	**32**	**34**	**35**	**36**	**37**
(wt. %)							
SiO_2	48.045	43.198	47.347	45.962	45.451	43.861	45.218
TiO_2	2.624	4.439	2.67	2.874	3.07	3.777	3.297
Al_2O_3	5.339	9.349	5.531	7.466	7.879	9.21	7.77
Cr_2O_3	-	0.015	-	0.454	0.01	0.377	0.084
NiO	0.004	-	0.013	0.022	0.002	0.02	-
FeO	9.33	8.727	8.647	7.312	8.694	7.995	7.824
MnO	0.18	0.131	0.165	0.067	0.134	0.087	0.085
MgO	12.596	11.092	12.415	12.792	12.124	11.654	12.245
CaO	22.702	23.007	22.901	23.156	23.022	22.993	23.146
Na_2O	0.391	0.44	0.446	0.398	0.473	0.469	0.427
Total	**101.211**	**100.398**	**100.135**	**100.503**	**100.859**	**100.443**	**100.096**
Wo %	47.79	50.85	48.81	49.63	49.33	50.60	50.01
Fs %	15.33	15.05	14.38	12.23	14.54	13.73	13.19
En %	36.88	34.10	36.80	38.14	36.13	35.67	36.80

Sample:	12 (middle basalt)						
Phenocryst:	Clinopyroxene						
No.	**41**	**42**	**45**	**46**	**53**	**54**	**55**
(wt. %)							
SiO_2	48.474	50.437	50.177	50.06	50.188	49.203	46.484
TiO_2	2.045	1.226	1.246	1.399	1.369	1.78	2.412
Al_2O_3	4.879	3.638	3.897	3.782	3.521	4.157	6.684
Cr_2O_3	0.113	0.174	0.308	0.09	0.236	0.006	0.235
NiO	-	0.007	0.022	-	0.019	0.002	0.039
FeO	7.929	7.686	8.401	8.754	8.724	9.173	8.606
MnO	0.186	0.187	0.156	0.226	0.224	0.177	0.153
MgO	12.983	14.836	14.608	14.529	12.966	13.889	12.626
CaO	22.594	21.564	21.207	21.391	22.707	21.744	21.939
Na_2O	0.558	0.452	0.496	0.433	0.529	0.369	0.562
Total	**99.761**	**100.207**	**100.518**	**100.664**	**100.483**	**100.5**	**99.74**
Wo %	48.24	44.74	44.11	44.17	47.75	45.09	47.47
Fs %	13.21	12.45	13.64	14.11	14.32	14.85	14.53
En %	38.55	42.81	42.26	41.72	37.93	40.06	38.00

Sample:	12 (middle basalt)					
Phenocryst:	Clinopyroxene					
No.	**56**	**57**	**59**	**64**	**65**	**69**
(wt. %)						
SiO_2	49.836	49.136	49.234	48.2	46.989	49.851
TiO_2	1.488	1.791	1.293	1.7	2.256	0.913
Al_2O_3	3.689	3.856	4.885	6.223	6.867	6.056
Cr_2O_3	0.009	0.002	0.676	0.361	0.101	0.978
NiO	0.025	0.003	0.018	0.03	0.001	0.001
FeO	7.835	8.773	7.529	8.466	9.067	7.032
MnO	0.15	0.156	0.166	0.169	0.165	0.157
MgO	14.183	13.633	14.334	13.171	12.501	15.616
CaO	22.284	22.027	21.206	21.571	21.545	18.924
Na_2O	0.435	0.381	0.615	0.637	0.589	0.763
Total	**99.934**	**99.758**	**99.956**	**100.528**	**100.081**	**100.291**
Wo %	46.30	46.05	45.10	46.39	46.83	41.02
Fs %	12.71	14.31	12.50	14.21	15.38	11.90
En %	40.99	39.64	42.40	39.40	37.79	47.08

Sample:	13 (lower basalt)									
Phenocryst:	Clinopyroxene									
No.	**77**	**78**	**79**	**80**	**81**	**87**	**91**	**92**	**93**	**94**
(wt. %)										
SiO_2	46.914	46.647	41.477	44.068	44.105	45.583	45.357	42.437	48.694	46.511
TiO_2	2.67	2.761	5.422	3.819	3.91	2.995	3.01	4.784	2.164	2.899
Al_2O_3	6.225	6.957	11.156	8.491	8.596	7.68	7.591	9.875	4.576	5.905
Cr_2O_3	-	0.277	0.008	0.301	0.108	0.442	-	-	0.017	0.016
NiO	-	0.011	-	-	-	0.029	0.005	-	0.022	-
FeO	8.658	7.658	9.339	8.22	8.531	6.857	7.998	9.699	7.592	8.854
MnO	0.163	0.114	0.122	0.103	0.083	0.139	0.121	0.146	0.119	0.096
MgO	12.488	12.808	10.056	11.81	11.704	12.527	12.121	10.383	13.726	12.637
CaO	23.002	23.032	22.824	23.2	23.259	23.023	23.066	22.664	22.887	22.712
Na_2O	0.376	0.408	0.53	0.486	0.457	0.441	0.437	0.481	0.336	0.36
Total	**100.496**	**100.673**	**100.934**	**100.498**	**100.753**	**99.716**	**99.706**	**100.469**	**100.133**	**99.99**
Wo %	48.81	49.19	51.76	50.39	50.35	50.27	49.96	50.73	47.78	48.12
Fs %	14.34	12.77	16.53	13.93	14.41	11.69	13.52	16.94	12.37	14.64
En %	36.85	38.05	31.72	35.68	35.24	38.04	36.52	32.33	39.85	37.24

Sample:	13 (lower basalt)								
Phenocryst:	Clinopyroxene								
No.	**96**	**101**	**102**	**103**	**104**	**106**	**107**	**109**	**110**
(wt. %)									
SiO_2	48.497	41.626	42.39	41.804	41.748	42.398	46.169	42.438	43.924
TiO_2	2.193	5.449	4.649	4.871	4.685	4.779	3.032	4.408	3.831
Al_2O_3	4.501	10.667	9.933	10.769	10.308	9.875	6.259	9.863	8.589
Cr_2O_3	0.032	0.005	0.004	-	0.017	0.003	0.017	0.172	0.037
NiO	0.005	-	-	0.02	-	0.017	0.014	-	0.037
FeO	7.673	9.766	9.285	9.387	9.073	8.97	8.779	8.298	8.116
MnO	0.145	0.107	0.112	0.157	0.149	0.092	0.114	0.085	0.066
MgO	13.779	10.173	10.546	10.444	10.814	10.752	12.446	11.108	11.617
CaO	23.157	22.803	22.806	22.723	23.12	23.063	22.672	22.982	23.178
Na_2O	0.358	0.513	0.439	0.457	0.483	0.497	0.367	0.438	0.453
Total	**100.34**	**101.109**	**100.164**	**100.632**	**100.397**	**100.446**	**99.869**	**99.792**	**99.848**
Wo %	47.93	51.16	51.00	50.98	51.10	51.23	48.41	51.18	50.75
Fs %	12.40	17.10	16.21	16.44	15.65	15.55	14.63	14.42	13.87
En %	39.67	31.74	32.80	32.59	33.25	33.22	36.96	34.40	35.38

Sample:	11 (upper basalt)								
Crystal:	Plagioclase								
No.	**4**	**5**	**6**	**7**	**8**	**9**	**11**	**12**	**13**
(wt. %)									
SiO_2	53.758	54.197	51.849	51.390	53.254	53.188	52.103	51.933	52.538
TiO_2	0.095	0.104	0.110	0.134	0.114	0.120	0.107	0.101	0.101
Al_2O_3	29.538	29.607	30.630	30.686	30.249	29.646	30.089	30.473	30.330
FeO	0.565	0.563	0.613	0.893	0.656	0.665	0.752	0.783	0.678
MnO	-	0.003	-	0.035	-	-	-	0.013	0.013
MgO	0.051	0.061	0.090	0.068	0.041	0.066	0.067	0.057	0.061
CaO	11.430	11.177	12.904	12.947	11.968	11.734	12.075	12.299	12.391
Na_2O	4.445	4.346	3.693	3.844	4.153	4.534	4.456	4.035	3.845
K_2O	0.479	0.413	0.323	0.305	0.358	0.391	0.360	0.476	0.325
Total	**100.361**	**100.471**	**100.212**	**100.302**	**100.792**	**100.344**	**100.010**	**100.170**	**100.282**
An %	57.02	57.22	64.61	63.88	60.11	57.51	58.71	60.99	62.79
Ab %	40.13	40.26	33.46	34.32	37.75	40.21	39.21	36.20	35.25
Or %	2.85	2.52	1.93	1.79	2.14	2.28	2.08	2.81	1.96

Sample:	11 (upper basalt)								
Crystal:	Plagioclase								
No.	**14**	**15**	**16**	**17**	**19**	**20**	**21**	**22**	**23**
(wt. %)									
SiO_2	52.278	51.981	52.404	53.158	51.912	51.727	51.789	51.702	52.210
TiO_2	0.140	0.102	0.085	0.112	0.095	0.103	0.110	0.124	0.119
Al_2O_3	30.738	30.858	30.460	29.314	30.624	30.573	30.963	30.705	30.342
FeO	0.692	0.730	0.687	0.674	0.671	0.729	0.717	0.726	0.729
MnO	-	-	0.012	-	0.006	-	-	0.014	0.004
MgO	0.063	0.077	0.078	0.062	0.057	0.093	0.093	0.072	0.068
CaO	12.624	13.053	12.504	11.131	12.711	12.929	13.021	13.237	12.755
Na_2O	3.755	3.700	4.072	4.726	3.737	3.698	3.476	3.818	3.927
K_2O	0.315	0.308	0.354	0.696	0.318	0.334	0.295	0.306	0.339
Total	**100.605**	**100.809**	**100.656**	**99.873**	**100.131**	**100.186**	**100.464**	**100.704**	**100.493**
An %	63.78	64.89	61.61	54.27	64.03	64.59	66.22	64.54	62.94
Ab %	34.33	33.28	36.31	41.69	34.06	33.43	31.99	33.69	35.07
Or %	1.89	1.82	2.08	4.04	1.91	1.99	1.79	1.78	1.99

Sample:	12 (middle basalt)									
Crystal:	Plagioclase									
No.	**27**	**28**	**29**	**30**	**31**	**32**	**34**	**35**	**36**	**37**
(wt. %)										
SiO_2	53.549	55.511	54.151	54.261	53.335	53.358	53.654	54.527	55.265	53.836
TiO_2	0.080	0.081	0.112	0.087	0.122	0.083	0.082	0.101	0.083	0.076
Al_2O_3	29.385	28.036	28.894	28.811	28.405	29.620	28.735	28.903	27.982	29.112
FeO	0.673	0.547	0.608	0.768	1.020	0.792	0.690	0.884	0.557	0.608
MnO	0.013	0.007	0.019	-	0.008	-	-	-	0.009	-
MgO	0.016	0.028	0.015	0.025	0.208	0.006	0.028	0.058	0.013	0.025
CaO	11.459	9.816	10.725	10.784	10.661	11.847	10.979	10.481	9.755	11.027
Na_2O	4.620	5.556	5.125	5.037	4.778	4.411	4.806	4.725	5.459	4.728
K_2O	0.238	0.368	0.298	0.310	0.297	0.243	0.278	0.553	0.342	0.294
Total	**100.033**	**99.949**	**99.947**	**100.082**	**98.834**	**100.359**	**99.252**	**100.232**	**99.465**	**99.706**
An %	57.00	48.34	52.69	53.21	54.23	58.89	54.88	53.23	48.68	55.32
Ab %	41.59	49.51	45.56	44.97	43.98	39.67	43.47	43.43	49.29	42.92
Or %	1.41	2.16	1.74	1.82	1.80	1.44	1.65	3.34	2.03	1.76

Sample:	12 (middle basalt)								
Crystal:	Plagioclase								
No.	**38**	**39**	**40**	**41**	**42**	**43**	**44**	**45**	**46**
(wt. %)									
SiO_2	55.633	54.234	54.107	54.231	54.680	53.516	54.219	54.436	55.809
TiO_2	0.104	0.109	0.090	0.104	0.081	0.067	0.089	0.080	0.086
Al_2O_3	27.999	29.378	29.148	28.003	28.931	29.147	28.459	28.184	27.671
FeO	0.639	0.790	0.721	0.691	0.549	0.738	0.702	0.747	0.635
MnO	-	-	0.013	-	0.005	-	-	0.010	0.001
MgO	0.025	0.028	0.015	0.024	0.034	0.026	-	0.051	0.013
CaO	9.761	10.989	10.752	9.946	10.663	11.299	10.382	10.294	9.497
Na_2O	5.513	4.768	4.783	5.312	4.845	4.774	5.373	5.389	5.731
K_2O	0.338	0.256	0.241	0.395	0.339	0.249	0.279	0.320	0.345
Total	**100.012**	**100.552**	**99.870**	**98.706**	**100.127**	**99.817**	**99.503**	**99.511**	**99.788**
An %	48.46	55.16	54.59	49.66	53.76	55.84	50.80	50.40	46.83
Ab %	49.54	43.31	43.95	47.99	44.21	42.70	47.58	47.74	51.14
Or %	2.00	1.53	1.46	2.35	2.03	1.47	1.63	1.87	2.03

Sample:	13 (lower basalt)											
Crystal:	Plagioclase											
No.	**51**	**52**	**53**	**54**	**55**	**57**	**58**	**60**	**61**	**62**	**65**	**68**
(wt. %)												
SiO_2	52.975	52.545	53.141	52.631	53.620	52.249	51.868	53.682	52.029	53.135	52.605	52.536
TiO_2	0.129	0.115	0.092	0.114	0.077	0.110	0.097	0.155	0.083	0.110	0.083	0.118
Al_2O_3	30.229	29.697	29.940	30.518	29.434	30.456	30.540	29.320	30.466	29.896	30.166	29.727
FeO	0.789	0.780	0.998	0.900	0.640	0.691	1.052	0.997	0.749	0.774	0.802	0.653
MnO	0.012	0.004	0.006	0.017	0.025	-	-	-	0.002	-	0.015	0.033
MgO	0.060	0.046	0.055	0.069	0.028	0.055	0.053	0.074	0.073	0.046	0.061	0.069
CaO	12.107	11.623	11.990	12.344	11.180	12.454	12.801	11.237	12.575	11.529	12.020	12.031
Na_2O	3.994	4.401	4.103	4.222	4.568	3.838	4.000	4.574	4.090	4.385	4.360	4.175
K_2O	0.348	0.599	0.300	0.313	0.399	0.278	0.254	0.373	0.359	0.422	0.334	0.322
Total	**100.644**	**99.809**	**100.624**	**101.127**	**99.971**	**100.132**	**100.665**	**100.412**	**100.426**	**100.297**	**100.446**	**99.664**
An %	61.30	57.26	60.64	60.64	56.12	63.12	62.93	56.30	61.63	57.74	59.19	60.25
Ab %	36.60	39.23	37.55	37.53	41.49	35.20	35.59	41.47	36.28	39.74	38.85	37.83
Or %	2.10	3.51	1.81	1.83	2.38	1.68	1.49	2.23	2.09	2.52	1.96	1.92

Appendix V

Raw XRF Data and CIPW Norm Calculations

	Upper Basalt						
	ne-hawaiite	basanite	basanite	basanite	basanite	ne-hawaiite	basanite
Equivalent thin section no.[1]	**7**	**11**	**28**	**33**	**41**	**44**	**45**
Major elements (wt. %)							
SiO_2	47.05	42.74	43.52	47.19	47.11	47.13	41.05
Al_2O_3	15.33	12.73	12.81	14.95	14.81	15.11	13.34
TiO_2	2.232	3.151	2.95	2.23	2.203	2.372	1.925
MnO	0.1831	0.1777	0.1877	0.1773	0.1902	0.1867	0.1535
Fe_2O_3	13.349	14.232	14.607	13.177	13.298	13.134	10.954
Na_2O	3.907	3.693	3.301	4.893	4.836	3.82	4.644
MgO	6.208	11.068	10.385	6.578	6.357	5.976	4.988
K_2O	1.838	1.438	1.073	1.87	1.918	1.813	1.708
CaO	7.757	10.365	10.272	7.997	7.648	7.854	6.04
P_2O_5	0.76	0.802	0.632	0.75	0.772	0.74	0.719
Total[2]	**100.24**	**101.07**	**100.11**	**100.43**	**100.23**	**100.13**	**102.35**
LOI[2]	1.32	0.25	0.05	0.3	0.75	1.66	16.55
Trace elements (ppm)							
F	364	782	455	403	516	472	364
S	0	578	162	5	38	0	0
Cl	158	135	89	258	296	180	258
Sc	11	11	15	13	10	11	6
V	167	263	306	170	161	170	129
Cr	184	285	330	215	205	205	113
Co	55	93	78	57	57	62	45
Ni	100	254	264	103	128	103	71
Cu	53	69	45	55	49	52	40
Zn	119	124	108	111	122	122	103
Ga	28	23	24	27	26	27	22
As	6	6	6	6	7	6	6
Rb	29	23	19	30	31	33	28
Sr	839	720	622	785	791	890	684
Y	23	23	22	23	24	23	18
Zr	370	271	223	351	363	371	338
Nb	59	52	42	54	58	59	46
Mo	6	7	5	6	6	6	5
Sn	3	0	2	3	3	4	0
Sb	0	0	0	0	0	0	0
Cs	13	19	18	13	12	13	10
Ba	291	258	199	275	293	300	265
La	62	48	41	56	52	61	50
Ce	101	99	78	102	112	107	98
Nd	39	40	31	41	41	37	37
Tl	0	0	0	0	0	0	0
Pb	3	3	3	3	3	3	3
Th	8	7	7	8	8	8	7
U	3	3	3	3	3	3	3

[1] Samples analysed correspond to thin sections.

[2] LOI and total are original figures.

LOI = Loss on ignition; Total Fe expressed as Fe_2O_3.

	Middle Basalt					
	ne-hawaiite	ne-hawaiite	ne-hawaiite	basanite	ne-hawaiite	ne-hawaiite
Equivalent thin section no.[1]	**1**	**3**	**5**	**6**	**12**	**20**
Major elements (wt. %)						
SiO_2	46.85	46.68	47.14	47.73	46.56	45.35
Al_2O_3	14.88	14.79	15.02	15.41	14.46	14.02
TiO_2	2.162	2.399	2.232	2.126	2.215	2.308
MnO	0.176	0.1904	0.1887	0.1788	0.1766	0.1831
Fe_2O_3	12.997	13.532	13.121	12.913	13.148	12.922
Na_2O	4.437	3.721	4.872	5.458	4.18	3.855
MgO	6.382	6.791	6.26	5.845	7.427	7.329
K_2O	1.831	1.767	1.902	2.063	1.768	1.673
CaO	7.767	7.806	7.758	7.269	7.806	7.694
P_2O_5	0.762	0.747	0.763	0.829	0.736	0.719
Total[2]	**98.95**	**100.44**	**99.96**	**100.45**	**99.89**	**98.17**
LOI[2]	0.4	1.66	0.38	0.31	1.09	1.78
Trace elements (ppm)						
F	245	493	517	289	503	475
S	0	100	0	0	30	58
Cl	221	163	254	389	220	140
Sc	10	11	10	9	10	11
V	166	178	162	148	164	170
Cr	189	225	197	143	216	224
Co	50	66	60	54	52	53
Ni	101	149	105	85	130	142
Cu	49	56	49	51	55	44
Zn	113	126	121	113	112	116
Ga	27	25	26	26	25	25
As	7	8	9	8	6	8
Rb	31	28	29	33	28	29
Sr	868	798	794	825	800	826
Y	25	29	23	23	24	25
Zr	364	350	360	386	347	338
Nb	61	57	58	59	55	59
Mo	6	6	6	6	6	6
Sn	3	1	2	2	3	5
Sb	0	0	0	0	1	1
Cs	12	13	12	12	13	13
Ba	308	501	280	305	292	288
La	58	59	53	51	56	55
Ce	103	105	110	114	99	97
Nd	45	42	38	35	37	41
Tl	0	0	0	0	0	0
Pb	3	3	3	3	3	3
Th	8	8	8	8	8	8
U	3	3	3	3	3	3

[1] Samples analysed correspond to thin sections.

[2] LOI and total are original figures.

LOI = Loss on ignition; Total Fe expressed as Fe_2O_3.

	Middle Basalt					
	ne-hawaiite	ne-hawaiite	ne-hawaiite	ne-hawaiite	ne-hawaiite	ne-hawaiite
Equivalent thin section no.[1]	22	23	25	27	30	35
Major elements (wt. %)						
SiO_2	47.87	47.18	47.03	46.18	47.53	46.83
Al_2O_3	15.39	14.55	14.79	14.04	15.22	14.38
TiO_2	2.17	2.347	2.301	2.257	2.25	2.293
MnO	0.1756	0.1855	0.1913	0.1882	0.1764	0.1771
Fe_2O_3	12.933	13.171	13.271	13.366	13.078	13.228
Na_2O	5.047	4.697	4.834	4.149	4.951	4.707
MgO	5.92	6.823	6.201	7.323	6.236	7.251
K_2O	1.999	1.876	1.923	1.828	1.922	1.829
CaO	7.303	7.769	7.848	7.983	7.691	7.954
P_2O_5	0.834	0.743	0.767	0.741	0.79	0.733
Total[2]	**100.18**	**99.77**	**99.65**	**98.45**	**100.25**	**100.35**
LOI[2]	0.22	0.08	0.15	0.05	0.1	0.64
Trace elements (ppm)						
F	321	361	443	444	287	398
S	0	0	93	0	0	98
Cl	304	503	353	194	293	276
Sc	11	9	10	11	10	11
V	147	168	165	172	157	167
Cr	148	209	217	213	168	208
Co	49	57	62	57	50	58
Ni	86	132	117	139	93	134
Cu	49	53	58	53	50	57
Zn	118	120	121	115	117	114
Ga	26	27	26	27	27	25
As	6	8	7	7	7	6
Rb	32	30	31	37	31	29
Sr	860	815	822	866	817	776
Y	24	24	24	25	23	23
Zr	393	361	365	353	373	339
Nb	61	60	60	60	60	54
Mo	6	6	6	6	6	6
Sn	3	3	3	4	2	2
Sb	0	1	0	2	0	1
Cs	12	13	13	13	13	13
Ba	314	297	308	302	299	281
La	63	59	56	55	58	53
Ce	106	107	101	107	106	96
Nd	42	44	35	43	40	38
Tl	0	0	0	1	1	0
Pb	3	3	3	3	3	3
Th	8	8	8	8	8	8
U	3	3	3	3	3	3

[1] Samples analysed correspond to thin sections.

[2] LOI and total are original figures.

LOI = Loss on ignition; Total Fe expressed as Fe_2O_3.

	Middle Basalt			Lower Basalt	
	ne-hawaiite	ne-hawaiite	ne-hawaiite	basanite	ne-hawaiite
Equivalent thin section no.[1]	**37**	**42**	**46**	**13**	**47**
Major elements (wt. %)					
SiO_2	47.36	46.32	46.75	42.56	46.12
Al_2O_3	14.98	14.3	14.51	12.43	14.63
TiO_2	2.299	2.332	2.333	3.031	2.535
MnO	0.1803	0.1886	0.1829	0.2004	0.1938
Fe_2O_3	13.150	13.065	13.266	15.190	13.576
Na_2O	4.978	4.074	4.649	3.972	3.597
MgO	6.59	7.415	7.197	10.987	6.943
K_2O	1.856	1.747	1.82	1.472	1.53
CaO	8.006	7.803	7.778	10.096	8.085
P_2O_5	0.759	0.731	0.735	0.774	0.74
Total[2]	**100.74**	**98.59**	**100.07**	**101.38**	**98.56**
LOI[2]	0.26	0.27	0.51	0.22	0.22
Trace elements (ppm)					
F	313	488	433	678	586
S	0	0	0	986	154
Cl	330	271	282	168	242
Sc	9	10	11	11	11
V	172	175	171	252	185
Cr	206	224	222	273	220
Co	59	53	136	72	62
Ni	105	138	146	241	160
Cu	52	53	60	69	57
Zn	114	118	117	114	130
Ga	26	26	25	22	27
As	8	7	8	7	8
Rb	29	30	30	23	25
Sr	786	827	786	673	848
Y	23	25	23	22	26
Zr	353	349	340	261	352
Nb	55	60	56	49	62
Mo	6	6	6	5	6
Sn	2	4	1	0	2
Sb	0	2	0	0	0
Cs	13	13	13	18	15
Ba	299	292	281	247	427
La	52	56	51	46	54
Ce	108	107	98	97	111
Nd	38	36	39	36	35
Tl	0	0	0	0	0
Pb	3	3	3	3	3
Th	8	8	8	7	8
U	3	3	3	3	3

[1] Samples analysed correspond to thin sections.

[2] LOI and total are original figures.

LOI = Loss on ignition; Total Fe expressed as Fe_2O_3.

CIPW Norm Calculations

Norm 4: norm calculation program Program run: 15/09/2016 HELP

Sample Number: 1

	Rock Analysis		Normalization Factors		Normalized Analysis	Normative Minerals	Weight % Norm	Volume % Norm
SiO2	47.69	%	Total=100%? Y/N	n	47.69	Quartz		
TiO2	2.20	%	Fe3+/(Total Iron)	0.1	2.20	Plagioclase	37.94	42.58
Al2O3	15.15	%			15.15	Orthoclase	11.02	12.92
Fe2O3		%	Total Fe as FeO	13.23	1.47	Nepheline	8.57	10.05
FeO	13.23	%	Desired Fe2O3	1.47	11.91	Leucite		
MnO	0.18	%	Desired FeO	11.91	0.18	Kalsilite		
MgO	6.50	%	Weight corr. factor	1.000	6.50	Corundum		
CaO	7.91	%			7.91	Diopside	15.43	13.73
Na2O	4.52	%			4.52	Hypersthene		
K2O	1.86	%			1.86	Wollastonite		
P2O5	0.78	%	Zero values not shown		0.78	Olivine	19.08	15.30
CO2		%				Larnite		
SO3		%				Acmite		
S		%				K2SiO3		
F		%	Norm calculation checks:			Na2SiO3		
Cl		%	Norm seems OK			Rutile		
Sr		ppm				Ilmenite	4.18	2.64
Ba		ppm				Magnetite	2.13	1.23
Ni		ppm				Hematite		
Cr		ppm	Macro-enabled			Apatite	1.80	1.69
Zr		ppm				Zircon		
Total	100.00				100.15	Perovskite		
						Chromite		
						Titanite		
						Pyrite		
						Halite		
						Fluorite		
						Anhydrite		
						Na2SO4		
						Calcite		
						Na2CO3		
						Total	100.15	100.15

Fe3+/(Total Fe) in rock	10.0	10.0
Mg/(Mg+Total Fe) in rock	46.7	46.7
Mg/(Mg+Fe2+) in rock	49.3	49.3
Mg/(Mg+Fe2+) in silicates	55.1	55.1
Ca/(Ca+Na) in rock	49.2	49.2
Plagioclase An content	39.6	39.6
Differentiation Index	57.5	65.6
Calculated density, g/cc	3.01	3.01
Calculated liquid density, g/cc	2.69	2.69
Calculated viscosity, dry, Pas	0.17	0.17
Calculated viscosity, wet, Pas	0.16	0.16
Estimated liquidus temp., °C	1257	1257
Estimated H2O content, wt. %	0.25	0.25

This program was written by Kurt Hollocher, Geology Department, Union College, Schenectady, NY, 12308, hollochk@union.edu

Norm 4: norm calculation program Program run: 15/09/2016 HELP

Sample Number: 3

	Rock Analysis	
SiO2	47.43	%
TiO2	2.44	%
Al2O3	15.03	%
Fe2O3		%
FeO	13.75	%
MnO	0.19	%
MgO	6.90	%
CaO	7.93	%
Na2O	3.78	%
K2O	1.80	%
P2O5	0.76	%
CO2		%
SO3		%
S		%
F		%
Cl		%
Sr		ppm
Ba		ppm
Ni		ppm
Cr		ppm
Zr		ppm
Total	100.00	

Normalization Factors	
Total=100%? Y/N	n
Fe3+/(Total Iron)	0.1
Total Fe as FeO	13.75
Desired Fe2O3	1.53
Desired FeO	12.37
Weight corr. factor	1.000

Zero values not shown

Norm calculation checks:
Norm seems OK

Macro-enabled

Normalized Analysis
47.43
2.44
15.03
1.53
12.37
0.19
6.90
7.93
3.78
1.80
0.76
100.15

Normative Minerals	Weight % Norm	Volume % Norm
Quartz		
Plagioclase	42.45	47.83
Orthoclase	10.61	12.51
Nepheline	4.48	5.29
Leucite		
Kalsilite		
Corundum		
Diopside	12.97	11.62
Hypersthene		
Wollastonite		
Olivine	21.04	17.01
Larnite		
Acmite		
K2SiO3		
Na2SiO3		
Rutile		
Ilmenite	4.63	2.94
Magnetite	2.22	1.29
Hematite		
Apatite	1.76	1.66
Zircon		
Perovskite		
Chromite		
Titanite		
Pyrite		
Halite		
Fluorite		
Anhydrite		
Na2SO4		
Calcite		
Na2CO3		
Total	100.15	100.15
Fe3+/(Total Fe) in rock	10.0	10.0
Mg/(Mg+Total Fe) in rock	47.2	47.2
Mg/(Mg+Fe2+) in rock	49.9	49.9
Mg/(Mg+Fe2+) in silicates	55.9	55.9
Ca/(Ca+Na) in rock	53.7	53.7
Plagioclase An content	42.7	42.7
Differentiation Index	57.5	65.6
Calculated density, g/cc	3.02	3.02
Calculated liquid density, g/cc	2.71	2.71
Calculated viscosity, dry, Pas	0.17	0.17
Calculated viscosity, wet, Pas	0.16	0.16
Estimated liquidus temp., °C	1262	1262
Estimated H2O content, wt. %	0.24	0.24

This program was written by Kurt Hollocher, Geology Department, Union College, Schenectady, NY, 12308, hollochk@union.edu

Norm 4: norm calculation program Program run: 15/09/2016 HELP

Sample Number: 5

	Rock Analysis	
SiO2	47.49	%
TiO2	2.25	%
Al2O3	15.13	%
Fe2O3		%
FeO	13.22	%
MnO	0.19	%
MgO	6.31	%
CaO	7.82	%
Na2O	4.91	%
K2O	1.92	%
P2O5	0.77	%
CO2		%
SO3		%
S		%
F		%
Cl		%
Sr		ppm
Ba		ppm
Ni		ppm
Cr		ppm
Zr		ppm
Total	100.00	

Normalization Factors	
Total=100%? Y/N	n
Fe3+/(Total Iron)	0.1
Total Fe as FeO	13.22
Desired Fe2O3	1.47
Desired FeO	11.90
Weight corr. factor	1.000

Zero values not shown

Norm calculation checks:

Norm seems OK

Macro-enabled

Normalized Analysis
47.49
2.25
15.13
1.47
11.90
0.19
6.31
7.82
4.91
1.92
0.77
100.15

Normative Minerals	Weight % Norm	Volume % Norm
Quartz		
Plagioclase	34.56	38.79
Orthoclase	11.32	13.27
Nepheline	11.14	13.06
Leucite		
Kalsilite		
Corundum		
Diopside	16.73	14.87
Hypersthene		
Wollastonite		
Olivine	18.21	14.56
Larnite		
Acmite		
K2SiO3		
Na2SiO3		
Rutile		
Ilmenite	4.27	2.70
Magnetite	2.13	1.23
Hematite		
Apatite	1.78	1.67
Zircon		
Perovskite		
Chromite		
Titanite		
Pyrite		
Halite		
Fluorite		
Anhydrite		
Na2SO4		
Calcite		
Na2CO3		
Total	100.15	100.15

Fe3+/(Total Fe) in rock	10.0	10.0
Mg/(Mg+Total Fe) in rock	46.0	46.0
Mg/(Mg+Fe2+) in rock	48.6	48.6
Mg/(Mg+Fe2+) in silicates	54.4	54.4
Ca/(Ca+Na) in rock	46.8	46.8
Plagioclase An content	37.9	37.9
Differentiation Index	57.0	65.1
Calculated density, g/cc	3.00	3.00
Calculated liquid density, g/cc	2.69	2.69
Calculated viscosity, dry, Pas	0.16	0.16
Calculated viscosity, wet, Pas	0.16	0.16
Estimated liquidus temp., °C	1261	1261
Estimated H2O content, wt. %	0.24	0.24

This program was written by Kurt Hollocher, Geology Department, Union College, Schenectady, NY, 12308, hollochk@union.edu

Norm 4: norm calculation program Program run: 15/09/2016 HELP

Sample Number: 6

	Rock Analysis	
SiO2	47.82	%
TiO2	2.13	%
Al2O3	15.44	%
Fe2O3		%
FeO	12.93	%
MnO	0.18	%
MgO	5.86	%
CaO	7.28	%
Na2O	5.47	%
K2O	2.07	%
P2O5	0.83	%
CO2		%
SO3		%
S		%
F		%
Cl		%
Sr		ppm
Ba		ppm
Ni		ppm
Cr		ppm
Zr		ppm
Total	100.00	

Normalization Factors	
Total=100%? Y/N	n
Fe3+/(Total Iron)	0.1
Total Fe as FeO	12.93
Desired Fe2O3	1.44
Desired FeO	11.64
Weight corr. factor	1.000

Zero values not shown

Norm calculation checks:
Norm seems OK

Macro-enabled

Normalized Analysis
47.82
2.13
15.44
1.44
11.64
0.18
5.86
7.28
5.47
2.07
0.83
100.14

Normative Minerals	Weight % Norm	Volume % Norm
Quartz		
Plagioclase	33.04	36.91
Orthoclase	12.21	14.22
Nepheline	13.38	15.58
Leucite		
Kalsilite		
Corundum		
Diopside	15.99	14.10
Hypersthene		
Wollastonite		
Olivine	17.46	13.80
Larnite		
Acmite		
K2SiO3		
Na2SiO3		
Rutile		
Ilmenite	4.05	2.54
Magnetite	2.08	1.19
Hematite		
Apatite	1.92	1.79
Zircon		
Perovskite		
Chromite		
Titanite		
Pyrite		
Halite		
Fluorite		
Anhydrite		
Na2SO4		
Calcite		
Na2CO3		
Total	100.14	100.14
Fe3+/(Total Fe) in rock	10.0	10.0
Mg/(Mg+Total Fe) in rock	44.7	44.7
Mg/(Mg+Fe2+) in rock	47.3	47.3
Mg/(Mg+Fe2+) in silicates	53.0	53.0
Ca/(Ca+Na) in rock	42.4	42.4
Plagioclase An content	33.4	33.4
Differentiation Index	58.6	66.7
Calculated density, g/cc	2.98	2.98
Calculated liquid density, g/cc	2.67	2.67
Calculated viscosity, dry, Pas	0.17	0.17
Calculated viscosity, wet, Pas	0.16	0.16
Estimated liquidus temp., °C	1255	1255
Estimated H2O content, wt. %	0.26	0.26

This program was written by Kurt Hollocher, Geology Department, Union College, Schenectady, NY, 12308, hollochk@union.edu

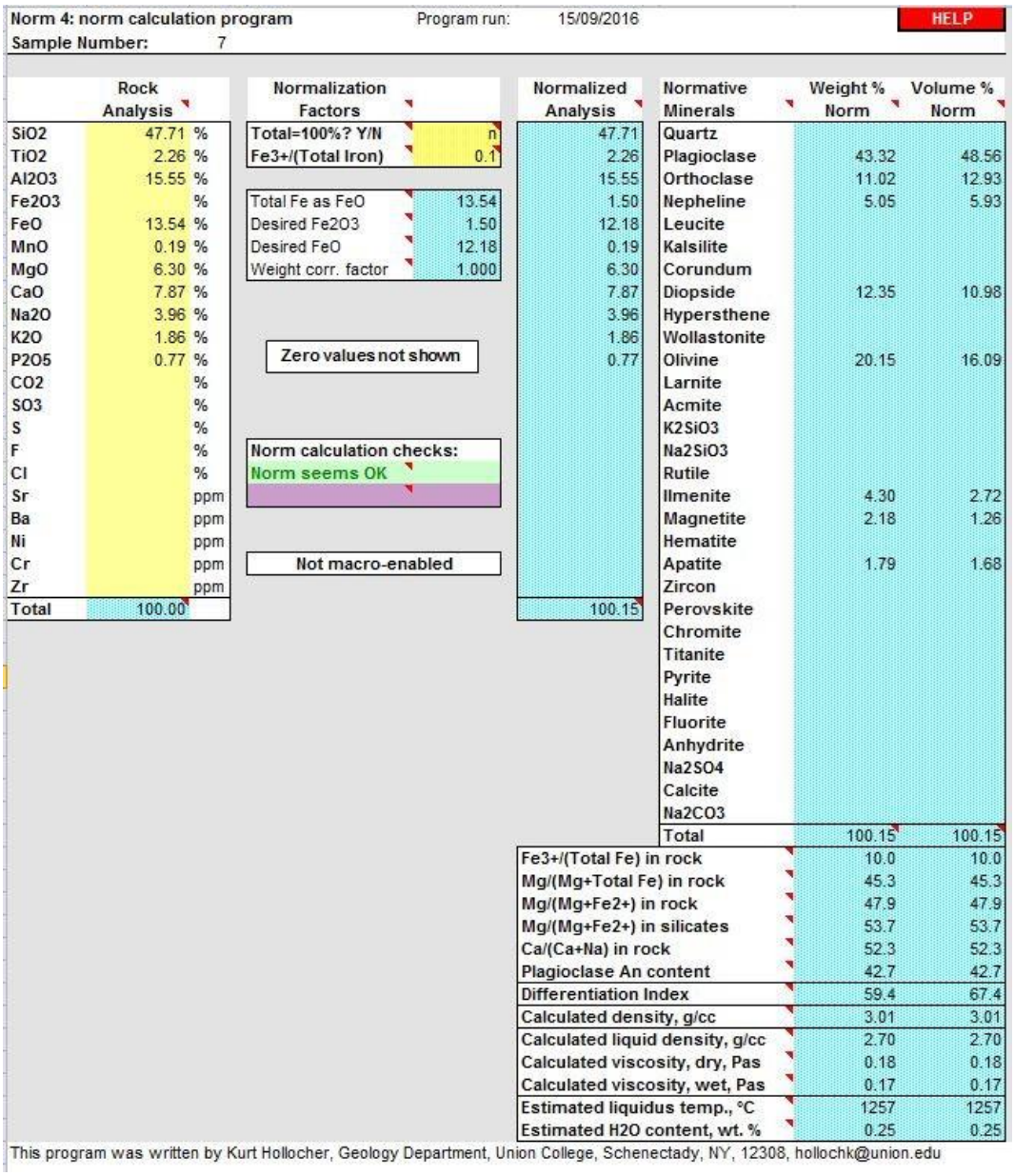

Norm 4: norm calculation program Program run: 15/09/2016 HELP

Sample Number: 7

	Rock Analysis	
SiO2	47.71	%
TiO2	2.26	%
Al2O3	15.55	%
Fe2O3		%
FeO	13.54	%
MnO	0.19	%
MgO	6.30	%
CaO	7.87	%
Na2O	3.96	%
K2O	1.86	%
P2O5	0.77	%
CO2		%
SO3		%
S		%
F		%
Cl		%
Sr		ppm
Ba		ppm
Ni		ppm
Cr		ppm
Zr		ppm
Total	100.00	

Normalization Factors	
Total=100%? Y/N	n
Fe3+/(Total Iron)	0.1
Total Fe as FeO	13.54
Desired Fe2O3	1.50
Desired FeO	12.18
Weight corr. factor	1.000

Zero values not shown

Norm calculation checks:

Norm seems OK

Not macro-enabled

Normalized Analysis
47.71
2.26
15.55
1.50
12.18
0.19
6.30
7.87
3.96
1.86
0.77
100.15

Normative Minerals	Weight % Norm	Volume % Norm
Quartz		
Plagioclase	43.32	48.56
Orthoclase	11.02	12.93
Nepheline	5.05	5.93
Leucite		
Kalsilite		
Corundum		
Diopside	12.35	10.98
Hypersthene		
Wollastonite		
Olivine	20.15	16.09
Larnite		
Acmite		
K2SiO3		
Na2SiO3		
Rutile		
Ilmenite	4.30	2.72
Magnetite	2.18	1.26
Hematite		
Apatite	1.79	1.68
Zircon		
Perovskite		
Chromite		
Titanite		
Pyrite		
Halite		
Fluorite		
Anhydrite		
Na2SO4		
Calcite		
Na2CO3		
Total	100.15	100.15

Fe3+/(Total Fe) in rock	10.0	10.0
Mg/(Mg+Total Fe) in rock	45.3	45.3
Mg/(Mg+Fe2+) in rock	47.9	47.9
Mg/(Mg+Fe2+) in silicates	53.7	53.7
Ca/(Ca+Na) in rock	52.3	52.3
Plagioclase An content	42.7	42.7
Differentiation Index	59.4	67.4
Calculated density, g/cc	3.01	3.01
Calculated liquid density, g/cc	2.70	2.70
Calculated viscosity, dry, Pas	0.18	0.18
Calculated viscosity, wet, Pas	0.17	0.17
Estimated liquidus temp., °C	1257	1257
Estimated H2O content, wt. %	0.25	0.25

This program was written by Kurt Hollocher, Geology Department, Union College, Schenectady, NY, 12308, hollochk@union.edu

Norm 4: norm calculation program Program run: 15/09/2016 HELP

Sample Number: 11

	Rock Analysis		Normalization Factors		Normalized Analysis	Normative Minerals	Weight % Norm	Volume % Norm
SiO2	42.57	%	Total=100%? Y/N	n	42.57	Quartz		
TiO2	3.14	%	Fe3+/(Total Iron)	0.1	3.14	Plagioclase	16.94	19.37
Al2O3	12.68	%			12.68	Orthoclase	8.46	10.33
Fe2O3		%	Total Fe as FeO	14.18	1.58	Nepheline	15.19	18.55
FeO	14.18	%	Desired Fe2O3	1.58	12.76	Leucite		
MnO	0.18	%	Desired FeO	12.76	0.18	Kalsilite		
MgO	11.02	%	Weight corr. factor	1.000	11.02	Corundum		
CaO	10.32	%			10.32	Diopside	26.19	24.59
Na2O	3.68	%			3.68	Hypersthene		
K2O	1.43	%	Zero values not shown		1.43	Wollastonite		
P2O5	0.80	%			0.80	Olivine	23.27	20.22
CO2		%				Larnite		
SO3		%				Acmite		
S		%				K2SiO3		
F		%	Norm calculation checks:			Na2SiO3		
Cl		%	Norm seems OK			Rutile		
Sr		ppm				Ilmenite	5.96	3.92
Ba		ppm				Magnetite	2.28	1.37
Ni		ppm				Hematite		
Cr		ppm	Not macro-enabled			Apatite	1.85	1.81
Zr		ppm				Zircon		
Total	100.00				100.16	Perovskite		
						Chromite		
						Titanite		
						Pyrite		
						Halite		
						Fluorite		
						Anhydrite		
						Na2SO4		
						Calcite		
						Na2CO3		
						Total	100.16	100.16
						Fe3+/(Total Fe) in rock	10.0	10.0
						Mg/(Mg+Total Fe) in rock	58.1	58.1
						Mg/(Mg+Fe2+) in rock	60.6	60.6
						Mg/(Mg+Fe2+) in silicates	67.6	67.6
						Ca/(Ca+Na) in rock	60.8	60.8
						Plagioclase An content	80.9	80.9
						Differentiation Index	40.6	48.3
						Calculated density, g/cc	3.13	3.13
						Calculated liquid density, g/cc	2.77	2.77
						Calculated viscosity, dry, Pas	0.07	0.07
						Calculated viscosity, wet, Pas	0.07	0.07
						Estimated liquidus temp., °C	1351	1351
						Estimated H2O content, wt. %	0.11	0.11

This program was written by Kurt Hollocher, Geology Department, Union College, Schenectady, NY, 12308, hollochk@union.edu

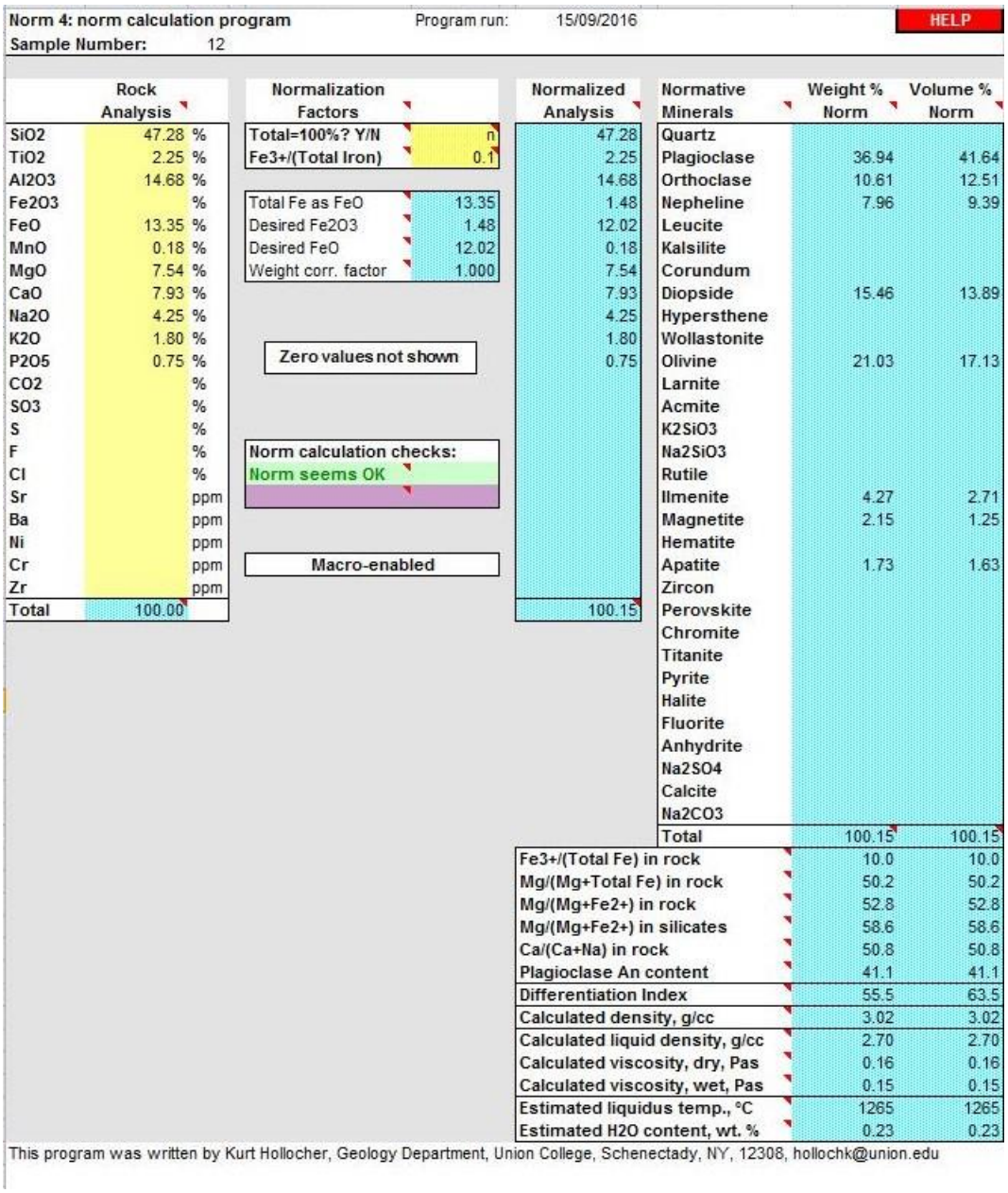

Norm 4: norm calculation program Program run: 15/09/2016 HELP

Sample Number: 12

	Rock Analysis	
SiO2	47.28	%
TiO2	2.25	%
Al2O3	14.68	%
Fe2O3		%
FeO	13.35	%
MnO	0.18	%
MgO	7.54	%
CaO	7.93	%
Na2O	4.25	%
K2O	1.80	%
P2O5	0.75	%
CO2		%
SO3		%
S		%
F		%
Cl		%
Sr		ppm
Ba		ppm
Ni		ppm
Cr		ppm
Zr		ppm
Total	100.00	

Normalization Factors	
Total=100%? Y/N	n
Fe3+/(Total Iron)	0.1
Total Fe as FeO	13.35
Desired Fe2O3	1.48
Desired FeO	12.02
Weight corr. factor	1.000

Zero values not shown

Norm calculation checks:

Norm seems OK

Macro-enabled

Normalized Analysis
47.28
2.25
14.68
1.48
12.02
0.18
7.54
7.93
4.25
1.80
0.75
100.15

Normative Minerals	Weight % Norm	Volume % Norm
Quartz		
Plagioclase	36.94	41.64
Orthoclase	10.61	12.51
Nepheline	7.96	9.39
Leucite		
Kalsilite		
Corundum		
Diopside	15.46	13.89
Hypersthene		
Wollastonite		
Olivine	21.03	17.13
Larnite		
Acmite		
K2SiO3		
Na2SiO3		
Rutile		
Ilmenite	4.27	2.71
Magnetite	2.15	1.25
Hematite		
Apatite	1.73	1.63
Zircon		
Perovskite		
Chromite		
Titanite		
Pyrite		
Halite		
Fluorite		
Anhydrite		
Na2SO4		
Calcite		
Na2CO3		
Total	100.15	100.15

Fe3+/(Total Fe) in rock	10.0	10.0
Mg/(Mg+Total Fe) in rock	50.2	50.2
Mg/(Mg+Fe2+) in rock	52.8	52.8
Mg/(Mg+Fe2+) in silicates	58.6	58.6
Ca/(Ca+Na) in rock	50.8	50.8
Plagioclase An content	41.1	41.1
Differentiation Index	55.5	63.5
Calculated density, g/cc	3.02	3.02
Calculated liquid density, g/cc	2.70	2.70
Calculated viscosity, dry, Pas	0.16	0.16
Calculated viscosity, wet, Pas	0.15	0.15
Estimated liquidus temp., °C	1265	1265
Estimated H2O content, wt. %	0.23	0.23

This program was written by Kurt Hollocher, Geology Department, Union College, Schenectady, NY, 12308, hollochk@union.edu

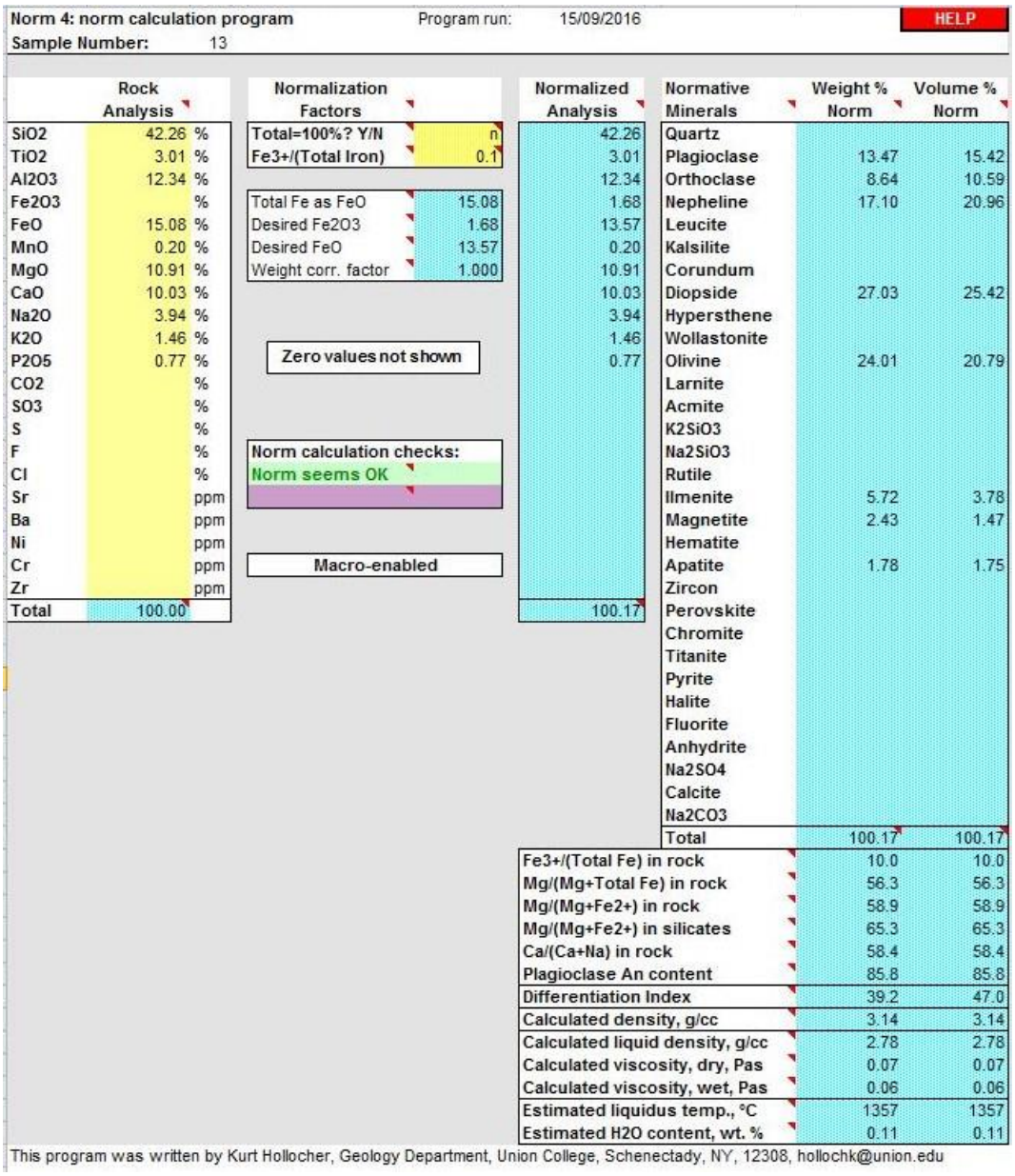

Norm 4: norm calculation program Program run: 15/09/2016 HELP

Sample Number: 13

	Rock Analysis	
SiO2	42.26	%
TiO2	3.01	%
Al2O3	12.34	%
Fe2O3		%
FeO	15.08	%
MnO	0.20	%
MgO	10.91	%
CaO	10.03	%
Na2O	3.94	%
K2O	1.46	%
P2O5	0.77	%
CO2		%
SO3		%
S		%
F		%
Cl		%
Sr		ppm
Ba		ppm
Ni		ppm
Cr		ppm
Zr		ppm
Total	100.00	

Normalization Factors	
Total=100%? Y/N	n
Fe3+/(Total Iron)	0.1
Total Fe as FeO	15.08
Desired Fe2O3	1.68
Desired FeO	13.57
Weight corr. factor	1.000

Zero values not shown

Norm calculation checks:
Norm seems OK

Macro-enabled

Normalized Analysis
42.26
3.01
12.34
1.68
13.57
0.20
10.91
10.03
3.94
1.46
0.77
100.17

Normative Minerals	Weight % Norm	Volume % Norm
Quartz		
Plagioclase	13.47	15.42
Orthoclase	8.64	10.59
Nepheline	17.10	20.96
Leucite		
Kalsilite		
Corundum		
Diopside	27.03	25.42
Hypersthene		
Wollastonite		
Olivine	24.01	20.79
Larnite		
Acmite		
K2SiO3		
Na2SiO3		
Rutile		
Ilmenite	5.72	3.78
Magnetite	2.43	1.47
Hematite		
Apatite	1.78	1.75
Zircon		
Perovskite		
Chromite		
Titanite		
Pyrite		
Halite		
Fluorite		
Anhydrite		
Na2SO4		
Calcite		
Na2CO3		
Total	100.17	100.17

Fe3+/(Total Fe) in rock	10.0	10.0
Mg/(Mg+Total Fe) in rock	56.3	56.3
Mg/(Mg+Fe2+) in rock	58.9	58.9
Mg/(Mg+Fe2+) in silicates	65.3	65.3
Ca/(Ca+Na) in rock	58.4	58.4
Plagioclase An content	85.8	85.8
Differentiation Index	39.2	47.0
Calculated density, g/cc	3.14	3.14
Calculated liquid density, g/cc	2.78	2.78
Calculated viscosity, dry, Pas	0.07	0.07
Calculated viscosity, wet, Pas	0.06	0.06
Estimated liquidus temp., °C	1357	1357
Estimated H2O content, wt. %	0.11	0.11

This program was written by Kurt Hollocher, Geology Department, Union College, Schenectady, NY, 12308, hollochk@union.edu

Norm 4: norm calculation program Program run: 15/09/2016 HELP

Sample Number: 20

	Rock Analysis	
SiO2	47.21	%
TiO2	2.40	%
Al2O3	14.60	%
Fe2O3		%
FeO	13.45	%
MnO	0.19	%
MgO	7.63	%
CaO	8.01	%
Na2O	4.01	%
K2O	1.74	%
P2O5	0.75	%
CO2		%
SO3		%
S		%
F		%
Cl		%
Sr		ppm
Ba		ppm
Ni		ppm
Cr		ppm
Zr		ppm
Total	100.00	

Normalization Factors	
Total=100%? Y/N	n
Fe3+/(Total Iron)	0.1
Total Fe as FeO	13.45
Desired Fe2O3	1.50
Desired FeO	12.11
Weight corr. factor	1.000

Zero values not shown

Norm calculation checks:

Norm seems OK

Macro-enabled

Normalized Analysis
47.21
2.40
14.60
1.50
12.11
0.19
7.63
8.01
4.01
1.74
0.75
100.15

Normative Minerals	Weight % Norm	Volume % Norm
Quartz		
Plagioclase	38.56	43.54
Orthoclase	10.29	12.16
Nepheline	6.54	7.72
Leucite		
Kalsilite		
Corundum		
Diopside	14.99	13.50
Hypersthene		
Wollastonite		
Olivine	21.30	17.41
Larnite		
Acmite		
K2SiO3		
Na2SiO3		
Rutile		
Ilmenite	4.56	2.91
Magnetite	2.17	1.26
Hematite		
Apatite	1.74	1.64
Zircon		
Perovskite		
Chromite		
Titanite		
Pyrite		
Halite		
Fluorite		
Anhydrite		
Na2SO4		
Calcite		
Na2CO3		
Total	100.15	100.15

Fe3+/(Total Fe) in rock	10.0	10.0
Mg/(Mg+Total Fe) in rock	50.3	50.3
Mg/(Mg+Fe2+) in rock	52.9	52.9
Mg/(Mg+Fe2+) in silicates	59.0	59.0
Ca/(Ca+Na) in rock	52.4	52.4
Plagioclase An content	41.8	41.8
Differentiation Index	55.4	63.4
Calculated density, g/cc	3.03	3.03
Calculated liquid density, g/cc	2.71	2.71
Calculated viscosity, dry, Pas	0.16	0.16
Calculated viscosity, wet, Pas	0.15	0.15
Estimated liquidus temp., °C	1266	1266
Estimated H2O content, wt. %	0.23	0.23

This program was written by Kurt Hollocher, Geology Department, Union College, Schenectady, NY, 12308, hollochk@union.edu

Norm 4: norm calculation program Program run: 15/09/2016 HELP

Sample Number: 22

	Rock Analysis	
SiO2	48.04	%
TiO2	2.18	%
Al2O3	15.45	%
Fe2O3		%
FeO	12.98	%
MnO	0.18	%
MgO	5.94	%
CaO	7.33	%
Na2O	5.07	%
K2O	2.01	%
P2O5	0.84	%
CO2		%
SO3		%
S		%
F		%
Cl		%
Sr		ppm
Ba		ppm
Ni		ppm
Cr		ppm
Zr		ppm
Total	100.00	

Normalization Factors	
Total=100%? Y/N	n
Fe3+/(Total Iron)	0.1
Total Fe as FeO	12.98
Desired Fe2O3	1.44
Desired FeO	11.68
Weight corr. factor	1.000

Zero values not shown

Norm calculation checks:
Norm seems OK

Macro-enabled

Normalized Analysis
48.04
2.18
15.45
1.44
11.68
0.18
5.94
7.33
5.07
2.01
0.84
100.14

Normative Minerals	Weight % Norm	Volume % Norm
Quartz		
Plagioclase	37.01	41.36
Orthoclase	11.85	13.81
Nepheline	10.47	12.20
Leucite		
Kalsilite		
Corundum		
Diopside	14.47	12.78
Hypersthene		
Wollastonite		
Olivine	18.17	14.39
Larnite		
Acmite		
K2SiO3		
Na2SiO3		
Rutile		
Ilmenite	4.14	2.60
Magnetite	2.09	1.20
Hematite		
Apatite	1.94	1.81
Zircon		
Perovskite		
Chromite		
Titanite		
Pyrite		
Halite		
Fluorite		
Anhydrite		
Na2SO4		
Calcite		
Na2CO3		
Total	100.14	100.14
Fe3+/(Total Fe) in rock	10.0	10.0
Mg/(Mg+Total Fe) in rock	44.9	44.9
Mg/(Mg+Fe2+) in rock	47.6	47.6
Mg/(Mg+Fe2+) in silicates	53.4	53.4
Ca/(Ca+Na) in rock	44.4	44.4
Plagioclase An content	35.1	35.1
Differentiation Index	59.3	67.4
Calculated density, g/cc	2.99	2.99
Calculated liquid density, g/cc	2.68	2.68
Calculated viscosity, dry, Pas	0.18	0.18
Calculated viscosity, wet, Pas	0.17	0.17
Estimated liquidus temp., °C	1251	1251
Estimated H2O content, wt. %	0.27	0.27

This program was written by Kurt Hollocher, Geology Department, Union College, Schenectady, NY, 12308, hollochk@union.edu

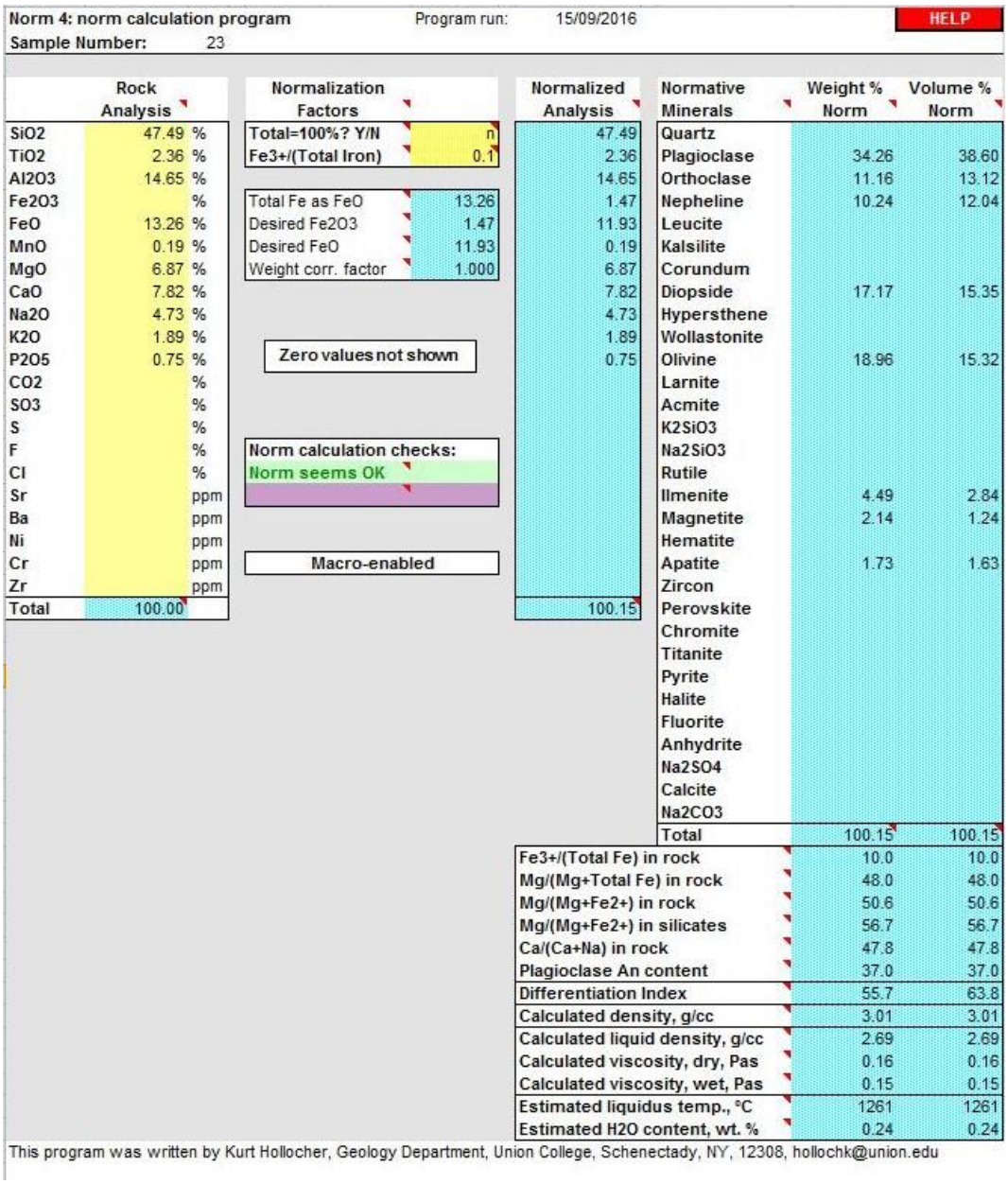

Norm 4: norm calculation program Program run: 15/09/2016 HELP

Sample Number: 23

	Rock Analysis	
SiO2	47.49	%
TiO2	2.36	%
Al2O3	14.65	%
Fe2O3		%
FeO	13.26	%
MnO	0.19	%
MgO	6.87	%
CaO	7.82	%
Na2O	4.73	%
K2O	1.89	%
P2O5	0.75	%
CO2		%
SO3		%
S		%
F		%
Cl		%
Sr		ppm
Ba		ppm
Ni		ppm
Cr		ppm
Zr		ppm
Total	100.00	

Normalization Factors	
Total=100%? Y/N	n
Fe3+/(Total Iron)	0.1
Total Fe as FeO	13.26
Desired Fe2O3	1.47
Desired FeO	11.93
Weight corr. factor	1.000

Zero values not shown

Norm calculation checks:

Norm seems OK

Macro-enabled

Normalized Analysis
47.49
2.36
14.65
1.47
11.93
0.19
6.87
7.82
4.73
1.89
0.75
100.15

Normative Minerals	Weight % Norm	Volume % Norm
Quartz		
Plagioclase	34.26	38.60
Orthoclase	11.16	13.12
Nepheline	10.24	12.04
Leucite		
Kalsilite		
Corundum		
Diopside	17.17	15.35
Hypersthene		
Wollastonite		
Olivine	18.96	15.32
Larnite		
Acmite		
K2SiO3		
Na2SiO3		
Rutile		
Ilmenite	4.49	2.84
Magnetite	2.14	1.24
Hematite		
Apatite	1.73	1.63
Zircon		
Perovskite		
Chromite		
Titanite		
Pyrite		
Halite		
Fluorite		
Anhydrite		
Na2SO4		
Calcite		
Na2CO3		
Total	100.15	100.15

Fe3+/(Total Fe) in rock	10.0	10.0
Mg/(Mg+Total Fe) in rock	48.0	48.0
Mg/(Mg+Fe2+) in rock	50.6	50.6
Mg/(Mg+Fe2+) in silicates	56.7	56.7
Ca/(Ca+Na) in rock	47.8	47.8
Plagioclase An content	37.0	37.0
Differentiation Index	55.7	63.8
Calculated density, g/cc	3.01	3.01
Calculated liquid density, g/cc	2.69	2.69
Calculated viscosity, dry, Pas	0.16	0.16
Calculated viscosity, wet, Pas	0.15	0.15
Estimated liquidus temp., °C	1261	1261
Estimated H2O content, wt. %	0.24	0.24

This program was written by Kurt Hollocher, Geology Department, Union College, Schenectady, NY, 12308, hollochk@union.edu

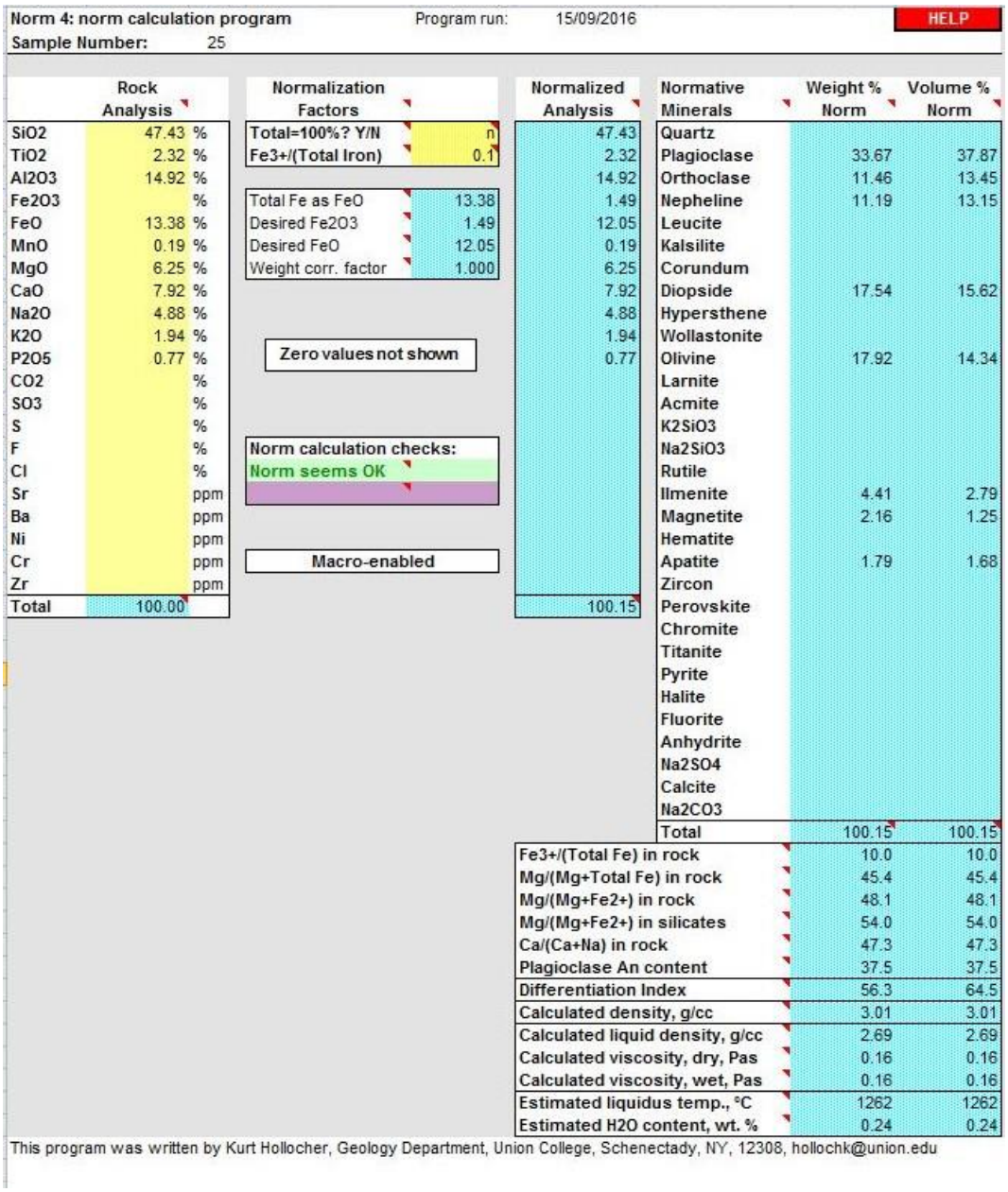

Norm 4: norm calculation program Program run: 15/09/2016 HELP
Sample Number: 25

	Rock Analysis	
SiO2	47.43	%
TiO2	2.32	%
Al2O3	14.92	%
Fe2O3		%
FeO	13.38	%
MnO	0.19	%
MgO	6.25	%
CaO	7.92	%
Na2O	4.88	%
K2O	1.94	%
P2O5	0.77	%
CO2		%
SO3		%
S		%
F		%
Cl		%
Sr		ppm
Ba		ppm
Ni		ppm
Cr		ppm
Zr		ppm
Total	100.00	

Normalization Factors	
Total=100%? Y/N	n
Fe3+/(Total Iron)	0.1
Total Fe as FeO	13.38
Desired Fe2O3	1.49
Desired FeO	12.05
Weight corr. factor	1.000

Zero values not shown

Norm calculation checks:
Norm seems OK

Macro-enabled

Normalized Analysis
47.43
2.32
14.92
1.49
12.05
0.19
6.25
7.92
4.88
1.94
0.77
100.15

Normative Minerals	Weight % Norm	Volume % Norm
Quartz		
Plagioclase	33.67	37.87
Orthoclase	11.46	13.45
Nepheline	11.19	13.15
Leucite		
Kalsilite		
Corundum		
Diopside	17.54	15.62
Hypersthene		
Wollastonite		
Olivine	17.92	14.34
Larnite		
Acmite		
K2SiO3		
Na2SiO3		
Rutile		
Ilmenite	4.41	2.79
Magnetite	2.16	1.25
Hematite		
Apatite	1.79	1.68
Zircon		
Perovskite		
Chromite		
Titanite		
Pyrite		
Halite		
Fluorite		
Anhydrite		
Na2SO4		
Calcite		
Na2CO3		
Total	100.15	100.15

Fe3+/(Total Fe) in rock	10.0	10.0
Mg/(Mg+Total Fe) in rock	45.4	45.4
Mg/(Mg+Fe2+) in rock	48.1	48.1
Mg/(Mg+Fe2+) in silicates	54.0	54.0
Ca/(Ca+Na) in rock	47.3	47.3
Plagioclase An content	37.5	37.5
Differentiation Index	56.3	64.5
Calculated density, g/cc	3.01	3.01
Calculated liquid density, g/cc	2.69	2.69
Calculated viscosity, dry, Pas	0.16	0.16
Calculated viscosity, wet, Pas	0.16	0.16
Estimated liquidus temp., °C	1262	1262
Estimated H2O content, wt. %	0.24	0.24

This program was written by Kurt Hollocher, Geology Department, Union College, Schenectady, NY, 12308, hollochk@union.edu

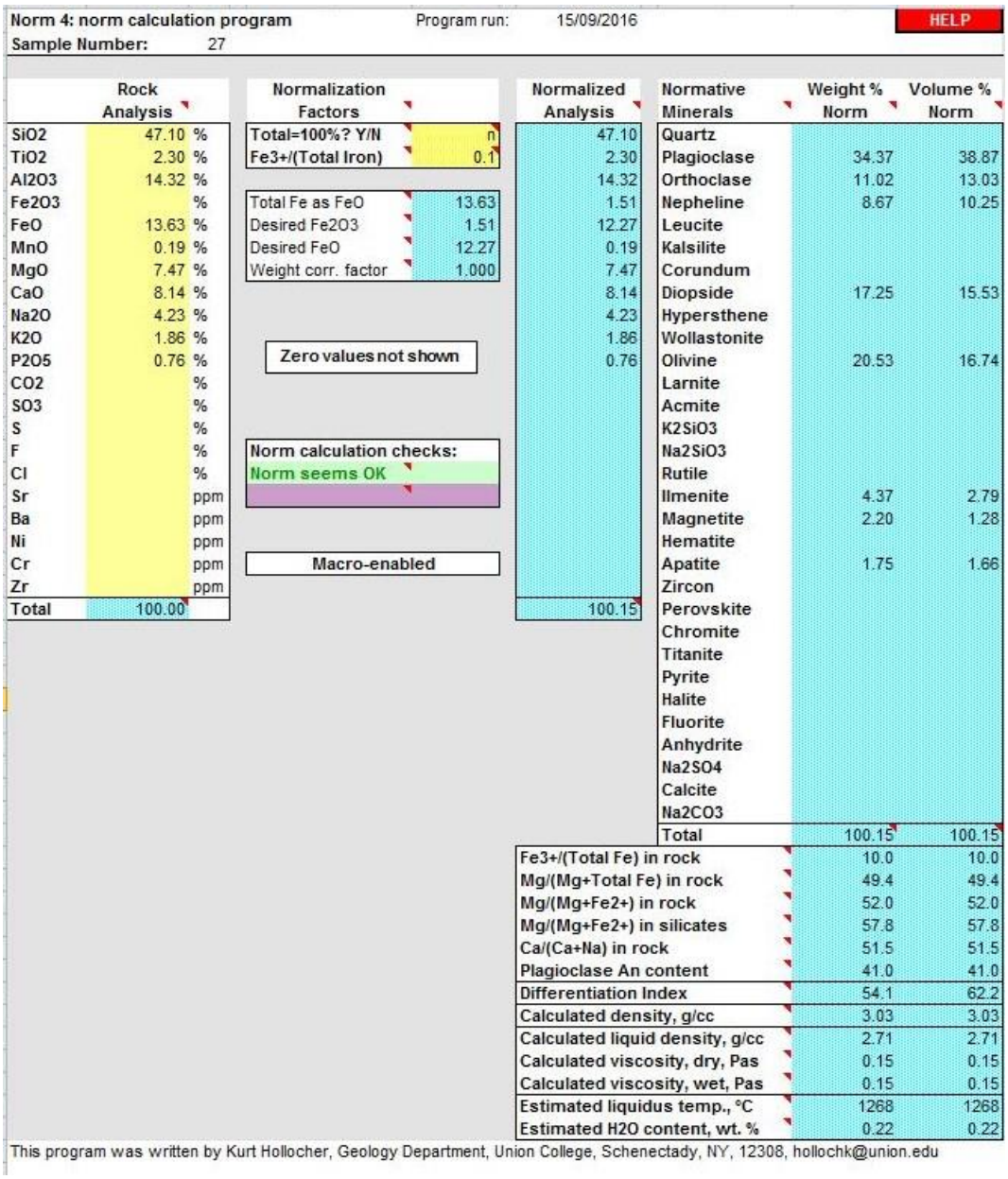

Norm 4: norm calculation program Program run: 15/09/2016 HELP

Sample Number: 27

	Rock Analysis	
SiO2	47.10	%
TiO2	2.30	%
Al2O3	14.32	%
Fe2O3		%
FeO	13.63	%
MnO	0.19	%
MgO	7.47	%
CaO	8.14	%
Na2O	4.23	%
K2O	1.86	%
P2O5	0.76	%
CO2		%
SO3		%
S		%
F		%
Cl		%
Sr		ppm
Ba		ppm
Ni		ppm
Cr		ppm
Zr		ppm
Total	100.00	

Normalization Factors	
Total=100%? Y/N	n
Fe3+/(Total Iron)	0.1
Total Fe as FeO	13.63
Desired Fe2O3	1.51
Desired FeO	12.27
Weight corr. factor	1.000

Zero values not shown

Norm calculation checks:

Norm seems OK

Macro-enabled

Normalized Analysis
47.10
2.30
14.32
1.51
12.27
0.19
7.47
8.14
4.23
1.86
0.76
100.15

Normative Minerals	Weight % Norm	Volume % Norm
Quartz		
Plagioclase	34.37	38.87
Orthoclase	11.02	13.03
Nepheline	8.67	10.25
Leucite		
Kalsilite		
Corundum		
Diopside	17.25	15.53
Hypersthene		
Wollastonite		
Olivine	20.53	16.74
Larnite		
Acmite		
K2SiO3		
Na2SiO3		
Rutile		
Ilmenite	4.37	2.79
Magnetite	2.20	1.28
Hematite		
Apatite	1.75	1.66
Zircon		
Perovskite		
Chromite		
Titanite		
Pyrite		
Halite		
Fluorite		
Anhydrite		
Na2SO4		
Calcite		
Na2CO3		
Total	100.15	100.15

Fe3+/(Total Fe) in rock	10.0	10.0
Mg/(Mg+Total Fe) in rock	49.4	49.4
Mg/(Mg+Fe2+) in rock	52.0	52.0
Mg/(Mg+Fe2+) in silicates	57.8	57.8
Ca/(Ca+Na) in rock	51.5	51.5
Plagioclase An content	41.0	41.0
Differentiation Index	54.1	62.2
Calculated density, g/cc	3.03	3.03
Calculated liquid density, g/cc	2.71	2.71
Calculated viscosity, dry, Pas	0.15	0.15
Calculated viscosity, wet, Pas	0.15	0.15
Estimated liquidus temp., °C	1268	1268
Estimated H2O content, wt. %	0.22	0.22

This program was written by Kurt Hollocher, Geology Department, Union College, Schenectady, NY, 12308, hollochk@union.edu

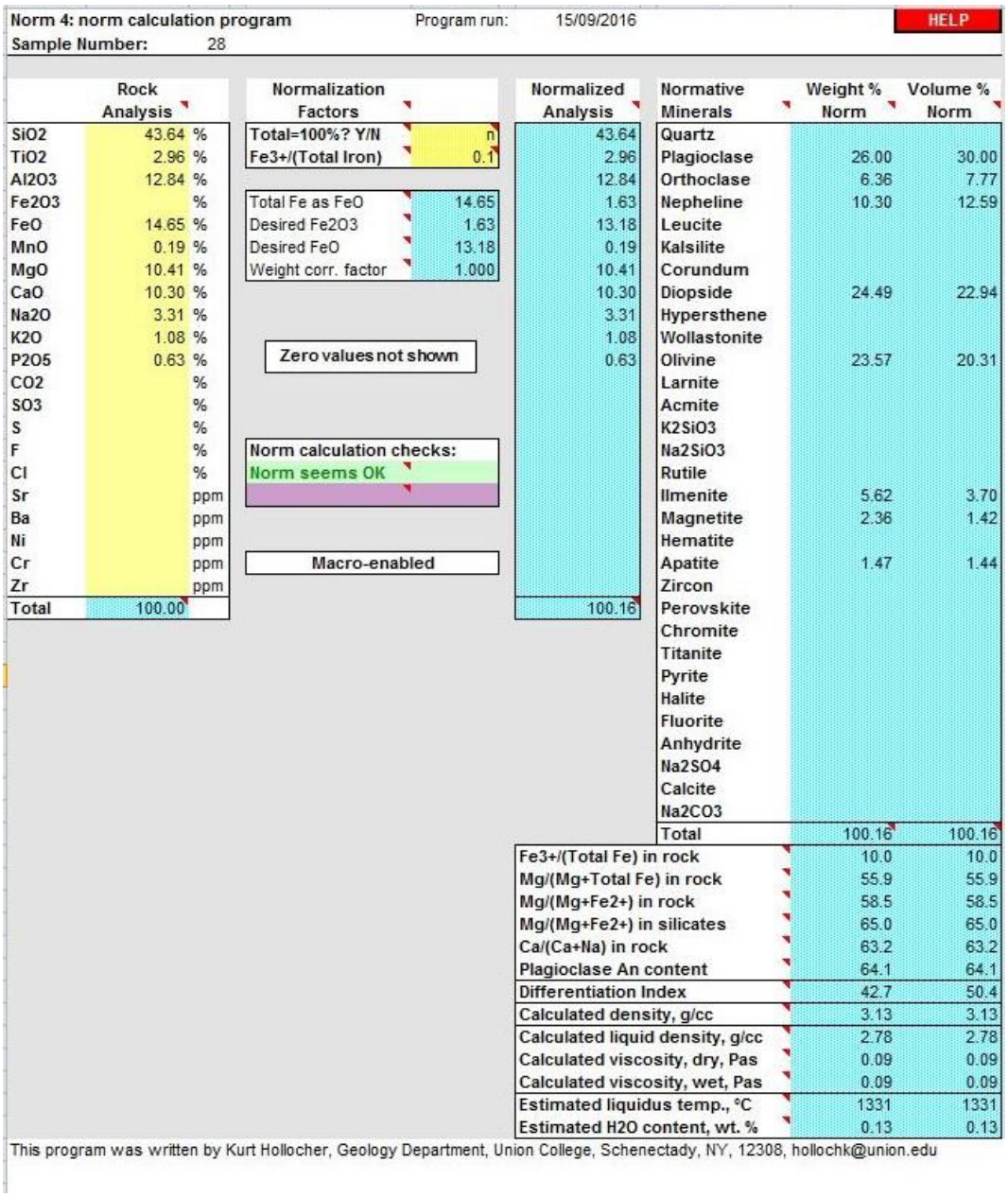

Norm 4: norm calculation program Program run: 15/09/2016 HELP

Sample Number: 28

	Rock Analysis		Normalization Factors		Normalized Analysis	Normative Minerals	Weight % Norm	Volume % Norm
SiO2	43.64	%	Total=100%? Y/N	n	43.64	Quartz		
TiO2	2.96	%	Fe3+/(Total Iron)	0.1	2.96	Plagioclase	26.00	30.00
Al2O3	12.84	%			12.84	Orthoclase	6.36	7.77
Fe2O3		%	Total Fe as FeO	14.65	1.63	Nepheline	10.30	12.59
FeO	14.65	%	Desired Fe2O3	1.63	13.18	Leucite		
MnO	0.19	%	Desired FeO	13.18	0.19	Kalsilite		
MgO	10.41	%	Weight corr. factor	1.000	10.41	Corundum		
CaO	10.30	%			10.30	Diopside	24.49	22.94
Na2O	3.31	%			3.31	Hypersthene		
K2O	1.08	%	Zero values not shown		1.08	Wollastonite		
P2O5	0.63	%			0.63	Olivine	23.57	20.31
CO2		%				Larnite		
SO3		%				Acmite		
S		%				K2SiO3		
F		%	Norm calculation checks:			Na2SiO3		
Cl		%	Norm seems OK			Rutile		
Sr		ppm				Ilmenite	5.62	3.70
Ba		ppm				Magnetite	2.36	1.42
Ni		ppm				Hematite		
Cr		ppm	Macro-enabled			Apatite	1.47	1.44
Zr		ppm				Zircon		
Total	100.00				100.16	Perovskite		
						Chromite		
						Titanite		
						Pyrite		
						Halite		
						Fluorite		
						Anhydrite		
						Na2SO4		
						Calcite		
						Na2CO3		
						Total	100.16	100.16
						Fe3+/(Total Fe) in rock	10.0	10.0
						Mg/(Mg+Total Fe) in rock	55.9	55.9
						Mg/(Mg+Fe2+) in rock	58.5	58.5
						Mg/(Mg+Fe2+) in silicates	65.0	65.0
						Ca/(Ca+Na) in rock	63.2	63.2
						Plagioclase An content	64.1	64.1
						Differentiation Index	42.7	50.4
						Calculated density, g/cc	3.13	3.13
						Calculated liquid density, g/cc	2.78	2.78
						Calculated viscosity, dry, Pas	0.09	0.09
						Calculated viscosity, wet, Pas	0.09	0.09
						Estimated liquidus temp., °C	1331	1331
						Estimated H2O content, wt. %	0.13	0.13

This program was written by Kurt Hollocher, Geology Department, Union College, Schenectady, NY, 12308, hollochk@union.edu

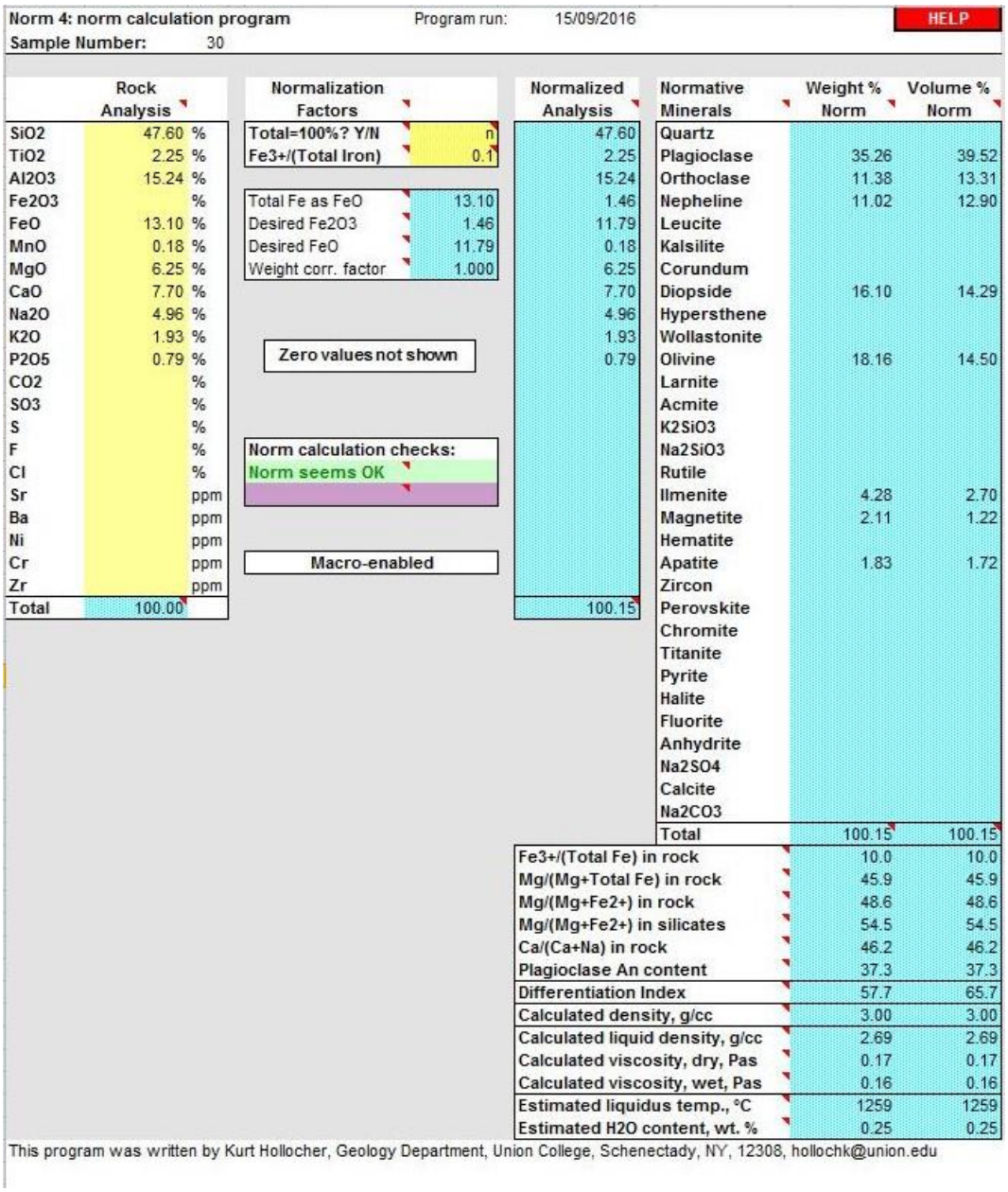

Norm 4: norm calculation program Program run: 15/09/2016 HELP

Sample Number: 30

	Rock Analysis	
SiO2	47.60	%
TiO2	2.25	%
Al2O3	15.24	%
Fe2O3		%
FeO	13.10	%
MnO	0.18	%
MgO	6.25	%
CaO	7.70	%
Na2O	4.96	%
K2O	1.93	%
P2O5	0.79	%
CO2		%
SO3		%
S		%
F		%
Cl		%
Sr		ppm
Ba		ppm
Ni		ppm
Cr		ppm
Zr		ppm
Total	100.00	

Normalization Factors	
Total=100%? Y/N	n
Fe3+/(Total Iron)	0.1
Total Fe as FeO	13.10
Desired Fe2O3	1.46
Desired FeO	11.79
Weight corr. factor	1.000

Zero values not shown

Norm calculation checks:

Norm seems OK

Macro-enabled

Normalized Analysis
47.60
2.25
15.24
1.46
11.79
0.18
6.25
7.70
4.96
1.93
0.79
100.15

Normative Minerals	Weight % Norm	Volume % Norm
Quartz		
Plagioclase	35.26	39.52
Orthoclase	11.38	13.31
Nepheline	11.02	12.90
Leucite		
Kalsilite		
Corundum		
Diopside	16.10	14.29
Hypersthene		
Wollastonite		
Olivine	18.16	14.50
Larnite		
Acmite		
K2SiO3		
Na2SiO3		
Rutile		
Ilmenite	4.28	2.70
Magnetite	2.11	1.22
Hematite		
Apatite	1.83	1.72
Zircon		
Perovskite		
Chromite		
Titanite		
Pyrite		
Halite		
Fluorite		
Anhydrite		
Na2SO4		
Calcite		
Na2CO3		
Total	100.15	100.15

Fe3+/(Total Fe) in rock	10.0	10.0
Mg/(Mg+Total Fe) in rock	45.9	45.9
Mg/(Mg+Fe2+) in rock	48.6	48.6
Mg/(Mg+Fe2+) in silicates	54.5	54.5
Ca/(Ca+Na) in rock	46.2	46.2
Plagioclase An content	37.3	37.3
Differentiation Index	57.7	65.7
Calculated density, g/cc	3.00	3.00
Calculated liquid density, g/cc	2.69	2.69
Calculated viscosity, dry, Pas	0.17	0.17
Calculated viscosity, wet, Pas	0.16	0.16
Estimated liquidus temp., °C	1259	1259
Estimated H2O content, wt. %	0.25	0.25

This program was written by Kurt Hollocher, Geology Department, Union College, Schenectady, NY, 12308, hollochk@union.edu

Norm 4: norm calculation program Program run: 15/09/2016 HELP

Sample Number: 33

	Rock Analysis	
SiO2	47.28	%
TiO2	2.23	%
Al2O3	14.98	%
Fe2O3		%
FeO	13.20	%
MnO	0.18	%
MgO	6.59	%
CaO	8.01	%
Na2O	4.90	%
K2O	1.87	%
P2O5	0.75	%
CO2		%
SO3		%
S		%
F		%
Cl		%
Sr		ppm
Ba		ppm
Ni		ppm
Cr		ppm
Zr		ppm
Total	100.00	

Normalization Factors	
Total=100%? Y/N	n
Fe3+/(Total Iron)	0.1
Total Fe as FeO	13.20
Desired Fe2O3	1.47
Desired FeO	11.88
Weight corr. factor	1.000

Zero values not shown

Norm calculation checks:
Norm seems OK

Macro-enabled

Normalized Analysis
47.28
2.23
14.98
1.47
11.88
0.18
6.59
8.01
4.90
1.87
0.75
100.15

Normative Minerals	Weight % Norm	Volume % Norm
Quartz		
Plagioclase	33.05	37.14
Orthoclase	11.07	13.00
Nepheline	11.79	13.84
Leucite		
Kalsilite		
Corundum		
Diopside	17.83	15.90
Hypersthene		
Wollastonite		
Olivine	18.30	14.71
Larnite		
Acmite		
K2SiO3		
Na2SiO3		
Rutile		
Ilmenite	4.24	2.69
Magnetite	2.13	1.23
Hematite		
Apatite	1.74	1.63
Zircon		
Perovskite		
Chromite		
Titanite		
Pyrite		
Halite		
Fluorite		
Anhydrite		
Na2SO4		
Calcite		
Na2CO3		
Total	100.15	100.15

Fe3+/(Total Fe) in rock	10.0	10.0
Mg/(Mg+Total Fe) in rock	47.1	47.1
Mg/(Mg+Fe2+) in rock	49.7	49.7
Mg/(Mg+Fe2+) in silicates	55.6	55.6
Ca/(Ca+Na) in rock	47.5	47.5
Plagioclase An content	38.9	38.9
Differentiation Index	55.9	64.0
Calculated density, g/cc	3.01	3.01
Calculated liquid density, g/cc	2.69	2.69
Calculated viscosity, dry, Pas	0.16	0.16
Calculated viscosity, wet, Pas	0.15	0.15
Estimated liquidus temp., °C	1265	1265
Estimated H2O content, wt. %	0.23	0.23

This program was written by Kurt Hollocher, Geology Department, Union College, Schenectady, NY, 12308, hollochk@union.edu

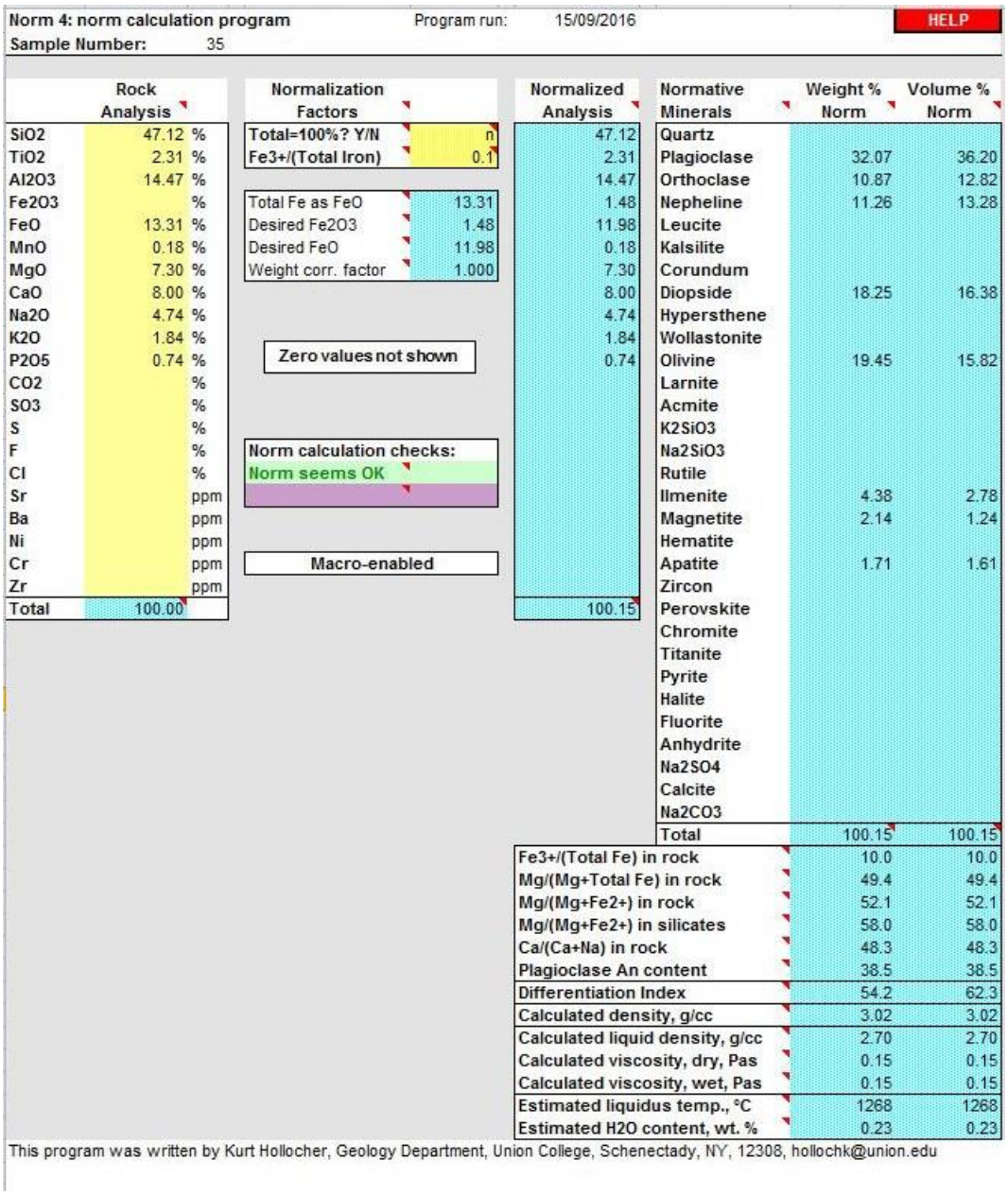

Norm 4: norm calculation program Program run: 15/09/2016 HELP

Sample Number: 35

	Rock Analysis	
SiO2	47.12	%
TiO2	2.31	%
Al2O3	14.47	%
Fe2O3		%
FeO	13.31	%
MnO	0.18	%
MgO	7.30	%
CaO	8.00	%
Na2O	4.74	%
K2O	1.84	%
P2O5	0.74	%
CO2		%
SO3		%
S		%
F		%
Cl		%
Sr		ppm
Ba		ppm
Ni		ppm
Cr		ppm
Zr		ppm
Total	100.00	

Normalization Factors	
Total=100%? Y/N	n
Fe3+/(Total Iron)	0.1
Total Fe as FeO	13.31
Desired Fe2O3	1.48
Desired FeO	11.98
Weight corr. factor	1.000

Zero values not shown

Norm calculation checks:

Norm seems OK

Macro-enabled

Normalized Analysis
47.12
2.31
14.47
1.48
11.98
0.18
7.30
8.00
4.74
1.84
0.74
100.15

Normative Minerals	Weight % Norm	Volume % Norm
Quartz		
Plagioclase	32.07	36.20
Orthoclase	10.87	12.82
Nepheline	11.26	13.28
Leucite		
Kalsilite		
Corundum		
Diopside	18.25	16.38
Hypersthene		
Wollastonite		
Olivine	19.45	15.82
Larnite		
Acmite		
K2SiO3		
Na2SiO3		
Rutile		
Ilmenite	4.38	2.78
Magnetite	2.14	1.24
Hematite		
Apatite	1.71	1.61
Zircon		
Perovskite		
Chromite		
Titanite		
Pyrite		
Halite		
Fluorite		
Anhydrite		
Na2SO4		
Calcite		
Na2CO3		
Total	100.15	100.15

Fe3+/(Total Fe) in rock	10.0	10.0
Mg/(Mg+Total Fe) in rock	49.4	49.4
Mg/(Mg+Fe2+) in rock	52.1	52.1
Mg/(Mg+Fe2+) in silicates	58.0	58.0
Ca/(Ca+Na) in rock	48.3	48.3
Plagioclase An content	38.5	38.5
Differentiation Index	54.2	62.3
Calculated density, g/cc	3.02	3.02
Calculated liquid density, g/cc	2.70	2.70
Calculated viscosity, dry, Pas	0.15	0.15
Calculated viscosity, wet, Pas	0.15	0.15
Estimated liquidus temp., °C	1268	1268
Estimated H2O content, wt. %	0.23	0.23

This program was written by Kurt Hollocher, Geology Department, Union College, Schenectady, NY, 12308, hollochk@union.edu

Norm 4: norm calculation program Program run: 15/09/2016 HELP

Sample Number: 37

	Rock Analysis	
SiO2	47.29	%
TiO2	2.30	%
Al2O3	14.96	%
Fe2O3		%
FeO	13.13	%
MnO	0.18	%
MgO	6.58	%
CaO	7.99	%
Na2O	4.97	%
K2O	1.85	%
P2O5	0.76	%
CO2		%
SO3		%
S		%
F		%
Cl		%
Sr		ppm
Ba		ppm
Ni		ppm
Cr		ppm
Zr		ppm
Total	100.00	

Normalization Factors	
Total=100%? Y/N	n
Fe3+/(Total Iron)	0.1
Total Fe as FeO	13.13
Desired Fe2O3	1.46
Desired FeO	11.82
Weight corr. factor	1.000

Zero values not shown

Norm calculation checks:
Norm seems OK

Macro-enabled

Normalized Analysis
47.29
2.30
14.96
1.46
11.82
0.18
6.58
7.99
4.97
1.85
0.76
100.15

Normative Minerals	Weight % Norm	Volume % Norm
Quartz		
Plagioclase	32.94	37.02
Orthoclase	10.95	12.86
Nepheline	12.00	14.08
Leucite		
Kalsilite		
Corundum		
Diopside	17.96	16.01
Hypersthene		
Wollastonite		
Olivine	18.08	14.54
Larnite		
Acmite		
K2SiO3		
Na2SiO3		
Rutile		
Ilmenite	4.36	2.76
Magnetite	2.12	1.22
Hematite		
Apatite	1.76	1.65
Zircon		
Perovskite		
Chromite		
Titanite		
Pyrite		
Halite		
Fluorite		
Anhydrite		
Na2SO4		
Calcite		
Na2CO3		
Total	100.15	100.15

Fe3+/(Total Fe) in rock	10.0	10.0
Mg/(Mg+Total Fe) in rock	47.2	47.2
Mg/(Mg+Fe2+) in rock	49.8	49.8
Mg/(Mg+Fe2+) in silicates	55.8	55.8
Ca/(Ca+Na) in rock	47.1	47.1
Plagioclase An content	38.1	38.1
Differentiation Index	55.9	64.0
Calculated density, g/cc	3.01	3.01
Calculated liquid density, g/cc	2.69	2.69
Calculated viscosity, dry, Pas	0.16	0.16
Calculated viscosity, wet, Pas	0.15	0.15
Estimated liquidus temp., °C	1265	1265
Estimated H2O content, wt. %	0.23	0.23

This program was written by Kurt Hollocher, Geology Department, Union College, Schenectady, NY, 12308, hollochk@union.edu

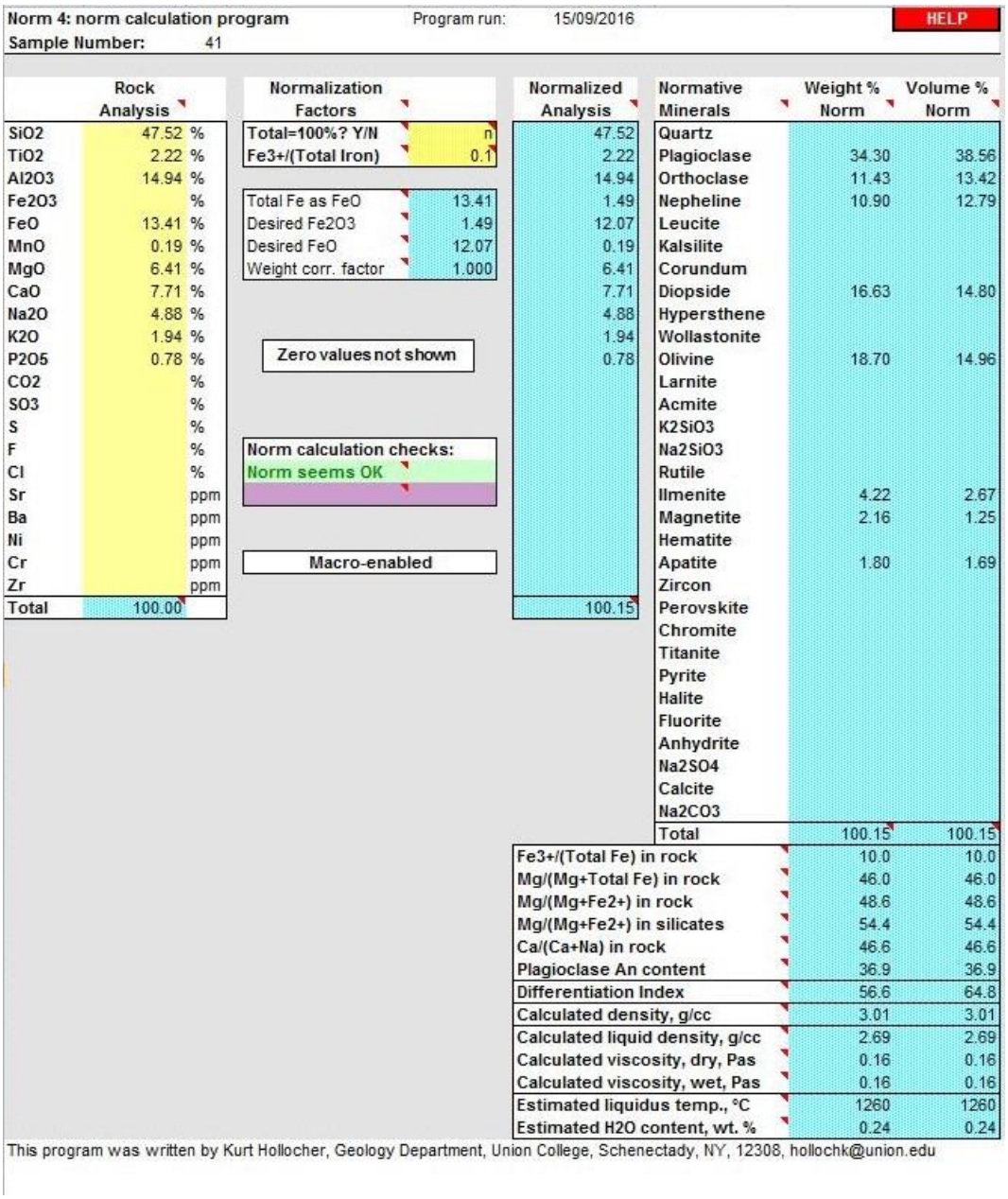

Norm 4: norm calculation program Program run: 15/09/2016 HELP

Sample Number: 41

	Rock Analysis	
SiO2	47.52	%
TiO2	2.22	%
Al2O3	14.94	%
Fe2O3		%
FeO	13.41	%
MnO	0.19	%
MgO	6.41	%
CaO	7.71	%
Na2O	4.88	%
K2O	1.94	%
P2O5	0.78	%
CO2		%
SO3		%
S		%
F		%
Cl		%
Sr		ppm
Ba		ppm
Ni		ppm
Cr		ppm
Zr		ppm
Total	100.00	

Normalization Factors	
Total=100%? Y/N	n
Fe3+/(Total Iron)	0.1
Total Fe as FeO	13.41
Desired Fe2O3	1.49
Desired FeO	12.07
Weight corr. factor	1.000

Zero values not shown

Norm calculation checks:

Norm seems OK

Macro-enabled

Normalized Analysis
47.52
2.22
14.94
1.49
12.07
0.19
6.41
7.71
4.88
1.94
0.78
100.15

Normative Minerals	Weight % Norm	Volume % Norm
Quartz		
Plagioclase	34.30	38.56
Orthoclase	11.43	13.42
Nepheline	10.90	12.79
Leucite		
Kalsilite		
Corundum		
Diopside	16.63	14.80
Hypersthene		
Wollastonite		
Olivine	18.70	14.96
Larnite		
Acmite		
K2SiO3		
Na2SiO3		
Rutile		
Ilmenite	4.22	2.67
Magnetite	2.16	1.25
Hematite		
Apatite	1.80	1.69
Zircon		
Perovskite		
Chromite		
Titanite		
Pyrite		
Halite		
Fluorite		
Anhydrite		
Na2SO4		
Calcite		
Na2CO3		
Total	100.15	100.15

Fe3+/(Total Fe) in rock	10.0	10.0
Mg/(Mg+Total Fe) in rock	46.0	46.0
Mg/(Mg+Fe2+) in rock	48.6	48.6
Mg/(Mg+Fe2+) in silicates	54.4	54.4
Ca/(Ca+Na) in rock	46.6	46.6
Plagioclase An content	36.9	36.9
Differentiation Index	56.6	64.8
Calculated density, g/cc	3.01	3.01
Calculated liquid density, g/cc	2.69	2.69
Calculated viscosity, dry, Pas	0.16	0.16
Calculated viscosity, wet, Pas	0.16	0.16
Estimated liquidus temp., °C	1260	1260
Estimated H2O content, wt. %	0.24	0.24

This program was written by Kurt Hollocher, Geology Department, Union College, Schenectady, NY, 12308, hollochk@union.edu

Norm 4: norm calculation program Program run: 15/09/2016 HELP

Sample Number: 42

	Rock Analysis		Normalization Factors		Normalized Analysis	Normative Minerals	Weight % Norm	Volume % Norm
SiO2	47.27	%	Total=100%? Y/N	n	47.27	Quartz		
TiO2	2.38	%	Fe3+/(Total Iron)	0.1	2.38	Plagioclase	37.51	42.32
Al2O3	14.60	%			14.60	Orthoclase	10.52	12.41
Fe2O3		%	Total Fe as FeO	13.34	1.48	Nepheline	7.37	8.69
FeO	13.34	%	Desired Fe2O3	1.48	12.01	Leucite		
MnO	0.19	%	Desired FeO	12.01	0.19	Kalsilite		
MgO	7.57	%	Weight corr. factor	1.000	7.57	Corundum		
CaO	7.96	%			7.96	Diopside	15.41	13.86
Na2O	4.16	%			4.16	Hypersthene		
K2O	1.78	%	Zero values not shown		1.78	Wollastonite		
P2O5	0.75	%			0.75	Olivine	20.94	17.09
CO2		%				Larnite		
SO3		%				Acmite		
S		%				K2SiO3		
F		%	Norm calculation checks:			Na2SiO3		
Cl		%	Norm seems OK			Rutile		
Sr		ppm				Ilmenite	4.52	2.87
Ba		ppm				Magnetite	2.15	1.25
Ni		ppm				Hematite		
Cr		ppm	Macro-enabled			Apatite	1.74	1.64
Zr		ppm				Zircon		
Total	100.00				100.15	Perovskite		
						Chromite		
						Titanite		
						Pyrite		
						Halite		
						Fluorite		
						Anhydrite		
						Na2SO4		
						Calcite		
						Na2CO3		
						Total	100.15	100.15
						Fe3+/(Total Fe) in rock	10.0	10.0
						Mg/(Mg+Total Fe) in rock	50.3	50.3
						Mg/(Mg+Fe2+) in rock	52.9	52.9
						Mg/(Mg+Fe2+) in silicates	59.0	59.0
						Ca/(Ca+Na) in rock	51.4	51.4
						Plagioclase An content	41.0	41.0
						Differentiation Index	55.4	63.4
						Calculated density, g/cc	3.03	3.03
						Calculated liquid density, g/cc	2.71	2.71
						Calculated viscosity, dry, Pas	0.16	0.16
						Calculated viscosity, wet, Pas	0.15	0.15
						Estimated liquidus temp., °C	1265	1265
						Estimated H2O content, wt. %	0.23	0.23

This program was written by Kurt Hollocher, Geology Department, Union College, Schenectady, NY, 12308, hollochk@union.edu

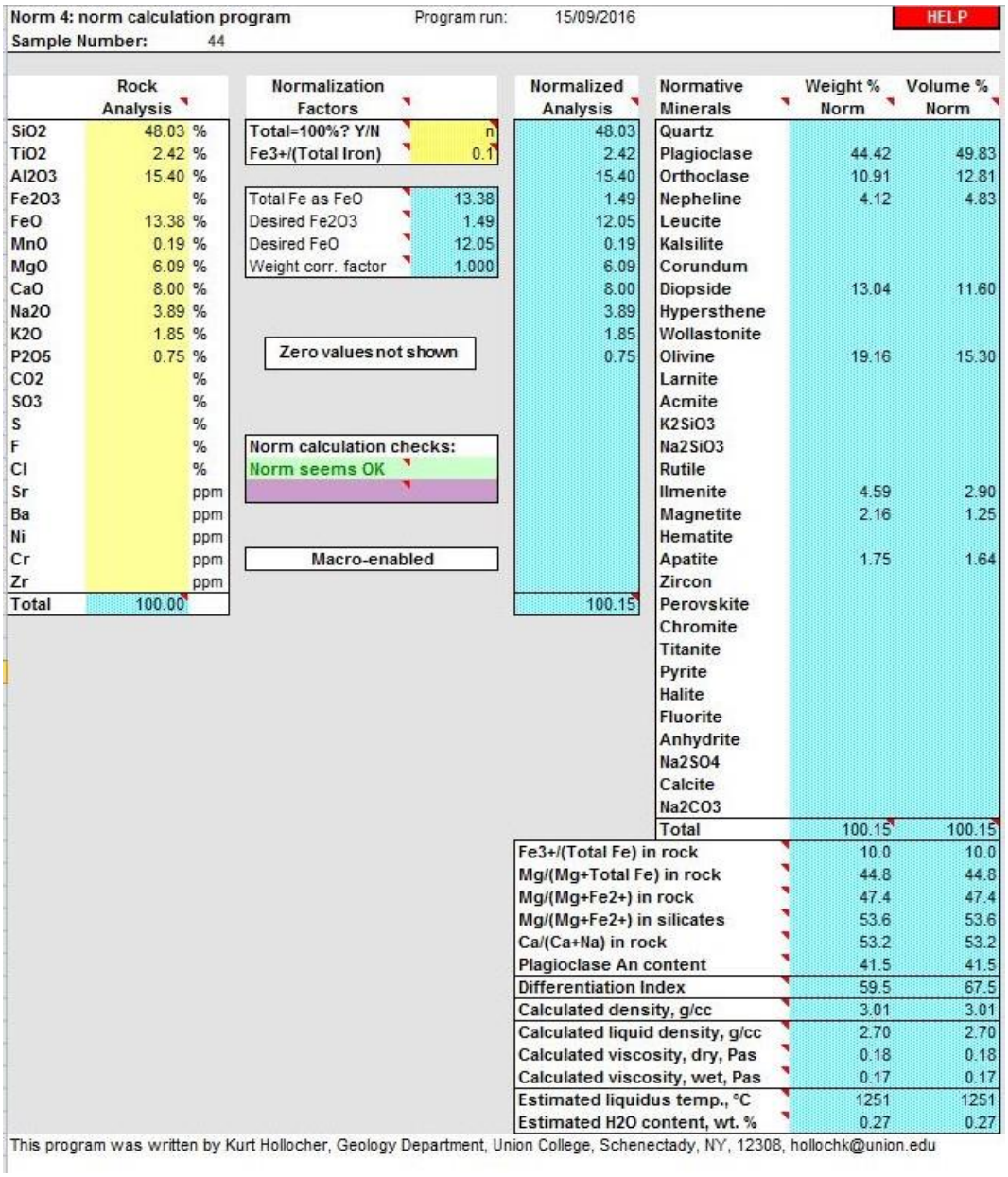

Norm 4: norm calculation program Program run: 15/09/2016 HELP

Sample Number: 44

	Rock Analysis	
SiO2	48.03	%
TiO2	2.42	%
Al2O3	15.40	%
Fe2O3		%
FeO	13.38	%
MnO	0.19	%
MgO	6.09	%
CaO	8.00	%
Na2O	3.89	%
K2O	1.85	%
P2O5	0.75	%
CO2		%
SO3		%
S		%
F		%
Cl		%
Sr		ppm
Ba		ppm
Ni		ppm
Cr		ppm
Zr		ppm
Total	100.00	

Normalization Factors	
Total=100%? Y/N	n
Fe3+/(Total Iron)	0.1
Total Fe as FeO	13.38
Desired Fe2O3	1.49
Desired FeO	12.05
Weight corr. factor	1.000

Zero values not shown

Norm calculation checks:
Norm seems OK

Macro-enabled

Normalized Analysis
48.03
2.42
15.40
1.49
12.05
0.19
6.09
8.00
3.89
1.85
0.75
100.15

Normative Minerals	Weight % Norm	Volume % Norm
Quartz		
Plagioclase	44.42	49.83
Orthoclase	10.91	12.81
Nepheline	4.12	4.83
Leucite		
Kalsilite		
Corundum		
Diopside	13.04	11.60
Hypersthene		
Wollastonite		
Olivine	19.16	15.30
Larnite		
Acmite		
K2SiO3		
Na2SiO3		
Rutile		
Ilmenite	4.59	2.90
Magnetite	2.16	1.25
Hematite		
Apatite	1.75	1.64
Zircon		
Perovskite		
Chromite		
Titanite		
Pyrite		
Halite		
Fluorite		
Anhydrite		
Na2SO4		
Calcite		
Na2CO3		
Total	100.15	100.15

Fe3+/(Total Fe) in rock	10.0	10.0
Mg/(Mg+Total Fe) in rock	44.8	44.8
Mg/(Mg+Fe2+) in rock	47.4	47.4
Mg/(Mg+Fe2+) in silicates	53.6	53.6
Ca/(Ca+Na) in rock	53.2	53.2
Plagioclase An content	41.5	41.5
Differentiation Index	59.5	67.5
Calculated density, g/cc	3.01	3.01
Calculated liquid density, g/cc	2.70	2.70
Calculated viscosity, dry, Pas	0.18	0.18
Calculated viscosity, wet, Pas	0.17	0.17
Estimated liquidus temp., °C	1251	1251
Estimated H2O content, wt. %	0.27	0.27

This program was written by Kurt Hollocher, Geology Department, Union College, Schenectady, NY, 12308, hollochk@union.edu

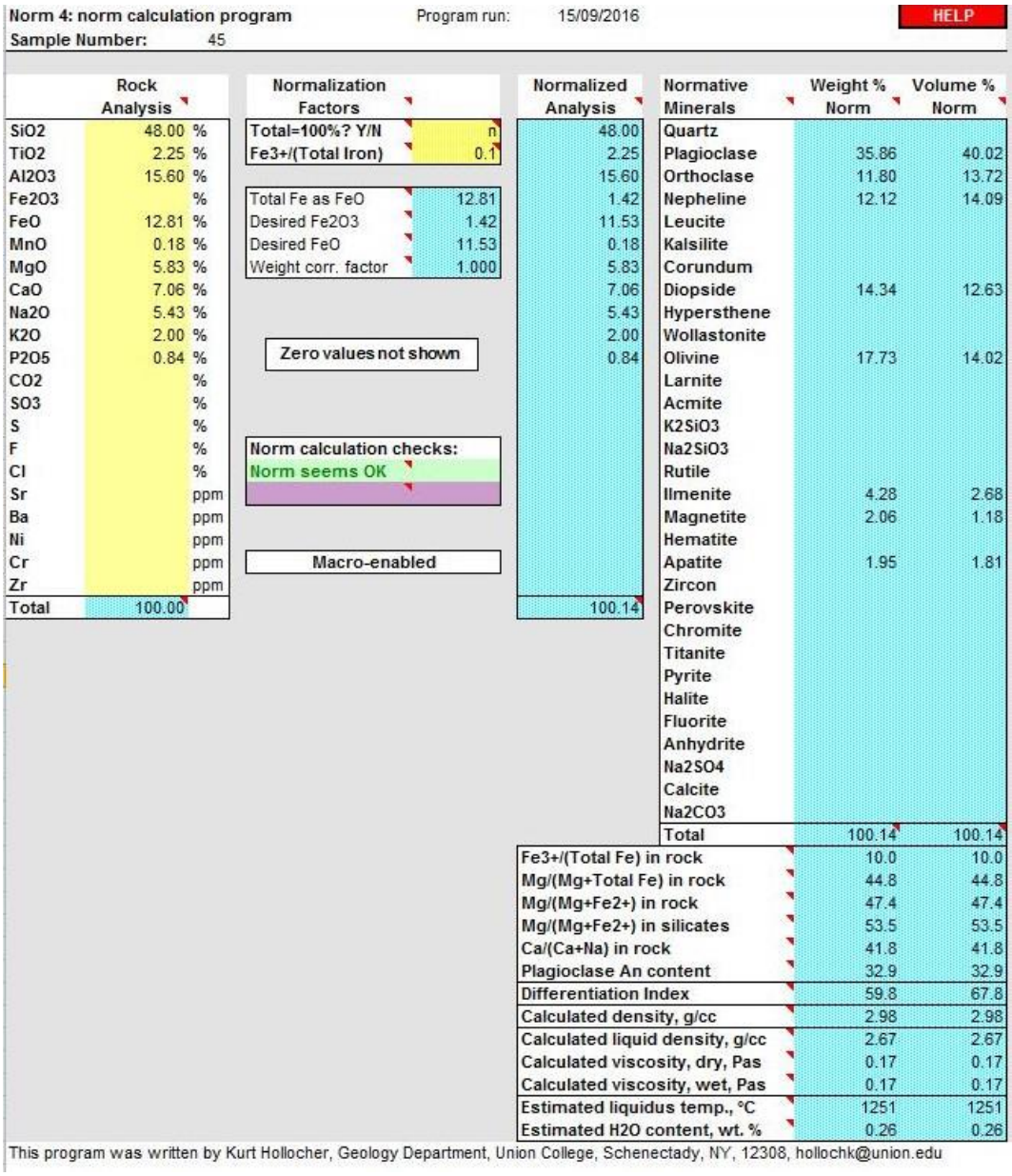

Norm 4: norm calculation program Program run: 15/09/2016 HELP

Sample Number: 45

	Rock Analysis	
SiO2	48.00	%
TiO2	2.25	%
Al2O3	15.60	%
Fe2O3		%
FeO	12.81	%
MnO	0.18	%
MgO	5.83	%
CaO	7.06	%
Na2O	5.43	%
K2O	2.00	%
P2O5	0.84	%
CO2		%
SO3		%
S		%
F		%
Cl		%
Sr		ppm
Ba		ppm
Ni		ppm
Cr		ppm
Zr		ppm
Total	100.00	

Normalization Factors	
Total=100%? Y/N	n
Fe3+/(Total Iron)	0.1
Total Fe as FeO	12.81
Desired Fe2O3	1.42
Desired FeO	11.53
Weight corr. factor	1.000

Zero values not shown

Norm calculation checks:
Norm seems OK

Macro-enabled

Normalized Analysis
48.00
2.25
15.60
1.42
11.53
0.18
5.83
7.06
5.43
2.00
0.84
100.14

Normative Minerals	Weight % Norm	Volume % Norm
Quartz		
Plagioclase	35.86	40.02
Orthoclase	11.80	13.72
Nepheline	12.12	14.09
Leucite		
Kalsilite		
Corundum		
Diopside	14.34	12.63
Hypersthene		
Wollastonite		
Olivine	17.73	14.02
Larnite		
Acmite		
K2SiO3		
Na2SiO3		
Rutile		
Ilmenite	4.28	2.68
Magnetite	2.06	1.18
Hematite		
Apatite	1.95	1.81
Zircon		
Perovskite		
Chromite		
Titanite		
Pyrite		
Halite		
Fluorite		
Anhydrite		
Na2SO4		
Calcite		
Na2CO3		
Total	100.14	100.14

Fe3+/(Total Fe) in rock	10.0	10.0
Mg/(Mg+Total Fe) in rock	44.8	44.8
Mg/(Mg+Fe2+) in rock	47.4	47.4
Mg/(Mg+Fe2+) in silicates	53.5	53.5
Ca/(Ca+Na) in rock	41.8	41.8
Plagioclase An content	32.9	32.9
Differentiation Index	59.8	67.8
Calculated density, g/cc	2.98	2.98
Calculated liquid density, g/cc	2.67	2.67
Calculated viscosity, dry, Pas	0.17	0.17
Calculated viscosity, wet, Pas	0.17	0.17
Estimated liquidus temp., °C	1251	1251
Estimated H2O content, wt. %	0.26	0.26

This program was written by Kurt Hollocher, Geology Department, Union College, Schenectady, NY, 12308, hollochk@union.edu

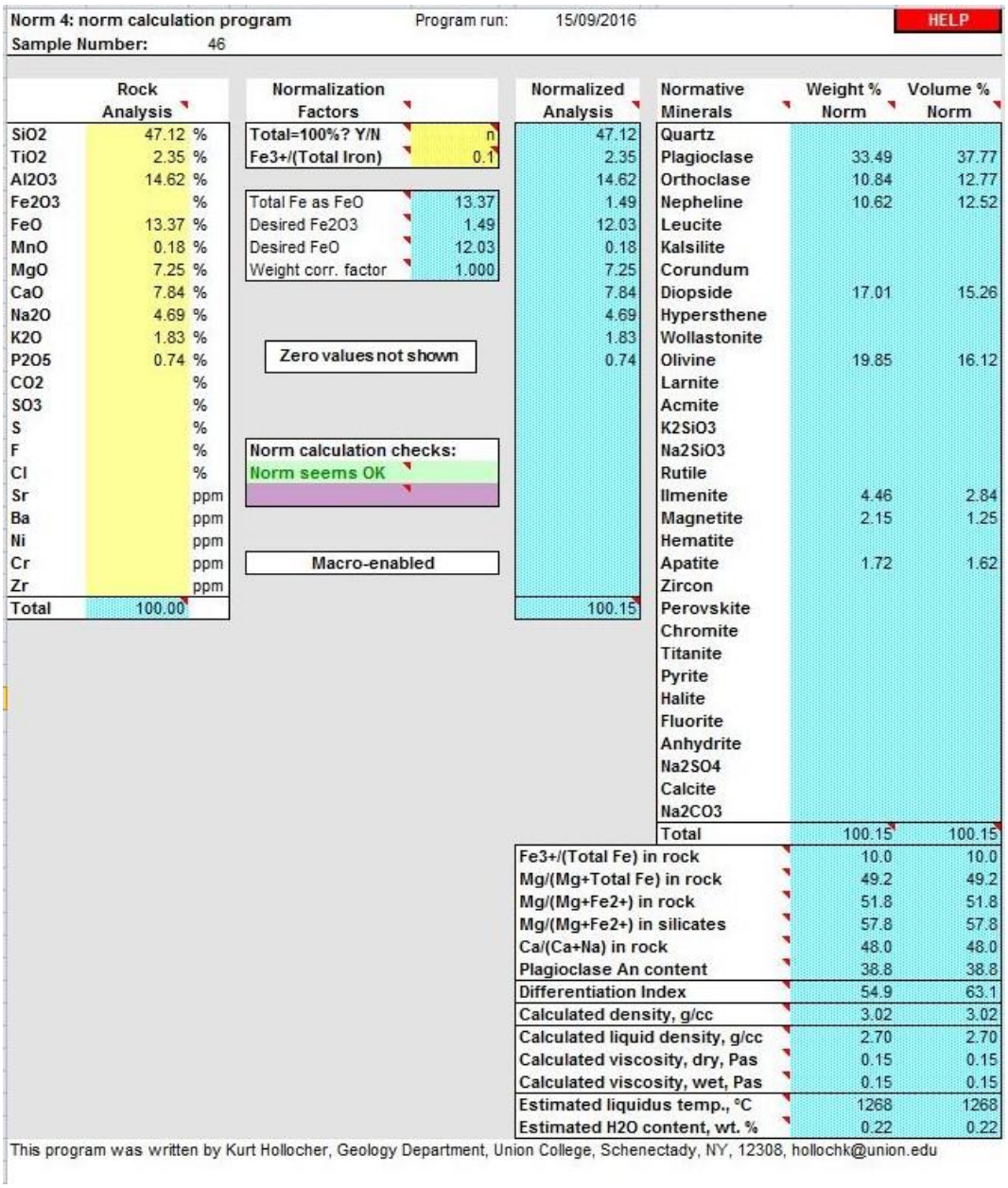

Norm 4: norm calculation program Program run: 15/09/2016 HELP

Sample Number: 46

	Rock Analysis	
SiO2	47.12	%
TiO2	2.35	%
Al2O3	14.62	%
Fe2O3		%
FeO	13.37	%
MnO	0.18	%
MgO	7.25	%
CaO	7.84	%
Na2O	4.69	%
K2O	1.83	%
P2O5	0.74	%
CO2		%
SO3		%
S		%
F		%
Cl		%
Sr		ppm
Ba		ppm
Ni		ppm
Cr		ppm
Zr		ppm
Total	100.00	

Normalization Factors	
Total=100%? Y/N	n
Fe3+/(Total Iron)	0.1
Total Fe as FeO	13.37
Desired Fe2O3	1.49
Desired FeO	12.03
Weight corr. factor	1.000

Zero values not shown

Norm calculation checks:

Norm seems OK

Macro-enabled

Normalized Analysis
47.12
2.35
14.62
1.49
12.03
0.18
7.25
7.84
4.69
1.83
0.74
100.15

Normative Minerals	Weight % Norm	Volume % Norm
Quartz		
Plagioclase	33.49	37.77
Orthoclase	10.84	12.77
Nepheline	10.62	12.52
Leucite		
Kalsilite		
Corundum		
Diopside	17.01	15.26
Hypersthene		
Wollastonite		
Olivine	19.85	16.12
Larnite		
Acmite		
K2SiO3		
Na2SiO3		
Rutile		
Ilmenite	4.46	2.84
Magnetite	2.15	1.25
Hematite		
Apatite	1.72	1.62
Zircon		
Perovskite		
Chromite		
Titanite		
Pyrite		
Halite		
Fluorite		
Anhydrite		
Na2SO4		
Calcite		
Na2CO3		
Total	100.15	100.15

Fe3+/(Total Fe) in rock	10.0	10.0
Mg/(Mg+Total Fe) in rock	49.2	49.2
Mg/(Mg+Fe2+) in rock	51.8	51.8
Mg/(Mg+Fe2+) in silicates	57.8	57.8
Ca/(Ca+Na) in rock	48.0	48.0
Plagioclase An content	38.8	38.8
Differentiation Index	54.9	63.1
Calculated density, g/cc	3.02	3.02
Calculated liquid density, g/cc	2.70	2.70
Calculated viscosity, dry, Pas	0.15	0.15
Calculated viscosity, wet, Pas	0.15	0.15
Estimated liquidus temp., °C	1268	1268
Estimated H2O content, wt. %	0.22	0.22

This program was written by Kurt Hollocher, Geology Department, Union College, Schenectady, NY, 12308, hollochk@union.edu

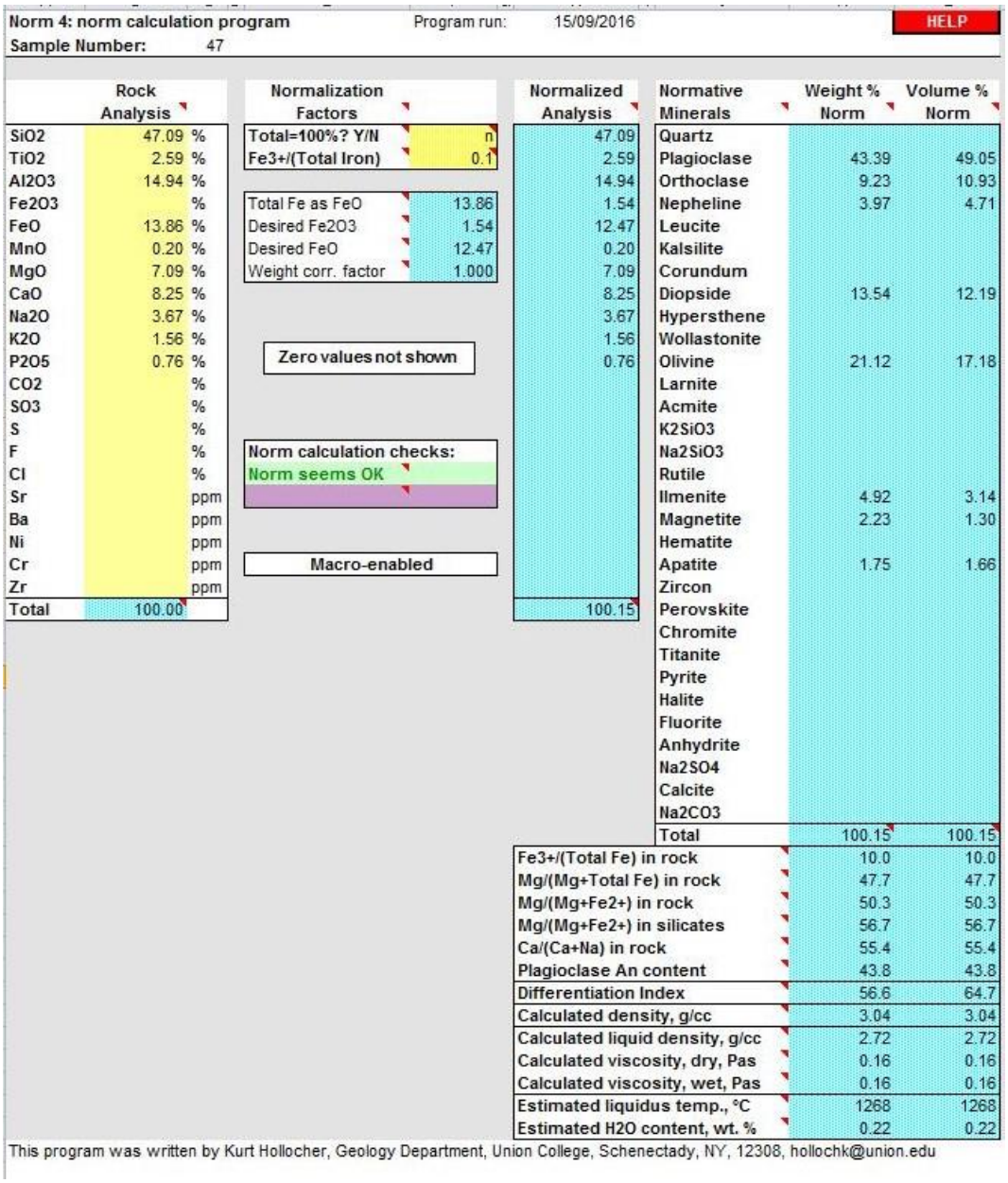

Norm 4: norm calculation program Program run: 15/09/2016 HELP

Sample Number: 47

	Rock Analysis		Normalization Factors		Normalized Analysis	Normative Minerals	Weight % Norm	Volume % Norm
SiO2	47.09	%	Total=100%? Y/N	n	47.09	Quartz		
TiO2	2.59	%	Fe3+/(Total Iron)	0.1	2.59	Plagioclase	43.39	49.05
Al2O3	14.94	%			14.94	Orthoclase	9.23	10.93
Fe2O3		%	Total Fe as FeO	13.86	1.54	Nepheline	3.97	4.71
FeO	13.86	%	Desired Fe2O3	1.54	12.47	Leucite		
MnO	0.20	%	Desired FeO	12.47	0.20	Kalsilite		
MgO	7.09	%	Weight corr. factor	1.000	7.09	Corundum		
CaO	8.25	%			8.25	Diopside	13.54	12.19
Na2O	3.67	%			3.67	Hypersthene		
K2O	1.56	%	Zero values not shown		1.56	Wollastonite		
P2O5	0.76	%			0.76	Olivine	21.12	17.18
CO2		%				Larnite		
SO3		%				Acmite		
S		%				K2SiO3		
F		%	Norm calculation checks:			Na2SiO3		
Cl		%	Norm seems OK			Rutile		
Sr		ppm				Ilmenite	4.92	3.14
Ba		ppm				Magnetite	2.23	1.30
Ni		ppm				Hematite		
Cr		ppm	Macro-enabled			Apatite	1.75	1.66
Zr		ppm				Zircon		
Total	100.00				100.15	Perovskite		
						Chromite		
						Titanite		
						Pyrite		
						Halite		
						Fluorite		
						Anhydrite		
						Na2SO4		
						Calcite		
						Na2CO3		
						Total	100.15	100.15
						Fe3+/(Total Fe) in rock	10.0	10.0
						Mg/(Mg+Total Fe) in rock	47.7	47.7
						Mg/(Mg+Fe2+) in rock	50.3	50.3
						Mg/(Mg+Fe2+) in silicates	56.7	56.7
						Ca/(Ca+Na) in rock	55.4	55.4
						Plagioclase An content	43.8	43.8
						Differentiation Index	56.6	64.7
						Calculated density, g/cc	3.04	3.04
						Calculated liquid density, g/cc	2.72	2.72
						Calculated viscosity, dry, Pas	0.16	0.16
						Calculated viscosity, wet, Pas	0.16	0.16
						Estimated liquidus temp., °C	1268	1268
						Estimated H2O content, wt. %	0.22	0.22

This program was written by Kurt Hollocher, Geology Department, Union College, Schenectady, NY, 12308, hollochk@union.edu